Immobilization of Homogeneous Catalysts on Nanoparticles and their Application in Semi-Heterogeneous Catalysis

Dissertation

Zur Erlangung des Doktorgrades

Dr. rer. nat.

der Fakultät für Chemie und Pharmazie

der Universität Regensburg

vorgelegt von

Alexander Schätz

aus Erlau

Regensburg 2009

Die Arbeit wurde angeleitet von:	Prof. Dr. O. Reiser
Promotionsgesuch eingereicht am:	16. März 2009
Promotionskolloquium am:	8. April 2009
Prüfungsausschuss:	Vorsitz: Prof. Dr. S. Elz 1. Gutachter: Prof. Dr. O. Reiser 2. Gutachter: Prof. Dr. F. E. Kühn 3. Prüfer: Prof. Dr. O. S. Wolfbeis

Der experimentelle Teil der vorliegenden Arbeit wurde unter der Leitung von Herrn Prof. Dr. Oliver Reiser in der Zeit von Januar 2006 bis März 2009 am Institut für Organische Chemie der Universität Regensburg angefertigt.

Herrn Prof. Dr. Oliver Reiser möchte ich herzlich für die Überlassung des äußerst interessanten Themas, die anregenden Diskussionen und seine stete Unterstützung während der Durchführung dieser Arbeit danken.

Meiner Familie

Of all human activities, writing is the one for which it is easiest to find excuses not to begin – the desk's too big, the desk's too small, there's too much noise, there's too much quiet, it's too hot, too cold, too early, too late.

Robert Harris

Table of Contents

	A. Introduction	**1**
1.	**Catalysts immobilized on monolayer-protected gold clusters**	**3**
1.1	**In-situ functionalized gold nanoparticles**	**4**
1.2	**Gold nanoparticles functionalized via place-exchange reaction**	**7**
2.	**Catalysts immobilized on magnetic nanoparticles**	**14**
2.1	**Magnetic nanoparticles stabilized with carboxylic- and phosphonic-acid derivatives**	**15**
2.2	**Dopamine stabilized ferrite nanoparticles**	**20**
2.3	**Silica coated iron oxide nanoparticles**	**24**
3.	***References***	**34**
	B. Main Part	**37**
	I. Catalysts immobilized on Monolayer-protected gold clusters	**37**
1.	**A short history of gold colloids**	**37**
2.	**Synthesis of monolayer-protected gold clusters**	**39**
2.1	**Reductants and stabilizers**	**39**
2.2	**The Brust-Schiffrin method**	**39**
3.	**Functionalization of monolayer-protected gold clusters via place-exchange reaction**	**42**
3.1	**Theoretical considerations concerning place-exchange reactions**	**43**
3.2	**Practical considerations concerning place-exchange reactions**	**44**
4.	**Immobilization of azabis(oxazolines) on AuMPCs**	**45**
4.1	**Classification and synthesis of azabis(oxazoline)-ligands**	**46**
4.2	**Immobilization of thiol-tagged azabis(oxazolines) via place-exchange reaction**	**46**
4.2.1	**Synthesis of thiol-modified azabis(oxazolines) via alkylation**	**49**
4.2.2	**Synthesis of thiol modified azabis(oxazolines) via copper(I)-catalyzed azide/alkyne cycloaddition**	**51**
4.2.2.1	**General remarks on the CuAAC-reaction**	**51**
4.2.2.2	**Synthesis of thiol-modified azabis(oxazolines) via CuAAC**	**54**

4.3	The CuAAC-reaction as a generally applicable tagging method for AuMPCs	58
4.3.1	Synthesis of azide-functionalized AuMPCs	59
4.3.2	CuAAC between propargylated azabis(oxazolines) and azide-functionalized AuMPCs	62
4.3.2.1	Copper(I)-salts and -complexes as catalysts	62
4.3.2.2	Heterogeneous copper(I)-sources as catalysts	63
4.3.2.2.1	Copper-in-charcoal (Cu/C)	63
4.3.2.2.2	Copper nanoparticles in aluminum oxyhydroxide nanofibers	64
4.4	Ruthenium catalyzed azide/alkyne cycloaddition (RuAAC)	64
4.5	Conclusions	66
5.	*References*	67
	II. Catalysts immobilized on Magnetic Nanoparticles	71
1.	Catalysts immobilized on silica coated magnetite nanoparticles	71
1.1	Synthesis of silica coated magnetite particles	71
1.2	The silica shell	73
1.3	Immobilization of azabis(oxazolines) on magnetite@silica-nanoparticles via CuAAC	74
2.	Catalysts immobilized on carbon coated cobalt nanoparticles	77
2.1	Characteristics of the shell	77
2.2	Synthesis of Co/C-nanoparticles via flame spray pyrolysis	78
2.3	Surface modification via reductive grafting of diazonium compounds	79
2.4	Synthesis of azide functionalized Co/C-nanoparticles	81
2.5	CuAAC as a generally applicable route for the immobilization of catalysts on Co/C-nanoparticles	82
2.5.1	Azabis(oxazolines) immobilized on Co/C-nanoparticles	85
2.5.2	Oxidation-catalysts immobilized on Co/C-nanoparticles	86
2.5.2.1	TEMPO immobilized on Co/C-nanoparticles	86
2.5.2.2	Co(II)-Schiff base complexes immobilized on Co/C-nanoparticles	90
3.	*References*	94

	III. Catalysis	**98**
1.	**Asymmetric catalysis with azabis(oxazolines)**	**98**
1.1	**Significance of ligand/metal-ratio**	**98**
1.2	**Asymmetric monobenzoylation of racemic 1,2-diols**	**99**
1.2.1	**Asymmetric monobenzoylation with homogeneous and polymer-supported azabis(oxazolines)**	**101**
1.2.2	**Asymmetric monobenzoylation with azabis(oxazolines) supported on magnetite@silica-nanoparticles**	**103**
1.2.2.1	**In-situ prepared Fe_3O_4@SiO_2@AzaBOX·$Cu(OTf)_2$-catalyst**	**103**
1.2.2.2	**Preformed Fe_3O_4@SiO_2@AzaBOX·$CuCl_2$-catalyst**	**105**
1.2.3	**Asymmetric monobenzoylation with azabis(oxazolines) supported on Co/C-nanoparticles**	**107**
1.2.3.1	**Catalysis under batch conditions**	**107**
1.2.3.2	**Catalysis under continuous-flow conditions**	**109**
1.3	**Asymmetric Michael-addition of indole to benzylidene malonates**	**113**
1.3.2	**Catalysis with nanoparticle-supported azabis(oxazolines)**	**125**
1.4	**Asymmetric Michael-addition of indole to nitroalkenes**	**127**
1.5	**Asymmetric intramolecular Cannizarro reaction**	**134**
2.	**Co/C-immobilized catalysts for oxidation reactions**	**138**
2.1	**TEMPO mediated oxidation of primary and secondary alcohols**	**138**
2.2	**Co(II)-Schiff base catalyzed oxidations with molecular oxygen**	**141**
3.	***References***	**148**

C. Summary 150

1.	**Significance of ligand/metal-ratio**	**150**
2.	**Azabis(oxazolines) immobilized on nanoparticles**	**152**
3.	**Oxidation-catalysts immobilized on Co/C-nanoparticles**	**155**
4.	***References***	**158**

D. Experimental 160

1. General comments 160
2. Syntheses of literature-known compounds 161
3. Syntheses of novel compounds 162
4. Nanoparticle syntheses 166
4.1 Syntheses of monolayer-protected gold clusters 166
4.2 Syntheses of magnetite@silica-nanoparticles 168
4.3 Syntheses of carbon coated cobalt-nanoparticles 174
5. Catalysis 179
6. *References* 193

E. Appendix 194

1. NMR spectra 194
2. List of publications 219
3. Congresses and scientific meetings 220
4. Curriculum vitae 221

F. Acknowledgement 223

Abbreviations

2D	2-dimensional
3D	3-dimensional
AAPS	*N*-(2-aminoethyl)-3-amino-propyltrimethoxysilane
abs.	absolute
APS	3-aminopropyltriethoxysilane
atm.	atmosphere
ATR	attenuated total reflection
ATRP	atom transfer radical polymerization
AuMPC	monolayer-protected gold cluster
AuNP	gold nanoparticle
AzaBOX	azabis(oxazoline)
BArF	tetrakis(3,5-trifluoromethyl-phenyl)borate
BINAP	binaphthol
BINOL	1,1´-bi-2-naphthol
Bn	benzyl
BOX	bis(oxazoline)
BTMSA	trimethylsilylacetylene
Bz	benzoyl
COD	1,5-cyclooctadiene
CuAAC	copper-catalyzed azide/ alkyne cycloaddition
d	day
DBS	dodecylbenzenesulfonate
DDB	4-diazonium decylbenzene fluoroborate
DIPEA	*N*,*N*-diisopropylethylamine
DMAP	4-dimethylaminopyridine
DMSO	dimethylsulfoxide
DOPA	dopamine
DPEN	1,2-diphenylethylene-diamine
DTT	1,4-dithiothreitol
EDTA	ethylenediamintetra-acetatic acid
ee	enantiomeric excess
EE	ethylacetate
EI	electron impact (MS)
ent	enantiomer
equiv.	equivalent
Et	ethyl
GaSB	Ga–Na-bis-(binaphthoxide)
GC	gas chromatography, glassy carbon
h	hour
HMDS	hexamethyldisilazane
HOPG	highly oriented pyrolytic graphite
HPLC	high performance liquid chromatography
^{i}Pr	*iso*-propyl
IR	infrared spectroscopy
L	ligand
M	arbitrary metal
MCF	mesocellular foam
Me	methyl
MeOH	methanol
MeOPEG	polyethylene glycol monomethyl ether
min	minute

MMA	methyl methacrylate
MOM	methoxymethl ether
MPC	monolayer-protected cluster
MPS	(3-mercaptopropyl)-trimethoxysilane
MRI	magnetic resonance imaging
MS	molecular sieves, mass spectroscopy
n.d.	not determined
NHC	*N*-heterocyclic carbene
NMR	nuclear magnetic resonance
NP	nanoparticle
OTf	triflate
PE	hexanes
Ph	phenyl
Phen	1,10-phenanthroline
PMAM	polyaminoamido
PMMA	polymethyl methacrylate
PS	polystyrene
PyOX	2-(2'-pyridyl)oxazoline
PYRPHOS	3,4-bis-diphenylphosphino-pyrrolidine
quant.	quantitative
R	arbitrary rest
rac	racemic
ROMP	ring opening metathesis polymerization
RT	room temperature
RuAAC	ruthenium catalyzed azide/ alkyne cycloaddition
S	solvent
s	second
SAM	self-assembled monolayer
SMAD	solvated metal atom dispersion
SPIO	superparamagnetic iron oxide
^{t}Bu	*tert*-butyl
T	temperature
TEM	transmission electron microscopy
TEMPO	2,2,6,6- tetramethyl-piperidine-1-oxyl
TEOS	tetraethylorthosilicate
THF	tetrahydrofurane
TLC	thin layer chromatography
TMS	tetramethylsilyl
TOF	turnover frequency
TON	turnover number
TOPO	trioctylphosphine oxide
TTCE	1,1,2,2-tetrachloroethane
X	arbitrary anion

A. Introduction

Catalysis is among the most important applications within the field of nanoscience.[1] The large surface area of metal nanoparticles qualifies them quite naturally to act either as heterogeneous promotors for catalytic reactions[2] or as a support for homogeneous catalysts.[3] Contrary to classic heterogeneous catalysts,[4] nanoparticles (NPs) are synthesized in a bottom-up approach from molecular precursors such as a metal salt, a stabilizer, and a reducing agent (with the latter two being sometimes identical). When catalytic applications of NPs are discussed, four general approaches can be considered in distinct form as well as in combinations thereof. They can be discriminated via the role exerted by the metal the nanoparticle consists of, the location of the ligand, if any, with respect to the particle surface and whether the ligand plays an active part in the catalytic process or acts solely as a stabilizer.

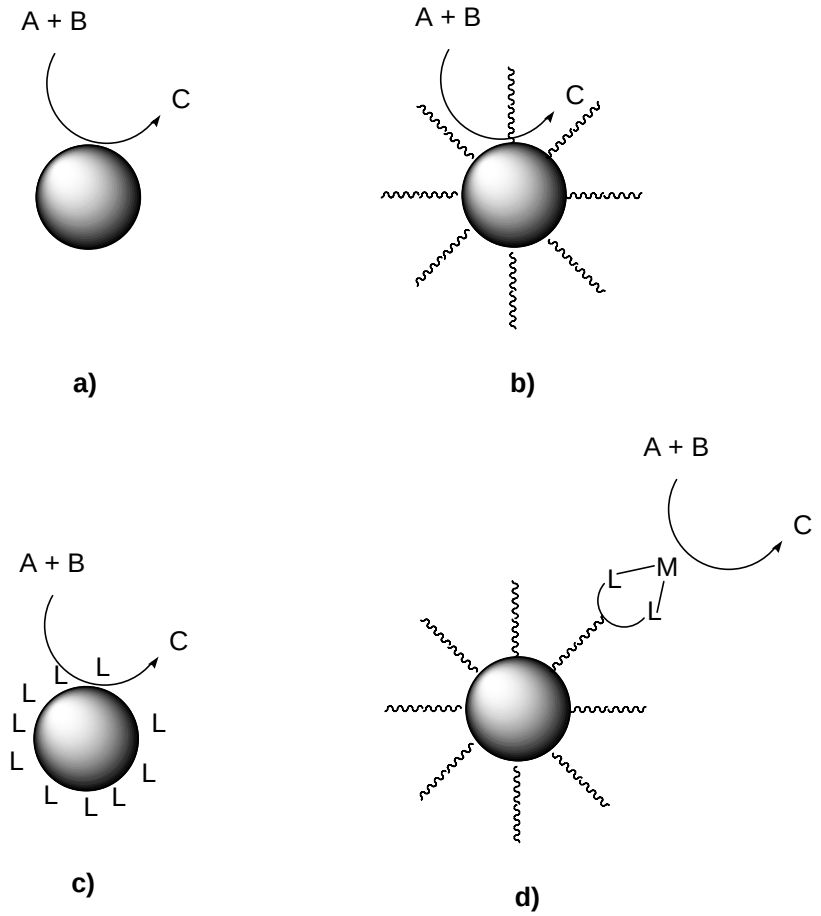

Figure 1. Catalysis with a) metal-nanoparticles, b) metal-nanoparticles capped with a protective shell, c) metal-nanoparticles capped with ligands contributing to the catalytical activity and d) metal-nanoparticles with catalysts supported on the protective shell. Only in the latter case the core material does not promote the reaction.

Even more complex morphologies are possible if bimetallic nanoparticles or multilayer shells are considered. The first three approaches involve the use of systems where the nanoparticle metal exerts the dominating influence on the catalytic activity (Figure 1a-c). In all these cases, the catalytic processes take place on the surface of the nanoparticles, affected only in one structure by ligands/capping agents that transmit influence to metal-coordinated substrates in their vicinity (Figure 1c). A plethora of clusters with constituent metals such as Pt, Pd, Ru and Rh was reported.[5] Since the catalytic properties of these metal nanoparticles, acting in principle as a heterogeneous catalyst, have been extensively reviewed,[2] the following chapters will focus on nanomaterials acting solely as carriers for soluble catalysts (Figure 1d), an approach which has been scarcely discussed.[6] In here the clusters act as a structuring element for an assembly of ligands, which are bonded to the core material through an additional function, different from the chelating functional groups defining the catalytic center. The activity arises from a metal different to the core material.

On these nanoclusters, catalysts are exposed on the particle surface, which makes them accessible almost like their homogeneous counterparts. Such a globular surface might be superior to conventional polymeric supports, representing the most popular scaffolds used for immobilization so far.[7] Amorphous resins have sometimes the problem that catalytic sites are buried in the polymer backbone, thus limiting the access of reactants.[8] This limitation was widely tolerated since the benefits which arise from the grafting of a soluble heavy-metal complex or organocatalyst, namely ease of separation and recyclability of the usually toxic and expensive species, outbalance the loss of activity and selectivity occasionally observed. Especially soluble transition-metal complexes are difficult to separate, a fact which limited their application in large-scale pharmaceutical processes due to metal contamination.[9] Furthermore, the separation of heterogeneous matrices from the reaction mixture is more feasible than via biphasic systems, e.g. extraction using perfluorinated tags.[10] The domain of nanoparticles acting as a recyclable scaffold is settled between these two orthogonal strategies, hence this approach is sometimes called “semi-heterogeneous”.[2f] The separation of the functionalized nanomaterial succeeds via different methods, depending on the nature of the particles. Such are centrifugation, precipitation–flocculation, nanofiltration, or magnetic decantation (in the case of magnetic nanoparticles). Since the core material is not meant to take part in the

catalytic reaction, this metal should be comparatively inactive or surrounded by a completely impermeable shell. The latter condition is rather difficult to accomplish, which explains why only very few metals are used as structural elements, despite the many different metal NPs that found application in heterogeneous catalysis. Therefore, gold-colloids tethered to a protective alkanethiol-monolayer were for a long time the dominating motif for nanosized core/shell-structures due to the insinuated inertness of Au(0), an assumption which can, however, not persist unrestricted.[11]

1. Catalysts immobilized on monolayer-protected gold cluster

The first nanosized core/shell-structures utilized as a support for catalysts were Au-colloids. Gold-nanoclusters sufficiently stable to act as a support for metal complexes usually feature a stabilizing alkanethiol-monolayer on which the catalysts are anchored. The exceptional stability of the Au-S-bond could result in the misguided association of a certain rigidness of the shell. In fact, the self-assembling-monolayer (SAM) on the particle surface is in his behaviour far more comparable to a two-dimensional fluid. Thiolates are constantly changing their position on the cluster, “hopping”[12] from one cluster to the next, or exchanging with thiols eventually present in the supernatant. Especially the latter behaviour offers a straightforward route for the attachment of functionalized thiols via the so-called place-exchange reaction.[13]

However, early studies feature examples for in-situ functionalization via passivation of preformed gold colloids or simultaneously to the growing of the gold nuclei which form upon reduction of tetrachloroaureate with sodium borohydride according to a procedure developed by Brust and Schiffrin.[14] Due to the exceptional simple and concise layout of the Schiffrin-reaction, chemistry using monolayer-protected gold clusters (AuMPCs) experienced an additional boost.

1.1 In-situ functionalized gold nanoparticles

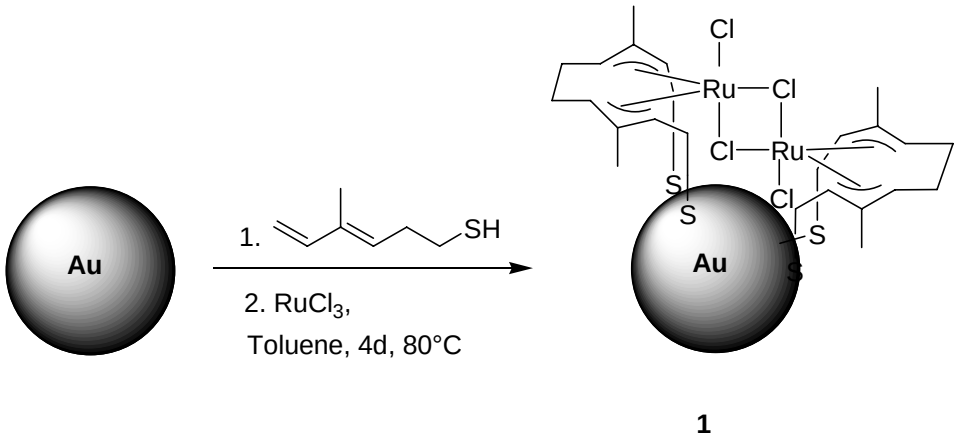

1

Scheme 1. Tagging of gold colloids with a Ru-complex for the ring opening metathesis polymerization (ROMP) of norbornene to polynorbornene.

The first transition-metal complex immobilized on metal nanoparticles was developed by Tremel et al. in 1998.[15] Freshly prepared gold colloids were stirred with 4-methylhexa-3,5-diene-1-thiol in the presence of $RuCl_3$ under argon to yield a black powder which can be dissolved in acetone and precipitated from methanol (Scheme 1). The gold-grafted Ru-complex **1** was able to catalyze the ring opening metathesis polymerization (ROMP) of norbornene, providing turnover frequencies (TOF: 16.000 h^{-1}) superior to those obtained with the homogeneous counterpart (TOF: 3.000 h^{-1}). It was reasoned that the orientation of the catalyst on the surface of the MPCs favours the coordination of the monomer and the orientation of the growing polymer chain. However, Ru-complexes on 2D-Au-surfaces exceeded both values by far (TOF: 80.000 h^{-1}).

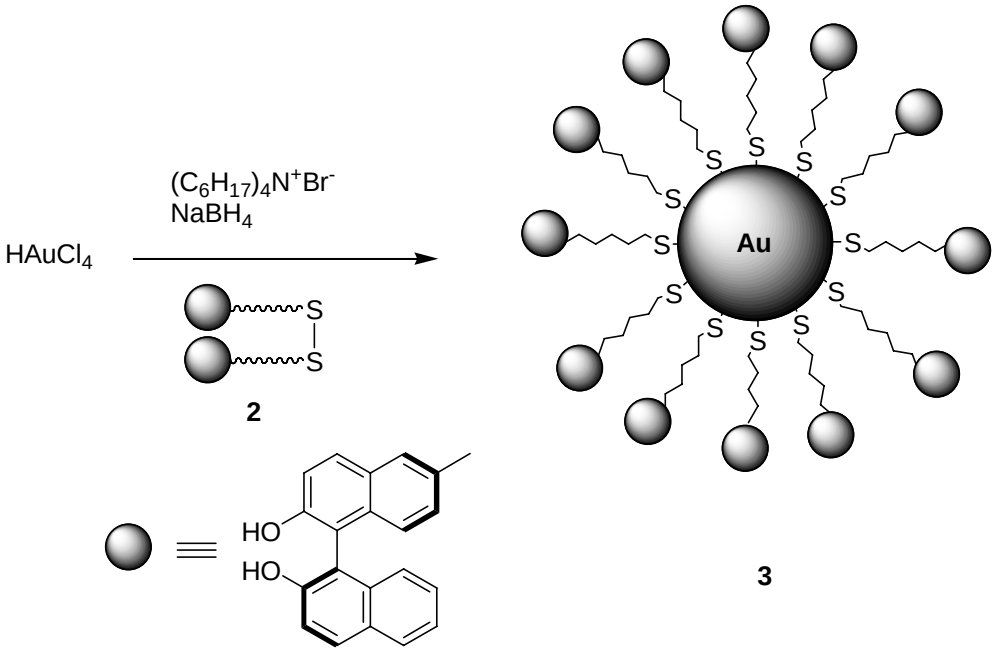

Scheme 2. Synthesis of ω-1,1`-bi-2-naphthol-alkanethiolated AuMPCs.

In an elegant study, Sasai et al.[16] reported on Au-clusters stabilized by thiols bearing chiral 1,1`-bi-2-naphthol (BINOL) moieties using exclusively disulfides with (*R*)-BINOL at terminal position. Since functionalized disulfides were employed already during the Schiffrin reaction, core passivation and functionalization succeeded in a one-pot reaction that makes this route comparatively simple (Scheme 2). Furthermore, this represents the first application of a chiral catalyst immobilized on AuNPs. A Ti-BINOLate-complex was able to catalyze the asymmetric alkylation of benzaldehyde using Et_2Zn in up to 98% yield and with 86% ee (Scheme 3).

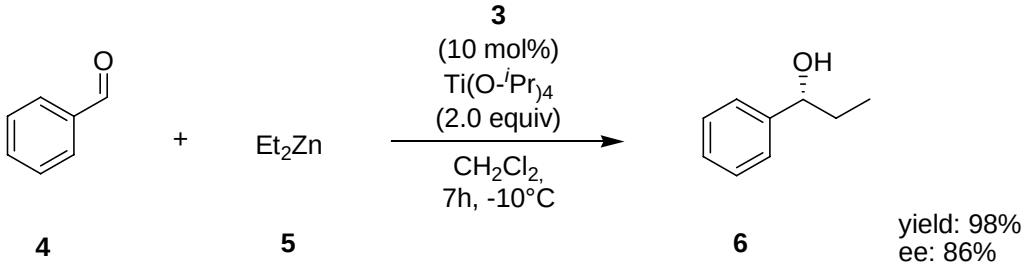

Scheme 3. Asymmetric alkylation of benzaldehyde (**4**) with diethylzinc (**5**) catalyzed by Ti-BINOLated-AuMPCs

Thus, BINOL-functionalized MPCs **3** gave results comparable to the homogeneous catalyst (95% yield, 90% ee) and clearly superior to polystyrene-supported Ti-BINOLate-complexes (61% yield, 83% ee).[16c] Recycling of the nanocomposite was

possible via precipitation from EtOH and redispersion in CH_2Cl_2, although this procedure was accompanied by an explicit drop in enantioselectivity (62% ee). In addition, the length of the alkanethiol-spacer (C_4, C_5, C_6) was found to have quite an effect on the selectivity.

Recently, Sasai was expanding this concept to challenge the task of immobilizing multicomponent asymmetric catalysts such as Ga–Na-bis(binaphthoxide) complexes (GaSB, Figure 2).[16b]

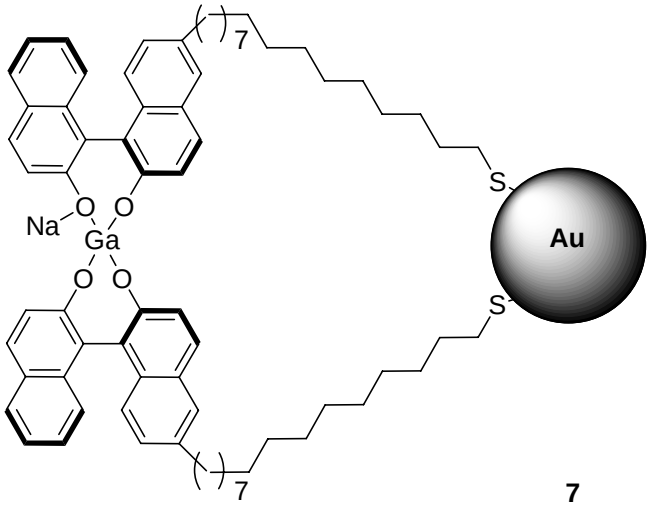

7

Figure 2. AuMPC supported asymmetric Ga–Na-bis(binaphthoxide) multicomponent catalyst.

The synthesis was similar to the one depicted in Scheme 2, using MOM-protected BINOL-terminated disulfides but with a significantly longer (C_{16}) alkyl-spacer. The as-prepared AuMPC-supported BINOL **7** (20 mol%) was treated with $GaCl_3$ (20 mol%) and NaO^tBu (85 mol%) in the presence of cyclohex-2-enone (**8**) and dibenzyl malonate (**9**) to afford the corresponding Michael adduct **10** in 67% yield and 98% ee, which is comparable to the parent homogeneous catalyst (Scheme 4).

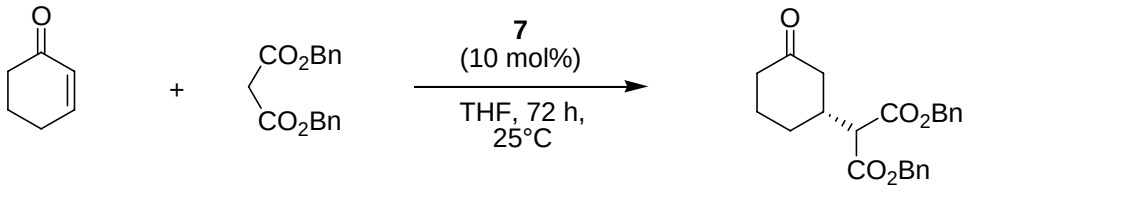

8 **9** **10** yield: 67%
ee: 98%

Scheme 4. Asymmetric Michael-addition of dibenzyl malonate (**9**) to cyclohex-2-enone (**10**) using in-situ created multicomponent catalyst **7**.

1.2 Gold nanoparticles functionalized via place-exchange reaction

The exchange of surface-bound thiolates against dissolved functionalized thiols represents a convenient post-grafting process. In contrast to the in-situ methods previously discussed, the size of the Au-particles can be controlled prior to particle modification following well-elaborated protocols since this reaction does not alter the core dimensions.

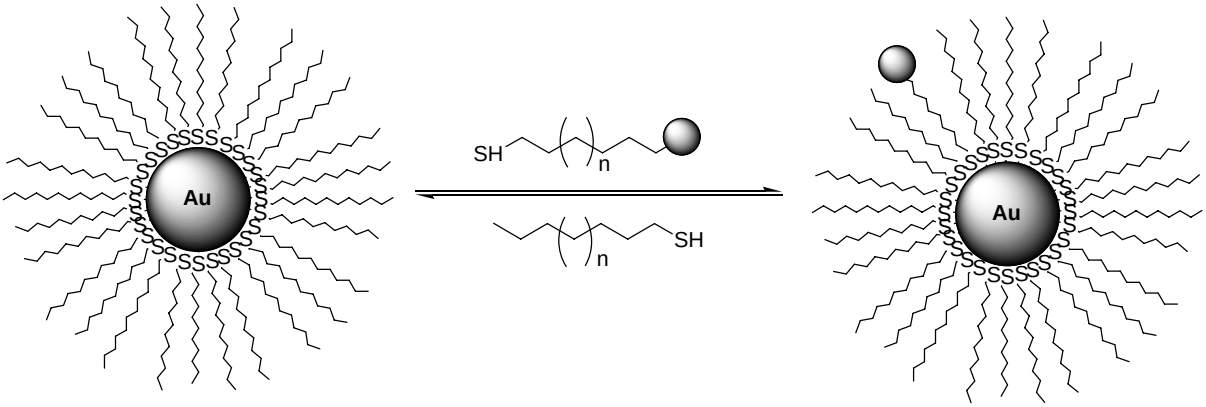

Scheme 5. Place-exchange reaction of surface-bound thiolates and dissolved ω-functionalized alkanethiols.

In addition, the formation of mixed alkanethiol-monolayers is possible, which enables higher degrees of complexity in the SAM. For instance, the use of alkanethiols with different chain length results in variably constructed catalytic sites. Complexes positioned on long-chained alkanethiols relative to the neighbouring thiolates form convex reaction sites, similar to homogeneous catalysts, whereas concave formations are possible with short-chained thiols resembling enzyme-like environments.

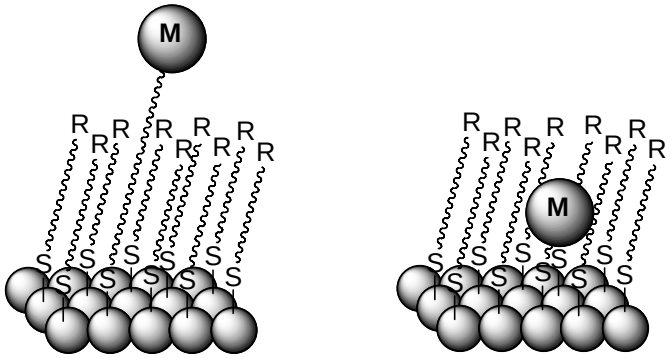

Figure 3. Different active sites for metal catalysts on thiolate-monolayers: Convex active site (homogeneous-like, left) and concave active site (enzyme-like, right).

Different termini of the surrounding alkanethiolates in the monolayer are apt to tune the solubility or reactivity of the cluster through interactions with the substrate or the catalytic center. In addition, the loading of the particles can be controlled in the place-exchange reaction by careful choice of concentrations and reaction times. In this regard, Stöhr and Pfaltz[17] have published a comprehensive study using a [Rh(COD)-(PYRPHOS)]BArF-catalyst.

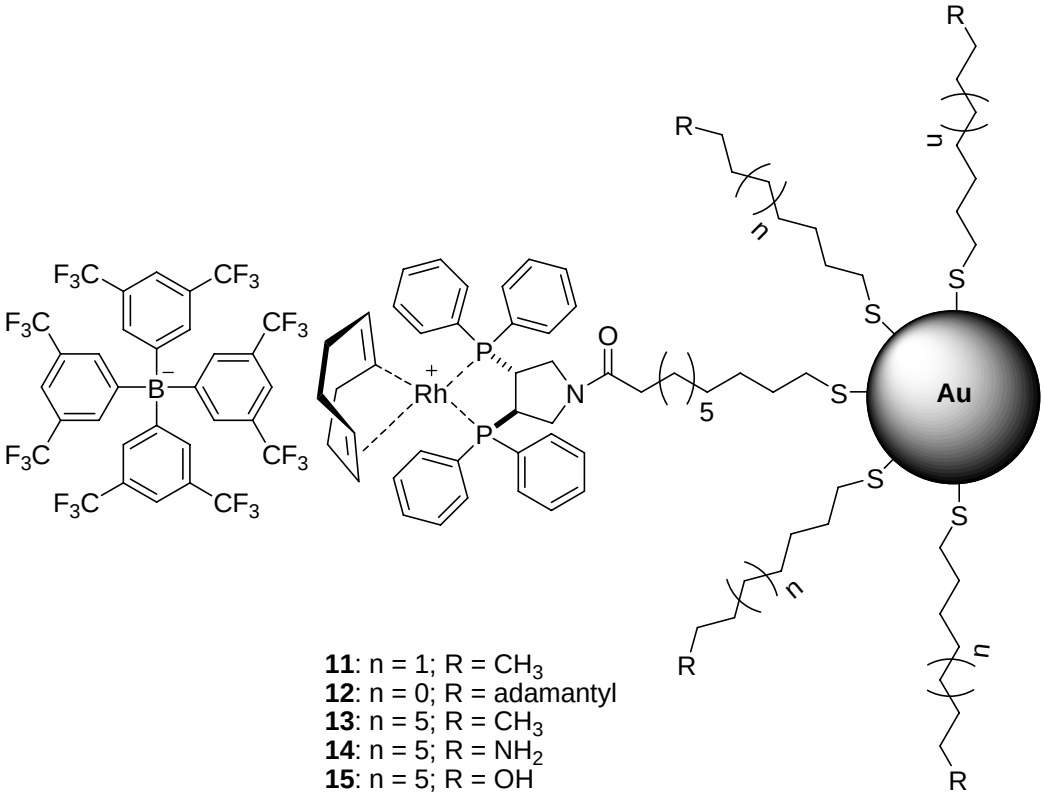

11: n = 1; R = CH_3
12: n = 0; R = adamantyl
13: n = 5; R = CH_3
14: n = 5; R = NH_2
15: n = 5; R = OH

Figure 4. Representation of different AuMPC-structures tagged with [Rh(COD)-(PYRPHOS)]BArF.

Different gold colloids were synthesized via place-exchange reaction of AuMPCs with unequal chain lengths (C_6-C_{12}) and end group polarity of the alkanethiolates in the shell against rhodium-PYRPHOS-bearing thiols (Figure 4). Almost all “heterogenized” catalysts gave yields (>99%) and enantioselectivities (93% ee) equalling those obtained with to the homogeneous [Rh(COD)(*n*-octanoyl-PYRPHOS)]BArF in the hydrogenation of methyl α-acetamidocinnamate **16** (Scheme 6). The colloids could be recovered by filtration and reused at least thrice without loss of enantioselectivity.

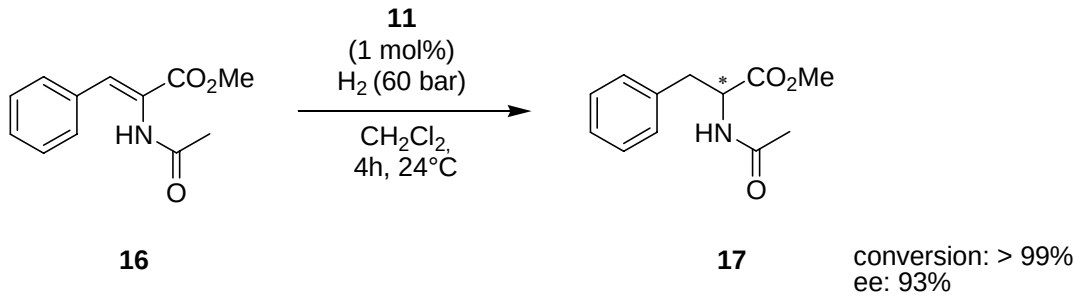

16 **17** conversion: > 99%
ee: 93%

Scheme 6. Asymmetric hydrogenation of methyl α-acetamidocinnamate (**16**) in the presence of **11**.

AuMPCs **14** and **15** are the exception in this regard. Both possess polar endgroups and deliver significantly lower yield (32-94%) and selectivity (82-86% ee). Thus, the promising strategy of creating AuNPs passivated with a ω-hydroxy/-amino-alkanethiolate layer, which was envisaged to result in particles compatible with polar-protic-reaction media, failed. Yields and selectivities achieved with **14** and **15** were clearly inferior when compared to homogeneous, but also heterogeneous catalysts **11**-**13** in EtOH. The anchoring of a preformed complex on gold nanoparticles, as reported by Stöhr and Pfaltz,[17] is a rather rare example.

However, according to Scheme 5, many alkanethiols tagged with ligands were grafted on preformed AuNPs via place-exchange. A very early example for a convex active site forming a homogeneous-like environment was reported by Mrksich.[18] A mixed monolayer was formed containing 25% of dihydroquinidine-functionalized alkanethiols neighbouring octanethiolate coated gold cores with an average diameter of 2.5 nm (Figure 5).

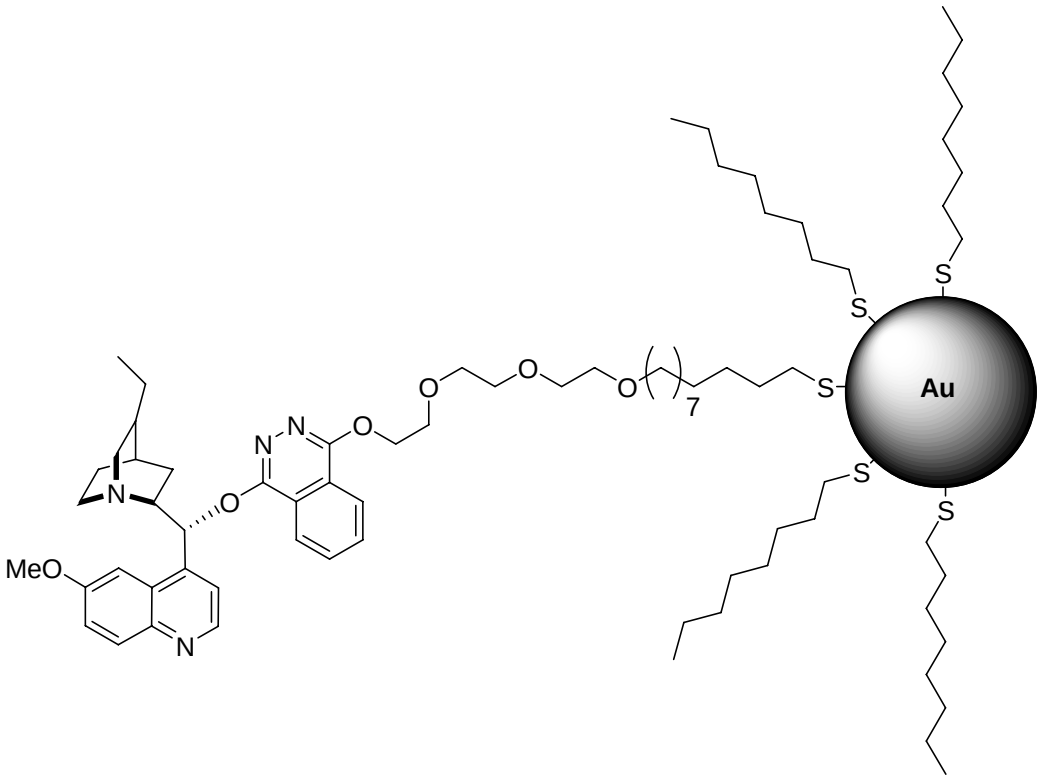

18

Figure 5. Representation of a mixed-monolayer coating of gold nanoparticles in which cinchona alkaloid derivatives are embedded.

The chiral cinchona alkaloid derivative **18** is used to activate oxidant osmium tetroxide in order to render the Sharpless asymmetric dihydroxylation of β-methyl styrene **19** highly enantioselective (90% ee). It is noteworthy that **18** was sufficiently stable to allow recycling via gel permeation chromatography at least twice, thus impressively demonstrating the versatility of this support even in aqueous media and under oxidative conditions.

19 **20**

yield: 72-81%
ee: 79-90%
3 cycles

Scheme 7. Asymmetric dihydroxylation of β-methyl styrene **19** using immobilized catalyst **18**.

However, the recovered material exhibited significant lower activity and selectivity in each cycle (Scheme 7).

If it comes to recyclability, an immobilized Ru-carbene complex developed by Lee et al.[19] sets the benchmark. Octanethiolate-passivated AuMPCs were exchanged with styrene-functionalized dodecanethiols. Treatment of cluster **21** thus obtained with second generation Grubbs Ru-complex **22** in the presence of CuCl yielded a AuMPC-Ru-carbene complex **23** which is soluble in CH_2Cl_2 and can be precipitated from methanol, ethanol or diethylether (Scheme 8).

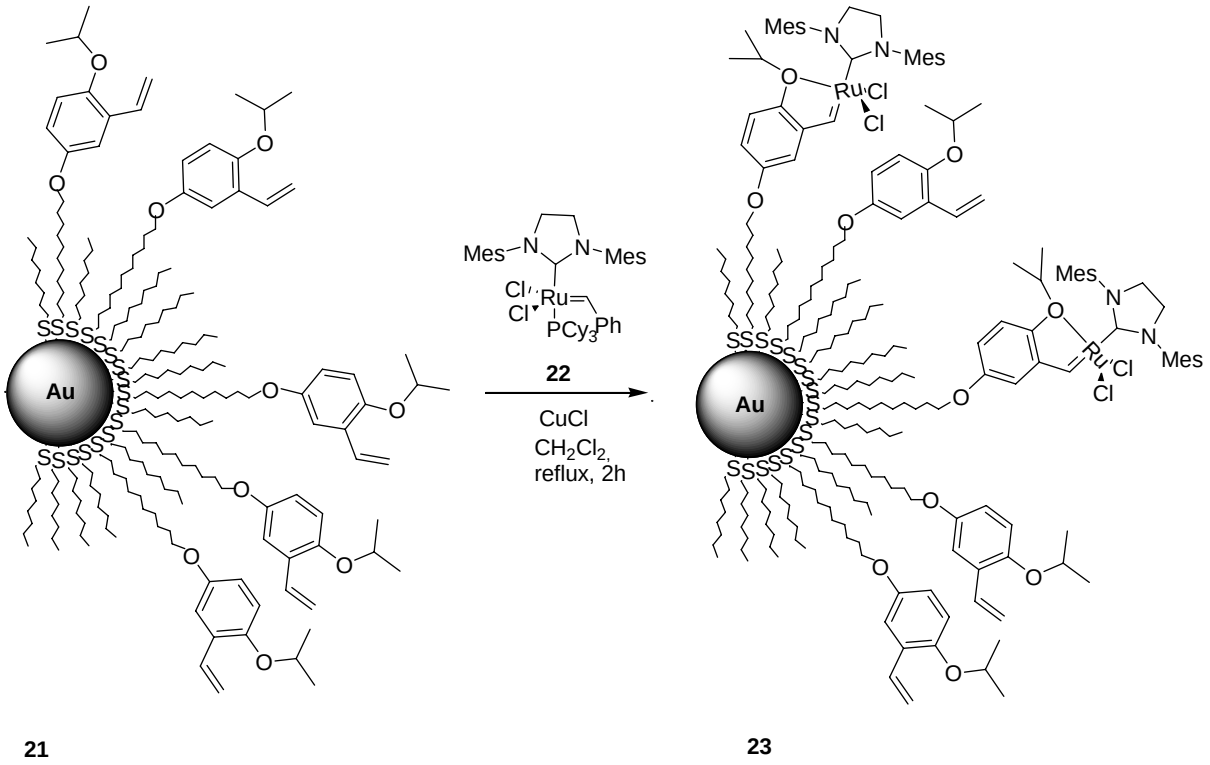

Scheme 8. Synthesis of AuMPC-bound Ru-carbene complex **23** for the ring-closing metathesis of dienes.

This material showed high reactivity (>98% conversion) in the ring-closing olefin metathesis of dienes to heterocyclic compounds with satisfying levels of reusability (Scheme 9).

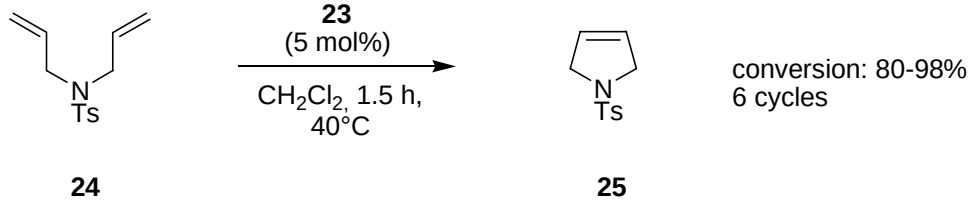

Scheme 9. Ring closing metathesis of *N*-allyl-*N*-tosylprop-2-en-1-amine (**24**) promoted by **23** (5 mol%).

After the 6th run, conversion decreased dramatically from 80% down to 20% accompanied by particle flocculation. Desorption of the coating monolayer followed by aggregation of the gold cores might be responsible for this effect, a suspicion which was substantiated by TEM-analysis (Figure 6).

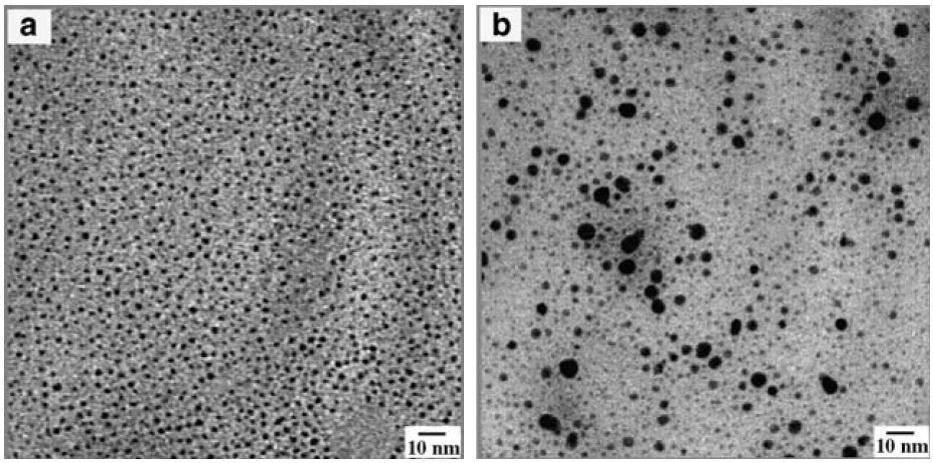

Figure 6. TEM photographs of **23** a) as-prepared and b) after 7th cycle in the ring closing metathesis of dienes (10 nm bar length).[19]

Tanaka et al. examined the influence of different spacer lengths (C_4, C_6, C_8, C_{10}) of the alkanethiols linked to the central carbon atom of a chiral bis(oxazoline) on the dispersability of the corresponding (*R*)-Ph-BOX-AuMPCs (Figure 7, left).[20]

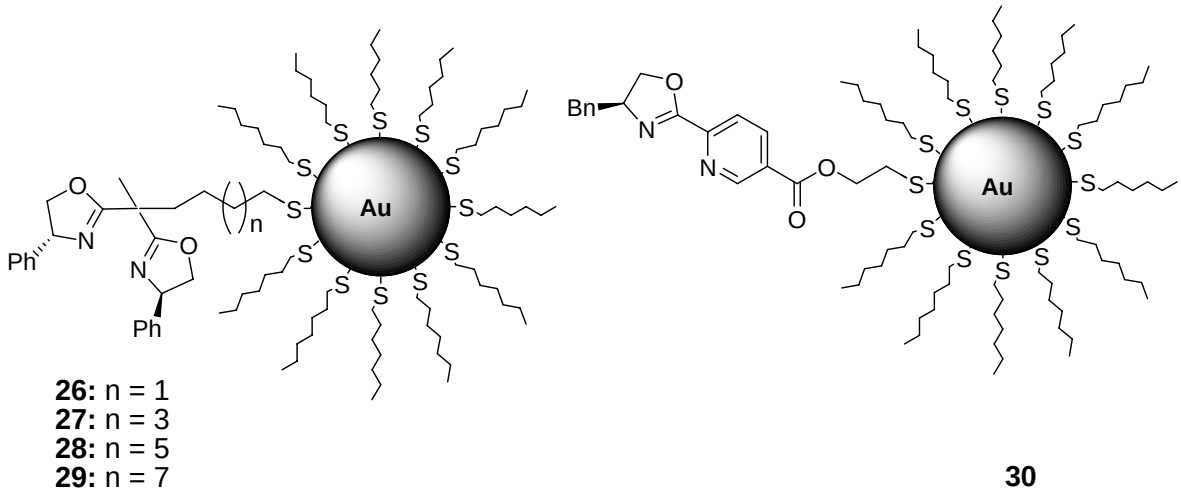

26: n = 1
27: n = 3
28: n = 5
29: n = 7

30

Figure 7. Chiral BOX ligand with different spacer length (C_4, C_6, C_8, C_{10}) (left) and chiral PyOX ligand (right) anchored on C_6-AuMPC.

The copper(II)-complexes of the functionalized AuMPCs **26**-**29** acted as nearly homogeneous catalysts in the ene reaction between 2-phenylpropene **31** and ethyl

glyoxylate **32**. It was found that ligands tethered with the shortest (C_4) linker show the highest level of dispersion and are the most effective in terms of catalytic activity and recycling utility. The authors reasoned that in the case of a concave active site, with copper(II)-complexes buried in the hexanthiolate-shell, aggregation of the particles is minimized. However, the recycling of these highly dispersed particles is a little laborious, involving shaking after dilution with hexane, centrifugation (10.000 min^{-1}, 10 min) and decantation. This procedure has to be repeated thrice before the remaining catalyst can be redispersed under sonication for the following cycle (Scheme 10). Yields decreased slightly from 99% to 80% in the 5th run whereas good enantioselectivites were achieved in each cycle (84-86% ee).

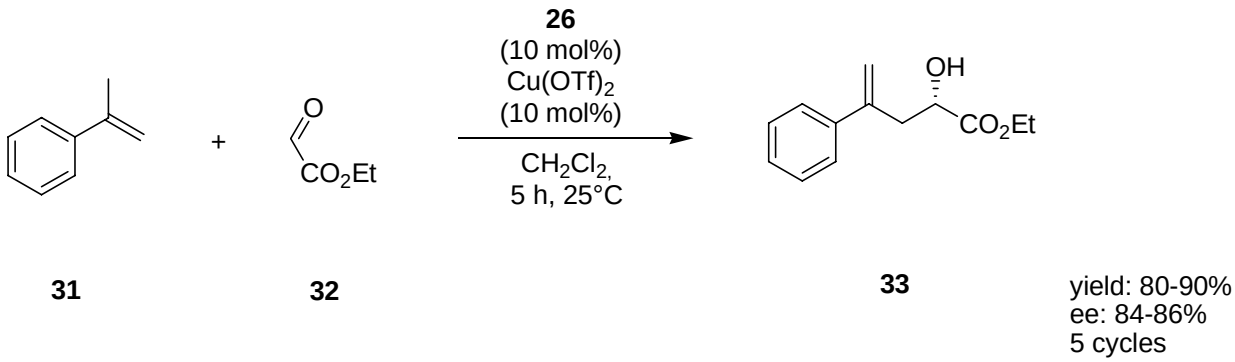

Scheme 10. Ene reaction between 2-phenylpropene **31** and ethyl glyoxylate **32** catalyzed by in-situ formed Cu(II)-**26** complex.

Koskinen and coworkers[21] extended this approach, forming concave PyOX binding sites buried even deeper in the hexanthiolate coating of the gold particle (Figure 7, right). The authors suggested that a 32-atom gold cluster was formed, resembling a hollow structure, which would be the smallest core diameter (1.2 ± 0.2 nm) ever used for AuMPCs serving as carriers for catalysts. However, the catalytic activity of the palladium-complexes of these MPCs in the alkylation of chalconol acetate **33** with dimethyl malonate **34** is limited (Scheme 11). It shows only neglible activity but slightly better enantioselectivity than a polystyrene bound analog. Complete conversions and selectivities up to 73% ee are possible with diverse homogeneous PyOX-ligands, thus suggesting that an enzyme-like binding site has a detrimental effect on this reaction (Scheme 11).

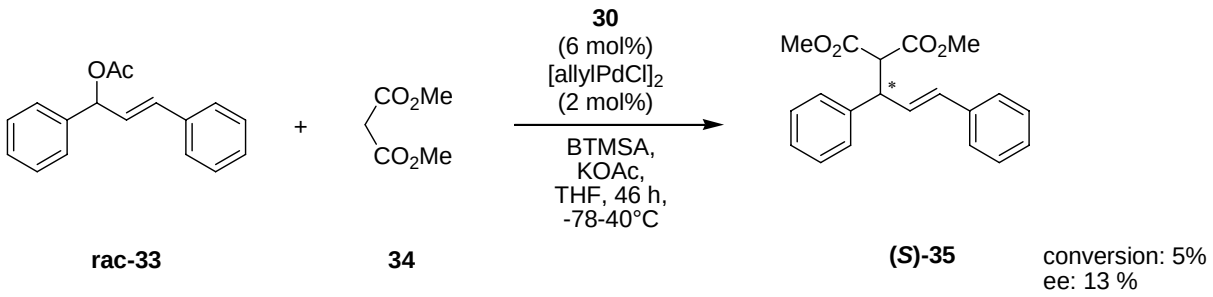

Scheme 11. Asymmetric alkylation of chalconol acetate **33** with dimethyl malonate **34** in the presence of 2 mol% $[allylPdCl]_2$ and 6 mol% **30**.

Nevertheless, such a poor performance is not usual for transition-metal complexes linked to gold nanoparticles. As shown in the previous examples, activities and selectivities reach levels that are often restricted to homogeneous catalysts and rarely equaled by complexes anchored on solid supports. This might be attributed to the excellent dispersibility of these particles, sometimes even considered “soluble”. In addition, the immobilization on AuMPCs offers many prospects, e.g. tuning of the environment of the catalytic sites. However, it has to be admitted that recycling is sometimes tedious and possible only in a limited number. After several cycles the monolayers start inevitably to desorb from the surface of the cluster, thus causing irreversible aggregation of the gold nuclei finally resulting in a material which can not be dispersed anymore.

Driven by the motivation to retain the beneficial properties of the AuMPCs and to simultaneoulsly overcome limitations in recycling, especially feasibility and deficiency in number, several groups disclosed nanoparticles that contain a magnetic core material.

2. Catalysts immobilized on magnetic nanoparticles

Recent advances in the synthesis of size-controlled and monodisperse magnetic ferrite nanoparticles without the need of size-selection facilitated the exploition of these particles in many applications.[22] Similar to gold nanoparticles, these materials allow a surface stabilization via simple organic compounds.

2.1 Magnetic nanoparticles stabilized with carboxylic- and phosphonic-acid derivatives

Carboxylic acid sites are predominant among the most common capping agents for ferrite nanoparticles.[23] Thus, a very early example for magnetic nanoparticles coated with a homogeneous catalyst is provided by a Rh-based cationic catalyst modified with benzoic acid, namely [Rh(COD)- η^6-benzoic acid]BF_4.[24] Co-ferrite ($CoFe_2O_4$) was chosen as support, possessing a deviation from the nominal structure of a spinel ferrite in the shell. An amorphous ferric hydroxide layer on the surface was proposed,[25] thus explaining the non-stoichiometric composition. The saturation magnetization of this nanomaterial with a size distribution ranging from 8 to 20 nm was reported to be approximately 60 emu/g. Similar to the place-exchange reaction, surface modification did not alter the chemical composition, resulting in the form $(CoFe_2O_4)_{core}(Fe_{0.19}O_x)_{shell}$-{[Rh(COD)-$\eta^6$-benzoic acid] BF_4}$_{0.013}$.

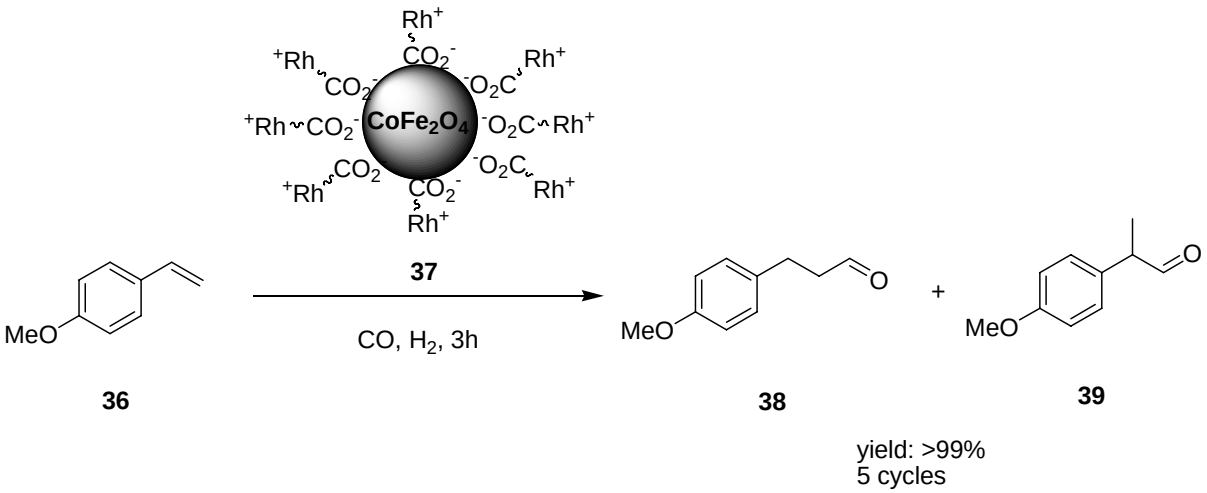

Scheme 12. Hydroformylation of 4-vinylanisole by the nanomagnet-supported catalyst **37**. **38**/**39** = 10/90.

The nanomagnet-supported catalyst **37** showed an activity and regioselectivity toward the hydroformylation of 4-vinylanisole **36**, which is comparable to its homogeneous counterpart, although it has to be stated that reactions with the unsupported catalyst require only one third of the reaction time (Scheme 12). However, the activity is still extraordinarily high relative to catalysts immobilized on conventional supports, e.g. polymers,[26] and shows no loss in activity upon recycling via magnetic decantation.

Not only ferrite-surfaces can be ligated with carboxylic acid derivatives. For instance, cobalt nanoclusters are known to be efficiently stabilized by oleic acid.[27] Very recently, the synthesis of cobalt nanoparticles, stabilized with oleic acid and long chained carboxylic acids ω-functionalized with chiral β-amino alcohols was reported (Scheme 13).[28] Without the use of oleic acid no nanomaterial can be obtained. Particle size and loading depend on the nature of the amino alcohol. With amino alcohol derivative **40** a loading of 1.4 mmol/g and a mean cluster diameter of 13 nm is achieved.

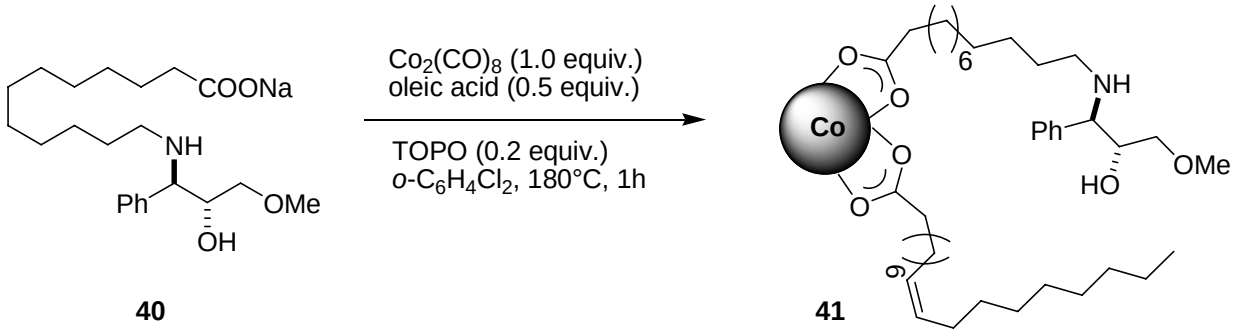

40 **41**

Scheme 13. Synthesis of oleic acid capped cobalt nanoparticles functionalized with chiral amino alcohol.

Pericàs et al. used this magnetically recyclable ligand for the ruthenium-catalyzed transfer hydrogenation of ketones, e.g. acetophenone **42** (Scheme 14). It was found, that activity as well as selectivity of the grafted complex were reasonably higher than those of the soluble analog. The authors reasoned that the concave active site formed on the surface of the nanostructure induces this beneficial effect.

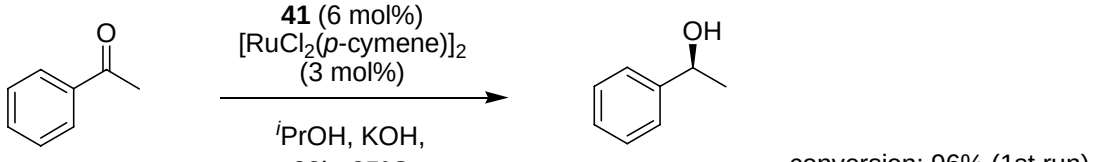

42 **43**

conversion: 96% (1st run)
ee: 77%
conversion: 61% (2nd run)
ee: 26%

Scheme 14. Ru-catalyzed transfer hydrogenation of acetophenone **42** with immobilized ligand **41**.

However, the recovered catalyst paled in means of yield and selectivity when applied in a second run, even when fresh $[RuCl_2(p\text{-cymene})]_2$ was added. Leaching of functionalized carboxylates from the nanoparticles might contribute to this explicit drop. Without the addition of ruthenium, virtually no conversion is observed.

Reduction of the ruthenium complex by metallic cobalt was made responsible for this effect.

Superparamagnetic materials, such as iron oxide nanoparticles (SPIO) are intrinsically nonmagnetic but readily magnetized in the presence of an external magnetic field. The unusual high magnetization moments allow the use of low-field magnets to recover these particles quantitatively from solution. The lack of magnetic remanence prevents the formation of aggregates in the reaction media.

Magnetite (Fe_3O_4) is not only a widespread representative of such SPIO-particles but the most common nanomagnetic support par excellence. Phosphonic acid derivatives were successfully used to stabilize the Magnetite NPs in a number of publications,[29] although they were assumed to be less effective in preventing aggregation upon solvent evaporation than oleic acid.[29a] Lin et. al[29a] used a Ruthenium(II) complex with phosphonic acid-substituted BINAP [Ru(BINAP-PO_3H_2)(DPEN)Cl_2] tethered to magnetite nanoparticles which were synthesized either by thermal decomposition[30] or a coprecipitation method (Figure 8).[31]

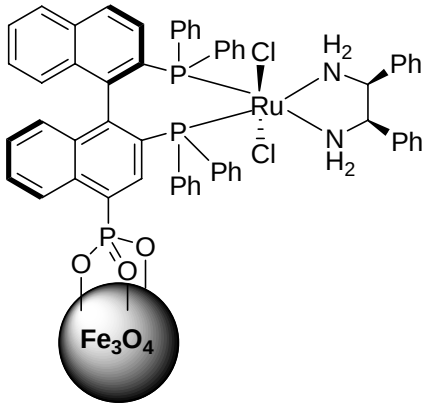

44

Figure 8. [Ru(BINAP-PO_3H_2)(DPEN)Cl_2] supported on magnetite nanoparticles.

Especially magnetite synthesized by the latter route demonstrated outstanding stability and catalyst **44** immobilized thereon possesses impressive efficacy and recyclability in the hydrogenation of 1-acetonaphtone **45** (Scheme 15).

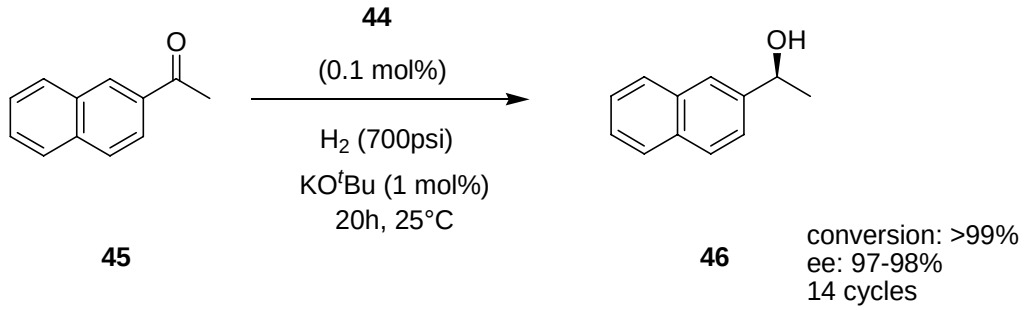

Scheme 15. Asymmetric hydrogenation of 1-acetonaphtone **45** using a Ru(II)-BINAP-phosphonic acid catalyst supported on Fe_3O_4-nanoparticles.

A drop in conversion was observed in the 15th cycle (35%) whereas selectivity remained high (95% ee). Catalyst **44** exhibits a saturation magnetization (σ_s) of 50 emu/g, which is smaller than that of bulk magnetite (92 emu/g). This is consistent with the presence of a surface coating.

Magnetite particles obtained from a similar coprecipitation method served as carriers for a proline ligand that promoted an Ullmann-type coupling between aryl/heteroaryl bromides and nitrogen heterocycles.[29b] In contrast to previous protocols, the phosphonic acid derivative was not ligand-functionalized prior to the coating of the particle surface but derivatized in a post-grafting process instead. To this end, an alkyne moiety was installed on a 4-hydroxy-proline derivative to yield compound **48**, which readily undergoes an azide/alkyne cycloaddition[32] reaction in the presence of catalytic amounts of Cu(I) (Scheme 16).[33] Thus, immobilization is achieved by reaction of **49** with simple 3-azidopropylphosphonic acid stabilized magnetite clusters **47** followed by deprotection.

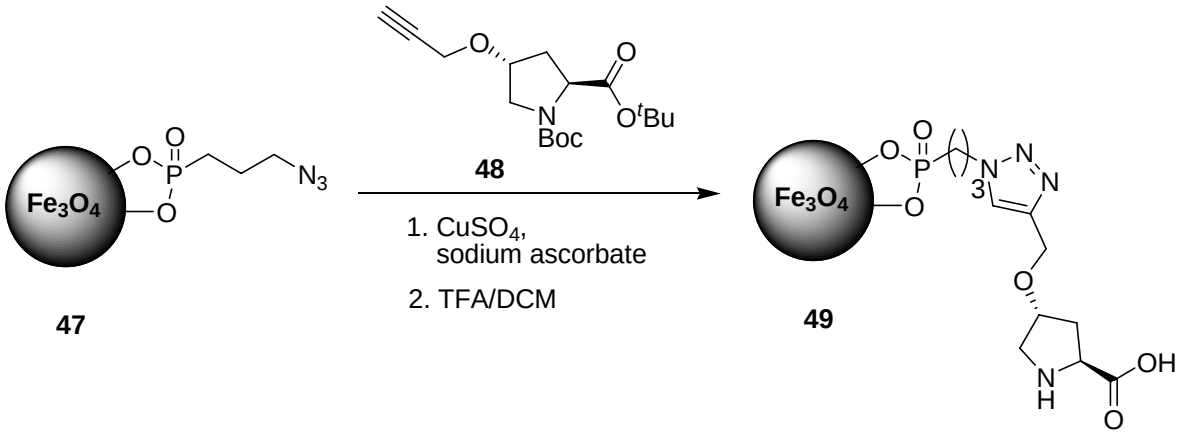

Scheme 16. Preparation of SPIO-immobilized proline **49** using a copper(I)-catalyzed azide/alkyne cycloaddition reaction.

The as-prepared magnetite proline nanocomposite **49** consists of partially aggregated particles with a diameter between 6 and 20 nm. The loading of ligand was determined to be approximately 2.0 mmol/g. The nanomagnet could be reused up to four times without any significant loss of activity (Scheme 17).

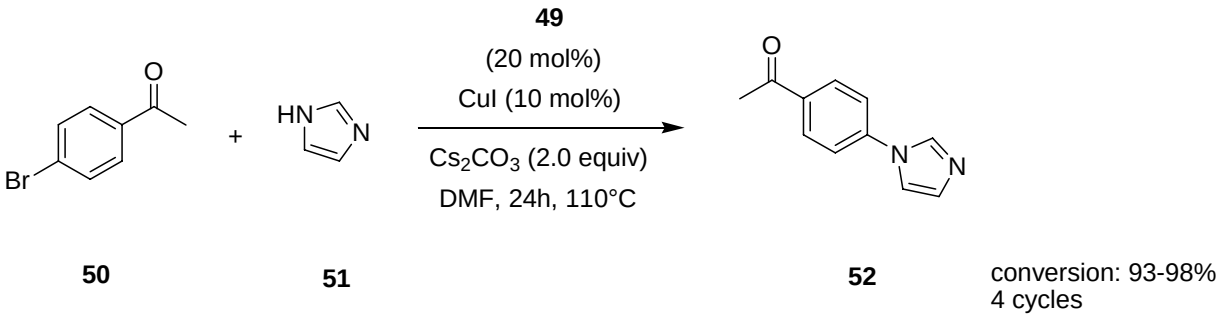

Scheme 17. Ullmann-type coupling reaction of *p*-bromoacetophenone **50** with imidazole **51** promoted by magnetite supported proline **49**.

Since phosphonic acids as well as oleate capped iron oxide nanoparticles have sometimes the problem of aggregation due to insufficient stabilization of the discrete clusters, effort was put into the design of additional mantle structures. Gao and coworkers[34a] used oleate protected γ-Fe_2O_3 nanocrystals and coated them with a thin (2 nm) film of crosslinked polystyrene via an emulsion polymerization approach.[35] 1,4-vinylbenzene chloride was copolymerized to allow the immobilization of 1-methylimidazole, which formed upon deprotonation N-heterocyclic carbenes (NHC). NHCs were chosen as ligands for chelating Pd because of the impressive complex stability of these compounds (Scheme 18).[36]

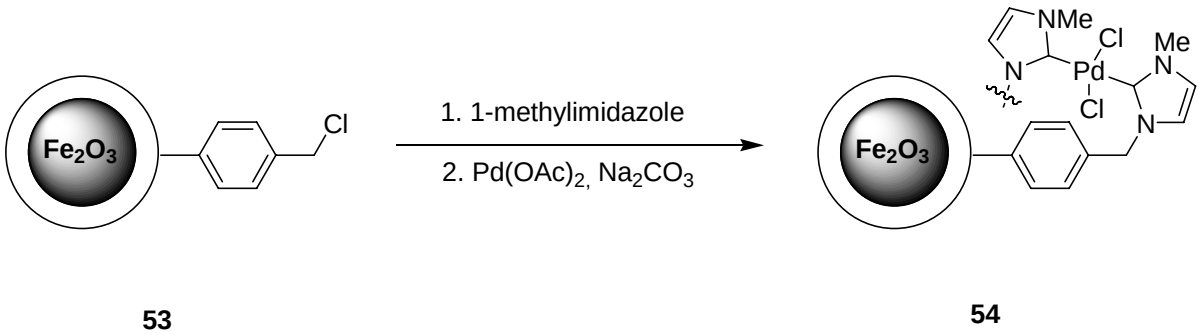

Scheme 18. Preparation of NHC-Pd complexes tagged on PS-coated SPIO-nanoparticles **53**

The catalytic power of this system was tested in a group of Suzuki cross-couplings of aryl halides with arylboronic acids.

An average yield of 82% was obtained for 20 reactions. Thus, SPIO-supported Pd catalyst **54** showed better catalytic activity than chloromethyl polystyrene resin-supported counterparts reported in the literature.[37] Finally, maghemite-supported Pd catalyst **54** was subjected to five iterative reactions between *p*-iodotoluene **55** and phenylboronic acid **56**. A yield of 88 ± 3% was obtained each time (Scheme 19).

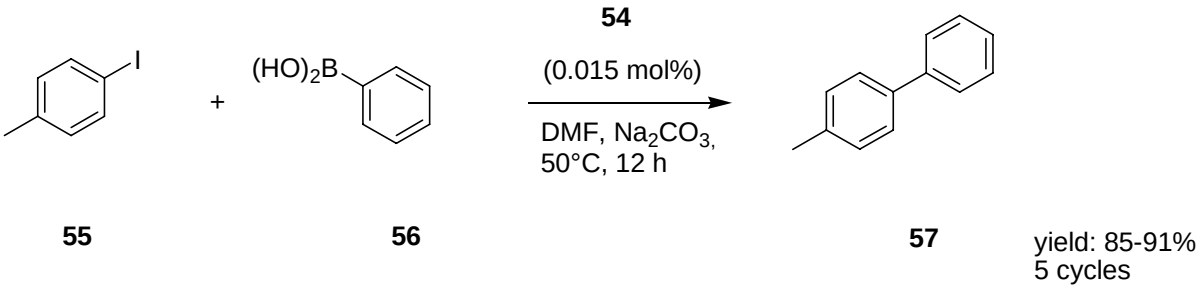

Scheme 19. Suzuki cross-couplings 4-iodotoluene **55** with phenylboronic acid **56** catalyzed by SPIO-immobilized NHC-Pd **54**.

2.2 Dopamine stabilized ferrite nanoparticles

Enediol-ligands such as catechols are known to have a high affinity to under-coordinated surface sites of metal oxide nanoparticles.[38] Therefore, dopamine has gathered attention, possessing an additional amine moiety which allows either immobilization of metal centers or further covalent modification.[39] Manorama and coworkers[40] reported several examples of Palladium(0) doped ferrite particles ($NiFe_2O_4$ and Fe_3O_4 respectively). The dopamine (DOPA) layer was formed by refluxing or sonicating the ferrites together with the catecholamine in water.

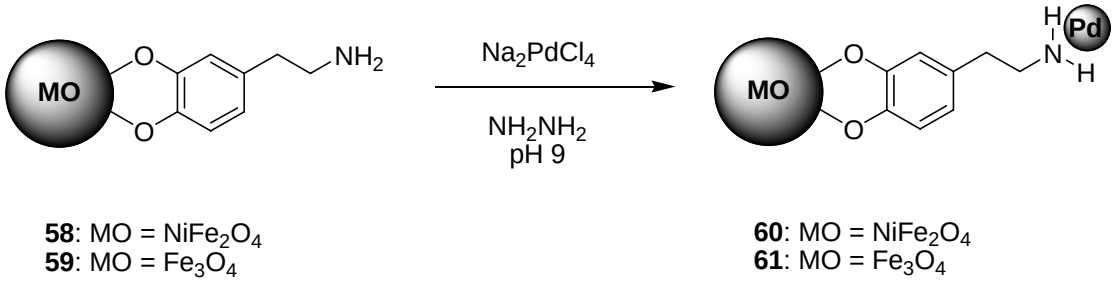

58: MO = $NiFe_2O_4$
59: MO = Fe_3O_4

60: MO = $NiFe_2O_4$
61: MO = Fe_3O_4

Scheme 20. Synthesis of ferrit-dopamine nanocomposite doped with Pd(0).

Once a palladium(0) source is anchored on the nanomagnets (Scheme 20), the saturation magnetization of the spinel ferrite and magnetite supported Pd-DOPA **60** and **61** respectively drops to 43 and 57 emu/g. For a series of hydrogenation reactions including aromatic nitro and azide compounds to their respective amine

derivatives with catalysts **60** and **61**, an activity is observed that exceeds those of previous studies.[41] The activity of **61** is somewhat inferior due to a lower palladium loading on the surface. Even after 10 cycles, no deterioration in the catalytic efficacy of both catalysts appeared.[40c] After each cycle, the catalyst was recycled with the aid of a external magnet (Figure 9).

Figure 9. Isolation of the dispersed magnetic NPs (left) with the aid of an external magnet (right) from the reaction mixture.[40c]

In addition, the spinel supported catalyst **60** was applied for Suzuki and Heck coupling reactions of aromatic halide derivatives (Scheme 21).

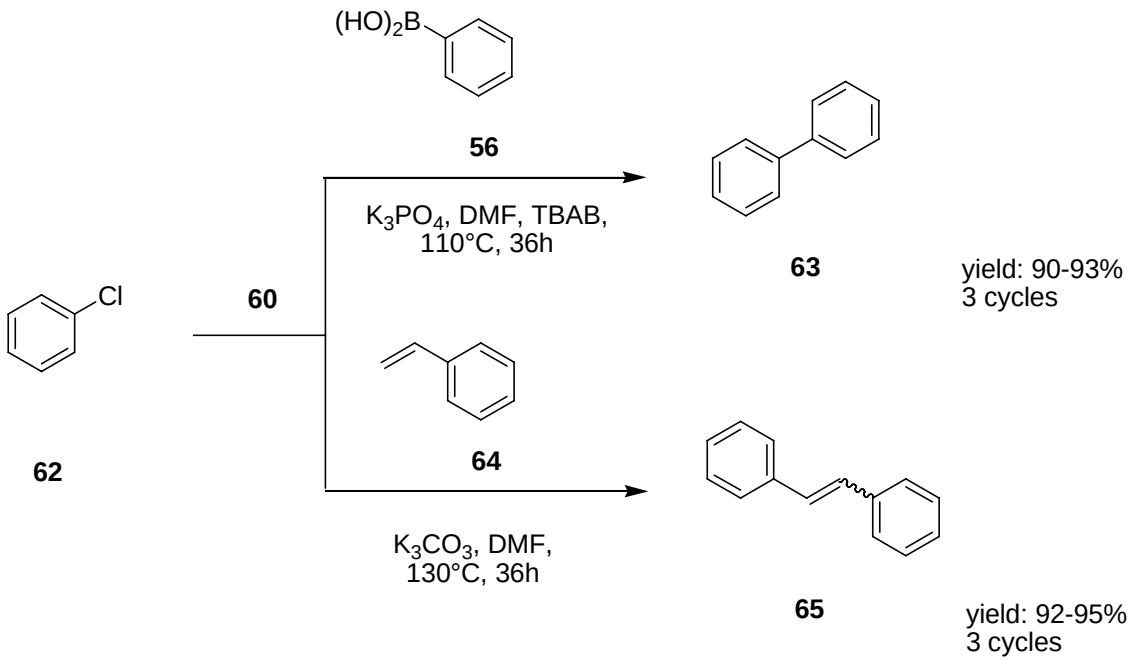

Scheme 21. Typical Suzuki (top) and Heck (bottom) coupling reactions of chlorobenzene (**62**) with phenylboronic acid (**56**) and styrene (**64**) respectively catalyzed by $NiFe_2O_4$-DOPA-Pd **60**.

Catecholamines can act as cornerstone for more complex molecular architecture on iron oxide nanoparticles which allows the tuning of solubility and enables complex formation at once. Gao et al.[42] reported on maghemite (γ-Fe_2O_3) protected with a shell of Simanek-type[43] (melamine) dendrons footing on a dopamine linker. Different generations of Simanek-type building blocks were modified with dopamine, which enables these dendritic branches to undergo a place-exchange reaction with oleate-surfactants.[44] Up to three dendron generations were anchored on a maghemite core in this way. Triphenylphospine moieties on the termini of generation-one dendrons could be used to allow the formation of Pd-complexes on the surface of the dendrimer-like core/shell-structure (Scheme 22). The as-prepared dendron coated iron oxide NPs were able to promote a Suzuki cross-coupling reaction of several arylhalides and phenylborate **56** at a catalyst concentration of 5 mol% under conditions comparable to those depicted in Scheme 21. In addition, **69** was found to maintain its activity upon recycling.

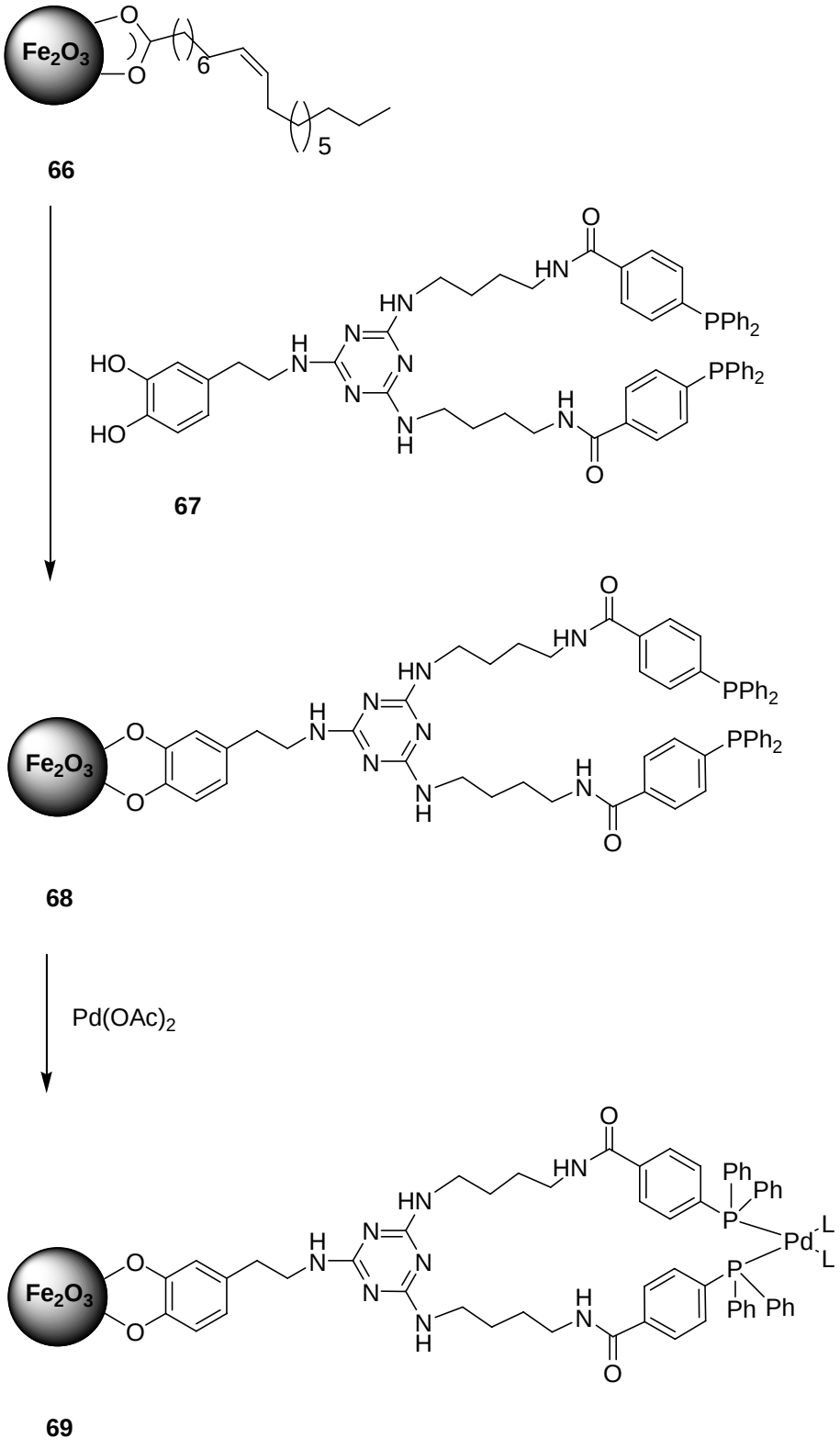

Scheme 22. Representative diagram for the synthesis of γ-Fe_2O_3 nanoparticles protected by first generation Simanek-type dendrons possessing Pd-triphenylphosphine moieties.

2.3 Silica coated iron oxide nanoparticles

Apart from enediol-ligands, silanes are frequently used to coat ferrites.[45] The deposition and adhesion of silica can be achieved via the hydrolysis of a sol-gel precursor to give shells with a thickness between 2 and 100 nm. Because of the strong affinity of iron oxide surfaces toward silica, no primer is required. An advantage of the silica coating is that this surface is terminated by silanol groups which can react with various coupling agents to covalently attach linkers, ligands, metals or complexes. Nanocomposites of this kind were extensively used for palladium catalyzed cross-coupling reactions.

Schüth and coworkers[46] disclosed the prospectives of magnetically separable mesoporous silica, however, Ying et al.[47] reported on SiO_2-coated maghemite nanoparticles that functioned as catalyst support. In a straight-forward synthesis, maghemite@silica **70** was refluxed with either (3-mercaptopropyl)-trimethoxysilane (MPS) or *N*-(2-aminoethyl)-3-aminopropyltrimethoxysilane (AAPS) in toluene for 30h to yield **71** and **73** respectively.[48]

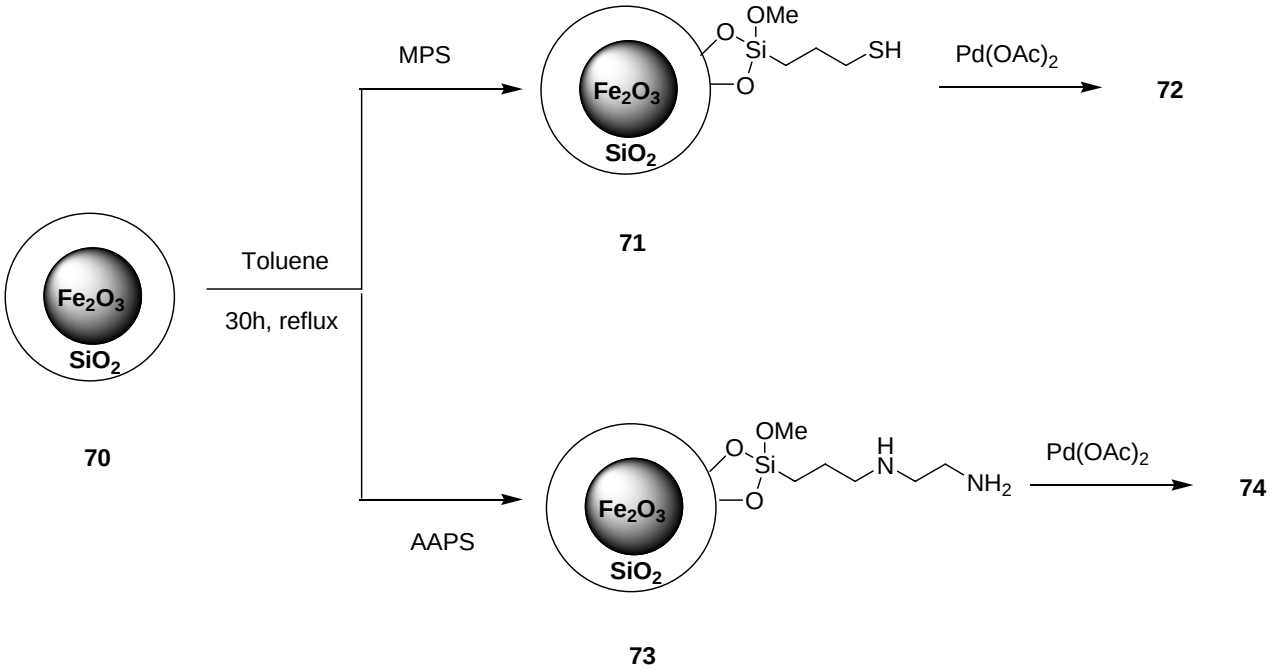

Scheme 23. Synthesis of thiol- (top) and amine- (bottom) functionalized silica coated maghemite nanoparticles.

Next, palladium nanoclusters were deposited on the surface of the affinity ligand functionalized Fe_2O_3@SiO_2-particles **71** and **73** in toluene under microwave irradiation (Scheme 23). Both Fe_2O_3@SiO_2@Pd-nanocomposites were examined as

catalysts for the hydrogenation of nitrobenzene to aniline. Both, Fe_2O_3@SiO_2-NH_2@Pd **72** and Fe_2O_3@SiO_2-SH@Pd **74** gave 99% conversion over 6 and 5 consecutive runs respectively. Their conversions then decreased gradually in subsequent runs to 87% and 76% respectively at run 14. The drawback in conversion after multiple catalyst recycling was rationalized with agglomeration of the Pd clusters, especially in the case of Fe_2O_3@SiO_2-SH@Pd **72**. TEM photographs taken before and after 14 runs affirmed this hypothesis (Figure 10).

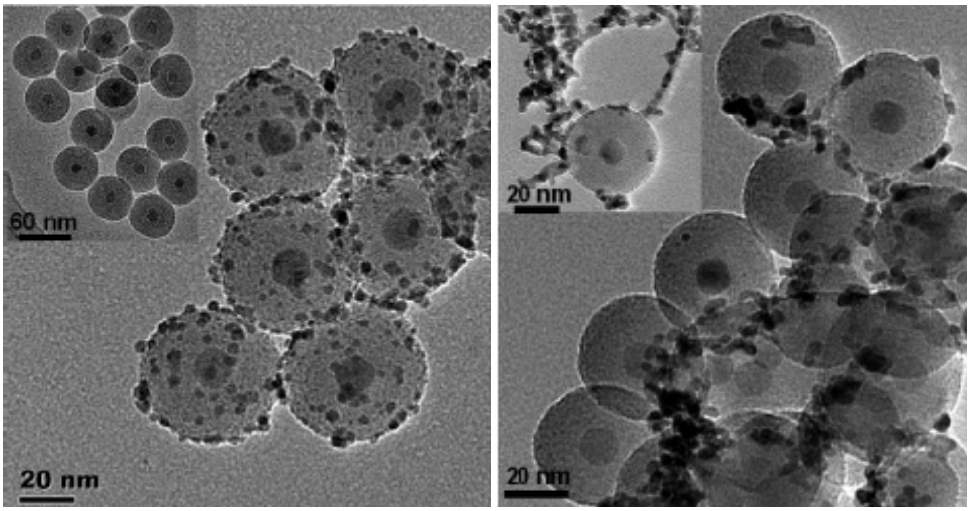

Figure 10. TEM photographs of Fe_2O_3@SiO_2-SH@Pd **72** taken before (left) the first and after the 14th run (right) of nitrobenzene hydrogenation. The inset in the right picture shows that Pd nanoclusters interconnected and some of them became detached from the support.[47]

The dependency of catalytic activity is known to relate with Pd cluster size and shape.[49] The authors concluded that AAPS might serve as a stronger affinity ligand than MPS, thus suppressing the aggregation of palladium.

Gao et al. broadened the scope of their protocol for the immobilization of Pd-NHC-complexes on PS-coated maghemite nanocrystals **54**[34a] to silica coated maghemite (Scheme 24).[34b]

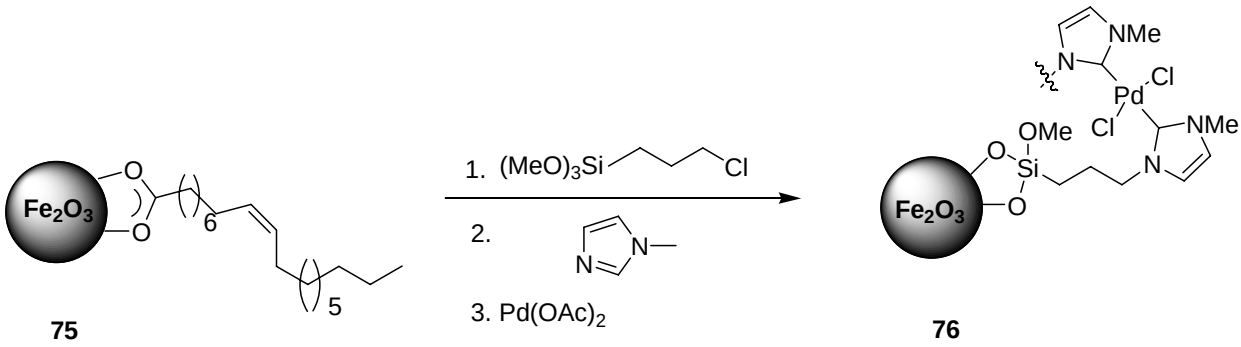

Scheme 24. Synthesis of NHC-Pd complex tagged on silica-coated maghemite-nanoparticle via place-exchange reaction with oleate stabilized iron oxide nanocrystals **75**.

Like its parent, the Fe_2O_3@SiO_2-NHC-Pd complex **76** shows high levels of efficacy and recyclability in the Suzuki cross-couping reaction. Furthermore, the authors demonstrated the catalyst applicability in Heck and Sonogashira cross-couplings (Scheme 25).

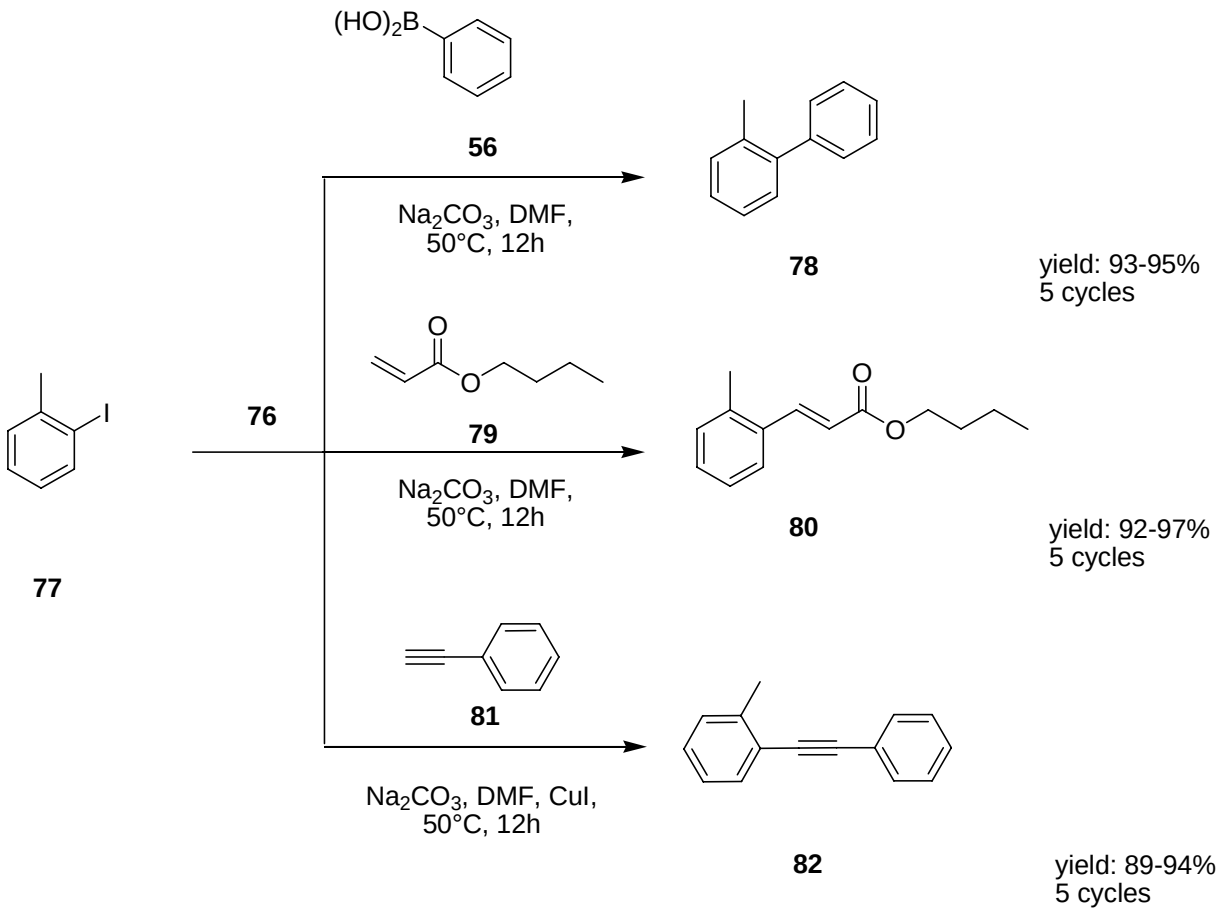

Scheme 25. Repeated use of recovered Fe_2O_3@SiO_2-NHC-Pd **76** for catalyzing Suzuki (top), Heck (middle) and Sonogashira (bottom) cross-coupling reactions respectively.

In addition, an interesting application of the nanosized NHC-Pd catalyst **76** was presented by the same group.[34c] They took advantage of the ability of the nanomagnet **76** to enter the polystyrene backbone (1% divinylbenzene-crosslinked polystyrene) of a solid-phase supported arylhalogenide. The two supports may be considered orthogonal due to the different separation procedure. Together with arylboronic acid in the solvent-phase, this system enables a three-phase Suzuki cross-coupling reaction (Scheme 26). The Pd catalyst was recovered from the reaction mixture with the aid of an external magnet. Subsequently, a filtration process was followed to remove the excess of dissolved borate reagent from the resin/product. Finally, the cross-coupling product was cleaved from the polymer by basic hydrolysis.

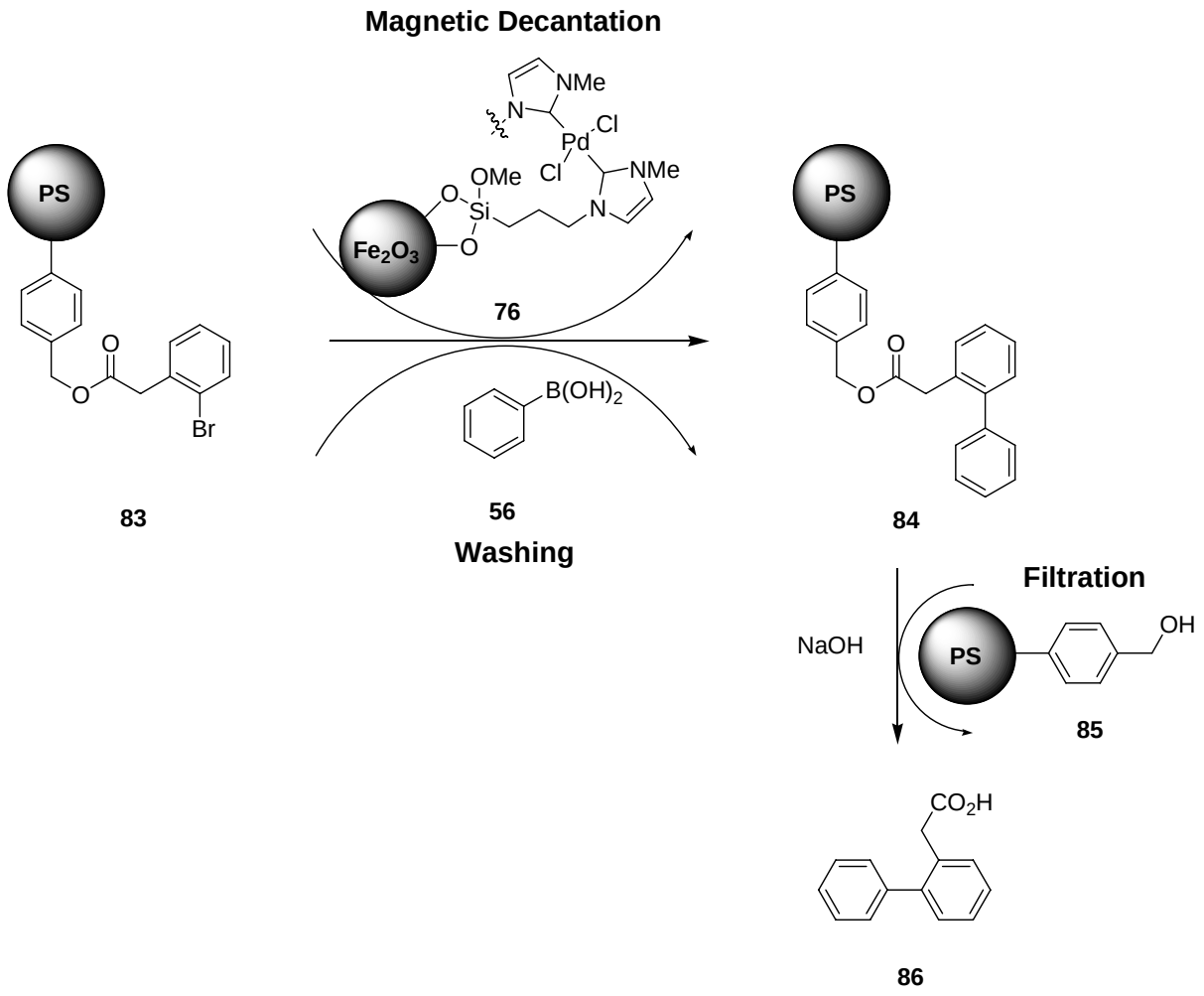

Scheme 26. Representation of a magnetic nanoparticle facilitated solid-phase Suzuki cross-coupling reaction.

The ability of nanoparticles to penetrate the pores of certain polymers has inspired their use in polymer synthesis. In general, the purification of polymers can be challenging already with a homogeneous catalyst since separation through copious washing is tedious. Therefore, a catalyst support being small enough to pass the polymer coils unhampered is a prerequisite for efficient recycling. Moreover, a support which can be attracted by an external magnetic field might be apt to reduce the amount of solvent necessary for complete removal of catalyst. Following this line of argument, Shen and coworkers[50] developed a magnetite anchored atom transfer radical polymerization (ATRP)[51] catalyst with an average diameter of 25 nm (Figure 11).

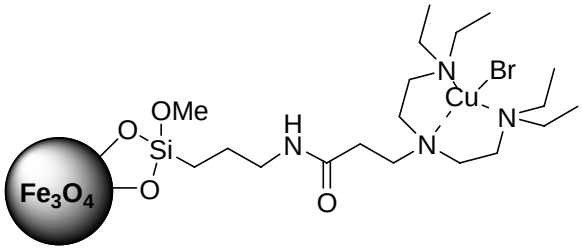

87

Figure 11. A tetraethyl-diethylenetriamine-copper(I)-complex for the polymerization of methyl methacrylate (MMA) supported on magnetite via a silane agent.

Catalyst **87** mediated the polymerization of methyl methacrylate (MMA) in a manner similar to homogeneous catalysts, thus being in contrast to catalysts immobilized on comparatively “large” particles, whose resulting polymers had uncontrolled molecular weights and high polydispersity. After recycling, **87** showed slightly diminished activity which further decreased after another cycle. The authors reasoned that oxidation of copper(I) might be responsible for this effect. To overcome this problem, in-situ catalyst regeneration methods were developed, e.g. triethylamine was used to reduce any Cu(II).[50b] Indeed, recycled catalyst **87** regained high activity and excellent control over polymerization after in-situ regeneration.

Connon et al. reported on an organocatalyst tethered to a Fe_3O_4@SiO_2-nanomagnet which was of unprecedented activity and recyclability.[52] They evaluated DMAP analog **88** (Figure 12) in the acetylation of 1-phenylethanol **89** by acetic anhydride where it furnished **90** in 14 iterative cycles with 94->98% conversion in each case (Scheme 27).

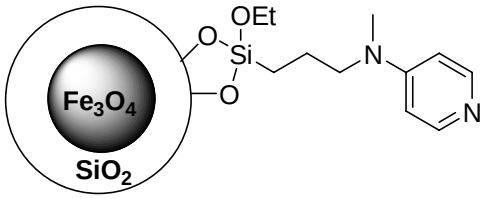

88

Figure 12. A magnetic nanoparticle supported organocatalyst: Magnetite@silica@4-*N*,*N*-dialkylaminopyridine **88**.

The recovered material was subsequently found to be even active when employed at loadings as low as 0.2 mol% (79%). The reaction scope was examined by subjecting recycled catalyst **88** to promote a range of distinct transformations where it acted as a nucleophilic catalyst. After 30 consecutive cycles, **88** (0.2 mol%) was still able to achieve an identical level of conversion (80%) in the acetylation of **89**.

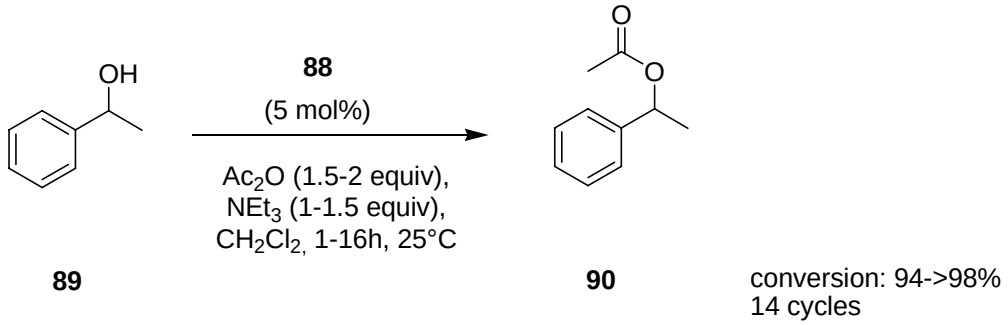

Scheme 27. 88 as a recyclable catalyst for the acetylation of 1-phenylethanol **89**.

Very recently, the “click”-reaction[33] has proved its versatility also on silica coated magnetite particles. A propargylated dipyridyl-ligand **92** was attached to 3-azidopropylsilane-capped Fe_3O_4@SiO_2 **91** under formation of a triazole moiety.[53] The corresponding Pd-complex was formed in refluxing toluene (Scheme 28).

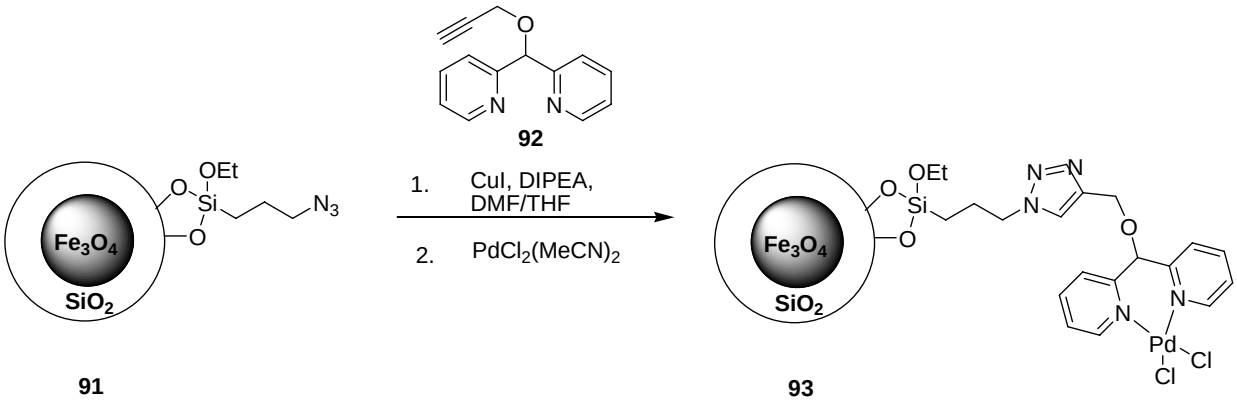

Scheme 28. Preparation of a magnetite@silica-supported di(2-pyridyl)methanol-Pd-complex **92** using a CuAAC protocol.

Catalyst **93** demonstrated its efficacy for a range of Suzuki-couplings and could be reused four times in the coupling of 4-bromoacetophenone **50** and phenylboronic acid **56** with only a slight gradual decrease in yield (95-99%).

Similar to catecholamine stabilized iron oxide nanocrystals, silica coated cores can be dendronized to make them more stable and soluble in organic solvents. Just like on dendronized Fe_2O_3@DOPA **68**, phosphonized moieties can be introduced to chelate transition metals. To this end, Post and coworkers[54] grew up to three generations of a polyaminoamido (PMAM) dendron silanized iron oxide. Interestingly, without silica coating a growth of dendrons could not be achieved. The dendrons were phosphonated by reaction of the terminal amino groups with diphenylphosphinomethanol prepared in-situ from diphenylphosphine with paraformaldehyde. Although the amount of amino groups increased with the growth of the dendrons to higher generations, the phosphorous content remained almost the same because of incomplete phosphination due to sterics. The phosphonated dendrons were complexed with $[Rh(COD)Cl]_2$ in dry and degassed toluene for 5 h at ambient temperature (Scheme 29).

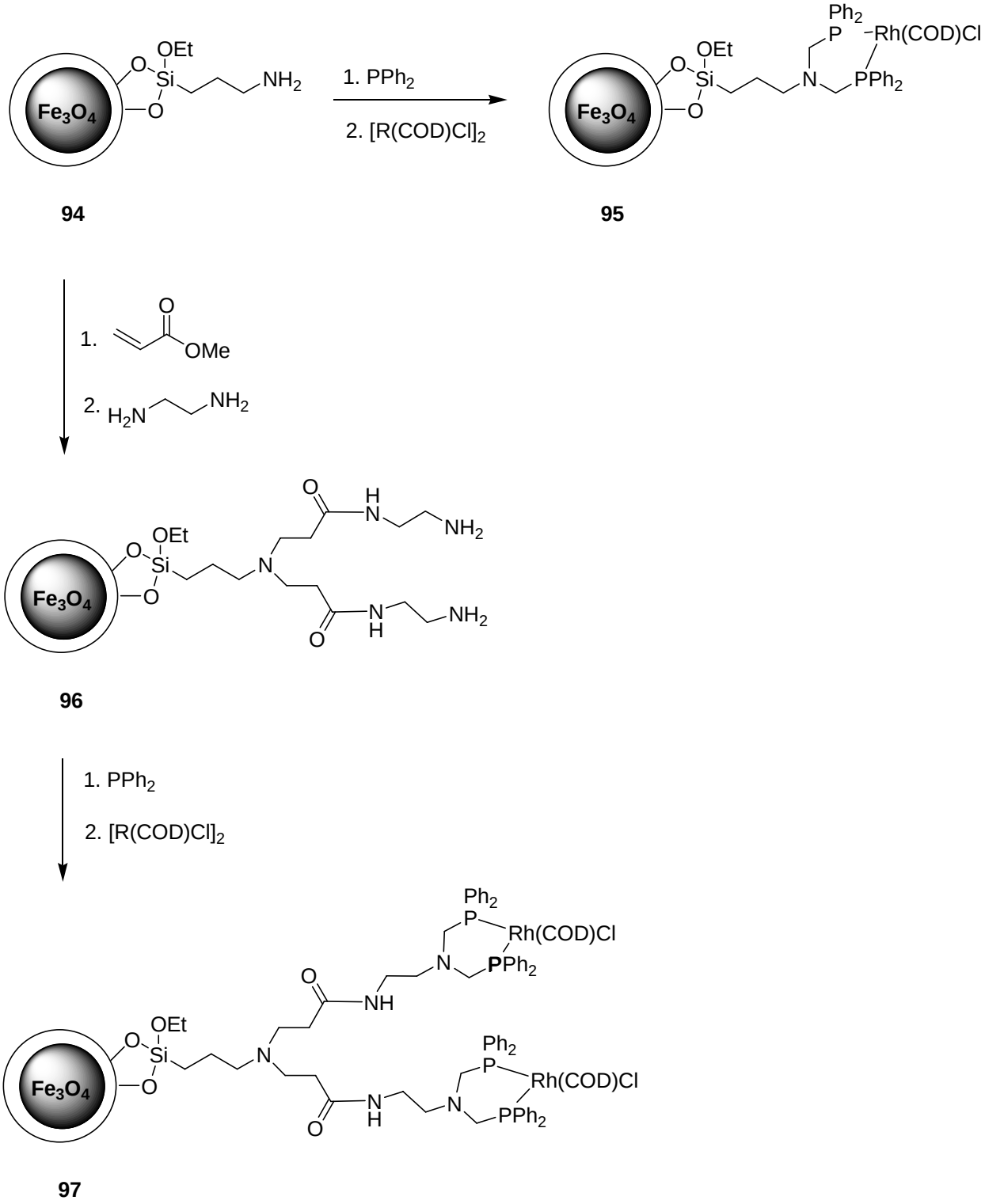

Scheme 29. Procedure for the dendronization, phosphination and complexation with $[Rh(COD)Cl]_2$ of silica coated iron oxide nanoparticles.

The resultant complexes **95** and **97** were tested in hydroformylation reactions using a 1:1 mixture of carbon monoxide and hydrogen pressurized to 1000 psi. Both, G(0) and G(1) dendrimers **95** and **97** respectively, performed well (Scheme 30). The selectivity toward the branched product was high and catalysts were more reactive and selective when compared with previous studies.[55] G(1) dendrimer based catalyst **97** was able to maintain its activity in at least five iterative runs whereas its counterpart **95** suffered from a significant decrease in the fifth cycle (69% conversion).

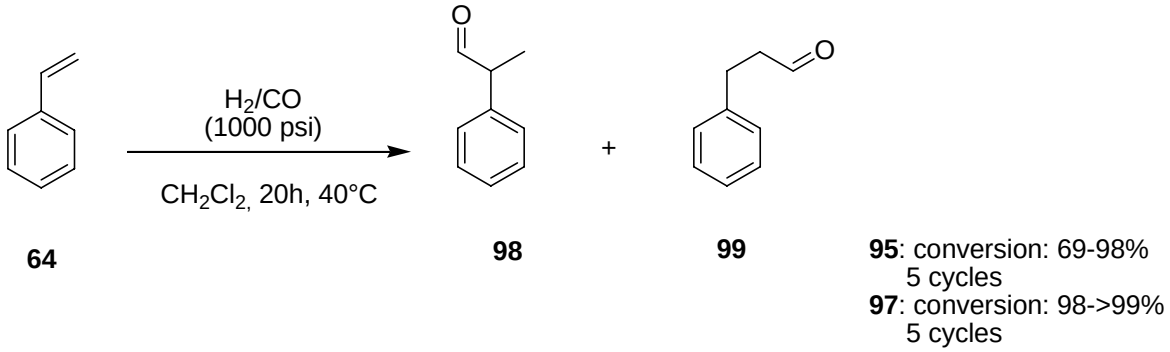

Scheme 30. Hydroformylation of sytrene (**64**) catalyzed by rhodium-complexes anchored on different generations of dendronized magnetite@silica NPs.

In contrast to previous studies,[55c] moving to higher generations does not involve loss of activity and selectivity. The present catalytic systems, engrafted on up to three dendron generations, retained its efficacy.

In conclusion, the recycling-handicap of the parent gold nanoparticles vanishes when magnetic nanoparticles are used. On the other hand, the heterogeneous character of this support increases, especially when intrinsically magnetic materials, e.g. cobalt, are used. But even superparamagnetic iron oxide nanoparticles without magnetic remanence might not be able to compete with gold clusters (typically 1-5 nm diameter) in terms of “solubility”, simply due to increased size (typically 5-20 nm). In addition, the different kinds of coating have to be considered.

In this regard, the work of Gao et al.[6] needs to be acknowledged. They designed a maghemite supported Ti-BINOLate complex **100** (Figure 13), which was envisaged to deliver results comparable to the AuNP-based catalyst **3** developed by Sasai et al.[16]

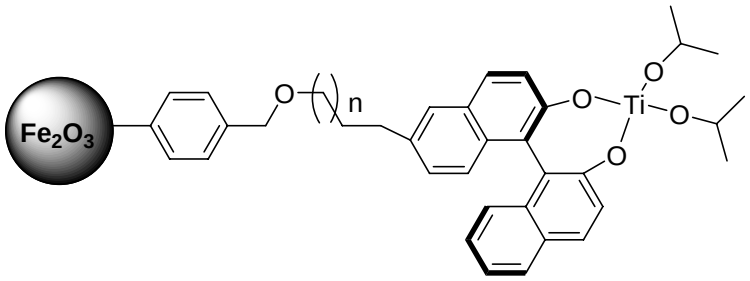

100

Figure 13. A maghemite@polymer supported Ti-BINOLate catalyst.

Under conditions silimar to those depicted in Scheme 3, moderate reaction yields (47-55%) and enantioselectivities (15-43% ee) were achieved. These values are by far lower than those obtained from unsupported Ti-BINOLate (90% yield, 84% ee)[6] or AuMPC **3** (98% yield, 86% ee).[16] Thus, the authors suggested that care has to be taken for selecting an appropriate nanoparticle matrix.

Such comparative studies are scarce. To the best knowledge of the author, no other example was reported so far. Furthermore, it should be mentioned that more than 50% of the publications highlighted in the last chapter appeared parallel to progressing research presented in this paper, thus demonstrating the current interest in this topic.

The development of a consistent protocol, that allows the efficient immobilization of different catalysts on various nanoparticles for comparative studies among each other and very same catalysts anchored on conventional supports, e.g. polymers, marks the aim of this dissertation.

3. References

1 J. Grunes, J. Zhu, G. A. Somorjai, *Chem. Commun.* **2003**, 2257.

2 Reviews: a) G. Schmid, *Chem. Rev.* **1992,** *92*, 1709; b) L. N. Lewis, *Chem. Rev.* **1993**, *93*, 2693; c) R. M. Crooks, M. Zhao, L. Sun, V. Chechik, L. K. Yeung, *Acc. Chem. Res*. **2001**, *34*, 181; d) J. Schulz, A. Roucoux, H. Patin. *Chem. Rev.* **2002**, *102*, 3757; e) M. Fernandez-Garcia, A. Martinez-Arias, J. C. Hanson, J. A. Rodriguez, *Chem. Rev.* **2004**, *104*, 4063; f) D. Astruc, F. Lu, J. R. Aranzaes, A*ngew. Chem. Int. Ed*. **2005**, *44*, 7852.

3 G. S. McCarty, P. S. Weiss, *Chem. Rev.* **1999**, *99*, 1983.

4 J. M. Thomas, W. J. Thomas, Principles and Practice of Heterogeneous Catalysis, VCH, Weinheim, **1997**.

5 Examples: a) M. Studer, H.-U. Blaser, C. Exner, *Adv. Synth. Catal.* **2003**, *345*, 45; b) S. Jansat, M. Gómez, K. Philippot, G. Müller, E. Guiu, C. Claver, S. Castillón, B. Chaudret, *J. Am. Chem. Soc.* **2004**, *126*, 1592; c) K. H. Park, Y. K. Chung, *Adv. Synth. Catal.* **2005**, *347*, 854; d) S. Jansat, D. Picurelli, K. Pelzer, K. Philippot, M. Gómez, G. Müller, P. Lecante, B. Chaudret, *New J. Chem.* **2006**, *30*, 115.

6 J. Fan, Y. Gao, *J. Exp. Nanosc*. **2006**, *1*, 457.

7 Reviews: a) C. A. McNamara, M. J. Dixon, M. Bradley, *Chem. Rev.* **2002**, *102*, 3275; b) D. E. Bergbreiter, *Chem. Rev.* **2002**, *102*, 3345; c) R. van Heerbeek, P. C .J. Kamer, P. W. N. M. van Leeuwen, J. N. H. Reek. *Chem. Rev.* **2002**, *102*, 3717; d) I. F. J. Vankelecom, *Chem. Rev*. **2002**, *102*, 3779.

8 A. R. Vaino, K. D. Janda, *J. Comb. Chem.* **2000**, *2*, 579.

9 A. Thayer, *Chem. & Eng. News* **2005**, 83, 55.

10 a) Z. Luo, Q. Zhang, Y. Oderaotoshi, D. P. Curran, *Science* **2001**, *291*, 1766; b) L. V. Dinh, J. A. Gladysz, *Chem. Comm.* **2004**, *8*, 998.

11 M.-C. Daniel, D. Astruc, *Chem. Rev.* **2004**, *104*, 293.

12 M. Zachary, V. Chechik, *Angew. Chem.* **2007**, *119*, 3368.

13 a) D. V. Leff, P. C. O'Hara, J. R. Heath, W. M. Gelbart, *J. Phys. Chem.* **1995**, *99*, 7036; b) M. J. Hostetler, S. J. Green, J. J. Stokes, R. W. Murray, *J. Am. Chem. Soc.* **1996**, *118*, 4212; c) R. S. Ingram, M. J. Hostetler, R. W. Murray, *J. Am. Chem. Soc.* **1997**, *119*, 9175; d) M. J. Hostetler, J. E. Wingate, C.-Z. Zhong, J. E. Harris, R. W. Vachet, M. R. Clark, J. D. Londono, S. J. Green, J. J. Stokes, G. D. Wignall, G. L. Glish, M. D. Porter, N. D. Evans, R. W. Murray, *Langmuir* **1998**, *14*, 17; e) A. C. Templeton, M. J. Hostetler, C. T. Kraft, R. W. Murray, *J. Am. Chem. Soc.* **1998**, *120*, 1906; f) M. J. Hostetler, A. C. Templeton, R. W. Murray, *Langmuir* **1999**, *15*, 3782; g) M. J. Hostetler, A. C. Templeton, R. W. Murray, *Langmuir* **1999**, *15*, 3782; h) A. C. Templeton, W. P. Wuelfing, R. W. Murray, *Acc. Chem. Res.* **2000**, *33*, 27; i) Y. Song, R. W. Murray, *J. Am. Chem. Soc*. **2002**, *124*, 7096; j) A. Kassam, G. Bremner, B. Clark, G. Ulibarri, R. B. Lennox, *J. Am. Chem. Soc.* **2006**, *128*, 3476.

14 a) M. Brust, A. Walker, D. Bethell, D. J. Schiffrin, R. Whyman, *J. Chem. Soc., Chem. Commun.* **1994**, 801; b) M. Brust, J. Fink, D. Bethell, D. J. Schiffrin, C. J. Kiely, *J. Chem. Soc., Chem. Commun*. **1995**, 1655.

15 M. Bartz, J. Küther, R. Seshadri, W. Tremel, *Angew. Chem.* **1998**, *110*, 2646.

16 a) K. Marubayashi, S. Takizawa, T. Kawakusu, T. Arai, H. Sasai, *Org. Lett.* **2003**, *23*, 4409; b) S. Takizawa, M. L. Patil, K. Marubayashi, H. Sasai, *Tetrahedron* **2007**, *63*, 6512; c) D. Jayaprakash, H. Sasai, *Tetrahedron: Asymmetry* **2001**, *12*, 2589.

17 T. Belser, M. Stöhr, A. Pfaltz, *J. Am. Chem. Soc.* **2005**, *127*, 8720.

18 H. Li, Y.-Y. Luk, M. Mrksich, *Langmuir* **1999**, *15*, 4957.

19 B. S. Lee, S. K. Namgoong, S.-G. Lee, *Tetrahedron Lett.* **2005**, 46, 4501.

20 F. Ono, S. Kanemasa, J. Tanaka, *Tetrahedron. Lett.* **2005**, *46*, 7626.

21 M. J. Oila, A. M. P. Koskinen, *ARKIVOK* **2006**, 76.

22 a) J. Rockenberger, J. Scher, A.P. Alivisatos, *J. Am. Chem. Soc.* **1999**, *121*, 11595; b) T. Hyeon, S. S. Lee, J. Park, Y. Chung, H. B. Na, *J. Am. Chem. Soc*. **2001**, *123*, 12789; c) S. Sun, H. Zeng, *J. Am. Chem. Soc.* **2002**, *124*, 8204; d) T. Hyeon. *Chem. Commun.* **2003**, 927; e) Y. Lee, J. Lee, C. J. Bae, J.-G. Park, H.-J. Noh, J.-H. Park, T. Hyeon, *Adv. Funct. Mater*. **2005**, *15*, 503.

23 J. Jin, T. Iyoda, C. Cao, Y. Song, L. Jiang, T. J. Li, D. B. Zhu, *Angew. Chem. Int. Ed.* **2001**, *40*, 2135.

24 T.-J. Yoon, W. Lee, Y.-S. Oh, J.-K. Lee, *New. J. Chem.* **2003**, *27*, 227.

25 M. H. Sousa, F. A. Tourinho, J. Depeyrot, G. J. da Silva, M. S. F. L. Lara, *J. Phys. Chem. B* **2001**, *105*, 1168.

26 a) S. C. Bourque, F. Maltais, W. J. Xiao, O. Tardif, H. Alper, P. Arya and L. E. Manzer, *J. Am. Chem. Soc.* **1999**, *121*, 3035; b) S. C. Bourque H. Alper, *J. Am. Chem. Soc.* **2000**, *122*, 956; c) J.-K. Lee, T.-J. Yoon,Y. K. Chung, *Chem. Commun.* **2001**, 1164; c) T. Malmström, H. Weigl, C. Andersson, *Organometallics* **1995**, *14*, 2593; d) K. Nozaki, Y. Itoi, F. Shibahara, E. Shirakawa, T. Ohta, H. Takaya and T. Hiyama, *J. Am. Chem. Soc.* **1998**, *120*, 4051.

27 N. Wu, L. Fu, M. Su, M. Aslam, K. C. Wong V. P. Dravid, *Nano Lett.* **2004**, *4*, 383.

28 F. Michalek, A. Lagunas, C. Jimeno, M. A. Pericàs, *J. Mater. Chem*. **2008**, *18*, 4692.

29 a) A. Hu, G. T. Yee, W. Lin, *J. Am. Chem. Soc.* **2005**, *127*, 12486; b) G. Chouhan, D. Wang, H. Alper, *Chem. Commun.* **2007**, 4809.

30 Sun, S.; Zeng, H. *J. Am. Chem. Soc.* **2002**, *124*, 8204.

31 Sahoo, Y.; Pizem, H.; Fried, T.; Golodnitsky, D.; Burstein, L.; Sukenik, C. N.; Markovich, G. *Langmuir* **2001**, *17*, 7907.

32 R. Huisgen, *Pure Appl. Chem.* **1989**, *61*, 613.

33 a) C. W. Tornøe, M. Meldal, *In American Peptide Symposium;* M. Lebl, R. A. Houghten, Eds, American Peptide Society and Kluwer Academic Publishers: San Diego, CA, **2001**, p 263; b) V. V. Rostovtsev, L. G. Green, V. V. Fokin, K. B. Sharpless, *Angew. Chem. Int. Ed*. **2002**, *41*, 2596; c) C. W. Tornøe, C. Christensen, M. Meldal, *J. Org. Chem*. **2002**, *67*, 3057.

34 a) P. D. Stevens, J. Fan, H. M. R. Gardimalla, M. Yen, Y. Gao, *Org. Lett.* **2005**, *7*, 2085; b) P. D. Stevens, G. Li, J. Fan, M. Yenb, Y. Gao, *Chem. Commun.* **2005**, 4435; c) Y. Zheng, P. D. Stevens, Y. Gao, *J. Org. Chem.* **2006**, *71*, 537.

35 J. Jang, H. Ha, *Langmuir* **2002**, *18*, 5613.

36 Review: W. A. Herrmann, *Angew. Chem., Int. Ed.* **2002**, *41*, 1290.

37 J.-W. Byun, Y.-S. Lee, *Tetrahedron Lett.* **2004**, 1837.

38 T. Rajh, L. X. Chen, K. Lukas, T. Liu, M. C. Thurnauer, D. M. Tiede, *J. Phys. Chem. B*. **2002**, *106*, 10543.

39 C. Xu, K. Xu, H. Gu, R. Zheng, H. Liu, X. Zhang, Z. Guo, B. Xu, *J. Am. Chem. Soc.* **2004**, *126*, 9938.

40 a) B. Baruwati, K. M. Reddy, S. V. Manorama, R. K. Singh, O. Parkash. *Appl. Phys. Lett.* **2004**, *85*, 2833; b) D. Guin, B. Baruwati, S. V. Manorama, *J. Mol. Catal. A, Chem.* **2005**, *242*, 26; c) D. Guin, B. Baruwati, S. V. Manorama, *Org. Lett.* **2007**, *9*, 1419; d) B. Baruwati, D. Guin. S. V. Manorama, *Org. Lett.* **2007**, *9*, 1419.

41 R. Raja, B. V. Glovko, M. J. Thomas, A. Berenguer-Murcia, W. Zhou, S. Xie, G. F. B. Johnson, *Chem. Commun*. **2005**, 2026.

42 C. Duanmu, I. Saha, Y. Zheng, B. M. Goodson, Y. Gao, *Chem. Mater.*, **2006**, *18*, 5973.

43 a) J. Lim, E. E. Simanek, *Mol. Pharm.* **2005**, *2*, 273. b) W. Zhang, E. E. Simanek, *Org. Lett.* **2000**, *2,* 843.

44 J. Park, K. An, Y. Hwang, J.-G. Park, H.-J. Noh, J.-Y. Kim, J.-H. Park, N.-M. Hwang, T. Hyeon, *Nat. Mater.* **2004**, *3*, 891.

45 a) Y. Yu, Y. Yin, B. T. Mayers, Y. Xia, Nano Lett. 2002, 2, 183; b) N. Kohler, G. E. Fryxell, M. Zhang, *J. Am. Chem. Soc.* **2004**, *126*, 7206.

46 A.-H. Lu, W. C. Li, A. Kiefer, W. Schmidt, E. Bill, G. Fink, F. Schüth, *J. Am. Chem. Soc.* **2004**, *126*, 8616.

47 D. K. Yi, S. S. Lee, J. Y. Ying, *Chem. Mater.* **2006**, *18*, 2459.

48 Kim, S. W.; Kim, M.; Lee, W. Y.; Hyeon, T. *J. Am. Chem. Soc.* **2002**, *124*, 7642.

49 Narayanan, R.; El-Sayed, M. A. *J. Phys. Chem. B* **2004**, *108*, 8572.

50 a) S. Ding, Y. Xing, M. Radosz, Y. Shen, *Macromolecules* **2006**, *39*, 6399; b) Tang, H.; Radosz, M.; Shen, Y. *Macromol. Rapid Commun.* **2006**, *27*, 1127.

51 a) M. Kato, M. Kamigaito, M. Sawamoto, T. Higashimura, *Macromolecules* **1995**, *28*, 1721; b) J. S. Wang, K. Matyjaszewski, *J. Am. Chem. Soc.* **1995**,*117*, 5614.

52 C. A. Dalaigh, S. A. Corr, Y. Gun`ko S. J. Connon, *Angew. Chem.* **2007**, *119*, 4407.

53 G. Lu, W. Mai, R. Jin, L. Gao, *Synlett* **2008**, *9*, 1418.

54 R. Abu-Reziq, H. Alper, D. Wang, M. L. Post, *J. Am. Chem. Soc*. **2006**, *128*, 5279.

55 a) S. M. Lu, H. Alper, *J. Am. Chem. Soc*. **2003**, *125*, 13126; b) P. Arya, G. Panda, N. V. Rao, H. Alper, S. C. Bourque, L. E. Manzer, *J. Am. Chem. Soc.* **2001**, *123*, 2889; c) S. C. Bourque, H. Alper, L. E. Manzer, P. Arya, *J. Am. Chem. Soc.* **2000**, *122*, 956.

B. Main Part

I. Catalysts immobilized on Monolayer-protected gold clusters

The concept of immobilizing a transition-metal complex on a self-assembled monolayer (SAM) of alkanethiolates on gold colloids was first reported in 1998 by Tremel et al. using a simple ruthenium catalyst.[1] In the following years, this account gained a lot of attention and was employed by many groups using different catalysts.[2] The immobilized catalysts proved to have activities and selectivities comparable to their homogeneous counterparts, a fact which was attributed to the excellent dispersibility of the thiol-protected gold particles. In addition, the accessibility of the catalysts on the surface of the particles was assumed to be superior to those on conventional supports, e.g. polymers. Recycling of the nanocomposite was usually accomplished by precipitation from the appropriate solvent, which depends on the nature of the coating and the catalyst.

However, grafting strategies are very straightforward but scarce. All foot on a rather simple place-exchange reaction of surface bound thiolates against functionalized thiols in solution. The ligands or complexes have to be tethered to a thiol in all established anchoring strategies. Thus, the development of an additional, generally applicable method for the efficient tagging of gold colloids with transition-metal complexes seems worthwhile, since incompatibilities between the (pre-)catalyst and the thiol tail might necessitate tedious protecting group chemistry. In extreme examples, the strong dependence on thiol linkers might rule out grafting of certain catalysts on AuMPCs. Azabis(oxazolines) will serve as prototypes for such a novel immobilization strategy that does not rely on a thiol linker.

1. A short history of gold colloids

Although the use of gold colloids, e.g. in ruby glass (Figure 14), dates back to Roman times,[3] their scientific exploration began in the middle of the nineteenth century.

Figure 14. Lycurgus cup at the British Museum in London, 5th to 4th century B.C. Gold colloids in the glass appear ruby red in transmitted light (right) and green in reflected light (left). (Images: British Museum)

In 1857, Michael Faraday reported in his groundbreaking research on “diffused gold”, obtained by the reduction of an aqueous solution of sodium tetrachloroaureate with white phosphorous in carbon disulfide.[4] He described qualitatively the reversible colour change of thin films, prepared from dried colloidal solutions, upon mechanical compression. Nowadays, the term “nanoparticle” has replaced its antecessor “colloid” in large part. Nevertheless, both mean a particle that consists of an assembly of atoms in the size range between 1 and usually not more than 50 nm.[5] Apart from that, the formation of gold nanoparticles is no longer restricted to chemical processes. Physical methods, e.g. the controlled condensation of gold atoms from the gas phase, known as metal-vapor synthesis,[6] have been developed but are still less predominant. However, it should be mentioned that gram-scale syntheses of thiol stabilized gold nanoparticles have been reported, e.g. based on the so-called solvated metal atom dispersion technique (SMAD).[7] Briefly, the Au-atoms are frozen at 77 K in acetone vapour and subsequently allowed to warm up to give gold colloids protected by acetone. Further stabilization was achieved by coating these clusters with dodecanethiol. Whereas the interest in gold colloids as colorants and pharmaceuticals has vanished, their current impact in science and technology is mostly due to the quantum size effect of mater.

2. Synthesis of monolayer-protected gold clusters

2.1 Reductants and stabilizers

In the past decades, the preparation of gold colloids was subject of a dramatically increased number of publications, which contributed to the new “gold rush” in catalysis.[8] In both, physical and chemical routes, it remains an important aspect to avoid coalescence between the distinct gold nanoparticles. Most relevant wet-chemical procedures still rely on Faraday’s route based on the reduction of Au^{III} in a two-phase system, although more convenient reducing agents have been established. In an elegant procedure introduced 1951 by Turkevitch et al.,[9] sodium citrate was used as reducing agent while citrate itself and its oxidation products could act as protecting ligands on the forming metal shell if no other stabiliser was used.[10] The size of the AuNPs could be influenced by the choice of the ratio between gold and the reducing/stabilizing agent as demonstrated later on by Frien et al.[11]

More powerful ligands, for instance phosphines, water soluble phosphanes (e.g. $P(C_6H_4SO_3Na)_3$) and thiols, allow the isolation of gold nanoparticles as a solid that can be redispersed in appropriate solvents. In general, the complete removal of the solvent makes the AuNPs loose their ability to form a colloidal solution due to the aforementioned tendency of the particles to agglomerate.

Schmidt’s cluster $[Au_{55}(PPh_3)_{12}Cl_6]$ attained popularity for its low size dispersion (1.4 ± 0.4 nm) despite its rather inconvenient synthesis by reduction of PPh_3AuCl using gaseous B_2H_6.[12] Both, phosphines and phosphanes can be usually substituted by thiols, hence it is an accepted assumption that thiolates bind more strongly to gold.[5]

AuNPs stabilized with alkanethiolates were first reported in 1993 by Mulvaney,[13] however, the most popular method for the preparation of thiol-capped gold nanoparticles came from the Schiffrin laboratories in 1994.

2.2 The Brust-Schiffrin method

Brust et al.[14] reported on the facile synthesis of air-stable AuNPs of reduced dispersity and controlled size. Particles thus obtained could be handled like simple chemical compounds. They allowed the repeated isolation from and redispersion in common organic solvents, especially apolar ones, without any sign of flocculation. This strategy combined Faraday`s two-phase approach with more recent techniques

of ion extraction and monolayer self-assembly of alkanethiols.[15] The growing of the metallic clusters succeeded simultaneously with the self-assembly of thiols on the surface of the nuclei. Therefore, it turned out to be necessary that surface passivation and the growing of the cluster take place in the same phase.

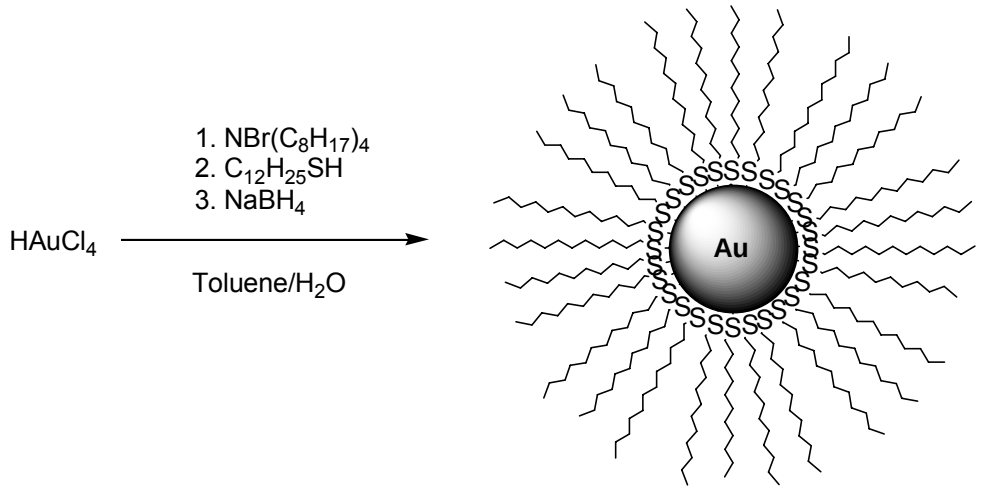

101

Scheme 31. Synthesis of monolayer-protected gold clusters by reduction of tetrachloroaureate with sodium borohydride in the presence of dodecanethiol according to Brust et al.[14]

In the first step, an excess of tetraoctylammonium bromide was used to transfer $AuCl_4$- from the aqueous into the toluene layer. The organic layer was separated from the aqueous one and treated with a freshly prepared aqueous $NaBH_4$-solution in the presence of dodecanethiol under vigorous stirring. The overall reaction taking place is summarized in equations (1) and (2), where BH_4^- is the source of electrons.

$$AuCl_4^-(aq) + N(C_8H_{17})_4^+ (C_6H_5Me) \rightarrow N(C_8H_{17})_4^+ AuCl_4^-(C_6H_5Me) \quad (1)$$

$$m AuCl_4^-(C_6H_5Me) + n C_{12}H_{25}SH(C_6H_5Me) + 3m\ e^- \rightarrow 4m\ Cl^-(aq) + [Au_m(C_{12}H_{25}SH)_n](C_6H_5Me) \quad (2)$$

High resolution TEM images revealed, that the diameters of the AuNPs obtained under these conditions were in a range between 1 and 3 nm with a maximum in the particle size distribution at 2.0-2.5 nm. The geometry of these particles, sometimes referred to as monolayer-protected clusters (MPCs), was found to show a

preponderance of cuboctahedral and icosahedral structures. In the following years, many publications reported on the successful use of the Schiffrin reaction and it was extensively investigated in how far size and size distribution of the clusters correlate to diverse reaction conditions.[16,17] It was concluded that larger thiol/gold mole ratios gave smaller average core sizes and fast borohydride addition as well as cooled solutions produced smaller, more monodisperse particles. This was attributed to the slowed growth of the metal cores relative to core passivation.

For instance, a cooled (0°C) reaction mixture with a $C_{12}H_{25}SH$/Au mole ratio of 2 resulted in an average cluster containing 106 Au atoms (~2 nm diameter), if the reductant was added within 10 s. On the other hand, at room temperature and with a $C_{12}H_{25}SH$/Au-ratio of 1/12, an average Au_{4794}-cluster with a diameter of approximately 5.2 nm was formed.[16d] In addition, a higher abundance of small core sizes (< 2 nm) was obtained by quenching the reaction immediately after the addition of borohydride.[17b,c]

In general, smaller MPCs are more stable due to slightly more polarized Au-S-bonds.[16b] However, having in mind that the gold nanoparticles are expected to serve as recyclable support for homogenous catalysts, it is not suggestive to decrease the cluster size below a certain level. Recycling via precipitation would be less feasible for such particles because they are also partly soluble in polar solvents, thus inevitably causing loss of substance during recovery.

Therefore, MPCs with an average diameter of 2 nm were synthesized according to a minute protocol developed by Murray et al.[16d] Briefly, a thiol/gold-ratio of 2 was adjusted before $NaBH_4$ was added to the solution at 0°C within 15 min. The number of Au atoms in an average cluster was assigned to be 225 and the number of alkanethiolates on the surface was assessed with 90.[16c] The clusters thus prepared were known to show a typical core size dispersity of ± 20%. However, because the clusters prefer certain “magic numbers” (closed shell structures), this rather small dispersity represented a large variation in the number of Au atoms per individual cluster.[16g]

The as-prepared particles were analyzed by transmission electron micrography (Figure 15).

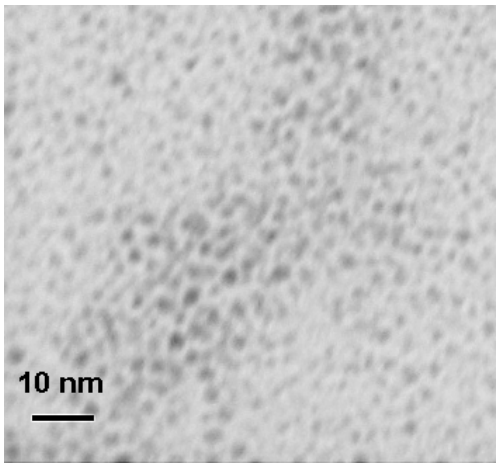

Figure 15. Transmission electron micrography of dodecanethiol coated gold nanoparticles with an average cluster diameter of 2 nm (recorded at the University of Regensburg).

It is well-known that some tetraoctylammonium cations remain as minor impurities in the alkanethiol shells of the particles. This residual phase-transfer agent was removed via Soxhlet extraction.[18]

The Schiffrin reaction is not limited to the use of simple alkanethiols. The use of *p*-mercaptophenol in a single-phase system shall be quoted in lieu of many others.[14b]

3. Functionalization of monolayer-protected gold clusters via a place-exchange reaction

Many different strategies for the modification of alkanethiolate stabilized AuNPs with simple chemical compounds were published.[16h] Comparatively few utilize functionalized thiols already during the synthesis of the MPCs, which is not surprising having the harsh reductive conditions in mind. Nevertheless, the pioneering work of Sasai et al.[2b] has to be mentioned in this regard. They subjected disulfides bearing (*R*)-1,1´-bi-2-naphthol ((*R*)-BINOL) moieties at each terminal position to the Schiffrin reaction. However, the vast majority takes advantage of a significant feature of self-assembled thiol monolayers on gold surfaces, the “place-exchange” of thiolate ligands in the shell by thiols in solution[19] (Scheme 32).

3.1 Theoretical considerations concerning place-exchange reactions

The place-exchange reaction of thiolates on 3D-surfaces, such as AuNPs, has been extensively studied.[16,20] In general, the tendency of thiolates ligating gold clusters to exchange with thiols in the supernatant is higher than on 2D-surfaces. Whereas terrace sites are the predominant motif on a flat Au(111) surface, the core surfaces of nanoclusters[21] contain a large fraction of classically defined defect sites. The different surface sites exhibited a substantial gradation in reactivity. Thiolates on vertexes and edges were significantly easier to exchange than the ones on the interior terrace sites.[16f] Evidence was found for both, associative[16f,22] (S_N2-like) and dissociative (S_N1-like)[20a,23] pathways as the rate determining step. Reaction kinetics were represented satisfactorily in a pseudo-first-order process.[20a] In an associative pathway, the thiol enters the monolayer, protonates and substitutes a bound thiolate ligand. This process does not alter the core dimensions. The rate of place-exchange decreases with an increase in the size of the entering ligand and the chain length of the protecting monolayer.[16f]

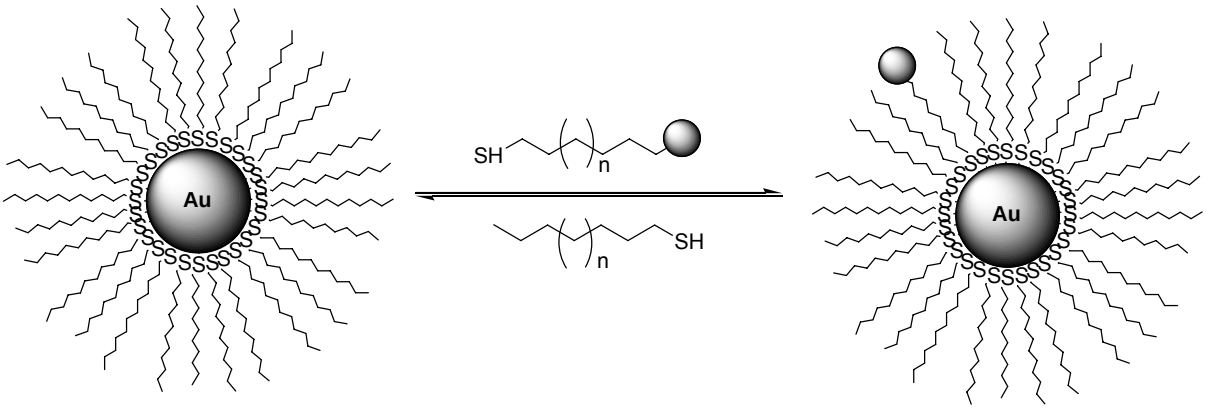

Scheme 32. General scheme for the place-exchange reaction between MPCs of the Brust type and functionalized thiols.

Other factors have to be considered, too. The extent of exchange is substantially enhanced by the presence of base and depressed by the presence of acid, hence it was rationalized that thiolates undergo the place-exchange reaction more rapidly than thiols. It should be mentioned that disulfides do not replace any bound thiolates. For the choice of the solvent, the solubility of the cluster has to be taken into account. Therefore, the less polar solvents in which the AuNPs are most rapidly “dissolved” showed also the largest extent of exchange. Suitable solvents are, e.g. toluene,

CH_2Cl_2 and THF. More polar, hydrogen bonding solvents such as methanol are unfavourable.[20a]

3.2 Practical considerations concerning place-exchange reactions

The place-exchange reaction is for sure the most straight-forward route for the functionalization of MPCs of the Brust-type with complex molecules. However, as a process driven by the force to equilibrate ligated thiolates and unbound thiols, a rather high concentration of functionalized thiols is necessary to obtain reasonable loadings. Functionalized thiols, which were not exchanged, are usually discarded after the equilibration process. In addition, the free thiol moieties might have incompatibilities with functional groups of more complex molecules. Thiol protected gold nanoparticles do usually not cause such incompatibilities because the gold core acts as some kind of “protecting-group” for the thiols.

Due to these limitations, many studies foot on the introduction of rather simple thiol building blocks, e.g. a ω-halogen-alkanethiol, on which more sophisticated chemistry can take place (Scheme 33). However, these chemistries are not always compatible with the desired applications, so that the development of an additional, general route toward nanoparticle functionalization still seems worthwhile.

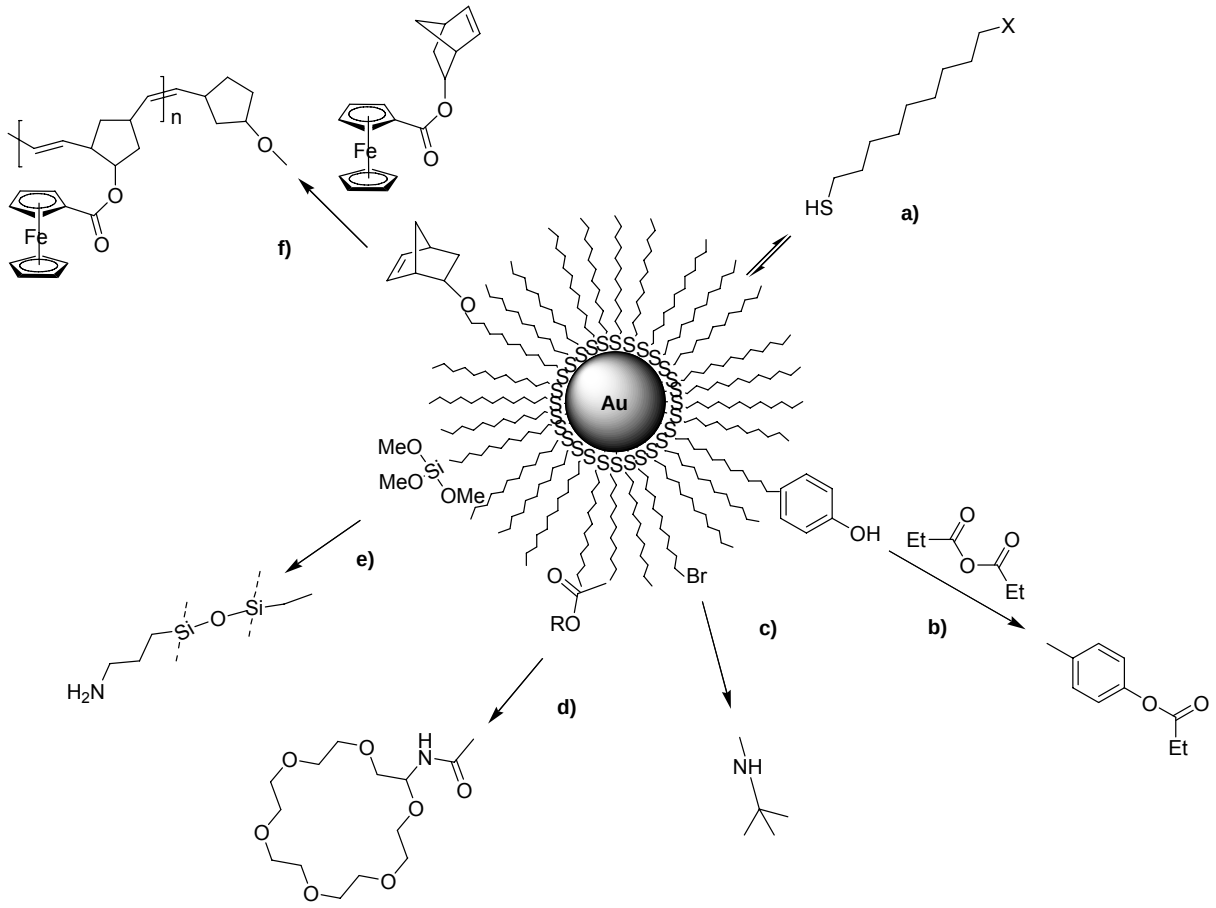

Scheme 33. Functionalization of MPCs of the Brust-type via a) a place-exchange reaction,[16] b) reaction of *p*-mercaptophenol with propionic anhydride,[14b] c) S_N2 reaction of ω-bromoalkanethiolated MPCs with primary alkylamines,[16e] d) amide and ester coupling reactions,[24a] e) siloxane formation reactions,[16g] and f) transition-metal-catalyzed ring-opening metathesis polymerization (ROMP).[24b]

Nevertheless, as an example for the successful grafting of a thiol-modified transition-metal-complex via direct place-exchange reaction on a MPC the work of Pfaltz[2c] shall be acknowledged. Preliminary investigations towards the immobilization of azabis(oxazolines) on monolayer-protected gold nanoparticles were inspired by this approach.

4. Immobilization of azabis(oxazolines) on monolayer-protected gold clusters

4.1 Classification and synthesis of azabis(oxazoline)-ligands

Azabis(oxazolines)[25] **103** (AzaBOX) can be seen as structural hybrids between bis(oxazolines) **102** and aza-semicorrines **104**.[26,27]

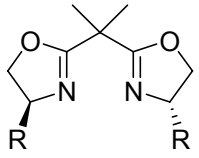

102a: R = ^{i}Pr
102b: R = ^{t}Bu
ent-102c: R = Ph

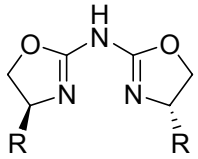

103a: R = ^{i}Pr
103b: R = ^{t}Bu
ent-103c: R = Ph
103d: R = Bn

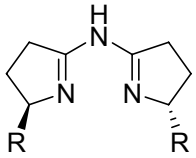

104a: R = ^{i}Pr
104b: R = ^{t}Bu
ent-104c: R = Ph

Figure 16. Different C_2-symmetric ligands.

They combine the advantage of being accessible from the chiral pool like the bis(oxazolines) and the structural variability of aza-semicorrins due to the possibility of functionalizing the central nitrogen bridge. In a concise route developed by H. Werner,[25b] chiral aminoalcohols, readily available from the corresponding amino acids by reduction with sodium borohydride in the presence of iodine, are transformed into the aminooxazolines **108** using in-situ created bromocyanide.[25] These compounds were found to react under acidic conditions with ethoxyoxazolines **107**,[28] accessible via selective alkylation of oxazolidinones **106**, to give rise to the desired azabis(oxazolines) **109** under cleavage of ethanol (Scheme 34).

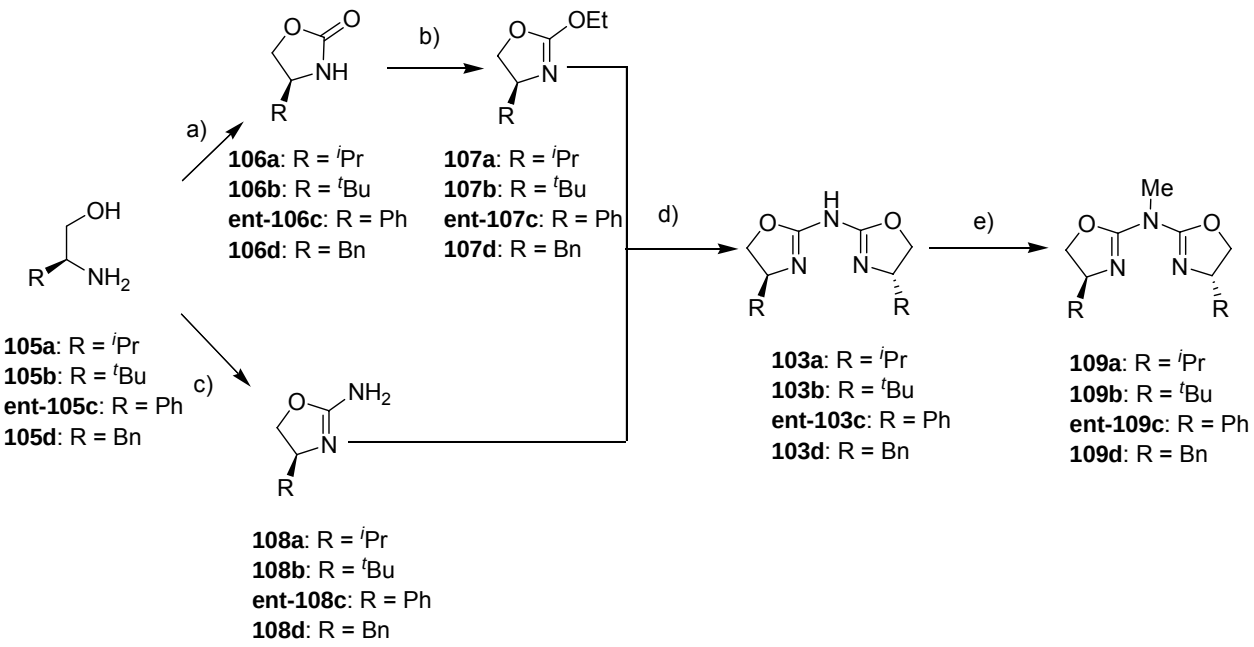

Scheme 34. Synthesis of azabis(oxazolines): a) $(EtO)_2CO$, NaOEt, EtOH, reflux, 87-93%; b) BF_4OEt_3, CH_2Cl_2, 0°C-RT, 81-98%; c) BrCN, MeOH, 0°C-RT, 38-89%; d) *p*-TsOH, Toluene, reflux; 35-92%; e) *n*-BuLi, MeI, THF, -78°C-RT, 95-98%.

Azabis(oxazolines) **103** form in general more electron rich complexes than bis(oxazolines) **102** or semicorrines **104**.[29] This can be a disadvantage, because the Lewis-acidity and therefore reactivity of the complexes is reduced. On the other hand, it provides an advantage for their immobilization since it means potentially less leaching of metal. Free metal centers would represent non-selective catalysts, an incisive limitation for recycling. Therefore, AzaBOX-complexes are able to maintain stable for an increased number of catalytic cycles. A second argument in favour for this comparatively novel class of chiral ligands deals with the complex geometry. The geometry on the metal center does not suffer from immobilization via alkylation on the central bridge atom as it is the case for bis(oxazolines) (Figure 17).[30] In conclusion, azabis(oxazolines) appear as privileged ligands for immobilization due to the central nitrogen atom.

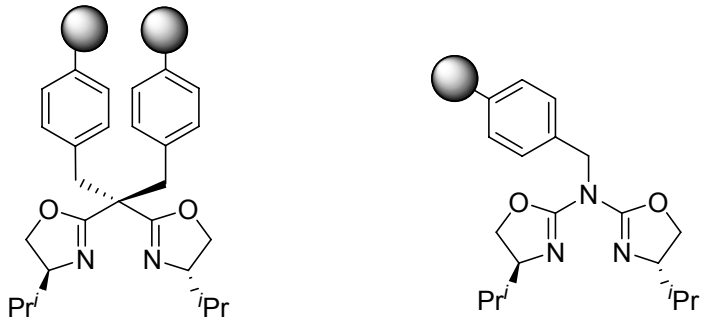

110 **111**

Figure 17. Bis(oxazolines)[30a] (left) and azabis(oxazolines) (right) grafted on polystyrene via alkylation of the central bridge atom. The immobilization has no substantial influence on the complex geometry in the case of the azabis(oxazolines).

Whereas the alkylation of the central nitrogen atom succeeds smoothly in the case of aza-semicorrines already via simple stirring with e.g. halogenalkanes, azabis(oxazolines) do not undergo this reaction that easily. Even after deprotonation with *n*-butyllithium the reactivity of the nitrogen nucleophile has only a limited scope.[25] However, azabis(oxazolines) were found to react quantitatively with methyliodide, allyl -and propargylbromide and benzyl bromide as well as certain derivatives thereof. Following this strategy, it was possible to covalently tag mesocellular silica foam,[31] dendrimers and different polymers such as MeOPEG, Tentagel™, a hybrid polymer with an insoluble polystyrene backbone and a PEG-periphery, and Merrifield resin[32] to azabis(oxazolines) (Figure 18).

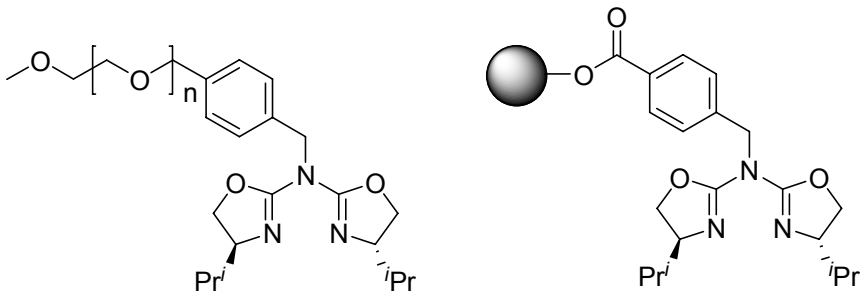

112 **113**

Figure 18. MeOPEG (left) and Tentagel™ (right) tagged with ^{i}Pr-AzaBOX **103a** via direct alkylation on the central nitrogen atom.

4.2 Immobilization of thiol-tagged azabis(oxazolines) via place-exchange reaction

4.2.1 Synthesis of thiol-modified azabis(oxazolines) via alkylation

In analogy to this work, efforts were concentrated on the alkylation of AzaBOX with 12-iodo-dodecanethiol. Success in this work would have yielded thiol modified ligand **114** which could have been grafted on monolayer-protected gold clusters via a simple place-exchange reaction (Scheme 35).

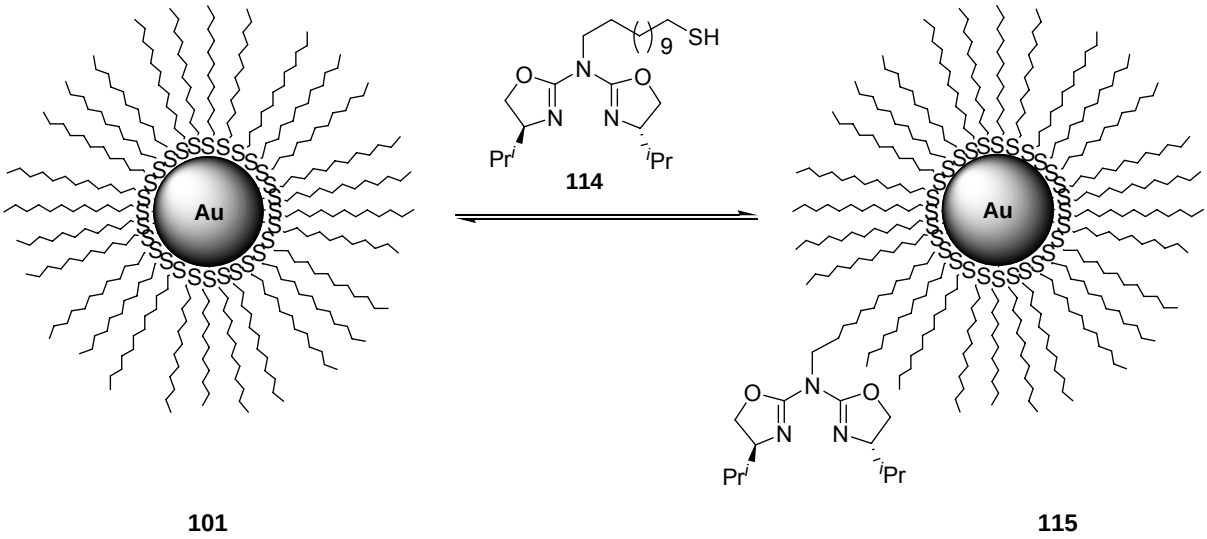

Scheme 35. Proposed Synthesis of azabis(oxazoline) tagged gold nanoparticles via place-exchange reaction with thiol-linked AzaBOX **114**.

Several attempts were undertaken using both, unprotected and acetyl-protected thiols at different reaction conditions (elevated temperatures, prolonged reaction times). Unfortunately, all endeavors were without success (Scheme 36). No signs which could be attributed to alkylated AzaBOX **114** were detected in ^{1}H-NMR and ^{13}C-NMR.

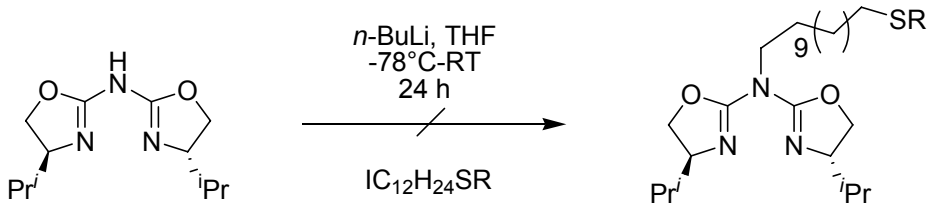

103a

114a: R = H
114b: R = Ac

Scheme 36. Attempted synthesis of thiol-functionalized ^{i}Pr-AzaBOX **103a** via direct alkylation with 12-iodo-dodecanethiol and 12-iodo-dodecane-acetyl-thiol respectively.

Inspired by the synthesis of substituted azabisbenzoxazoles (Scheme 37),[33] a modular approach towards thiol functionalized azabis(oxazoline) **114** was envisaged (Scheme 38). A similar method was investigated by A. Gissibl using ethoxyoxazolines **107** and simple diamines as well as aniline respectively. Since no or only little amount of product was obtained thereby, a more reactive oxazoline-derivative was employed. To test the viability of this route, (4*S*)-2-bromo-4-isopropyloxazoline (**117**)[34] was stirred together with decylamine. However, under various reaction conditions no product was obtained (Scheme 39).

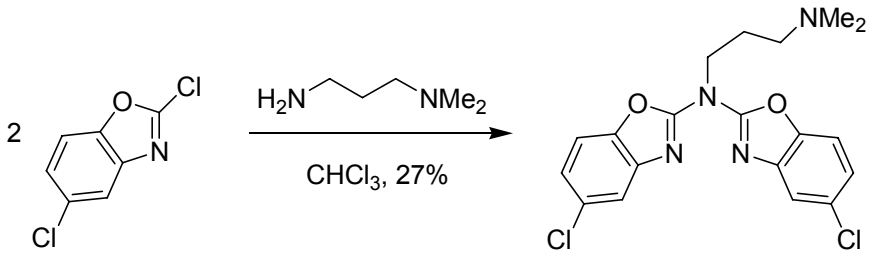

115 **116**

Scheme 37. Synthesis of substituted azabisbenzoxazole **116**.

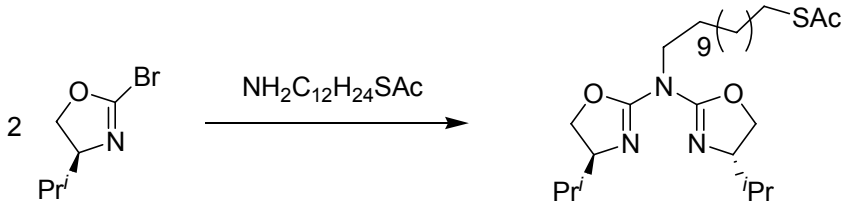

117 **114b**

Scheme 38. Proposed synthesis of thiol-linked azabis(oxazoline) **114b**.

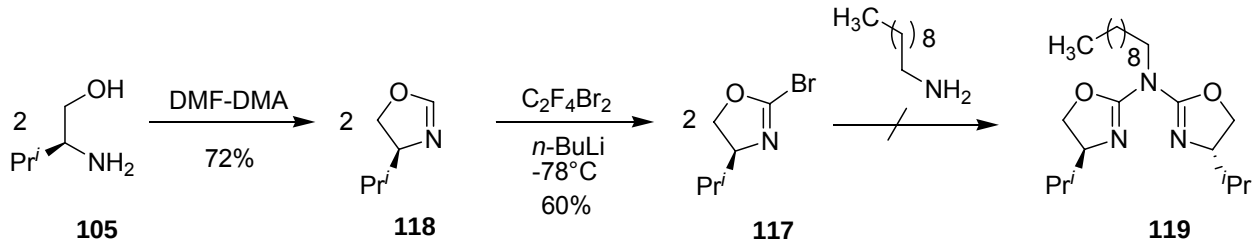

Scheme 39. Attempted preparation of substituted azabis(oxazoline) **119**.

Since the direct alkylation on the central nitrogen bridge with the appropriate alkanethiol was not successful, it seemed worthwhile to apply a different strategy, which had already proven its high versatility in order to install functionalities on the central nitrogen. It is known that azabis(oxazoline) **103** reacts quantitatively with propargylbromide (Scheme 40) and that alkyne-functionalized AzaBOX **120** obtained offers a suitable motif for the copper(I)-catalyzed alkyne/azide cylcloaddition reaction.

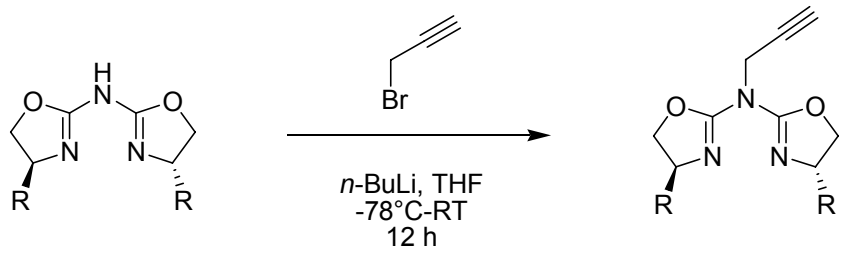

103a: R = ^{i}Pr
103d: R = Bn

120a: R = ^{i}Pr
120b: R = Bn

Scheme 40. Propargylation of azabis(oxazolines) **103a** and **103d**.

4.2.2 Synthesis of thiol modified azabis(oxazolines) via copper(I)-catalyzed azide/alkyne cycloaddition

4.2.2.1 General remarks on the CuAAC-reaction

The copper-catalyzed[35] azide/alkyne cycloaddition[36] reaction (CuAAC) has become very popular under the catchphrase “click”-reaction since it was developed almost simultaneously by Sharpless and Meldal in 2002. A 1,4-disubstituted 1,2,3-triazole is formed regioselectively in a Huisgen 1,3-dipolar cycloaddition of an azide with a terminal alkyne when the reaction is catalyzed by copper(I).

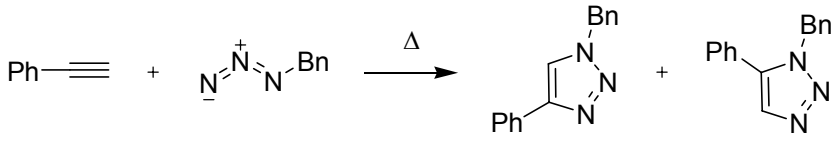

81 **121** **122** **123**

Scheme 41. Cycloaddition reaction of phenylacetylene **81** with benzylazide **121**.

Because of the high activation energy (ca. 24-26 kcal/mol), these cycloadditions are very slow even at elevated temperatures and produce mixtures of regioisomers if no catalyst is provided (Scheme 41). The mechanisms leading to the regioselectivity and rate enhancement for triazole formation under Cu(I)-catalysis have been extensively reviewed.[37] The addition of copper(I) to the alkyne results in the abstraction of a proton to form a highly polarized copper-acetylide-cluster. This copper-cluster is responsible for ligating the azide in order to enable an attack on the acetylide not via a concerted [2,3]-cycloaddition, but a stepwise annealing sequence. This is why the reaction is sometimes referred to as ligation of azides and alkynes. Two different transition states are possible, depending on whether the copper-cluster coordinates the terminal or the imine nitrogen of the azide. In any case, the final step involves the regioselective formation of a 1,4-disubstituted triazole (Scheme 42).

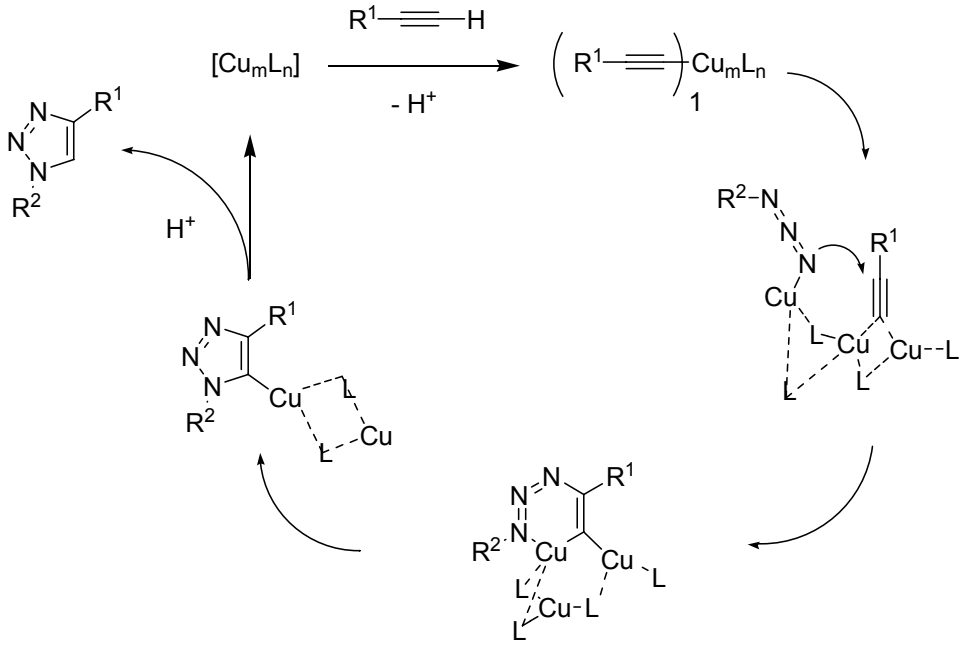

Scheme 42. Outline of a plausible mechanism for the CuAAC involving the formation of Cu(I)-clusters.[37]

Most methods use Cu(I)-salts[38] or –complexes (e.g. $Cu_2(OTf)_2 \cdot C_6H_6$, $Cu(PPh_3)_3Br$, [(SIMes)CuBr])[39] in a concentration of 0.25-5 mol% directly. Other strategies rely on the generation of Cu(I) in-situ by reduction of $Cu(II)SO_4 \cdot 5H_2O$ or $Cu(II)(OAc)_2$ using sodium ascorbate and metallic copper respectively.[38] Recently, the use of copper clusters of Cu/Cu oxide nanoparticles in activated charcoal,[40] PVP-polymers,[41] zeolites[42] and aluminum oxyhydroxide nanofibers[43] was described. At large, all common organic solvents and water can be used as reaction medium. Restrictions are due to particular properties of the copper source and can be avoided by choosing the appropriate catalyst carefully.

Despite the diversity of the different copper-sources, almost all demand the use of base. Common reagents for the "click"-reaction are triethylamine, 2,6-lutidine, and *N*,*N*-diisopropylethylamine (DIPEA).[38] Besides these rather simple bases, additives bearing triazole moieties have been shown to accelerate rates dramatically in some cases (Figure 19).[44] It was speculated that such compounds are capable of stabilizing the copper(I) oxidation state, thus preventing coupling reactions such as Ullman-, and Cadiot-Chodkiewizc-couplings.[45] Moreover, some additives were reported to inhibit the Cu(II)-catalyzed oxidative coupling of terminal alkynes to diynes.[45c]

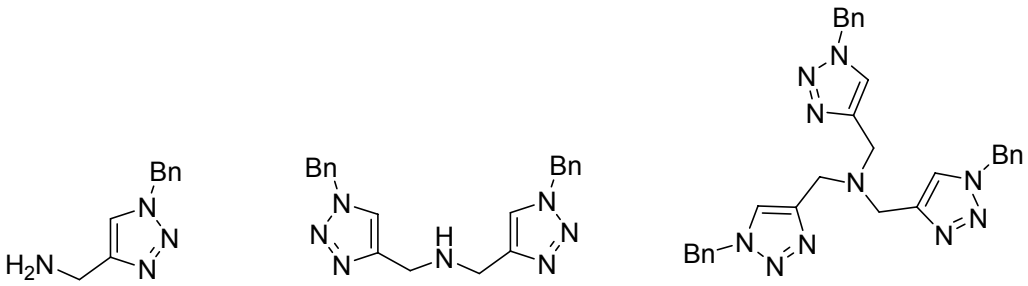

124 **125** **126**

Figure 19. Triazole-additives used in the copper-catalyzed azide/alkyne cycloaddition reaction.

Due to this impressive versatility, the "click"-reaction was already utilized for the grafting of azabis(oxazolines) on different polymers[32] or on fluorous tags.[46]

4.2.2.2 Synthesis of thiol-modified azabis(oxazolines) via “click”-chemistry

The synthesis of propargylated azabis(oxazolines) **120a** was expected to deliver thiol-linked azabis(oxazoline) **127** after a copper(I)-catalyzed “click”-reaction with ω-azido-dodecanethiol. The ligand derivatized thiol **127** could then be applied in a place-exchange reaction en-route to the desired azabis(oxazoline)-AuMPC **128** as depicted in Scheme 43.

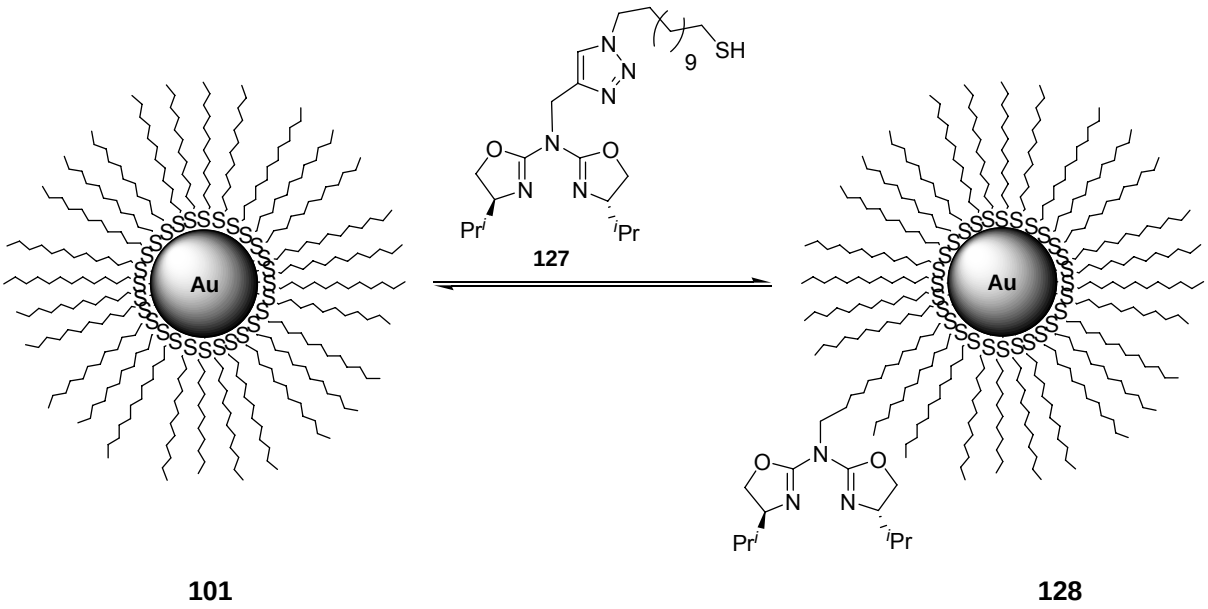

Scheme 43. Outline for the functionalization of AuNPs through a place-exchange reaction with thiol-modified azabis(oxazolines) created via “click”-chemistry.

Although the CuAAC is affected by very few incompatibilities, thiols range unfortunately among them. Azides are known to react with thiols, especially in the presence of Cu(I), to give sulfenylamides, amines and disulfides,[47] which makes a protecting group for the azido-dodecanethiol inevitable. An acetyl-group was envisaged to give the least problems due to very mild deprotection conditions applicable. This is an especially important issue, since azabis(oxazolines) functionalized on the central nitrogen bridge decompose in the presence of strong nucleophiles and even under mild acidic conditions. Thus, it is not even possible to perform column chromatography using untreated silica gel.

It was found that propargylated AzaBOX **120a** reacts in the presence of 5 mol% CuI and 1.1 equiv. triethylamine quantitatively with 12-azidododecyl ethanethiolate (**131**), prepared in a two-step synthesis from commercially available 1,12-dibromododecane (**129**) in 42% overall yield, (Scheme 44).[35c]

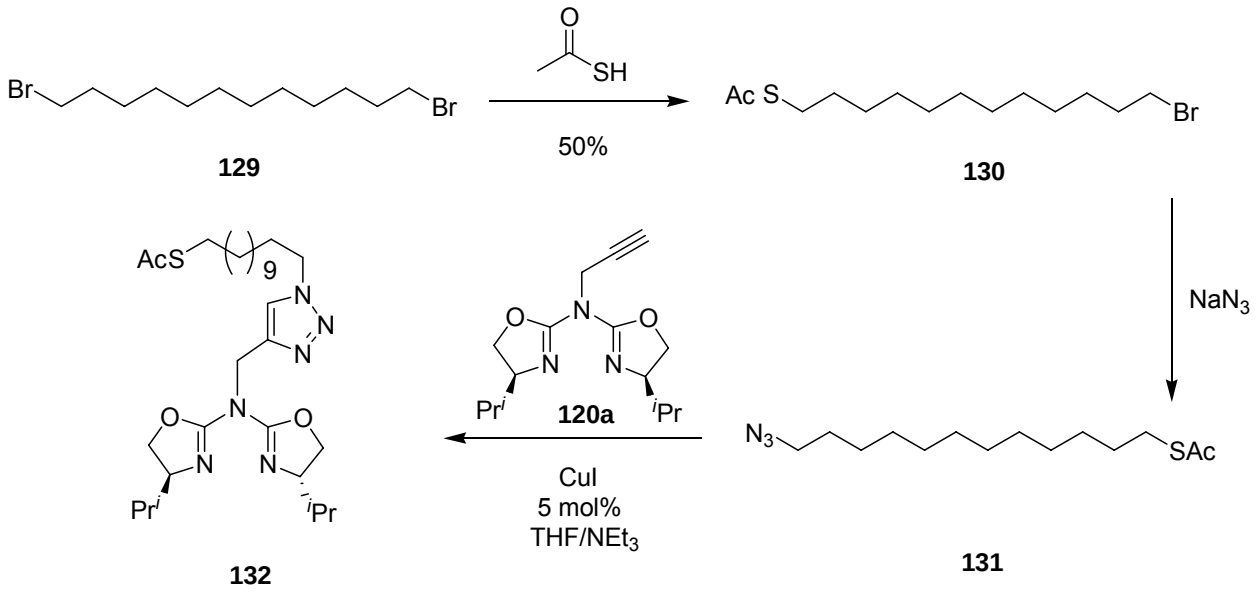

Scheme 44. Synthesis of acetyl-protected thiol functionalized azabis(oxazoline) **134** via "click"-chemistry.

However, unanticipated problems occurred during the deprotection step. Extensive decomposition was observed under deprotection conditions[48] which were not under the suspicion to harm *N*-alkylated azabis(oxazolines) **132** (Table 1).

Table 1. Reagents and conditions used for thiol deprotection.

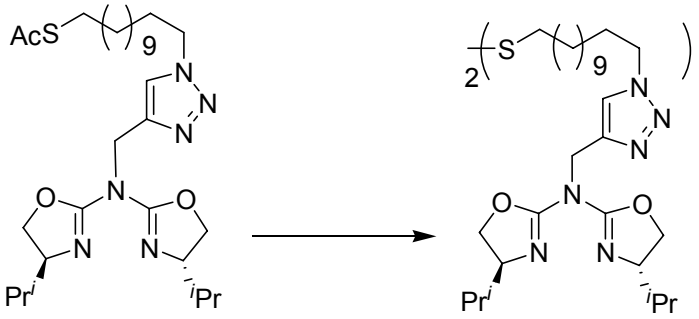

132 **133**

entry	reagents and conditions	yield (%)
1	$NaBH_4$, 2 h, THF,0°C-RT	-[a]
2	1. NH_3 (25% aq.), 1 h, MeOH, RT; 2. HCl (0.1 M aq.), pH = 7	-[a]
3	1. NaOH (0.2 M), 10 min, MeOH, RT; 2. HCl (0.1 M aq.), pH = 7	-[a]
4	1. NaOH (0.1 M), 15 min, MeOH, RT; 2. Amberlite IR120	-[a]
5	NaOMe, 5 min, MeOH, RT	-[b]
6	KCN, 3h, MeOH, RT	-[a]
7	K_2CO_3 (0.5 M aq.)/Dioxane/MeOH (1/0.5/0.5 v/v); Microwave Irradiation (5 min, 300W, Tmax = 60°C)	-[a]

[a] Decomposition; [b] Disulfide formation.

Only deprotection conditions which resulted in disulfide formation gave the expected product **133**. Since disulfides do not undergo the place-exchange reaction, the very mild reductants 1,4-dithiothreitol (DTT) and 1,2-ethanedithiol respectively were applied to yield the corresponding thiols (Scheme 45).

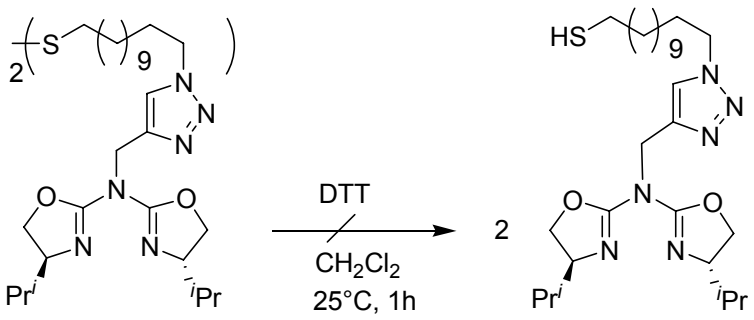

133 **127**

Scheme 45. Attempted reduction of disulfide **135** with 1,4-dithiothreitol.

Again, the expected product could not be observed and decomposition took place. In a control reaction, functionalized azabis(oxazoline) **132** was stirred together with 1 equiv. of 12-dodecanethiol in CH_2Cl_2 for 3 h. Decomposition was observed, thus indicating that not the deprotection conditions are responsible for the decay of the oxazoline moieties but the free thiol itself. This unprecedented reaction between thiols and azabis(oxazolines) might be similar to the formation of thioxazolines out of oxazolines, starting with a nucleophile attack of H_2S on the C*2*-carbon of the oxazoline.[49] However, the ^{1}H-NMR and ^{13}C-NMR spectra obtained were too complex to be analyzed.

The apparent incompatibility of thiols and azabis(oxazolines) points out the limitations of the place-exchange reaction, the hitherto predominant strategy for the functionalization of AuMPCs. This emphasized the demand for a generally applicable strategy for the immobilization of catalysts on gold clusters of the Brust-type.

4.3 The CuAAC-reaction as a generally applicable tagging method for AuMPCs

The CuAAC has already found broad application in polymer and material science,[38,50] since it allows the facile modification of various surfaces including 2D-SAMs of the thiol/gold-type.[51] The incompatibilities between azides and thiols have not hampered the use of a copper(I)-source ($CuSO_4$/ascorbate)[51b,c] to catalyze the "click"-reaction on thiolated Au(111)-surfaces. Once the ω-azidothiol has formed a SAM on the gold surface, the use of Cu(I) is apparently less problematic as disclosed by the studies of Binder et al. These results were quite encouraging since they implicate that the gold surface itself could act as some kind of protecting-group for the thiol. Therefore, a copper(I)-catalyzed cycloaddition between azide modified MPC **134** and propargylated azabis(oxazoline) **120a** appeared promising (Scheme 46).

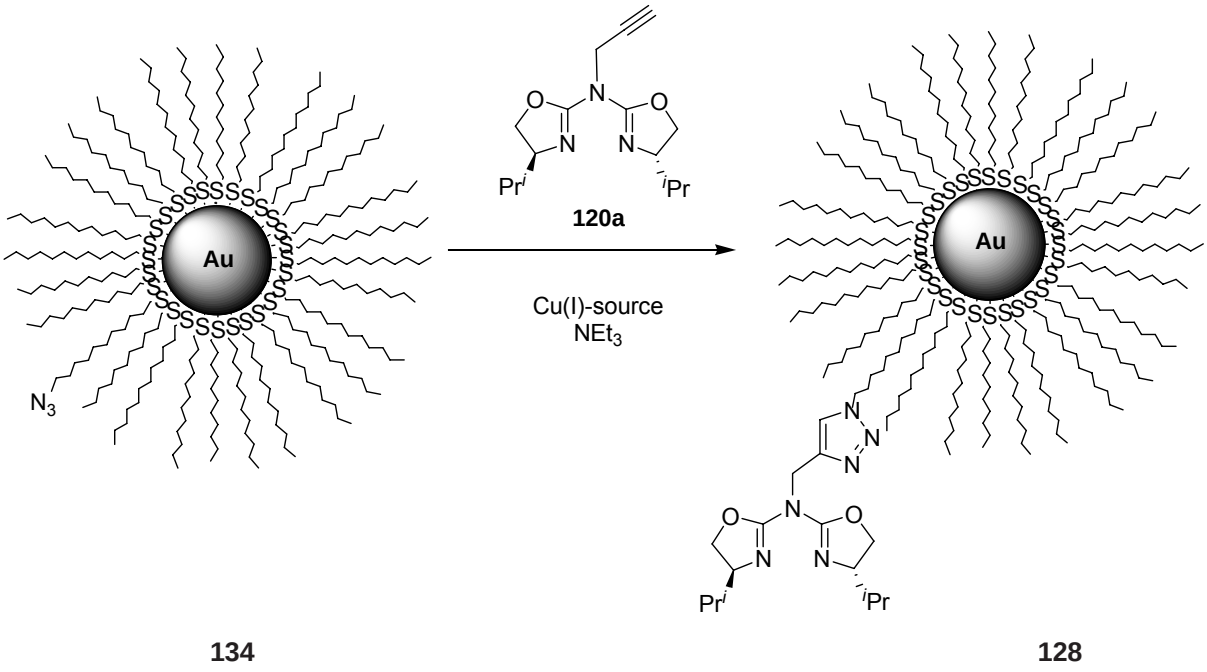

134 **128**

Scheme 46. Proposed synthesis of AuMPC-grafted azabis(oxazoline) **130** using a copper(I)-catalyzed azide/alkyne cycloaddition between azide functionalized MPC **134** and propargylated AzaBOX **120a**.

Nevertheless, it has been mentioned already in previous chapters that the difference between 2D- and 3D-SAMs are numerous due to the enlarged number of defect sites on a cluster.

4.3.1 Synthesis of azide-functionalized AuMPCs

The synthesis of azide-functionalized MPCs was unpretentious. In principle, such particles are accessible via place-exchange reaction of clusters obtained by the Schiffrin-reaction with ω-azidothiol. However, substantial amounts of this compound would be lost during the place-exchange reaction with its rather long reaction time (24- 48h) because those thiols are known to decompose slowly under loss of nitrogen to give sulfenylamides. Thus, 12-bromododecanethiol was used instead for the ligand-exchange and the bromo-functionalized cluster **135** reacted with an excess of tetrabutylammoniumazide to yield the azide-functionalized MPC **134** (Scheme 47). A two phase approach using sodium azide in DMSO and Br-MPCs **135** in CH_2Cl_2 together with catalytic amounts of tetrabutylammonium bromide gave inferior azide loading. The separation of the as-prepared NPs from the reactants succeeded through precipitation from MeOH (Figure 20).

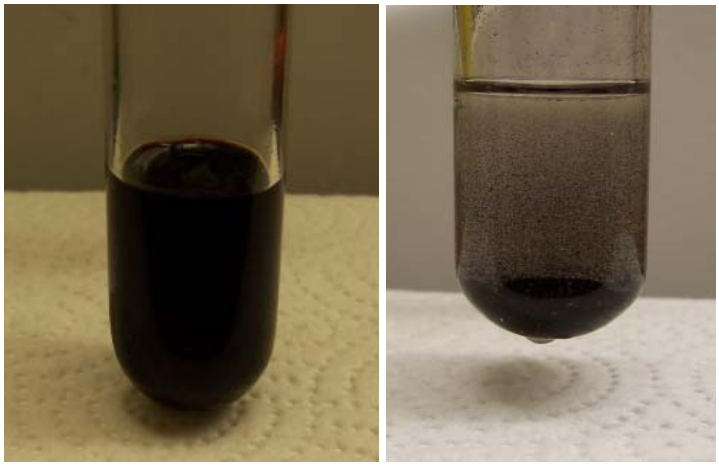

Figure 20. AuMPCs dispersed in CH_2Cl_2 (left) and after precipitation from MeOH (right).

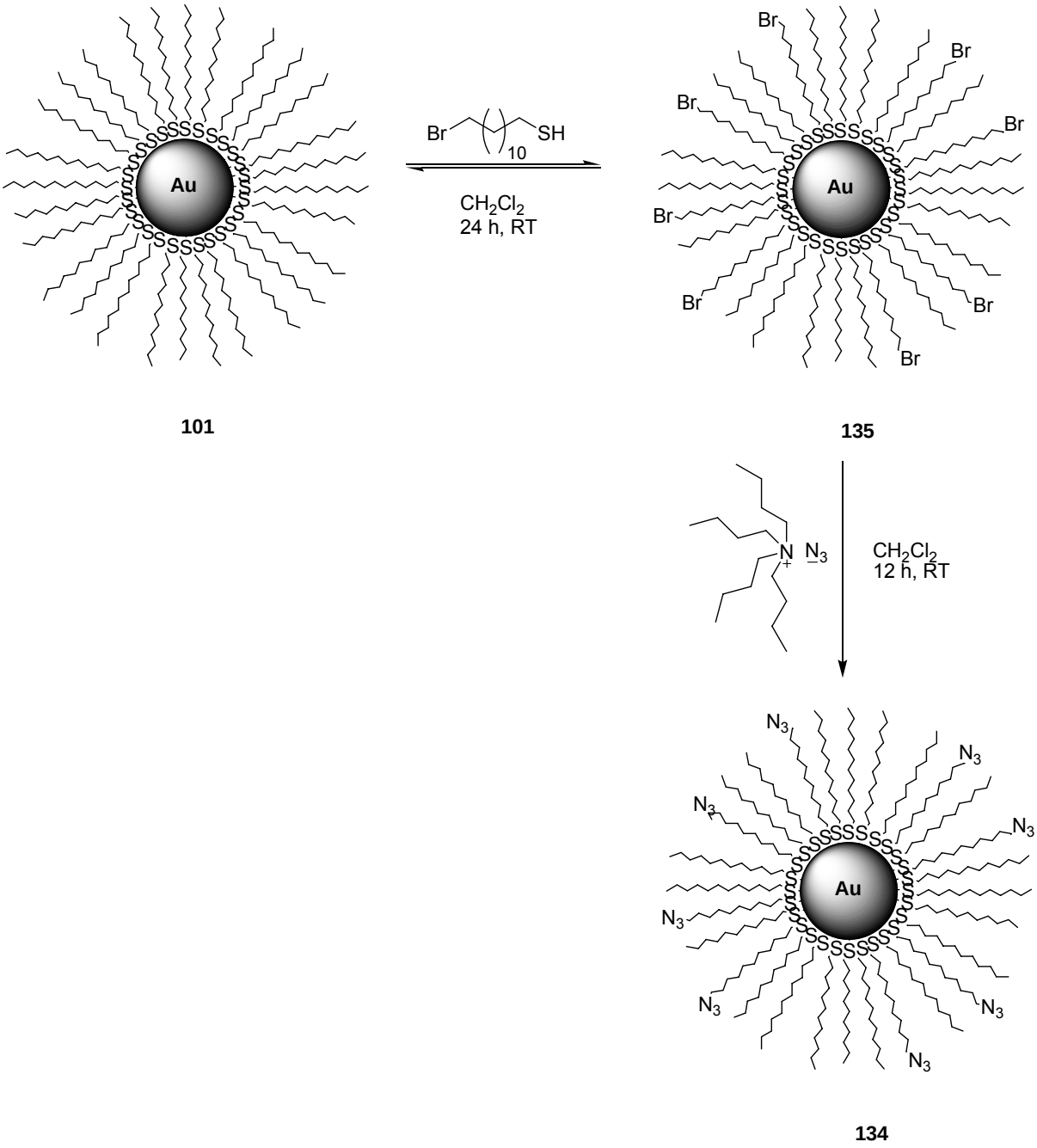

Scheme 47. Synthesis of azide-functionalized AuMPCs **134** via place-exchange reaction of dodecanethiol-capped MPCs **101** with 12-bromododecanethiol and subsequent substitution of Br-AuMPCs **135** with tetrabutylammoniumazide.

Although many reports provide empirical data correlating reaction time, concentration of clusters and functionalized thiols in solution to the extent of exchanged thiols,[16] it is still necessary to determine the amount of bromine moieties on the cluster. This can be easily achieved by ^{1}H-NMR-analysis. The ratio of 12-bromo-dodecanethiol and dodecanethiol can be determined via integration of the methylene peak vicinal to the bromine at 3.38 ppm and the terminal CH_3-group at 0.85 ppm. Having knowledge of the amount of residual thiols in the supernatant, conclusions can be drawn about the loading of the MPCs. In principle, a similar assessment is possible using the functionalized AuNPs after copious washing, albeit more sophisticated. Analyzing the MPCs does not allow precise integration of the spectra since the methylene peaks in the proximity of the particle surface are significantly broadened (Figure 21).[52]

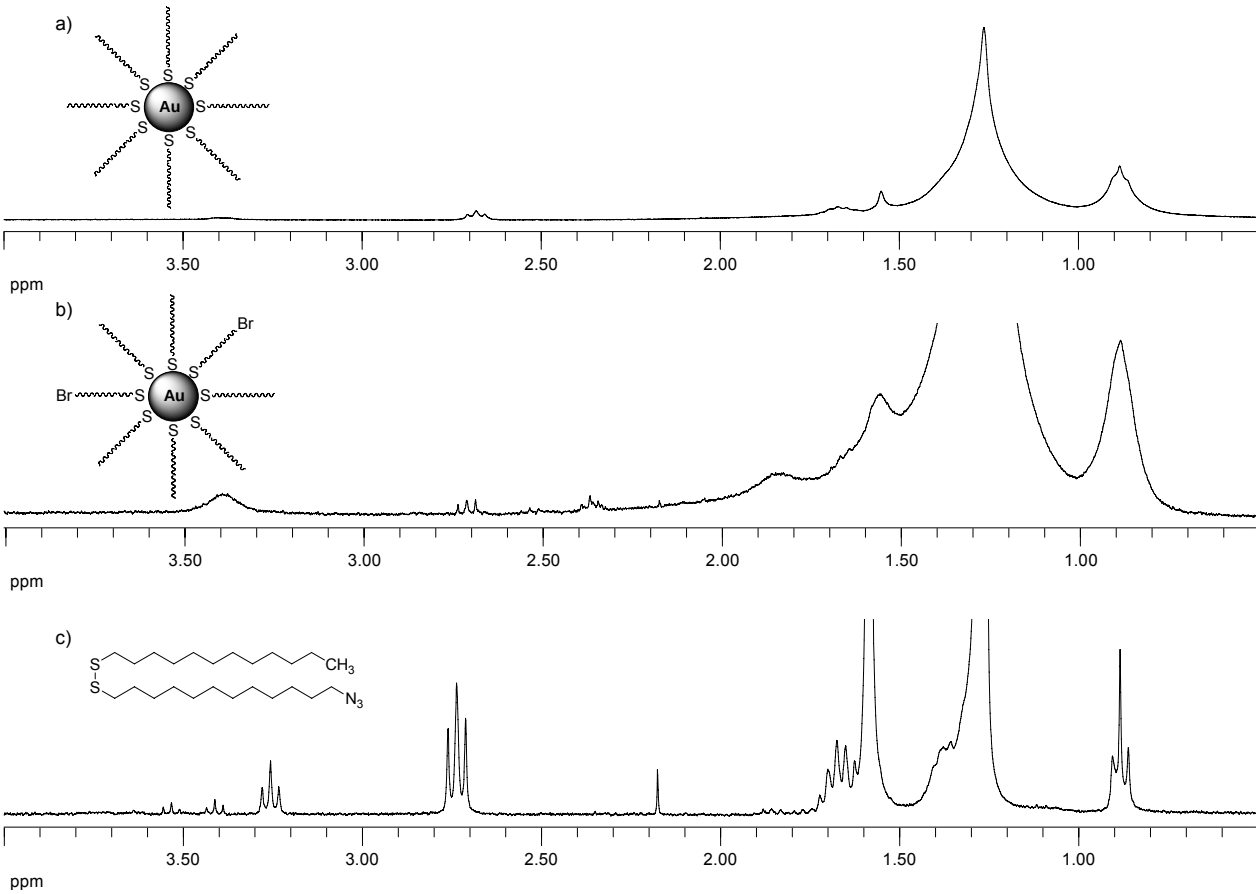

Figure 21. ^{1}H-NMR spectra obtained from a) Au-MPCs **101** b) Br-functionalized Au-MPCs **135** and c) N_3-functionalized Au-MPCs **134** after oxidative cleavage of thiols with I_2 in $CDCl_3$. The CH_2-units in the proximity of the cluster show a significant T_2-broadening.

Multiple factors contribute to the spectral broadening: Methylenes close to the thiolate/gold interface are more densely packed and solid like, whereas CH_2-units furthermost from the Au core experience freedom of motion and show spin relaxations similar to those of the dissolved species. Apart from that, chemical shifts of the methylene groups in the proximity of the cluster are inequivalent because of different binding sites (terraces, edges, verteces). The width of the spin-spin relaxation (T_2) broadening decreases with increasing core size, thus giving information about the Au cluster.

As a result, quantification of ligand exchange in the monolayer can be difficult. A solution for this problem is to cleave the alkanethiols oxidatively from the AuNPs by treatment with I_2 and to analyze the disulfides instead. Without the protective thiol shell, the gold cores flocculate immediately and can be filtered off the supernatant containing the disulfides.

Thus it was concluded that 20% of the thiolates were exchanged against 12-bromo-dodecanethiol. The success of the substitution of the bromide against the azide can be monitored qualitatively by recording the IR-spectra of the MPCs. It shows a significant peak at 2100 cm^{-1} if azide moieties are present. A quantitative analysis is possible in the same manner as discussed above. The CH_2-groups next to the N_3 are found at approximately 3.22 ppm, thus the extent of N_3-functionalized thiols in the protective shell was assessed to be ca. 16%.

4.3.2 CuAAC between propargylated azabis(oxazolines) and azide-functionalized AuMPCs

Tagging of azide-capped gold colloids **134** with propargylated azabis(oxazolines) **120a** was envisaged to be possible under various conditions since many “click”-protocols are applicable in apolar solvents.

4.3.2.1 Copper(I)-salts and –complexes as catalysts

Unfortunately, upon addition of any copper(I)-salt or –complex (CuI, $Cu_2(OTf)_2{\cdot}C_6H_6$, CuI(phen)), the AuNPs started to flocculate within minutes. A recent study, which was published in parallel to investigations presented in this work, substantiated the suspicion that MPCs of the Brust-type are destroyed by Cu(I)-sources.[53] In detail, Williams et al. reported immediate and extensive aggregation of the MPCs upon addition of CuI, $Cu(PPh_3)_3Br$ and CuBr/2,6-lutidine, most probably caused by

coordination of copper to the thiolates in the protective shell. The use of polytriazole-additives such as TBTA **126** was not able to suppress this effect.[44]

4.3.2.2 Heterogeneous copper(I)- sources as catalysts

Heterogeneous copper-sources offer an interesting, albeit hardly disclosed alternative to common systems. Most methods provide only a limited scope and diminished activity. However, some recent studies show an impressive scope including bulky substrates. Since migration of copper(I) to the thiol/Au-interface is presumably hampered when copper nanoparticles are immobilized within a stable matrix, such a catalyst might not destroy the protective shell of the gold clusters.

4.3.2.2.1 Copper-in-charcoal (Cu/C)

An exceptionally simple way to create “heterogenized” copper(I) was reported by Lipshutz and coworkers.[40] They impregnated commercially available wood charcoal with $Cu(NO_3)_2$ in water under sonication. Upon this treatment, CuO and Cu_2O were proposed to be present within the charcoal matrix, thus suggesting that a reducing agent might not be needed. Only the latter species is known to possess some catalytic activity in the CuAAC.[43] The Cu/C-catalyst, suspended together with N_3-MPC **134**, propargylated AzaBOX **120a** and NEt_3, proved to be an unsuitable catalyst for this system. No traces of product could be isolated at various reaction conditions (Table 2).

Table 2. Reagents and conditions used in the Cu/C-catalyzed 1,3-dipolar azide/alkyne cycloaddition.

entry	reagents and conditions	yield (%)
1	THF, NEt_3 (1.1 equiv.), 25°C, 96h	-
2	CH_2Cl_2, NEt_3 (1.1 equiv.), 25°C, 96h	-
3	Dioxane/Toluene (1:2, v/v), NEt_3 (1.1 equiv.), 60°C, 96h	-
4	Dioxane/Toluene (1:2, v/v), NEt_3 (1.1 equiv.), 60°C, 96h, Microwave Irradiation (5 min, 300W, Tmax = 60°C)	-

Moreover, the MPCs could be recovered in only 30% average yield, even after copious washing. This is most probably not due to decomposition of the AuNPs upon mild heating because selfsame yield was observed at ambient temperature. However, the as-prepared copper-charcoal-matrix proved to be an efficient catalyst, allowing the formation of the 1,4-disubstituted triazole to take place quantitatively in a test reaction between benzylazide **121** and 1-ethynylbenzene (**81**).

4.3.2.2.2 Copper nanoparticles in aluminum oxyhydroxide nanofibers

Another promising heterogeneous catalyst was generated by heating a mixture of cupric chloride dihydrate, ethanol, aluminum tri-*sec*-butoxide, and pluronic P123 at 160°C.[43] Without pluronic, the copper nanoparticles aggregated before gelation. The surface of these particles, stabilized in a matrix of aluminum oxyhydroxy-fibers, was reported to consist of Cu_2O and CuO as shown by XPS analysis.[43] The catalytically active species is likely again Cu_2O. The copper content of this material was calculated to be 4.0 wt% and the catalyst thus obtained was reported to be sufficiently active even without additional base.

Unfortunately, N_3-MPCs **134** and propargylated azabis(oxazoline) **120a** dissolved in refluxing *n*-hexane did not undergo 1,2,3-triazole formation in the presence of up to 20 mol% Cu/AlO(OH) within 96 h, although this catalyst demonstrated its activity in the simple benzylazide **121**/1-ethynylbenzene (**81**) –system. However, no aggregation of the gold cores was observed, thus indicating that catalysts of such a fashion are indeed capable of preventing migration of copper(I) into the thiol-SAMs. Nevertheless, also the MPCs are most probably unable to enter the aluminum matrix in which the copper is incorporated.

4.4 Ruthenium catalyzed azide/alkyne cycloaddition (RuAAC)

Other metal sources, such as Ni, Pd, and Pt salts, have been reported to promote the [3+2] Huisgen cycloaddition as well, but their reactivity pales in comparison with copper(I).[54] A highly promising alternative was investigated by Sharpless and co-workers.[55] They found that a variety of Ru-complexes (Cp*RuCl(PPh_3), [Cp*$RuCl_2$]$_2$, Cp*RuCl(NBD), Cp*RuCl(COD) and [Cp*RuCl]$_4$) promote the azide/alkyne click reaction. Interestingly, not only the 1,4-adduct is favored by some catalysts (i.e., $Ru(OAc)_2(PPh_3)_2$), but also the 1,5-adducts can be obtained as the only product. A

catalytic cycle that relies on a pathway similar to the cyclotrimerization reaction of alkynes via a six-membered ruthenacycle has been proposed (Scheme 48).[55b]

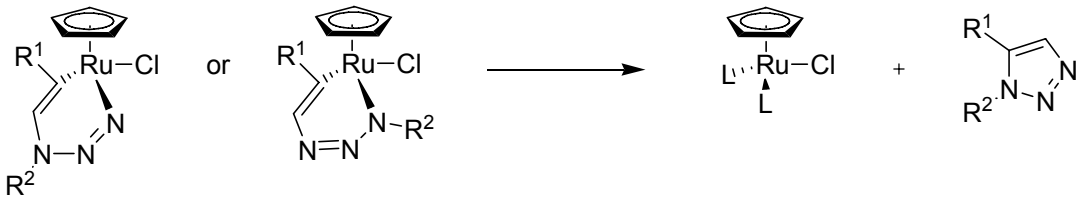

Scheme 48. Proposed Intermediates in the Ru-catalyzed reaction of azides and alkynes.[55b]

Typically 1-5 mol% of Ru-catalyst were applied to obtain moderate to excellent yields within reasonable reaction times, which could even be shortened when reactions were carried out under microwave irradiation.[55c] However, the scope of the Ru-catalyzed cycloaddition reaction still seems inferior when compared to its Cu-catalyzed counterpart.

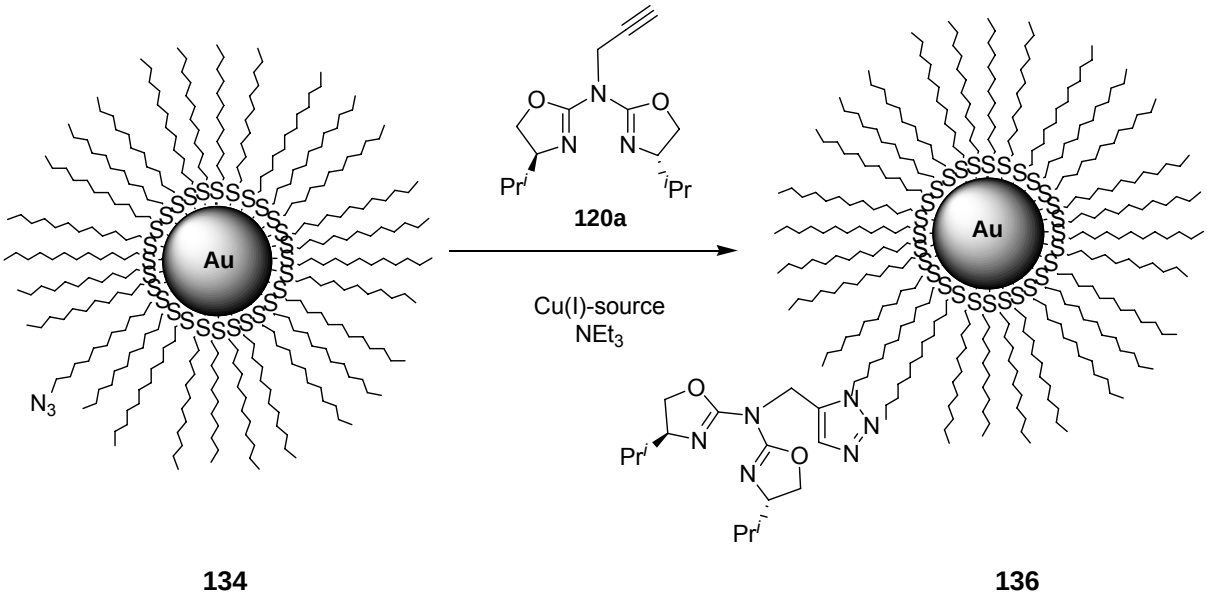

Scheme 49. Proposed synthesis of AuMPC-immobilized azabis(oxazolines) **138** via RuAAC.

Attempts to utilize a RuAAC reaction for the tagging of AuMPCs with azabis(oxazolines) were unsuccessful (Scheme 49). Decomposition of the gold nanoparticles was observed to some extent after refluxing in THF for 24 h, but no NMR-signals could be assigned to the 1,5-triazol.

4.5. Conclusion

In conclusion, several factors impeded a successful tagging of AuMPC **101** with azabis(oxazoline)-ligands. On the one hand, azabis(oxazolines) were destroyed by thiols, whereas on the other hand the protective thiolate shell was cleaved from the gold cores when exposed to copper(I). This ruled out the use of thiol-modified azabis(oxazolines) in a place-exchange reaction as well as a “click”-reaction between azide functionalized AuMPCs **134** and propargylated AzaBOX **120a**. Thus, it seemed reasonable to explore alternatives to gold nanoparticles rather than investigating more circumstantial strategies in order to achieve grafting of azabis(oxazolines) on monolayer- protected gold clusters.

5. References

1 M. Bartz, J. Küther, R. Seshadri, W. Tremel, *Angew. Chem.* **1998**, *110*, 2646.

2 a) H. Li, Y.-Y. Luk, M. Mrksich, *Langmuir* **1999**, *15*, 4957; b) K. Marubayashi, S. Takizawa, T. Kawakusu, T. Arai, H. Sasai, *Org. Lett.* **2003**, *23*, 4409; c) T. Belser, M. Stöhr, A. Pfaltz, *J. Am. Chem. Soc.* **2005**, *127*, 8720; d) F. Ono, S. Kanemasa, J. Tanaka, *Tetrahedron Lett*. **2005**, *46*, 7623.

3 M.-C. Daniel, D. Astruc, *Chem. Rev.* **2004**, *104*, 293.

4 a) M. Faraday, *Phil. Trans. Roy. Soc.* **1857**, *147*, 145; b) P. P. Edwards, J. M. Thomas, *Angew. Chem.* **2007**, *119*, 5576.

5 G. Schmid, B. Corain, *Eur. J. Inorg. Chem.* **2003**, 3081.

6 *Metal Vapour Synthesis;* J. R. Blackborow, D. Young, Eds.; Springer Verlag, New York **1979**.

7 S. Stoeva, K. J. Klabunde, Ch. M. Sorensen, I. Dragieva, *J. Am. Chem. Soc.* **2002**, *124*, 2305.

8 a) M. A. Hayat, *Colloidal Gold, Principles, Methods and Applications*; Academic Press: New York, **1989**; b) *Clusters and Colloids*; Schmid, G., Ed.; VCH: Weinheim, **199**4. c) Bradley, J. S. In *Clusters and Colloids*; Schmid, G., Ed.; VCH: Weinheim, **1994**; pp 459-544. d) G. Schmid, *Chem. Rev*. **1992**, *92*, 1709; e) G. Schmid, M. Bäumle, M. Geerkens, I. Heim, C. Osemann, T. Sawitowski, *Chem. Soc. Rev.* **1999**, *28*, 179; f) G. Schmid, B. Corain, *Eur. J. Inorg. Chem.* **2003**, 3081; g) H. Zhang, G. Schmid, U. Hartmann, *Nano Lett.* **2003**, *3*, 305.

9 J. Turkevitch, P. C. Stevenson, J. Hillier, *Discuss. Faraday Soc*. **1951**, *11*, 55.

10 a) A. Henglein, M. Giersig, *J. Phys. Chem. B* **1999**, *103*, 9533; b) S. Link, Z. L. Wang, M. A. El-Sayed, *J. Phys. Chem. B* **1999**, *103*, 3529.

11 G. Frens, G. *Nature: Phys. Sci.* **1973**, *241*, 20.

12 G. Schmid, R. Pfeil, R. Boese, F. Bandermann, S. Meyer, G. H. Calis, J. W. van der Velden, *Chem. Ber.* **1981**, *114*, 3634.

13 M. Giersig, P. Mulvaney, *Langmuir* **1993**, *9*, 3408.

14 a) M. Brust, A. Walker, D. Bethell, D. J. Schiffrin, R. Whyman, *J. Chem. Soc., Chem. Commun.* **1994**, 801; b) M. Brust, J. Fink, D. Bethell, D. J. Schiffrin, C. J. Kiely, *Chem.Commun*. **1995**, 1655.

15 a) M. D. Porter, T. B. Bright, D. L. Allara and C. E. D. Chidsey, *J. Am. Chem. Soc.* **1987**, *109*, 3559; b) P. E. Libinis, R. G. Muzzo, *G.* M. Whitesides, *J. Phys. Chem.* **1992**, *96*, 5097.

16 a) D. V. Leff, P. C. O'Hara, J. R. Heath, W. M. Gelbart, *J. Phys. Chem.* **1995**, *99*, 7036; b) M. J. Hostetler, S. J. Green, J. J. Stokes, R. W. Murray, *J. Am. Chem. Soc.* **1996**, *118*, 4212; c) R. S. Ingram, M. J. Hostetler, R. W. Murray, *J. Am. Chem. Soc.* **1997**, *119*, 9175; d) M. J. Hostetler, J. E. Wingate, C.- Z. Zhong, J. E. Harris, R. W. Vachet, M. R. Clark, J. D. Londono, S. J. Green, J. J. Stokes, G. D. Wignall, G. L. Glish, M. D. Porter, N. D. Evans, R. W. Murray, *Langmuir* **1998**, *14*, 17; e) A. C. Templeton, M. J. Hostetler, C. T. Kraft, R. W. Murray, *J. Am. Chem. Soc.* **1998**, *120*, 1906; f) M. J. Hostetler, A. C. Templeton, R. W. Murray, *Langmuir* **1999**, *15*, 3782; g) M. J. Hostetler, A. C. Templeton, R. W. Murray, *Langmuir* **1999**, *15*, 3782; h) A. C. Templeton, W. P. Wuelfing, R. W. Murray, *Acc. Chem. Res.* **2000**, *33*, 27.

17 a) R. L. Whetten, J. T. Khoury, M. M. Alvarez, S. Murthy, I. Vezmar, Z. L. Wang, P. W. Stephen, C. L. Cleveland, W. D. Luedtke, U. Landman, *Adv. Mater.* **1996**, *5*, 428; b) T. G. Schaaff, M. N.

Shafigullin, J. T. Khoury, I. Vezmar, R. L. Whetten, W. Cullen, P. N. First, C. Gutierrez-Wing, J. Ascensio, M. J. Jose-Yacaman, *J. Phys. Chem. B* **1997**, *101*, 7885; c) M. M. Alvarez, J. T. Khoury, T. G. Schaaff, M. Shafigulin, I. Vezmar, R. L. Whetten, *Chem. Phys. Lett*. **1997**, *266*, 91.

18 C. A. Waters, A. J. Mills, K. A. Johnson, D. J. Schiffrin, *Chem. Commun.* **2003**, 540.

19 M. Brust, C. J. Kiely, *Colloids Surf., A* **2002**, *202*, 175.

20 Y. Song, R. W. Murray, *J. Am. Chem. Soc*. **2002**, *124*, 7096; b) A. Kassam, G. Bremner, B. Clark, G. Ulibarri, R. B. Lennox, *J. Am. Chem. Soc.* **2006**, *128*, 3476.

21 a) M. M. Alvarez, J. T. Khoury, T. G. Schaaf, M. N. Shafigullin, I. Vezmar, R. L. Whetten, *J. Phys. Chem. B* **1997**, *101*, 3706; b) R. L. Whetten, J. T. Khoury, M. M. Alvarez, S. Murthy, I. Vezmar, Z. L. Wang, P. W. Stephens, C. L. Cleveland, W. D. Luedtke, U. Landman, *Adv. Mater.* **1996**, *8*, 428; c) W. D. Luedtke, U. J. Landman, *Phys. Chem. B* **1998**, *102*, 6566; d) S. L. Logunov, T. S. Ahmadi, M. A. El-Sayed, J. T. Khoury, R. L. Whetten, *J. Phys. Chem. B* **1997**, *101*, 3713.

22 M. Montalti, L. Prodi, N. Zaccheroni, R. Baxter, G. Teobaldi, F. Zerbetto, *Langmuir* **2003**, *19*, 5172.

23 P. Ionita, A. Caragheorgheopol, B. C. Gilbert, V. Chechik, *J. Am. Chem. Soc.* **2002**, *124*, 9048; b) P. Ionita, A. Caragheorgheopol, B. C. Gilbert, V. Chechik, *Langmuir* **2004**, *20*, 11536.

24 a) A. C. Templeton, M. J. Hostetler, E. K. Warmoth, S. Chen, C. M. Hartshorn, V. M. Krishnamurthy, M. D. E. Forbes, R. W. Murray, *J. Am. Chem. Soc.* **1998**, *120*, 4845; b) K. J. Watson, J. Zhu, S. T. Nguyen, C. A. Mirkin, *J. Am. Chem. Soc.* **1999**, *121*, 462.

25 a) M. Glos, O. Reiser, *Org. Lett.* **2000**, *14*, 2045; b) H. Werner, R. Vicha, A. Gissibl, O. Reiser, *J. Org. Chem.* **2003**, *68*, 10166.

26 Reviews: a) A. K. Ghosh, P. Mathivanan, J. Cappiello, *Tetrahedron: Asymmetry* **1998**, *9*, 1; b) K. A. Jørgensen, M. Johannsen, S. Yao, H. Audrain, J. Thorhauge, *Acc. Chem. Res.* **1999**, *32*, 605; c) J. S. Johnson, D. A. Evans, *Acc. Chem. Res.* **2000**, *33*, 325.

27 a) H. Fritschi, U. Leutenegger, K. Siegmann, A. Pfaltz, W. Keller, C. Kratky, *Helv. Chim. Acta* **1988**, *71*, 1541; b) H. Fritschi, U. Leutenegger, A. Pfaltz, *Helv. Chim. Acta* **1988**, *71*, 1553; c) U. Leutenegger, G. Umbricht, C. Fahrni, P. von Matt, A. Pfaltz, *Tetrahedron* **1992**, *48*, 2143; d) U. Leutenegger, A. Madin, A. Pfaltz, *Angew. Chem.* **1989**, *101*, 61; *Angew. Chem., Int. Ed. Engl.* **1989**, *28*, 60.

28 R. E. Gawley, G. Hart, M. Goicochea-Pappas, A. L. Smith, *J. Org. Chem.* **1986**, *51*, 3076.

29 J. M. Fraile, J. I. García,. C. I. Herrerías, J. A. Mayoral, O. Reiser, A. Socuéllamos, H. Werner. *Chem. Eur. J.* **2004**, *10*, 2997.

30 a) M. I. Burguete, J. M. Fraile, J. I. Garcia, E. García-Verdugo, S. V. Luis, J. A. Mayoral, *Org. Lett.* **2000**, *2*, 3905; b) M. I. Burguete, J. M. Fraile, J. I. Garcia, E. García-Verdugo, C. I. Herrerías, S. V. Luis, J. A. Mayoral, *J. Org. Chem.* **2001**, *66*, 8893; c) S. Orlandi, A. Mandoli, D. Pini, P. Salvadori, *Angew. Chem.,Int. Ed.* **2001**, *40*, 2519.

31 J. Lim, S. N. Riduan, S. S. Lee, J. Y. Yinga, *Adv. Synth. Catal.* **2008**, *350*, 1295.

32 A. Gissibl, M. G. Finn, O. Reiser, *Org. Lett.* **2005**, *7*, 2325.

33 J. N. Plampin, J. Sam, *J. Pharm. Sci*. **1964**, *53*, 538.

34 V. César, S. Bellemin-Laponnaz, H. Wadepohl, L. H. Gade, *Chem. Eur. J.* **2005**, *11*, 2862.

35 a) C. W. Tornøe, M. Meldal, *In American Peptide Symposium;* M. Lebl, R. A. Houghten, Eds, American Peptide Society and Kluwer Academic Publishers: San Diego, CA, **2001**, p 263; b) V. V. Rostovtsev, L. G. Green, V. V. Fokin, K. B. Sharpless, *Angew. Chem. Int. Ed*. **2002**, *41*, 2596; c) C. W. Tornøe, C. Christensen, M. Meldal, *J. Org. Chem*. **2002**, *67*, 3057.

36 R. Huisgen, *Pure Appl. Chem.* **1989**, *61*, 613.

37 M. Meldal, C. W. Tornøe, *Chem.Rev.* **2008**, *108*, 2952.

38 Reviews: a) W. H. Binder, C. Kluger, *Current Organic Chemistry* **2006**, *10*, 1791; b) W. H. Binder, R. Sachsenhofer, *Macromol. Rapid Commun*. **2007**, *28*, 15.

39 a) L. Bosch, J. Vilarrasa, *Angew. Chem. Int. Ed.* **2007**, *46*, 3926; b) R. Zirbs, F. Kienberger, P. Hinterdorfer, W. H. Binder, *Langmuir* **2005**, 8414; c) S. Díez-González, A. Correa, L. Cavallo, S. P. Nolan, *Chem. Eur. J.* **2006**, *12*, 7558.

40 a) B. H. Lipshutz, B. A. Frieman, A. E. Tomaso, *Angew. Chem. Int. Ed.* **2006**, *45*, 1259; b) B. H. Lipshutz, B. R. Taft, *Angew. Chem*. **2006**, *118*, 8415.

41 A. Sarkar, T. Mukherjee, S. Kapoor, *J. Phys. Chem. C* **2008,** *112,* 3334.

42 S. Chassing, M. Kumarraja, A. S. S. Sido, P. Pale, J. Sommer, *Org. Lett.* **2007**, *9*, 883.

43 I. S. Park, M. S. Kwon, Y. Kim, J.S. Lee, J. Park, *Org. Lett.* **2008**, *10*, 497.

44 T. R. Chan, R. Hilgraf, K. B. Sharpless, V. V. Fokin, *Org. Lett*. **2004**, *6*, 2853.

45 a) F. Ullman, *Liebigs Ann. Chem.* **1904**, *332*, 38; b) P. Cadiot, W. Chodkiewicz, *Chemistry of Acetylenes*, H. G. Viehe, Ed., Dekker, New York **1969**, pp. 597–647; c) I. D. Campbell, G. Eglinton, *Org. Synth.* **1965**, *45*, 39.

46 A. Gissibl, C. Padie, M. Hager, F. Jaroschik, R. Rasappan, E. Cuevas-Yanez, C.-O.Turrin, A.-M. Caminade, J.-P. Majoral, O. Reiser, *Org. Lett.* **2007,** *9*, 2895.

47 T. Saegusa, Y. Ito, V. Fokin, T. Schimizu, *J. Org. Chem.* **1970***, 35*, 2979.

48 T. W. Greene, P. G. M. Wuts, *Protective Groups in Organic Synthesis*, Wiley-Interscience Publication, New York, **1999**.

49 G. Stork, H. T. Cheung *J. Am. Chem. Soc.* **1965**, *87*, 3783.

50 J. F. Lutz, *Angew.Chem.Int.Ed.* **2007**, *46*, 1018.

51 a) J. P. Collman, N. K. Devaraj, C. E. D. Chidsey, *Langmuir* **2004**, *20*, 1051; b) R. Zirbs, F. Kienberger, P. Hinterdorfer, W. H. Binder, *Langmuir* **2005**, *21*, 8414; c) J. K. Lee, Y. S. Chi, I. S. Choi, *Langmuir* **2004**, *20*, 3844.

52 a) R. H. Terrill, T. A. Postlethwaite, C. Chen, C.-D. Poon, A. Terzis, A. Chen, J. E. Hutchison, M. R. Clark, G. Wignall, J. D. Londono, R. Superfine, M. Falvo, C. S. Johnson, E. T. Samulski, R. W. Murray, *J. Am. Chem. Soc.* **1995**, *117*, 12537; b) A. Badia, W. Gao, S. Singh, L. Demers, L. Cuccia, L. Reven, *Langmuir* **1996**, *12*, 1262.

53 D. A. Fleming, C. J. Thode, M. E. Williams, *Chem. Mater.* **2006**, *18*, 2327.

54 P. L. Golas, N. V. Tsarevsky, B. S. Sumerlin, K. Matyjaszewski, *Macromolecules* **2006**, *39*, 6451.

55 a) L. Zhang, X. Chen, P. Xue, H. H. Y. Sun, I. D. Williams, K. B. Sharpless, V. V. Fokin, G. Jia, *J. Am. Chem. Soc*. **2005**, *127*, 15998; b) L. Zhang, X. Chen, P. Xue, H. Y. Sun, I. D. Williams, K. B. Sharpless, V. V. Fokin, G. Jia, *J. Am. Chem. Soc.* **2005**, *127*, 15998; c) L. K. Rasmussen, B. C. Boren, V. V. Fokin, *Org. Lett.* **2007**, *9*, 5337.

II. Catalysts immobilized on Magnetic Nanoparticles

1. Catalysts immobilized on silica coated magnetite nanoparticles

Magnetic metal oxide nanoparticles, in particular magnetite nanoparticles, have demonstrated their versatility in a plethora of applications, e.g. ferrofluids were envisioned as magnetic storage media,[1] vessels for drug delivery,[2] contrast agents for magnetic resonance imaging (MRI)[3] and for cancer treatment through hyperthermia.[4] In addition, the use of magnetite NPs attracted a lot of attention in the field of catalysis.[5] The magnetic nature of superparamagnetic iron oxide (SPIO) particles provides a prerequisite for the effective and fast recycling of this material.[6] The nanocomposite is intrinsically nonmagnetic but the particles are readily magnetized in the presence of an external magnetic field. On the other hand, the lack of magnetic remanence prevents the agglomeration of the nanocrystals. Aforementioned properties, combined with the high accessibility of the globular arranged active sites on silica coated Fe_3O_4-particles, encouraged their application as supports for noble metals,[7] several palladium-based catalysts for C-C-bond formations,[8] or organocatalysts such as 4-*N,N*-dimethylaminopyridine (DMAP).[9] The immobilization of catalyst on a silica coating turned out to be especially beneficial in the latter case, giving rise to an invariant high activity and improved numbers of recycle and reuse referring to DMAP immobilized on conventional polymeric supports.[10] Moreover, a chiral transition-metal complex “heterogenized” on magnetite@silica-nanoparticles, had not been disclosed before. Therefore, the “click”-chemistry route for the grafting of Cu(II)-azabis(oxazoline)-complexes was reattempted using magnetite nanoparticles coated with amorphous silica.

1.1 Synthesis of silica coated magnetite particles

Much attention has been focused on the synthesis of magnetic core-shell structures by coating a SiO_2-shell around a preformed nanoparticle in the recent years.[11] Especially one large scale synthesis of discrete and uniformly sized superparamagnetic Fe_3O_4@SiO_2 seems attractive due to its simplicity.[12] In this strategy, the coating is achieved by addition of silane agents, e.g. tetraethyl orthosilicate (TEOS), to reverse micelles **137** during the formation of uniformly sized magnetite nanoparticles in a simple one-pot reaction. An interesting aspect lies in the addition of derivatized silane agents, such as 3-azidopropyltriethoxysilane, which can

be embedded in the silica shell already during the passivation of the iron oxide cores. Thus, nanocrystals can be synthesized and functionalized within one single step, starting from a 1:2 mixture of $FeCl_2 \cdot 4H_2O/Fe(NO_3)_3 \cdot 9H_2O$ and a microemulsion of dodecylbenzenesulfonate (DBS) in xylene. However, post-grafting on the surface of the particle shell is a more common alternative to the single-step functionalization and can be conveniently carried out by stirring 3-azidopropyltriethoxysilane together with the particles in THF for 48 h (Scheme 50).[9]

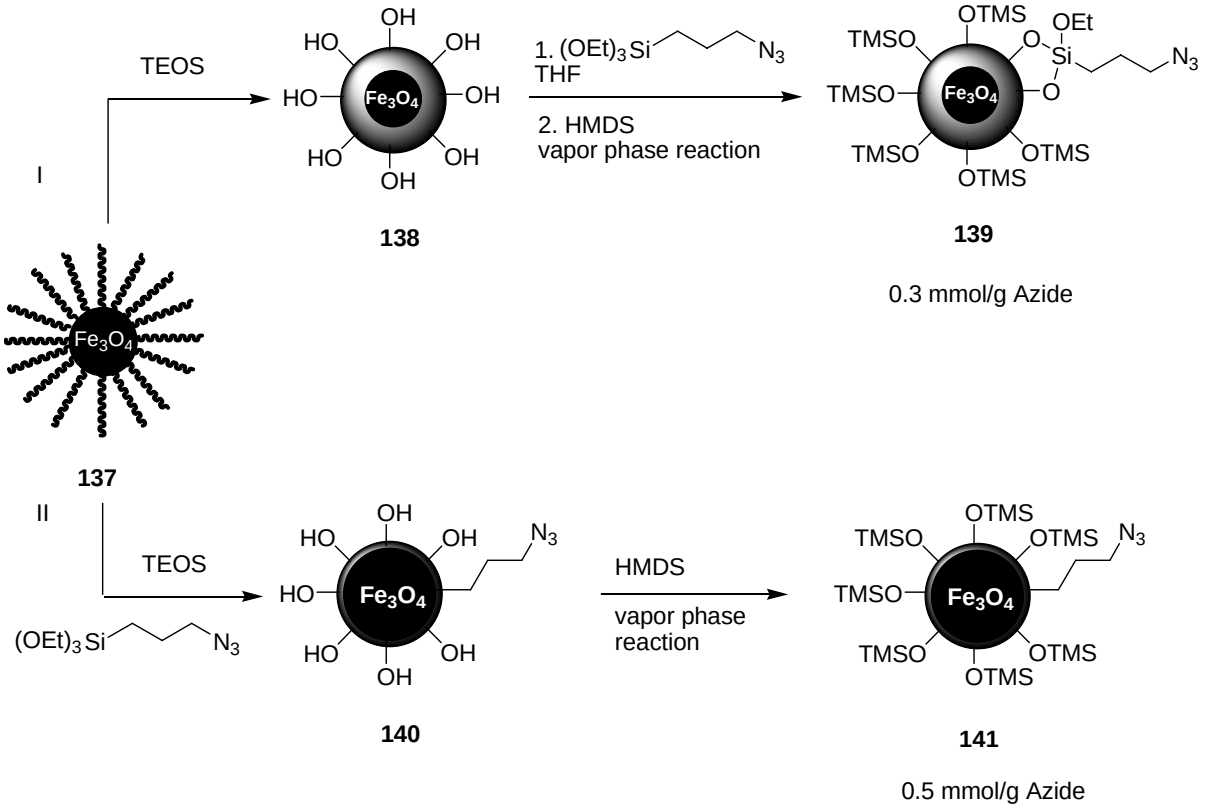

Scheme 50. Synthesis of azide-functionalized magnetite@silica-nanoparticles out of reverse micelles **137** via a post-grafting (path I) and a single-step protocol (path II) followed by TMS-endcapping of the surface silanol groups.

These two strategies did not only result in an altered amount of azide moieties - 0.3 mmol/g and 0.5 mmol/g respectively as determined by elemental microanalysis - but, more striking, in a different thickness of the silica shell (Figure 22).

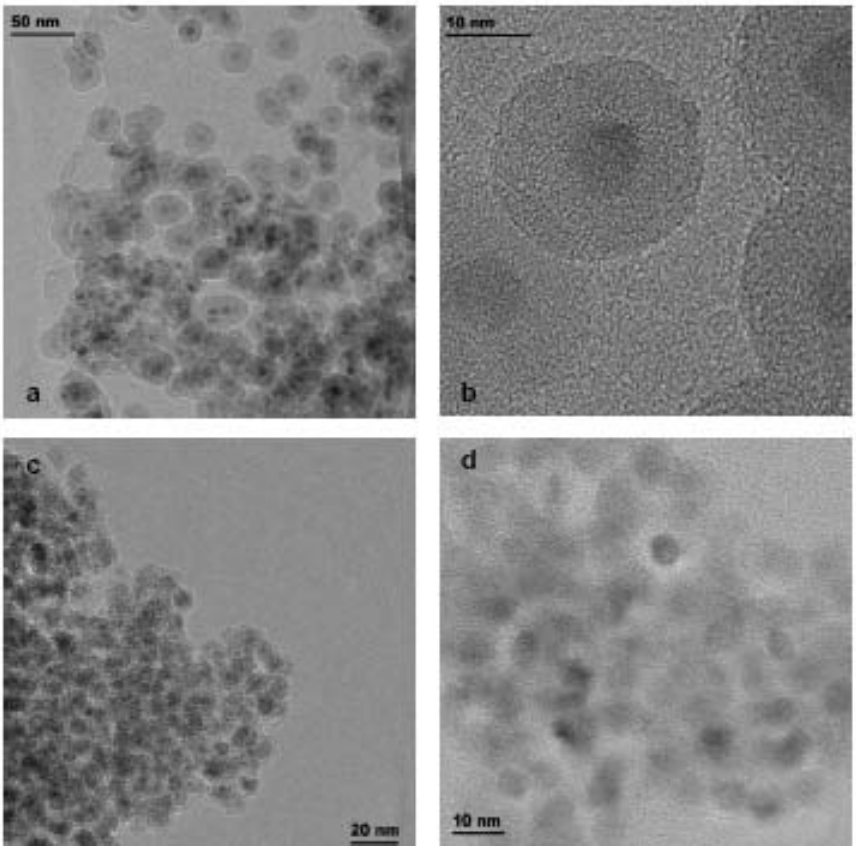

Figure 22. TEM images of particles **138** modified through a post-grafting process (Fig. 22a: 50 nm; Fig. 22b: 10 nm bar length) and single-step synthesized particles **140** (Fig. 22c: 20 nm; Fig. 22d: 10 nm bar length): The particles **138** synthesized via a post-grafting process form a thick silica shell (b) whereas only a thin SiO_2-coating, not visible in the TEM, is obtained for the nanoparticles **140** produced by the single-step pathway (d).

Aforementioned reaction conditions applied led to particles with a mean diameter of 7 nm for the magnetite core and an average diameter of 25 nm for magnetite@silica-particle **138** synthesized via the post-grafting process. In the case of the single-step synthesized particle **140**, the radius of the silica shell could not be determined by TEM even at higher resolutions (Figure 22b), whereas the size of the magnetite core remained unaltered. These dimensions were in agreement with the initial characterization of Hyeon et al. using 3-aminopropyltriethoxysilane (APS) instead of 3-azidopropyltriethoxysilane.

1.2 The silica shell

Following the line of argument that a high surface area is beneficial for catalyst activity, one would consider a coating with mesoporous rather than amorphous silica. From another point of view, a high catalyst density on the surface might even be

detrimental for both activity and selectivity. Indeed, a direct comparison between a Cu(II)-bis(oxazoline) complex anchored on MCM-41 and amorphous silica revealed that in the enantioselective Friedel-Crafts hydroxyalkylation of 1,3-dimethoxybenzene with 3,3,3-trifluoroppyruvate the complex grafted on mesoporous silica was inferior in means of selectivity (82% vs. 92% ee).[13] Although the authors reasoned that this effect might be caused by uncapped silanol groups, further studies demonstrated that even excessive TMS-endcapping of siliceous mesocellular foam (MCF) supported bis(oxazolines) using hexamethyldisilazane (HMDS) in a vapour phase reaction did not equal the results obtained when the surface of the MCF was precapped in large part before catalyst immobilization, thus limiting catalyst density on the surface.[14] In general, a complete TMS-postcapping of the residual surface silanol is beneficial, so avoiding interactions of the silanol moieties with metal salts.[13,14,15] Nevertheless, some reports indicated that TMS-capped silica exerts some catalytic activity, e.g. in the Diels-Alder reaction even at -70°C.[16]

1.3 Immobilization of azabis(oxazolines) on magnetite@silica-nanoparticles via CuAAC

As-prepared and endcapped particles were subjected to a copper(I)-catalyzed[17] azide/alkyne cycloaddition[18] reaction with propargylated azabis(oxazoline) derivative **120d** (Scheme 51). The loading typically achieved under these conditions was assessed by reacting **139** and **141** respectively with alkyne **142** bearing a *para*-nitrophenolester (Scheme 51).[19] Briefly, the particles were separated from excess of **142** in the supernatant, washed copiously and dried. Subsequently, **143** and **145** were subjected to basic hydrolysis (1 M $NaOH_{aq.}$/dioxane, 1:1 (v/v), 1 h) and the concentration of nitrophenolate was detected by UV/vis-spectroscopy measured against a standard solution. Thus, it appeared that 0.1 mmol/g of **142** could be immobilized on **139** and 0.3 mmol/g on **141** respectively. These data were confirmed by elemental microanalysis. Following a slightly modified protocol, propargylated azabis(oxazoline) **120d** was grafted onto **139** and **141** to yield the heterogeneous catalysts **144** and **146**.

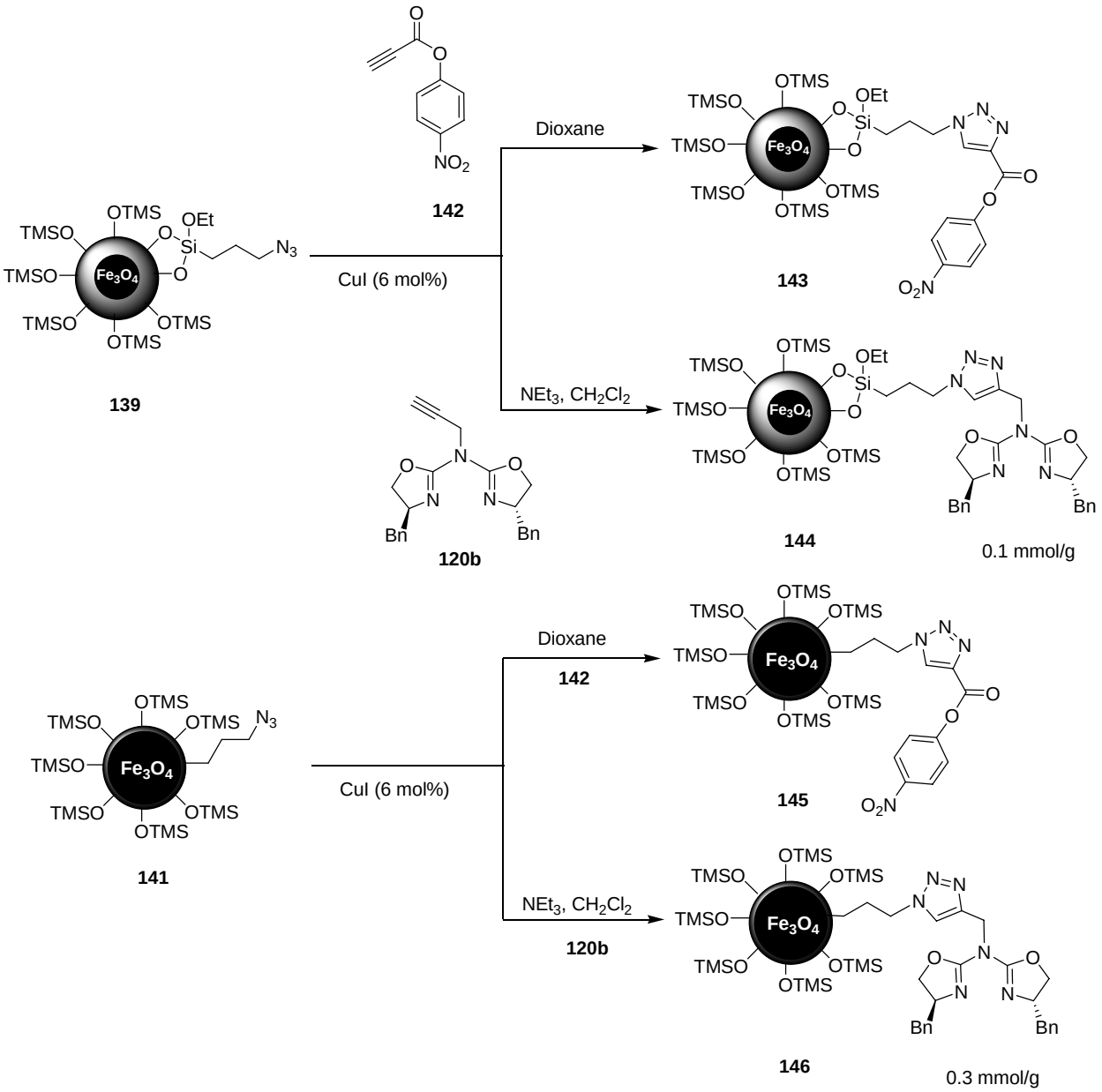

Scheme 51. Copper(I)-catalyzed azide/alkyne cycloaddition-reaction of azide functionalized magnetite@silica-nanoparticles **139** and **141** with 1-(nitrophenyl)-2-propyn-1-one (**142**) and propargylated azabis(oxazoline) **120b**, respectively.

The functionalization chemistry of the Fe_3O_4@SiO_2-nanomagnets was monitored by IR spectroscopy (Figure 23). The unfunctionalized silica coated magnetite particles showed stretches at 565, 1055, 1630 and 3300 cm^{-1} which were attributed to the Fe-O, Si-O-Si and –OH bonds respectively. In the case of the azide functionalized particles **139** and **141**, the characteristic absorption bands at 2100 cm^{-1} could only be observed for **141**, bearing just a thin silica layer. Intensities remained too weak for a distinct identification of functionalities upon further surface modification for **138** due to the intense Si-O-Si-bands at 1050 cm^{-1} with one exception: The vanishing –OH

signal at 3300 cm^{-1} gave hint of a successful TMS-postcapping. Various new signals between 1550 and 1670 cm^{-1} related to azabis(oxazolines) linked via a triazole moiety on the single-step synthesized Fe_3O_4@SiO_2 **146**.

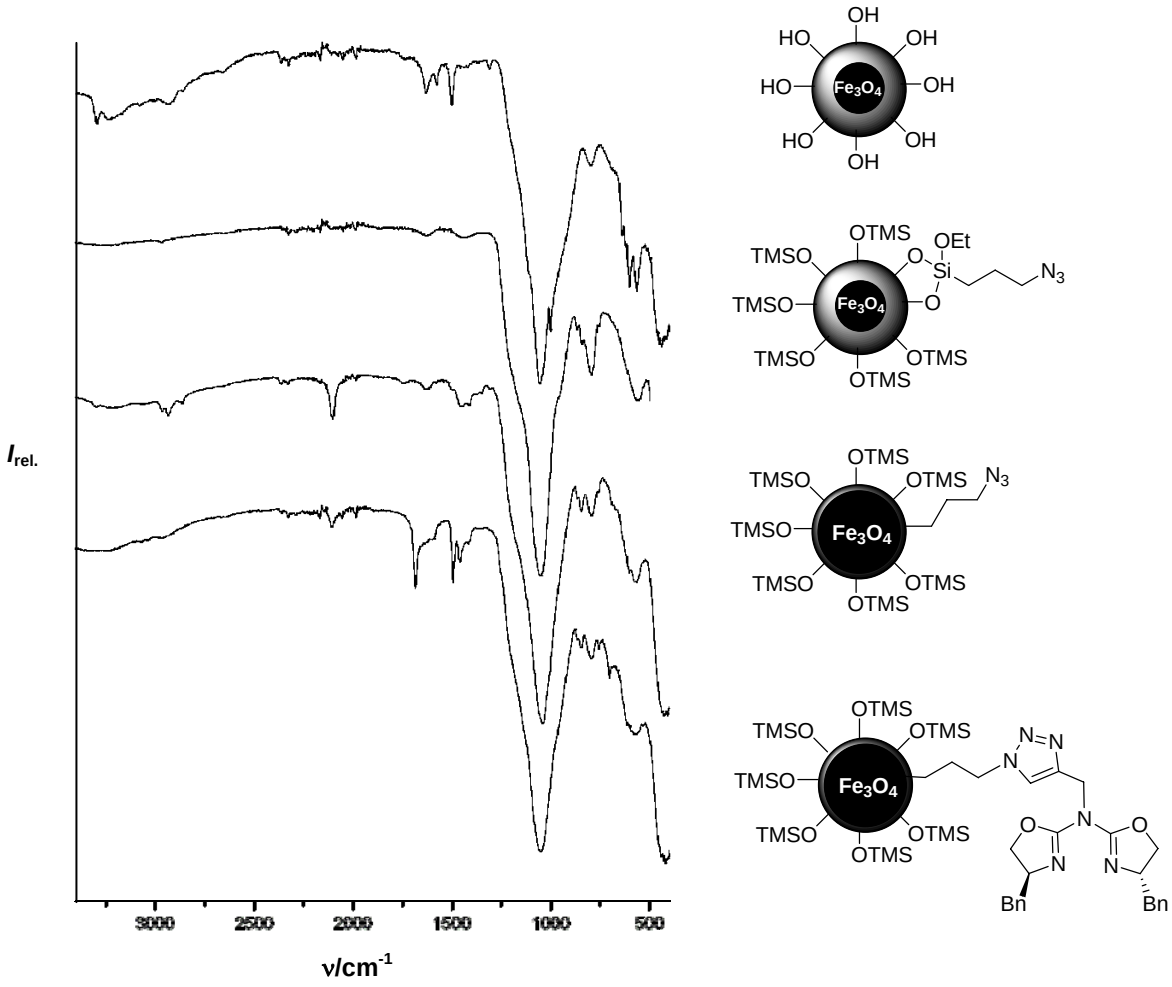

Figure 23. ATR-IR spectra of unfunctionalized (**138**), different azide functionalized magnetite@silica nanoparticles (**139, 141**) and of azabis(oxazolines) immobilized thereon (**146**) (top to bottom).

The azide/alkyne cycloaddition reaction as a tagging method which runs under mild conditions and with tremendous tolerance towards different functionalities provided the possibility to “click” preformed complexes directly onto the support. Hence, in an alternative strategy **120b**·$CuCl_2$ was subjected to CuAAC (Scheme 52).

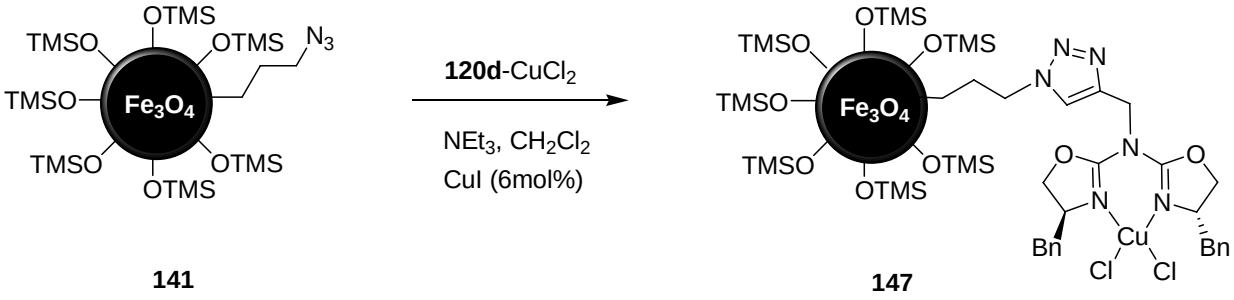

141 **147**

Scheme 52. Copper(I)-catalyzed azide/alkyne cycloaddition reaction between **120b**·$CuCl_2$ and single-step azide functionalized magnetite@silica nanoparticles **141**.

0.9 equivalents of $CuCl_2$ with respect to azabis(oxazoline) **120b** were applied in the complexation reaction, thus ensuring that the 6 mol% of copper(I) iodide subsequently used for the Huisgen cycloaddition were all ligated thereafter. The magnetite supported catalyst **147** was removed from the reaction mixture with the aid of an external magnet and redispersed in CH_2Cl_2 after decantation of the supernatant. This procedure was repeated five times before the retained material was applied in catalysis.

2. Catalysts immobilized on carbon coated cobalt nanoparticles

Apart from the magnetic metal oxides, pure metals such as Fe, Co, and Ni and their metal alloys, were used in various fields requiring magnetic materials.[20] The saturation magnetization of these ferromagnets exceeds the values obtained with ferrites by far. Compared to iron oxide nanoparticles, these levels are hardly diminished upon surface modification.

On the other hand, nanoparticles out of pure metals are highly sensitive to air and can even be pyrophoric, whereas oxidation of aforementioned magnetite particles to ferrimagnetic maghemite is potentially less problematic. The sensitivity towards oxygen is not necessarily a disadvantage. Metal nanoparticles can be coated with a layer of its metal oxide during a controlled oxidation process, e.g. Co/CoO-nanoparticles were prepared in such a manner. This is of particular interest because of the exchange bias effect between ferromagnetic Co and antiferromagnetic CoO.[21] Nevertheless, other core/shell motifs are more promising for further functionalization.

2.1 Characteristics of the shell

The intrinsic instability of all nanoparticles is caused by the tendency to agglomerate, thus reducing the energy associated with the high surface area/volume-ratio.

Naturally, the affinity to coalescence is enhanced in ferromagnetic particles. Moreover, the coating should be able to exclude oxygen. This problem is best addressed with shells derived from inorganic components, including silica,[22] precious metals, such as Ag and Au,[23] and carbon[24] rather than organic compounds (e.g. surfactants, polymers).[25] Nevertheless, a recent example shows that even cobalt nanoparticles stabilized by a rather penetrable oleic acid layer can act as recyclable carrier for a ligand promoting the ruthenium-catalyzed transfer hydrogenation of ketones (Scheme 14).[26] Reduction of the ruthenium complex by metallic cobalt was a major drawback, demonstrating once more the need for an impermeable coating which would also rule out catalytic action of Co.

Two problems arise from the coating of Co with precious-metals such as Au, which was reported by Luov et al.[27] Apart from economic considerations, further functionalization of the gold surface can create problems that were extensively discussed beforehand.

Silica coatings are sufficiently stable as long as harsh basic conditions are avoided and have therefore gained a predominant position for the passivation of iron oxide nanoparticles. However, a primer has to be used to make the surface of metal nanoparticles glasslike (“vitreophilic”)[28] in order to create an additional barrier for oxygen and other species which could diffuse through pores in the silica.

Carbon layers provide definitely the highest level of chemical and thermal stability over all aforementioned organic and inorganic compounds.[29] Despite this benefit, the formation of carbon coated metal particles is challenging and was possible only in small-scale operations (< 1 g/h) via arc discharge techniques,[30] chemical vapour depositions[31] and pyrolysis of metal complexes.[32] Recently, Stark et al.[33] reported on cobalt nanoparticles (50 nm average diameter) on which a graphene layer (1 nm) was deposited via reducing flame-spray pyrolysis.[34] In contrast to all literature precedents, this procedure gave rise to substantial amounts of Co/C nanoparticles (> 30 g/h).

2.2 Synthesis of Co/C-nanoparticles via flame spray pyrolysis

Cobalt(II)-2-ethylhexanoate was dispersed by an oxygen jet forming a spray, which was subsequently ignited by a premixed flame. In a conventional spray reactor (Figure 24, left), this precursor would combust to H_2O, CO_2 and metal oxide nanoparticles.

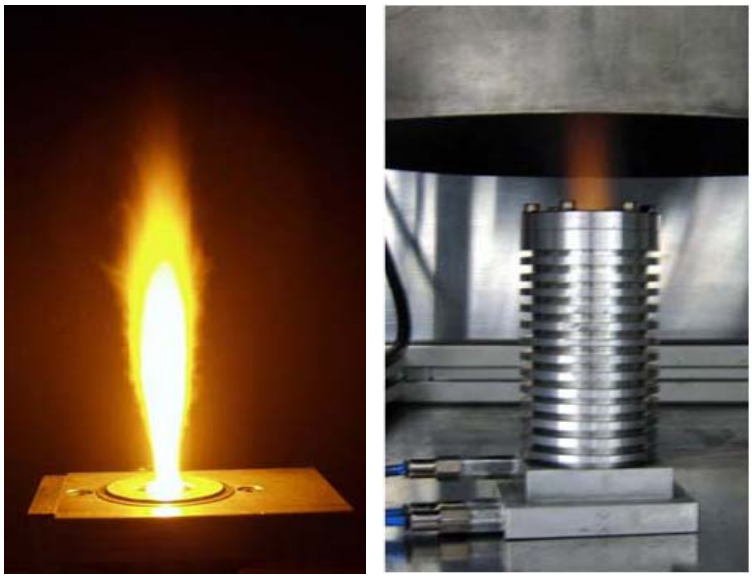

Figure 24. Photograph of a burning spray flame (left) and a spray flame operating in a glove box under oxygen limitation and encased in a doublewalled tube (right). The latter is used for the synthesis of Co/C-nanoparticles.[33]

Since the flame was operated in a nitrogen filled glove box under oxygen limitation, the combustion yielded CO and H_2 instead. The metal oxide nanoparticles were simultaneously reduced to the metal. Addition of acetylene through the side walls of a double walled tube (Figure 24, right) allowed the controlled coating of the nanoparticles by depositing carbon. The saturation magnetization of this material was close to bulk cobalt (158 emu/g), thus exceeding values obtained with the SPIO-particles **138**-**141** by far (ca. 20 emu/g).

2.3 Surface modification via reductive grafting of diazonium compounds

Covalent modification of a carbon surface is possible via aryl radicals generated from reduction of diazonium compounds (Scheme 53).[35]

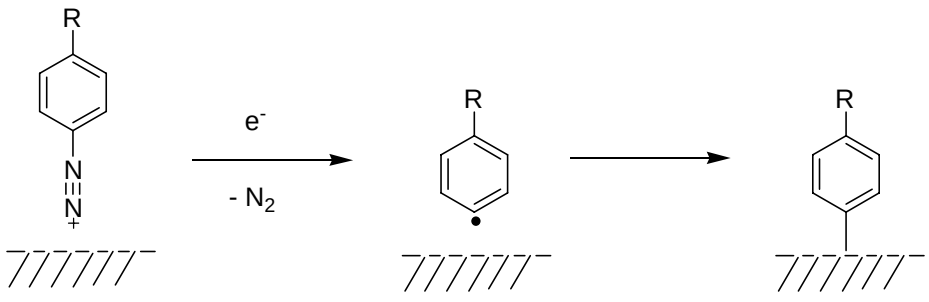

Scheme 53. Reduction grafting of diazonium compounds.

This strategy seemed highly versatile since most of the methods previously used for modifying the carbon surface involved harsh oxidation processes, e.g. boiling in HNO_3 leads to the formation of carboxy, quinone, keto or hydroxyl groups on the surface[36] that allow coupling with the molecules to be attached. In addition, the formation of oxygenated functionalities is hard to control in number and nature and often accompanied by roughening or even degradation of the carbon surface. Initial studies[35] focused on the electrochemical reduction of diazonium salts on glassy carbon (GC) and highly oriented pyrolytic graphite (HOPG) which were in the following expanded to any kind of carbon scaffolds and modifications including nanotubes and diamond.[37] The procedure is applicable for surfaces different than carbon, for instance hydrogenated silicon[38] and diverse metals and metal oxides.[39] A study which deserves to be mentioned in this regard was reported by Schiffrin and coworkers.[40] They demonstrated that Au and Pt nanoparticles can be stabilized by reduction grafting of 4-diazonium decylbenzene fluoroborate (DDB) (Figure 25).

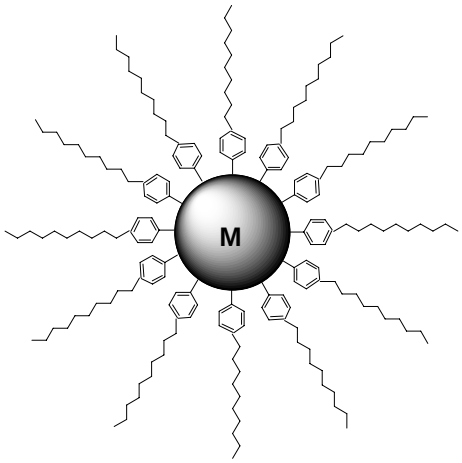

148: M = Au
149: M = Pt

Figure 25. Au and Pt nanoparticles stabilized with carbon-metal bonds formed upon reduction of DDB.

The calculated bonding energies of the covalent bonds[41] that result from the attack of the aryl radical range from 24 kcal/mol on gold to 70 kcal/mol on Si and up to 105 kcal/mol on carbon. This demonstrates once more the supremacy of carbon shells in this regard.

2.4 Synthesis of azide functionalized Co/C-nanoparticles

Two options were established by Stark et al.[33] for the grafting of functionalized aryl radicals on the graphene layer of cobalt particles.

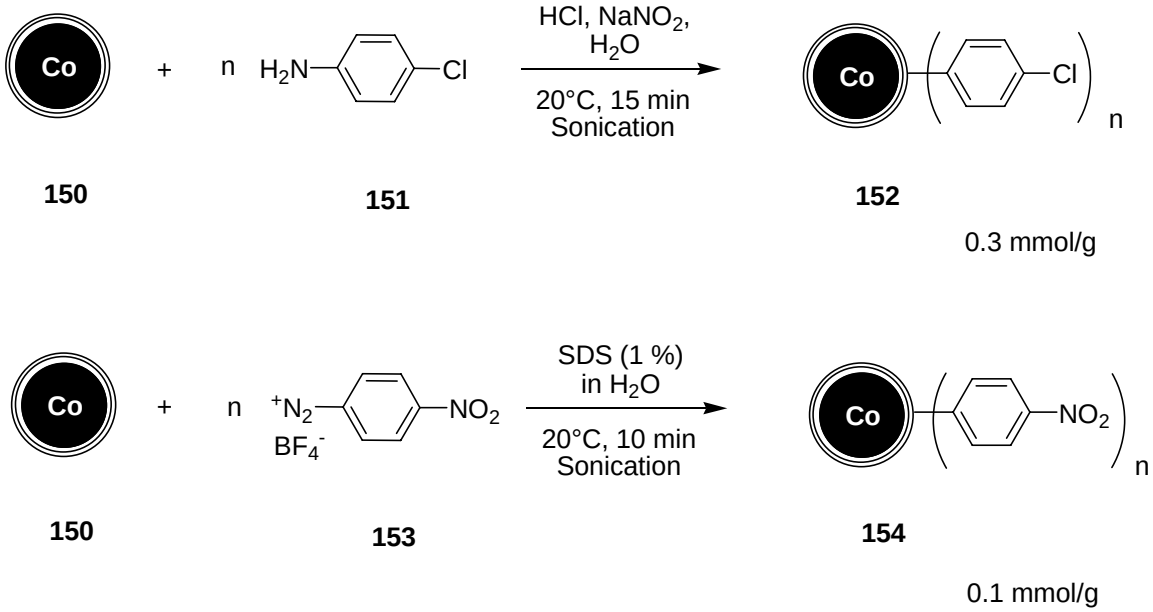

Scheme 54. Grafting of in-situ prepared (top) and preformed (bottom) diazonium compounds on carbon coated cobalt nanoparticles.[33]

Since in-situ prepared diazonium-salts seemed to result in superior loading, a similar approach was followed to install 4-aminobenzylalcohol **155** on the surface of the Co/C-nanoparticles **150**. Sonication was necessary to reduce the aggregation of the nanomagnets, a prerequisite for the grafting of the arylradicals which form upon loss of nitrogen. Keeping in mind the various side reactions possible with the sensitive diazonium moiety created in-situ and the excess of reagent that has to be applied in the course of the reaction, the grafting is apparently limited to quite simple aniline-derivatives. Hence, the tagging with more complex molecules had to be realized following a different route. In order to functionalize the nanobeads with more complex molecules, the phenylethanol-derivative **156** was transformed into the (azidomethyl)phenyl counterpart **157** using a modified Mitsunobu reaction to enable a copper(I)-iodide[17] catalyzed azide/alkyne cycloaddition[18] on the particle surface (Scheme 55).

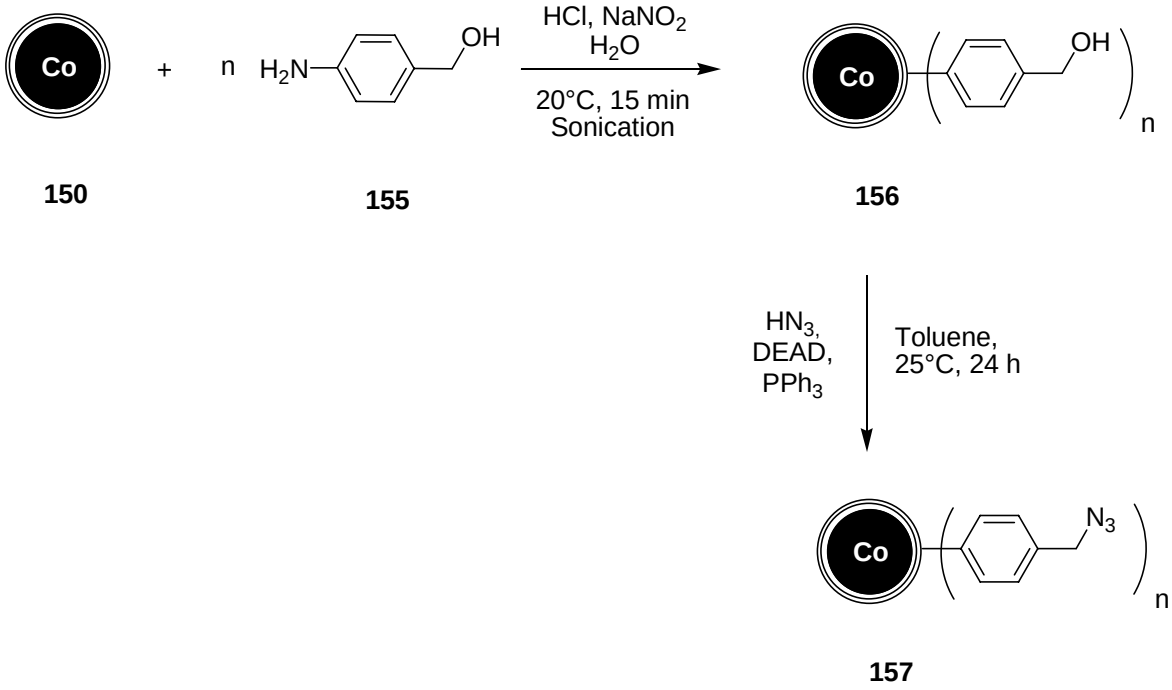

150 **155** **156**

157

Scheme 55. Grafting of the diazonium salt of 4-aminobenzyl alcohol (**155**) onto carbon coated cobalt particles and subsequent substitution of the alcohol against an azide under modified Mitsunobu conditions.

2.5 CuAAC as a generally applicable route for the immobilization of catalysts on Co/C-nanoparticles

In a preliminary investigation, the reactivity of the azide functionalized Co/C-particles in the “click”-reaction and the loading typically obtained under these conditions was assessed by reacting **157** with alkyne **142** bearing a *para*-nitrophenolester[19] (Scheme 56). The necessity of a rather high concentration of copper salt (20 mol%) for a quantitative reaction course within 36 h might be attributed to solvation effects since the reaction proceeds within a heterogeneous environment (proximity of the particle surface). In order to maintain a maximum level of dispersion, the particles were sonicated in an ultrasound bath throughout the reaction.

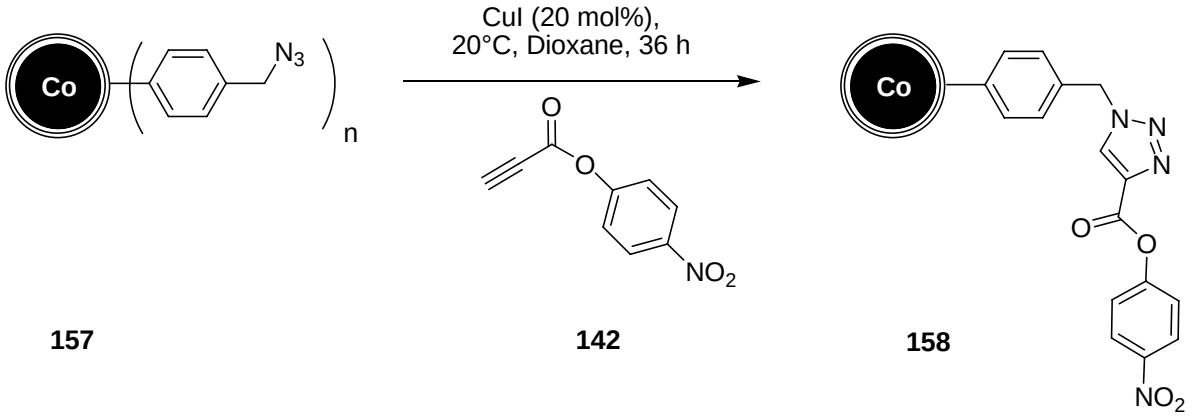

157 **142** **158**

Scheme 56. Copper(I)-catalyzed "click"-reaction of (azidomethyl) benzene functionalized nanoparticles **147** with 4-nitrophenylpropiolate (**142**).

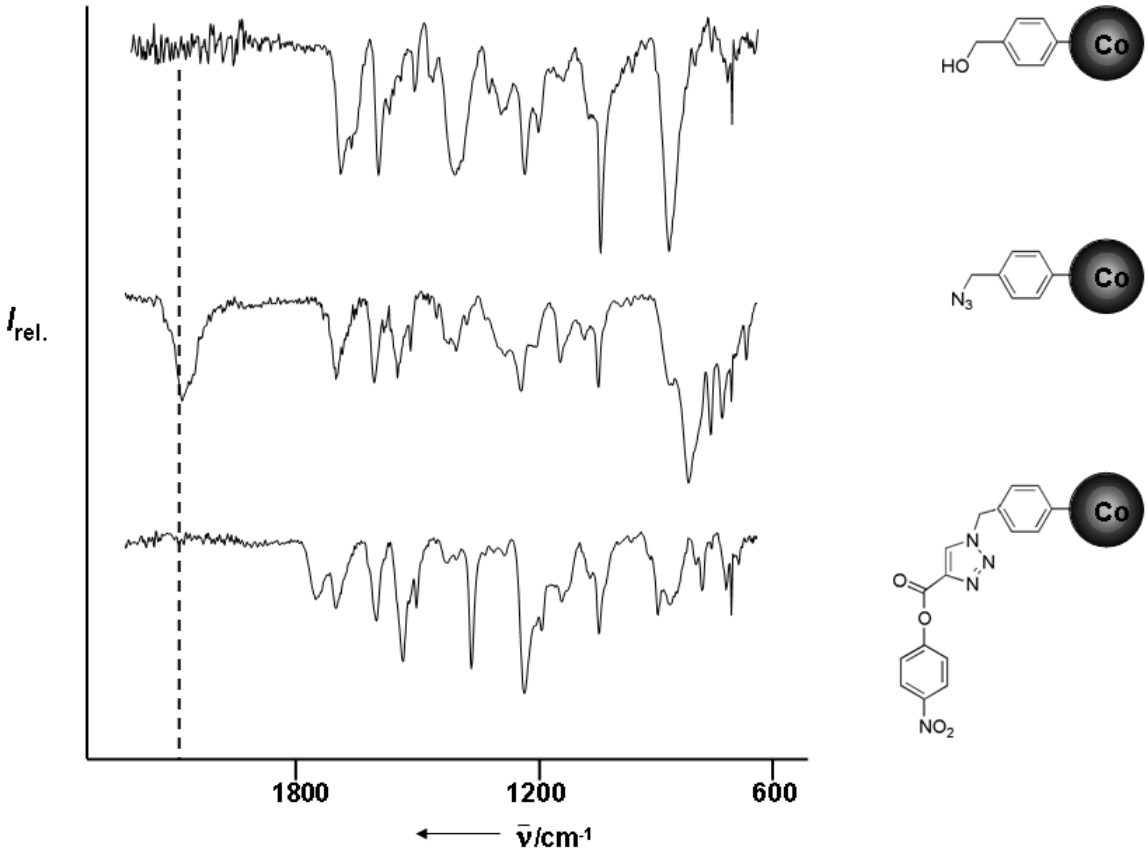

Figure 26. IR-spectra of Co/C powder after functionalization with phenylmethanol, (azidomethyl) benzene and after subsequent "click"-reaction of the latter with 4-nitrophenylpropiolate (**142**).

After accomplished immobilization – monitored by the vanishing azide peak at 2100 cm^{-1} (Figure 26) – the particles were separated from excess of **142** in the supernatant via repeated magnetic decantation and dried. The concept of magnetic decantation

takes advantage of the fact that a separation of the magnetic nanobeads is achieved within seconds after applying an external magnet to the reaction vessel (Figure 27).

Figure 27. Co/C-nanoparticles dispersed in dichloromethane before (left) and after the application of an external neodymium based magnet (right).

The supernatant can be decanted while the nanomaterial is retained. Recovered material was redispersed in the same volume of fresh solvent for another washing cycle until the waters remained colorless for three iterative washing cycles. Subsequently, the ester moieties immobilized on the Co/C-nanoparticles were subjected to basic hydrolysis (1M $NaOH_{aq.}$/dioxane, 1:1 (v/v), Scheme 57) and the concentration of nitrophenolate in the supernatant was measured by UV/vis-spectroscopy against a standard solution of 4-nitrophenolate **160**.

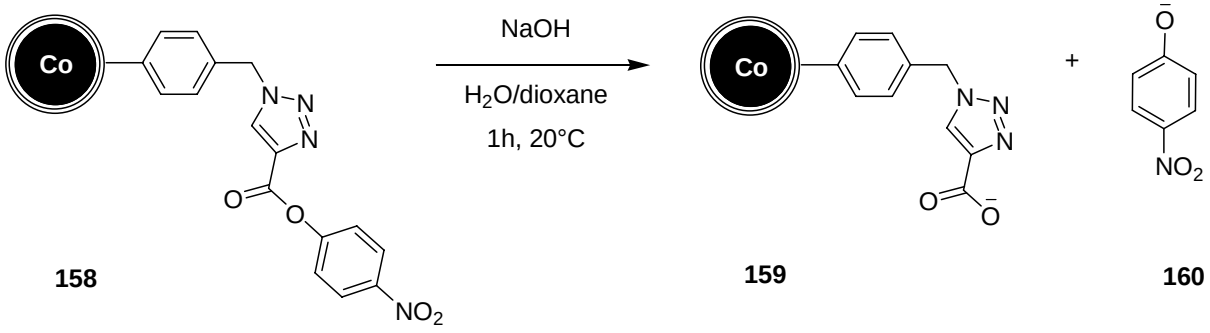

Scheme 57. Basic hydrolysis of Co/C-grafted nitrophenolester.

It is known that phenolates can be adsorbed on carbon surfaces to some extent.[42] Therefore, a reference solution was measured in which a standard solution of nitrophenolate was incubated together with **150** for 1 h. No significant loss of

concentration was detected, thus indicating that no physisorbtion of phenolates on the graphene layer is taking place. The maximum loading of the azide-functionalized cobalt-nanoparticles **158** was assessed to be approximately 0.1 mmol/g, a value which was affirmed by elemental microanalysis.

2.5.1 Azabis(oxazolines) immobilized on Co/C-nanoparticles

Based on promising results obtained with SPIO-particle immobilized catalyst **147**, a $CuCl_2$-complex of propargylated azabis(oxazoline) **120b** was subjected to the CuAAC reaction instead of the propargylated ligand itself (Scheme 58).

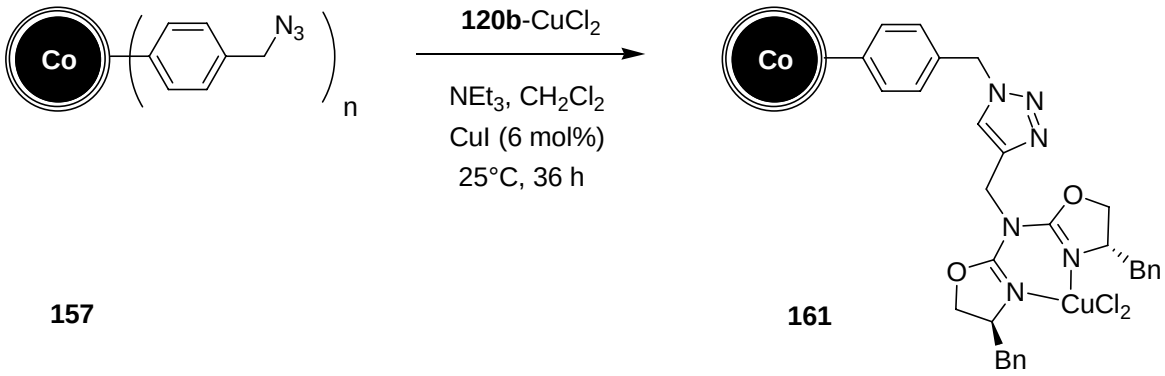

157 **161**

Scheme 58. Copper(I)-catalyzed "click"-reaction of (azidomethyl) benzene functionalized nanoparticles **157** with propargylated azabis(oxazoline)-copper complex **161**.

However, agitating the reaction mixture in an ultrasound bath did not deliver catalytically active material although the azide-peak vanished in the IR-spectrum of **161** (Figure 58). Extensive leaching of metal centers through continuous sonication might account for this effect. Hence, an alternative procedure was chosen in order to circumvent this drawback. The explicit ferromagnetism of the cobalt cores turned out to be sufficient for keeping the particles in dispersion when the reaction vessel was placed between adjacent parallel flanks of two magnetic stirrers. Indeed, the nanomaterial isolated after magnetic agitation under otherwise unchanged reaction conditions delivered catalytically active material.

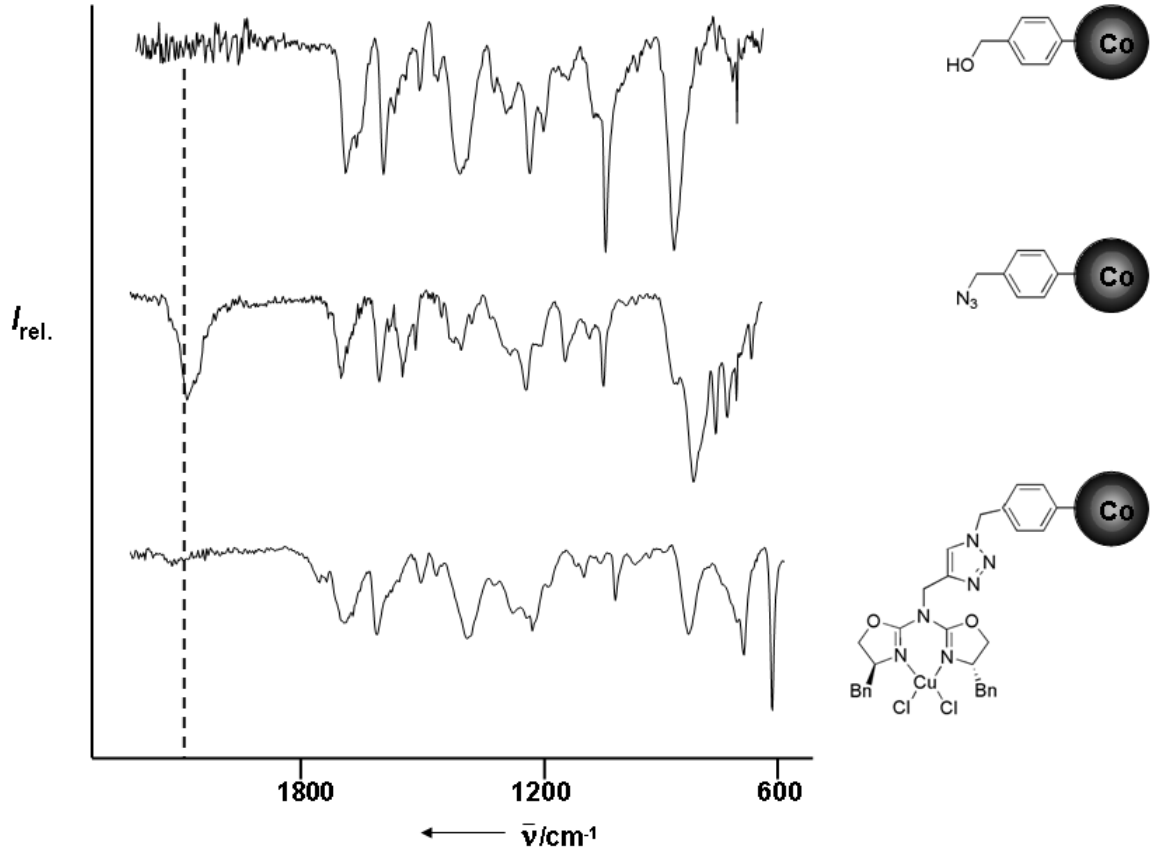

Figure 28. IR-spectra of Co/C powder after functionalization with phenylmethanol, (azidomethyl) benzene and after subsequent ”click”-reaction of the latter with propargylated azabis(oxazoline)-copper complex **120b**·$CuCl_2$.

2.5.2 Oxidation-catalysts immobilized on Co/C-nanoparticles

As mentioned afore, the ability of the shell to protect the metallic core material from oxygen is most crucial for the stability of such materials. In order to elucidate how efficiently the graphene layers are shielding the cobalt core, two different oxidation catalysts were anchored on the Co/C-nanoparticles and the condition of the nanocatalysts was examined after several consecutive oxidation reactions.

2.5.2.1 TEMPO immobilized on Co/C-nanoparticles

The selective oxidation of primary and secondary alcohols into the corresponding carbonyl compounds is one of the most important transformations in organic chemistry ever since.[43] Common reagents for these oxidation reactions are usually toxic chromium(VI) salts in stoichiometric amounts, which exhibits a severe

environmental issue.[44] Therefore, the development of systems using comparatively harmless oxidants such as oxygen, peroxide or hypochlorite seems worthwhile.[45]

The stoichiometric oxidation of primary alcohols to the corresponding aldehydes by the oxoammonium cation was first reported by Golubev and coworkers in 1965.[46] The oxoammonium cation could also be generated from TEMPO in-situ using single oxygen donors such as *m*-chloroperbenzoic acid,[47] sodium bromite,[48] persulfate,[49] and sodium hypochlorite.[50]

The stable nitroxyl radical 2,2,6,6- tetramethylpiperidine-1-oxyl (TEMPO) demonstrated benign properties such as low toxicity[51] and a reversible redox behaviour which motivated its application in combination with diverse primary oxidants. Examples of TEMPO-catalyzed reactions involved the oxidation of secondary alcohols into ketones with *m*-CPBA,[47] oxidation of primary, secondary and benzylic alcohols in an electrochemical process,[52] and the oxidation of allylic and benzylic alcohols to aldehydes by oxygen/CuCl.[53]

Especially the protocol developed 1987 by Anelli et al., using buffered household bleach at 0°C in combination with 10 mol% of sodium bromide and 1 mol% of 4-methoxy-TEMPO in dichloromethane/water is widely applied in organic synthesis.[54] Both, primary and secondary alcohols are converted to carbonyl compounds in high yields, even in large-scale operations. In addition, the oxidation of primary alcohols could be modified to give carboxylic acids by adding a phase-transfer catalyst to the biphasic system.[54b] Whichever oxidant was used, product isolation and catalyst recovery remained key issues. Although low catalyst concentrations are required (typically 1-2.5 mol%), TEMPO is quite expensive. Therefore, it is highly eligible to separate the catalyst after the oxidation reaction and reuse it. Hence, several groups have addressed this problem by anchoring TEMPO to solid supports such as different polymers,[55] silica,[56] or by entrapping TEMPO in a silica sol-gel.[57] TEMPO was even immobilized on thiol-protected gold nanoparticles utilizing a place-exchange reaction.[58] However, no nanoparticle support had proven to be stable under conditions required for the TEMPO mediated oxidation. In fact, initial studies revealed that AuMPCs (oxidation of thiols to disulfides) as well as silica coated magnetite particles (oxidation of iron(II) to iron(III)[59]) are affected under the reaction conditions used for TEMPO oxidations, although oxidation of magnetite to maghemite is not necessarily a disadvantage since both are ferrimagnetic.

However, cobalt nanoparticles were expected to be more stable under these conditions due to their protecting graphene layers. In contrast to the well studied behavior of the nitroxyl radical on silica surfaces,[56,57] no report had addressed its catalytic activity on carbon surfaces so far although examples of TEMPO grafted on carbon, i.e. fullerenes,[60] were known.

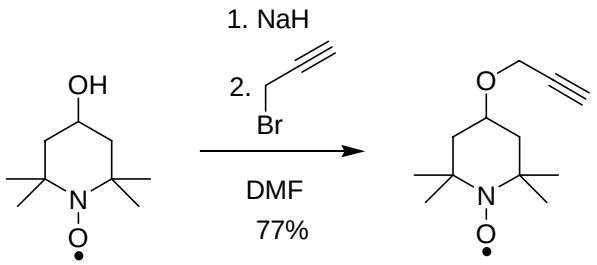

162 **163**

Scheme 59. Synthesis of propargyl ether TEMPO **163**.

To enable a "click"-reaction between the organocatalyst and azide-modified nanomagnet **157**, 4-hydroxy-TEMPO **163** was transformed into propargyl ether TEMPO **163** (Scheme 59).

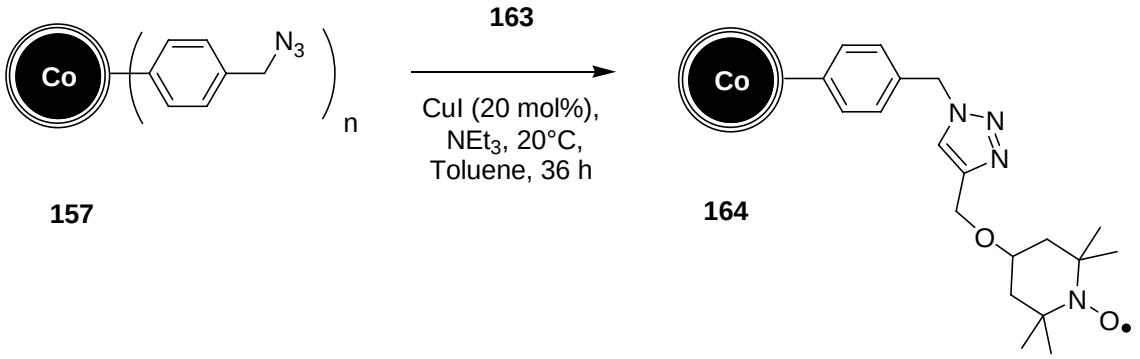

157 **164**

Scheme 60. Copper(I)-catalyzed "click"-reaction of (azidomethyl) benzene functionalized nanoparticles **157** with propargyl ether TEMPO **163**.

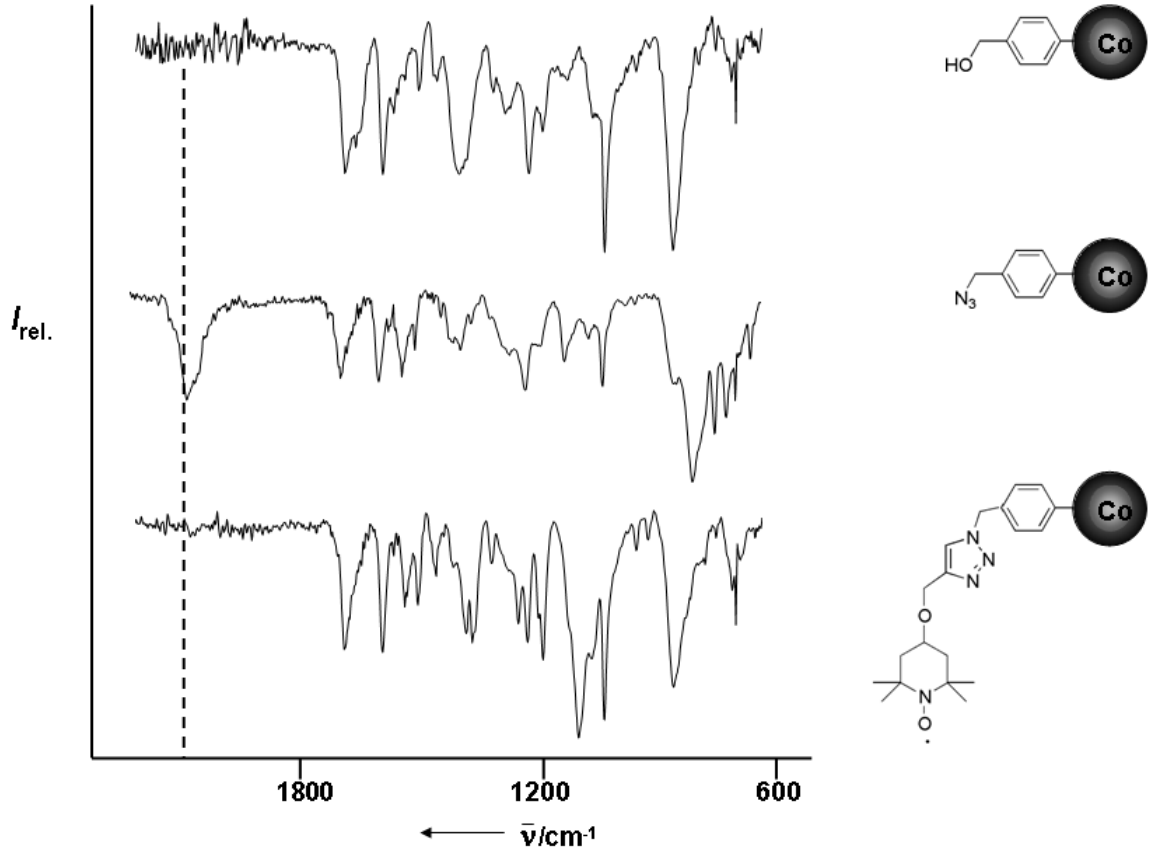

Figure 29. IR-spectra of Co/C powder after functionalization with phenylmethanol, (azidomethyl) benzene and after subsequent ”click”-reaction of the latter with propargyl ether TEMPO **163** respectively (top to bottom).

The grafting of the propargyl ether derivative of 4-hydroxy-TEMPO succeeded smoothly in the presence of catalytic amounts of CuI (Scheme 60) and was conveniently monitored by IR spectroscopy as described above (Figure 29). The oxidation of Cu(I) by TEMPO is seemingly not a problem.[61] In contrast to the protocol applied for the immobilization of azabis(oxazoline)-copper complexes, sonication in an ultrasound bath was used to keep the particles in dispersion. This strategy, which did not impede a quantitative course of the CuAAC reaction using 4-nitrophenylpropiolate, proved to be likewise successful. The heterogeneous CoNP-TEMPO was purified via magnetic decantation as described above. The as-prepared catalyst was envisaged to be an efficient promotor for the selective oxidation of alcohols to carbonyl compounds.

2.5.2.2 Co(II)-Schiff base complexes immobilized on Co/C-nanoparticles

Molecular oxygen is an abundant and ubiquitous oxidant. Since it was discovered that cobalt(II)-β-diketonate complexes allow trapping and activation of oxygen,[62] many Co(II)-based systems for the aerobic oxidation have been developed. Early examples were reported by Mukaiyama et al.[63] using Co(II)-bis(1,3-diketonato) complexes for the oxidation of secondary alcohols into the corresponding ketones [63a] or for the conversion of olefins to the hydrated products.[63b] In any case, the presence of an excess of secondary alcohol, which was stoichiometrically co-oxidized to the corresponding ketone, was crucial for the success of the reaction. The secondary alcohol could also be used as solvent. Furthermore, the authors concluded that water inhibits the catalytic activity of the cobalt(III) superoxide complexes[64] formed. Addition of molecular sieves had proven to be an efficient dehydrating method.[63a] However, especially the hydration of olefins resulted in a mixture of products, namely secondary alcohols, ketones and alkanes, thus limiting the synthetic value of the "oxidation-reduction hydration".[63b] Interestingly, Co(salen)-complexes were unsuitable catalyst in the presence of secondary alcohols.

Nevertheless, studies carried out by the same group showed that cobalt(II)-Schiff base complexes[65] are superior catalysts for the oxygenation of olefins into epoxides when cyclic ketones are used as reductants instead of secondary alcohols.[66] Further investigations by Iqbal and coworkers substantiated the versatility of these complexes in the epoxidation of olefins, oxidation of secondary alcohols and allylic as well as benzylic oxidations.[67] Isobutyraldehyde and cyclic ketoesters respectively were reported to be equally active reductants. Cobalt(II)-Schiff base complexes have been anchored on silica[68] and diverse polymers[69] applying different strategies and forming highly active and recyclable catalysts, which outperformed even their homogenous counterparts in means of activity and selectivity in some cases.[69e,h,i] Since carbon coated cobalt particles were expected to endure the oxidative conditions without alterations, their application as support seemed promising.

To this end, propargylated Schiff base **165b** was "clicked" onto azide functionalized Co/C-nanoparticles **157** (Scheme 61). Imine **165b** was accessed via Schiff-base reaction between salicylaldehyde and propargylated *L*-tyrosine derivative **167b** (Scheme 62).

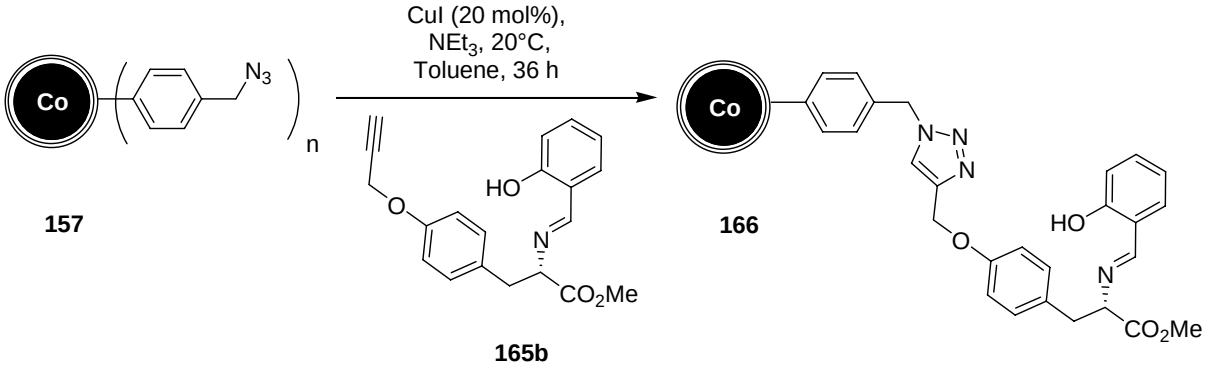

Scheme 61. Copper(I)-catalyzed "click"-reaction of (azidomethyl) benzene functionalized nanoparticles **157** with propargylated Schiff base **165b**.

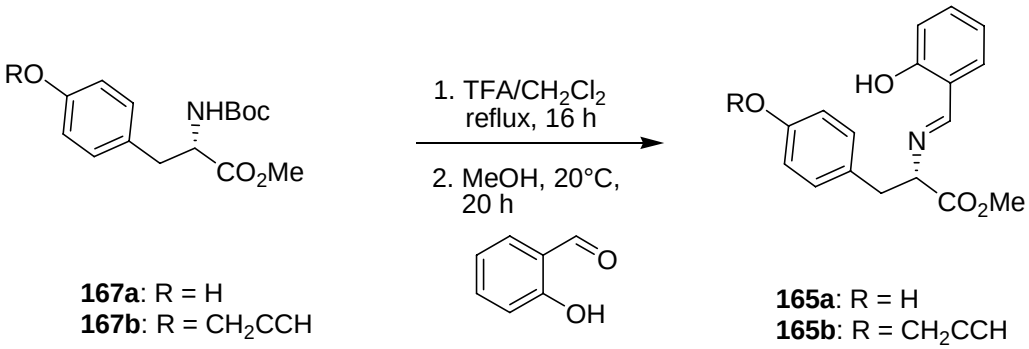

167a: R = H
167b: R = CH_2CCH

165a: R = H
165b: R = CH_2CCH

Scheme 62. Synthesis of different Schiff base ligands.

In analogy to previous reports,[69] it was attempted to form a cobalt(II)-Schiff base complex in-situ by agitating the nanoparticle linked imine **166** in an external magnetic field together with anhydrous $CoCl_2$ and ligand **165a** in dry acetonitrile (Scheme 63).

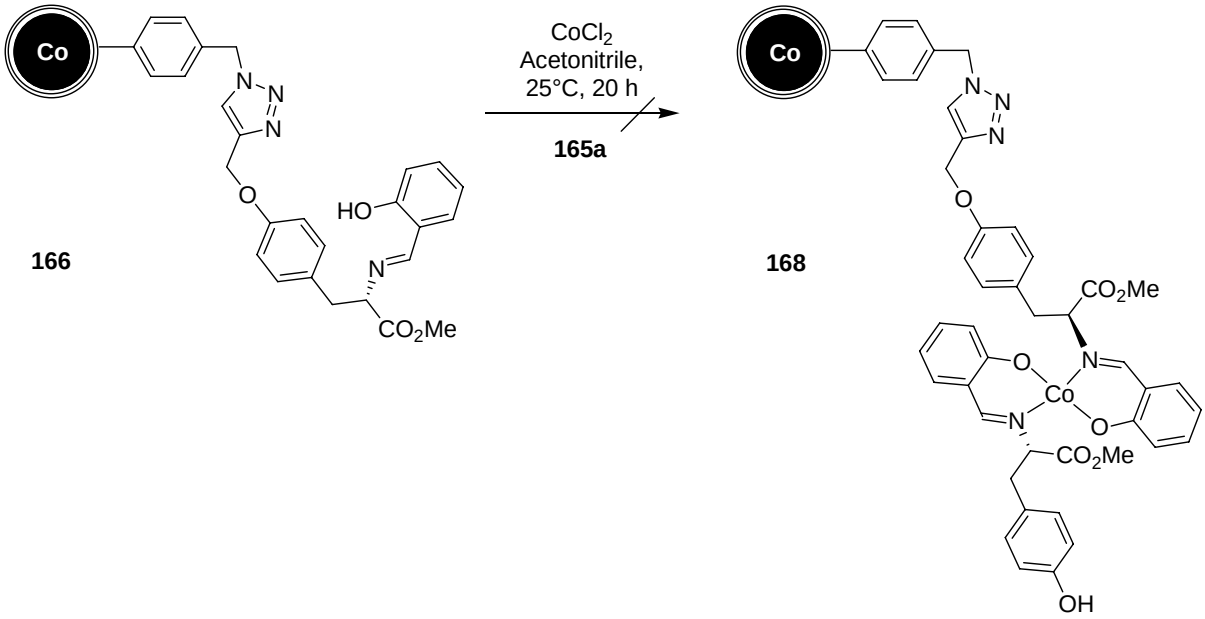

Scheme 63. Attempted synthesis of Co-NP immobilized Co(II)-Schiff base complex **168** via complexation of Co-NP grafted Schiff base **166** with $CoCl_2$ in the presence of **165a**.

Elemental microanalysis revealed that this protocol did not result in formation of the desired immobilized Co(II)-Schiff base complex **168**.

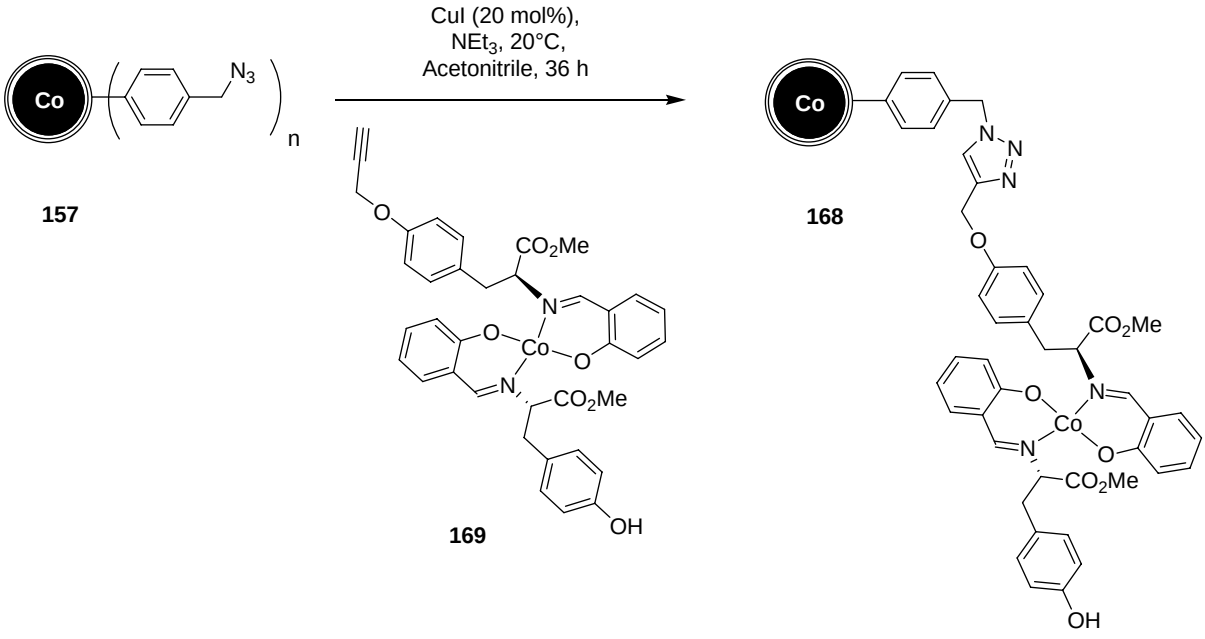

Scheme 64. Copper(I)-catalyzed "click"-reaction of (azidomethyl) benzene functionalized carbon coated cobalt nanoparticles **157** with propargylated Co(II)-Schiff-base complex **169**.

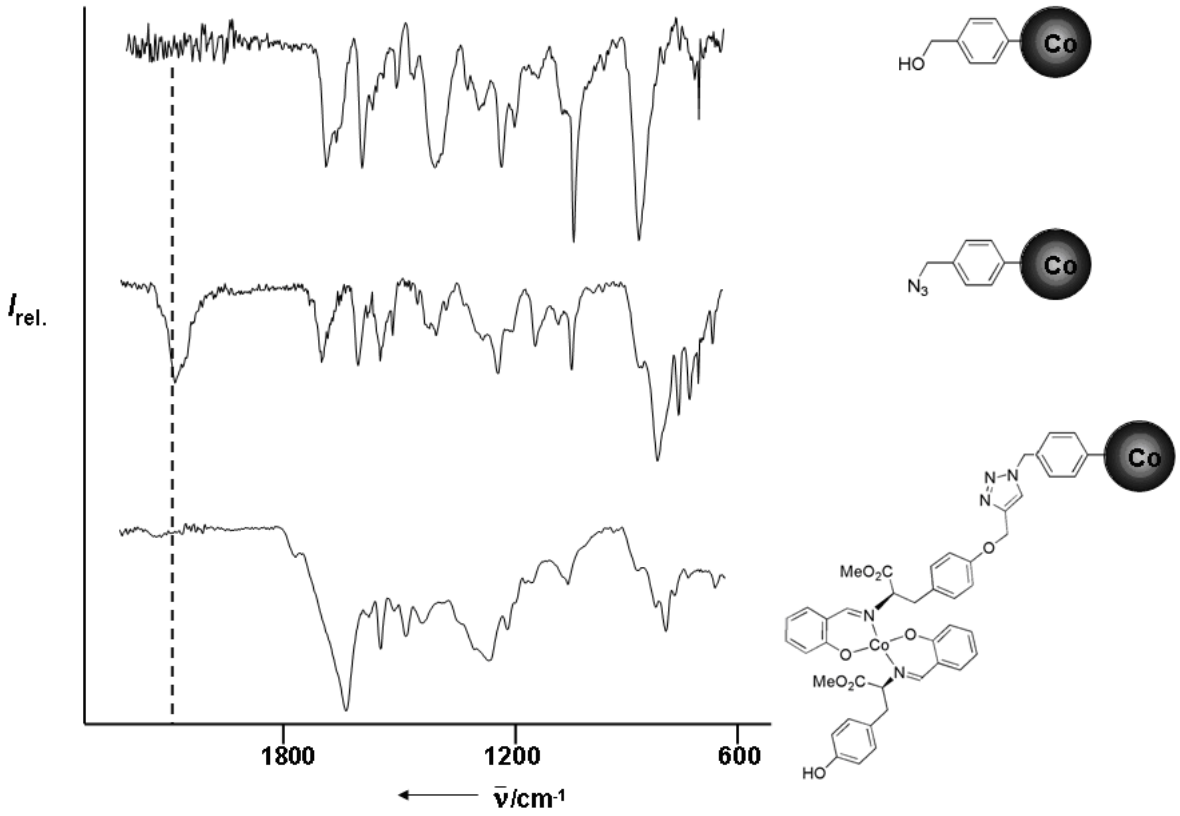

Figure 30. IR-spectra of Co/C powder after functionalization with phenylmethanol, (azidomethyl) benzene and after subsequent ”click”-reaction of the latter with Co(II)-Schiff-base complex **169** respectively (top to bottom).

Hence, the preformed complex **169** was applied in the CuAAC reaction instead, thus resulting in the depicted catalyst **168** (Scheme 64).

IR spectroscopy revealed that all azide moieties on the graphene layer underwent triazole formation in the presence of an excess (5 equiv.) of propargylated complex **169** (Figure 30). The loading was determined by elemental analysis und found to be in accordance with the one assessed via UV/vis spectroscopy using nitrophenolester derivatized particles **158**.

3. References

1 Huber, D. L. *Small* **2005**, *1*, 482.

2 Z. P. Xu, Q. H. Zeng, G. Q. Lu, A. B. Yu, *Chem. Eng. Sci.* **2006**, *61*,1027.

3 a) Y. M. Huh, Y. W. Jun, H. T. Song, S. Kim, J. S. Choi, J. H. Lee, S. Yoon, K. S. Kim, J. S. Shin, J. S. Suh, J. Cheon, *J. Am. Chem. Soc.* **2005**, *127*, 12387; b) H. T. Song, J. S. Choi, Y. M. Huh, S. Kim, Y. W. Jun, J. S. Suh, J. Cheon, *J. Am. Chem*. *Soc*. **2005**, *127*, 9992.

4 a) S. Benderbous, C. Corot, P. Jacobs, B. Bonnemain, *Acad. Radiol.* **1996**, *3*, 292; b) Q. A. Pankhurst, *BT Technology J.* **2006**, *24*, 33; c) P. Tartaj, M. P. Morales, S. Veintemillas-Verdaguer, T. Gonzalez-Carreco, C. J. Serna, *J. Phys. D* **2003**, *36*, 182.

5 Review: J. Fan, Y. Gao, *J. Exp. Nanosc*. **2006**, *1*, 457.

6 a) T.-J. Yoon, W. Lee, Y.-S. Oh, J.-K. Lee, *New J. Chem*. **2003**, *27*, 227; b) A.-H. Lu, W. Schmidt, N. Matoussevitch, H. B. Gönnemann, B. Spliethoff, B. Tesche, E. Bill, W. Kiefer, F. Schüth, *Angew. Chem.* **2004**, *116*, 4403; *Angew. Chem. Int. Ed*. **2004**, *43*, 4303; c) H. M. R. Gardimalla, D. Mandal, P. D. Stevens, M. Yen, Y. Gao, *Chem. Commun.* **2005**, 4432; d) A. Hu, G. T. Yee, W. Lin, *J. Am. Chem. Soc.* **2005**, *127*, 12486; e) P. D. Stevens, J. Fan, H. M. R. Gardimalla, M. Yen, T. Gao, *Org. Lett.* **2005**, *7*, 2085; f) Y. Zheng, P. D. Stevens, Y. Gao, J. Org. Chem. **2006**, *71*, 537; g) D. Lee, J. Lee, H. Lee, S. Jin, T. Hyeon, B. M. Kim, *Adv. Synth. Catal*. **2006**, *348*, 41; h) R. Abu-Reziq, H. Alper, D. Wang, M. L. Post, *J. Am. Chem. Soc.* **2006**, *128*, 5279.

7 D. K. Yi, S. S. Lee, J. Y. Ying, *Chem. Mater.* **2006**, *18*, 2459.

8 a) D. Stevens, G. Li, J. Fan, M. Yenb, Y. Gao, *Chem. Commun.* **2005**, 4435; b) G. Lu, W. Mai, R. Jin, L. Gao, *Synlett* **2008**, *9*, 1418.

9 C. A. Dalaigh, S. A. Corr, Y. Gun`ko, S. J. Connon, *Angew. Chem. Int. Ed*. **2007**, *119*, 4407.

10 Reviews: a) M. Benaglia, A. Puglisi, F. Cozzi, *Chem. Rev.* **2003**, *103*, 3401; b) F. Cozzi, *Adv. Synth. Catal.* **2006**, *348*, 1367.

11 a) Y. Lu, Y. Yin, B. T. Mayers, Y. Xia, Nano Lett. **2002**, *2*, 183; b) D. K. Yi, S. S. Lee, J. Y. Ying, *Chem.Mater .* **2006**, *18*, 2459; c) D. K. Yi, S. S. Lee, G. C. Papaefthymiou, J. Y. Ying, *Chem. Mater.* **2006**, *18*, 614; d) D. C. Lee, F. V. Mikulec, J. M. Pelaez, B. Koo, B. A. Korgel, *J. Phys. Chem. B* **2006**, *110*, 11160; d) C. R. Vestal, Z. J. Zhang, *Nano Lett.* **2003**, *3*, 1739; e) T.-J. Yoon, K. N. Yu, E. Kim, J. S. Kim, B. G. Kim, S.-H. Yun, B.-H. Sohn, M.-H. Cho, J.-K. Lee, S. B. Park, *Small* **2006**, *2*, 209.

12 J. Lee, Y. Lee, J. K. Youn, H. B. Na, T. Yu, H. Kim, S. M. Lee, Y. M. Koo, J. H. Kwak, H. G. Park, H. N. Chang, M. Hwang, J. G. Park, J. Kim, T. Hyeon, *Small* **2008**, *4*, 143.

13 A. Corma, H. García, A. Moussaif, M. J. Sabater, R. Zniber, A. Redouane, *Chem. Commun.* **2002**, 1058.

14 S. S. Lee, S. Hadinoto, J. Y. Ying, *Adv. Synth. Catal.* **2006**, *348*, 1248.

15 J. Lim, S. N. Riduan, S. S. Lee, J. Y. Ying, *Adv. Synth. Catal.* **2008**, *350*, 1295.

16 J. K. Park, S.-W. Kim,. T. Hyeonb, B. M. Kima, *Tetrahedron: Asymmetry* **2001**, *12*, 2931.

17 a) C. W. Tornøe, M. Meldal, *In American Peptide Symposium;* M. Lebl, R. A. Houghten, Eds, American Peptide Society and Kluwer Academic Publishers: San Diego, CA, **2001**, p 263; b) V. V.

Rostovtsev, L. G. Green, V. V. Fokin, K. B. Sharpless, *Angew. Chem. Int. Ed*. **2002**, *41*, 2596; c) C. W. Tornøe, C. Christensen, M. Meldal, *J. Org. Chem*. **2002**, *67*, 3057.

18 R. Huisgen, *Pure Appl. Chem.* **1989**, *61*, 613.

19 *cf*. T. Belser, M. Stöhr, A. Pfaltz, *J. Am. Chem. Soc*. **2005**, *127*, 8720.

20 S. Sun, H. Zeng, *J. Am. Chem. Soc*. **2002**, *124*, 8204.

21 H. Bönnemann, W. Brijoux, R. Brinkmann, N. Matoussevitch, N. Waldoefner, N. Palina, H. Modrow, *Inorg. Chim. Acta.* **2003**, *350*, 617.

22 Y. Kobayashi, M. Horie, M. Konno, B. Rodriguez-Gonzalez, L. M. Liz-Marzan, *J. Phys. Chem. B* **2003**, *107*, 7420.

23 a) N. S. Sobal, M. Hilgendorff, H. Moehwald, M. Giersig, M. Spasova, T. Radetic, M. Farle, *Nano Lett.* **2002**, *2*, 621; b) M. Chen, S. Yamamuro, D. Farrell, S. A. Majetich, *J. Appl. Phys.* **2003**, *93*, 7551.

24 a) A.-H. Lu, W. Li, N. Matoussevitch, B. Spliethoff, H. B. Pennemann, F. Schüth, *Chem. Commun.* **2005**, 98; b) M. Chen, S. Yamamuro, D. Farrell, S. A. Majetich, *J. Appl. Phys.* **2003**, *93*, 7551.

25 a) L. E. Euliss, S. G. Grancharov, S. O`Brien, T. J. Deming, G. D. Stucky, C. B. Murray, G. A. Held, *Nano Lett*. **2003**, *3*, 1489; b) X. Liu, Y. Guan, Z. Ma, H. Liu, *Langmuir* **2004**, *20*, 10278; c) R. Hong, N. O. Fischer, T. Emrick, V. M. Rotello, *Chem. Mater.* **2005**, *17*, 4617; d) Y. Sahoo, H. Pizem, T. Fried, D. Golodnitsky, L. Burstein, C. N. Sukenik, G. Markovich, *Langmuir* **2001**, *17*, 7907; e) M. Kim, Y. Chen, Y. Liu, X. Peng, *Adv. Mater.* **2005**, *17*, 1429.

26 F. Michalek, A. Lagunas, C. Jimeno, M. A. Pericàs, *J. Mater. Chem*. **2008**, *18*, 4692.

27 Z. Lu, M. D. Prouty, Z. Guo, V. O. Golub, C. S. S. R. Kumar, Y. M. Luov, *Langmuir* **2005**, *21*, 2042.

28 L. M. Liz-Marzàn, M. Giersig, P. Mulvaney, *Chem. Commun.* **1996**, 731.

29 A. H. Lu, E. L. Salabas, F. Schüth, *Angew. Chem.* **2007**, *119*, 1242; *Angew. Chem. Int. Ed.* **2007**, *46*, 1222.

30 a) Y. Saito, *Carbon* **1995**, *33*, 979; b) J. H. J. Scott, S. A. Majetich *Phys. Rev. B* **1995**, 52, 12564; c) J. Jiao, S. Seraphin, X. Wang, J. C. Withers, *J. Appl. Phys.* **1996**, *80*, 103.

31 a) Z. H. Wang, C. J. Choi, B. K. Kim J. C. Kim, Z. D. Zhang, *Carbon* **2003**, *41*, 1751; b) E. Flahaut, F. Agnoli, J. Sloan, C. O'Connor, M. L. H. Green, *Chem. Mater.* **2002**, *14*, 2553.

32 a) Y. Lu, Z. Zhu Z. Liu, *Carbon* **2005**, *43*, 36; b) N. Sano, H. Akazawa, T. Kikuchi, T. Kanki *Carbon* **2003**, *41*, 2159; c) J. Nishijo, C. Okabe, O. Oishi, N. Nishi, *Carbon* **2006**, *44*, 2943.

33 R. N. Grass, E. K. Athanassiou, W. J. Stark, *Angew. Chem.* **2007**, *119*, 4996.

34 W. J. Stark, L. Madler, M. Maciejewski, S. E. Pratsinis, A. Baiker, *Chem. Commun.* **2003**, 588.

35 a) M. Delamar, R. Hitmi, J. Pinson, J.-M. Savéant, *J. Am. Chem. Soc*. **1992**, *114*, 5883; b) R. Hitmi, J. Pinson, J.-M. Savéant, Fr. Pat. 91 011172; c) C. Bourdillon, C. Demaille, R. Hitmi, J. Moiroux, J. Pinson, *J. Electroanal. Chem*. **1992**, *336*, 113; d) P. Allongue, M. Delamar, B. Desbat, O. Fagebaume, R. Hitmi, J. Pinson, J.-M. Savéant, *J. Am. Chem. Soc.* **1997**, *119*, 201.

36 a) R. W. Murray, *Electroanalytical Chemistry*; A. J. Bard, Ed.; Marcel Dekker: New York, **1984**; Vol. 13, pp 191-368; b) H. P. Boehm, *Angew. Chem., Int. Ed. Engl*. **1966**, *5*, 533; c) J. P. Randin, In *Encyclopedia of the Electrochemistry of the Elements*; A. J. Bard, Ed.; Marcel Dekker: New York, **1976**; Vol. 7, p 22; d) J. O. Besenhard, H. P. Fritz, *Angew. Chem., Int. Ed. Engl*. **1983**, *22*,

950; e) J. O. Besenhard, J. Jakob, U. Krebber, P. Möller, R. F. Sauter, A. Kurtze, N. Kanani, H. Meyer, J. K. H. Hörber, A. D. Z. Jannakoudakis, *Naturforsch*. **1989**, *44*, 729.

37 a) P. Allongue, M. Delamar, B. Desbat, O. Fagebaume, R. Hitmi, J. Pinson, J.-M. Savéant, *J. Am. Chem. Soc.* **1997**, *119*, 201; b) C. A. Dyke, J. M. Tour, *J. Am. Chem. Soc.* **2003**, *125*, 1156; c) H. Uetsuka, D. Shin, N. Tokuda, K. Saeki, C. E. Nebel, *Langmuir* **2007**, *23*, 3466.

38 Henry de Villeneuve, C.; Pinson, J.; Allongue, P *J. Phys. Chem. B* **1997**,*101*, 2415.

39 a) A. Adenier, M.-C. Bernard, M. M. Chehimi, E. Deliry, B. Desbat, O. Fagebaume, J. Pinson, F. Podvorica, *J. Am. Chem. Soc.* **2001**, *123*, 4541; b) A. Laforgue, T. Addou, D. Bélanger, *Langmuir* **2005**, *21*, 6855; c) M.-C. Bernard, A. Chausse, E. Cabet-Deliry, M. M. Chehimi, J. Pinson, F. Podvorica, C. Vautrin-Ul, *Chem. Mater.* **2003**, *15*, 3450; d) S. Maldonado, T. J. Smith, R. D. Williams, S. Morin, E. Barton, K. J. Stevenson, *Langmuir* **2006**, *22*, 2884; e) C. Combellas, F. Kanoufi, J. Pinson, F. I. Podvorica, *J. Am. Chem. Soc.* **2008**, *130*, 8576.

40 F. Mirkhalaf, J. Paprotny, D. J. Schiffrin, *J. Am. Chem. Soc.* **2006**, *128*, 7400.

41 a) D.-E. Jiang, B. G. Sumpter, S. Dai, *J. Am. Chem. Soc.* **2006**, *128*, 6030; b) D.-E. Jiang, B. G. Sumpter, S. Dai, *J. Phys. Chem. B* **2006**,*110*, 23628.

42 Kamegawa, K.; Yoshida, H. Bull. *Chem. Soc. Jpn.* **1990**, *63*, 3683.

43 M. Hudlicky, *Oxidations in Organic Chemistry*, American Chemical Society, Washington, DC, **1990**.

44 F. A. Luzzio, *Org. React*. **1998**, *53,* 1.

45 a) P. Anastas, M. Kirchhoff, *Acc. Chem. Res.* **2002**, *35*, 686; b) R. Sheldon, I. Arends, G. J. Brink, A. Dijksman, *Acc. Chem. Res.* **2002**, *35*, 774.

46 V. A. Golubev, E. G. Rozantsev, M. B. Neiman, *Bull. Acad. Sci. USSR, Chem. Ser.* **1965**, *14*, 1898.

47 a) J. A. Cella, J. A. Kelley, E. F. Kenehan, *J. Org. Chem.* **1975**, *40*, 1850; b) S. D. Rychovsky, R. Vaidyanathan, *J. Org. Chem*. **1999**, *64*, 310.

48 D. H. Hunter, D. H. R. Barton, W. B. Motherwell, *Tetrahedron Lett.* **1984**, *25*, 603.

49 C. Bolm, A. S. Magnus, J. P. Hildebrand, *Org. Lett*. **2000**, *2*, 1173.

50 a) P. L. Anelli, C. Biffi, F. Montanari, S. Quici, *J. Org. Chem*. **1987**, *52*, 2559; b) P. L. Anelli, S. Banfi, F. Montanari, S. Quici, *J. Org. Chem*. **1989**, *54*, 2970; c) P. L. Anelli, F. Montanari, S. Quici, *Org. Synth*. **1990**, *69*, 212.

51 LD_{50} (oral, rat, 4-hydroxy-TEMPO) = 1053 mg kg^{-1}; CAS database.

52 M. F. Semmelhack, C. S. Chou, D. A. Cortes, *J. Am.Chem. Soc.* **1983**, *105*, 4492.

53 M. F. Semmelhack, C. R. Schmid, D. A. Cortes, C. S. Chou, *J. Am. Chem. Soc.* **1984**, *106*, 3374.

54 a) P. L. Anelli, C. Biffi, F. Montanari, S. Quici, *J. Org. Chem*. **1987**, *52*, 2559; b) P. L. Anelli, S. Banfi, F. Montanari, S. Quici, *J. Org. Chem*. **1989**, *54*, 2970; c) P. L. Anelli, F. Montanari, S. Quici, *Org. Synth*. **1990**, *69*, 212.

55 a) A. Dijksman, I. W. Arends, R. A. Sheldon, *Chem. Commun.* **2000**, 271; b) A. Dijksman, I. W. Arends, R. A. Sheldon, *Synlett* **2001**, 102; c) P. Ferreira, W. Hayes, E. Phillips, D. Rippon, S. C. Tsang, *Green Chemistry* **2004**, *6*, 310; d) G. Pozzi, M. Cavazzini, S. Quici, M. Benaglia, G. Dell'Anna, *Org. Lett.* **2004***, 6*, 441; e) A. Gheorghe, A. Matsuno, O. Reiser, *Adv. Synth. Catal.* **2006**, *348*, 1016.

56 a) C. Bolm, T. Fey, *Chem. Commun.* **1999**, 1795; b) T. Fey, H. Fischer, S. Bachmann, K. Albert, C. Bolm, *J. Org. Chem*. **2001**, *66*, 8154; c) D. Brunel, P. Lentz, P. Sutra, B. Deroide, F. Fajula, J. B. Nagy, *Stud. Surf. Sci. Catal.* **1999**, *125*, 237.

57 a) R. Ciriminna, J. Blum, D. Avnis, M. Pagliaro, *Chem. Commun.* **2000**, 1441; b) R. Ciriminna, M. Pagliaro, *Adv. Synth. Catal.* **2002**, *344*, 159.

58 K. Hata, H. Fujihara, *Chem. Commun*. **2002**, 2714.

59 *cf*. a) F. Vereda, J. de Vicente, M. del Puerto Morales, F. Rull, R. Hidalgo-Alvarez, *J. Phys. Chem. C.* **2008**, *112*, 5843; b) Y-k. Sun, M. Ma, Y. Zhang, N. Gu, *Coll. Surf. A* **2004**, *245*, 15.

60 T. Ishida, T. Shinozuka, M. Kubota, M. Ohashi, T. Nogami, *Tetrahedron* **1996**, *52*, 5103.

61 a) A. Gheorghe, A. Matsuno, O. Reiser, *Adv. Synth. Catal.* **2006**, *348*, 1016; b) A. Gheorghe, E. Cuevas-Yañez, J. Horn, W. Bannwarth, B. Narsaiah, O. Reiser, *Synlett* **2006**, 2767.

62 E. P. Talsi, Y. S. Zimin, V. M. Nekipelov, *React. Kinet. Catal. Lett.* **1985**, *27*, 361.

63 a) T. Yamada, T. Mukaiyama, *Chem. Lett.* **1989**, 519; b) K. Kato, T. Yamada, T. Takai, S. Inoki, S. Isayama, *Bull. Chem. Soc. Jpn.* **1990**, *63*, 179; c) S. Inoki, T. Mukaiyama, *Chem. Lett.* **1990**, 67.

64 A. L. Crumbliss, F. J. Basolo, *J. Am. Chem. Soc.* **1970**, *92*, 55.

65 a) D. E. Hamilton, R. S. Drago, A. Zombeck, *J. Am. Chem. Soc.* **1987**, *109*, 374; b) B. B. Corden, R. S. Drago, R. P. Perito, *J. Am. Chem. Soc.* **1985**, *107*, 2903.

66 T. Takai, E. Hata, K. Yorozu, T. Mukaiyama, *Chem. Lett.* **1992**, 2077.

67 a) T. Punniyamurthy, J. Iqbal, *Tetrahedron Lett.* **1994**, *35*, 4003; b) S. J. S. Singh Kaira, T. Punniyamurthy, J. Iqbal, *Tetrahedron Lett.* **1994**, *35*, 4847; c) G. C. Maikap, D. Guhathakurta, J. Iqbal, *Synlett* **1995**, 189; d) T. Punniyamurthy, B. Bhatia, M. M. Reddy, G. C. Maikap, J. Iqbal, *Tetrahedron*, **1997**, *53*, 7649.

68 A. Kumar, G. S. Mishra, A. Kumar, *Transition Metal Chem.* **2003**, *28*, 913.

69 a) K. C. Gupta, H. K. Abdulkadir, S. Chand, *J. Appl. Polym. Sci.* **2003**, *90*, 1398; b) K. C. Gupta, H. K. Abdulkadir, S. Chand, *J. Mol. Catal. A* **2003**, *202*, 253; c) A. Syamal, M. M. Singh, D. Kumar, *React. Funct. Polym.* **1999**, *39*, 27; d) S. Kulkarni, M. Alurkar, A. Kumar, *Appl. Catal. A* **1996**, 142, 243; e) K. C. Gupta, A. K. Sutar, *J. Mol. Catal. A* **2007**, *272*, 64; f) R. M. Wang, C. J. Hao, Y. F. He, Y. P. Wang, C. G. Xia, *Polym. Adv. Technol.* **2002**, *13*, 6; g) R. M. Wang, C. J. Hao, Y. F. He, Y. P. Wang, C. G. Xia, *J. Macromol. Sci.* **2002**, *39*, 1361; h) R. S. Drago, J. Gaul, A. Zombeck, D.-K. Straub, *J. Am. Chem. Soc.* **1980**, *102*, 1033; i) S. Jain, O. Reiser, *ChemSusChem* **2001**, *1*, 534.

III. Catalysis

1. Asymmetric catalysis with azabis(oxazolines)

If it comes to the application of “heterogenized” organometallic catalysts, a distinction can be drawn whether preformed complexes are anchored on the support or catalysts are prepared in-situ via complexation of the scaffold-grafted ligand with metal salt. Either approach was employed but the latter needs to be discussed in detail under the aspect of recent studies by Reiser et al.[1] focussing on the importance of ligand/metal-ratio in asymmetric catalysis.

1.1 Significance of ligand/metal-ratio

The determination of the optimum ligand/metal ratio has been an issue in many pioneering works in the field of asymmetric catalysis with chiral oxazoline ligands. An early example was reported by Brunner and co-workers[2] demonstrating that in general the rhodium/ligand ratio in the enantioselective hydrosilylation of acetophenone with $[Rh(COD)Cl]_2$ using pyridineoxazoline ligands as cocatalysts is crucial for asymmetric induction. An excess of rhodium was found to be as detrimental as an equimolar ratio of ligand to metal whereas a fivefold ligand surplus proved to give best optical induction. The same group showed that the $Cu(OAc)_2$-catalyzed monophenylation of meso-diols with $Ph_3Bi(OAc)_2$ can be rendered enantioselective with an even higher excess of pyridineoxazoline.[3] Indeed, it appears reasonable to assume that at least a small excess of ligand is required in order to suppress a background reaction promoted by ligand-free and therefore unselective metal centers. Consequently, a slight excess of ligand was applied in various asymmetric catalyses ever since. Evans[4] and Pfaltz[5] have developed highly enantio-selective processes for the copper(I)-catalyzed cyclopropanation of olefins utilizing bis(oxazolines) and semicorrines respectively in small overspill, the latter also applied at a ligand/copper ratio of 2 but accompanied by a diminutive loss of selectivity. The same ligands proved to be very efficient in palladium-catalyzed allylic alkylations at a ligand/Pd ratio of 1.25.[5b]

However, the stereoelectronic outcome of the asymmetric monobenzoylation of 1,2-diols was found to be affected neither by a slight excess of copper(II) nor bis(oxazoline) ligand.[6] This made the kinetic resolution of vicinal diols highly interesting for catalysis with any immobilized ligand, since the ligand/metal-ratio can

not be adjusted that accurately as it is possible in homogeneous catalysis. Therefore, it seemed reasonable to examine the efficacy of the novel nanoparticle supported catalysts first with such an unpretentious reaction.

1.2 Asymmetric monobenzoylation of racemic 1,2-diols

Asymmetric acylations using enzymes are possible with a broad range of substrates and include the desymmetrization or kinetic resolution of alcohols.[7] Such highly enantioselective transformations are also possible with transition-metal- or organocatalysts. For instance, Matsumura et al. developed a protocol for the kinetic resolution of vicinal 1,2-diols via asymmetric benzoylation using bis(oxazoline)-copper(II) complexes.[8] The monobenzoylated product was obtained in 49% yield (theoretical maximum: 50%) and in >99% enantioselectivity (Scheme 61).

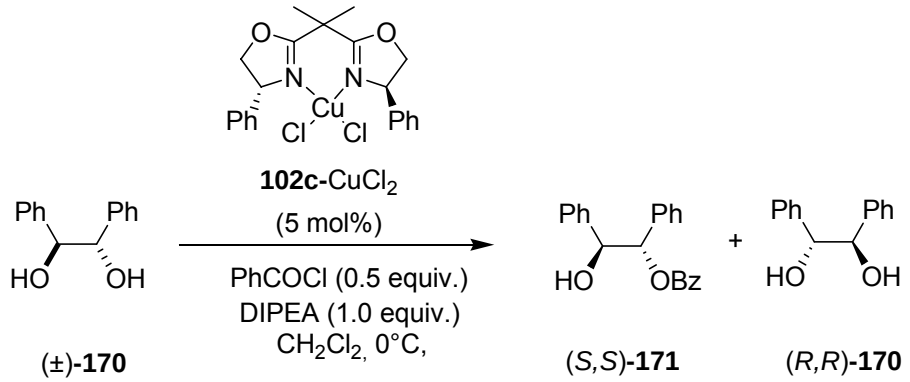

Scheme 61. Kinetic resolution of racemic diol **170** through asymmetric benzoylation.[8]

The authors suggested that coordination of one enantiomer of 1,2-diol **170** should result in the formation of product **171,** depending on which chiral environment is provided by the copper-bis(oxazoline) catalyst. A complex of type **B** forms, in which **170** is prone to the attack of a weak base. The metal-alkoxide complex **C** can be trapped with the electrophile **172**. Provided that the copper-bis(oxazoline) complex is regenerated after the formation of an acylated product **171**, a catalytic cycle concerning **A** is completed (Scheme 62).

The enantiodiscrimination in the kinetic resolution of (±)-**170** was explained with a shielding of the copper center against the electrophile **172** as depicted for complex **D** (Figure 29, left). If one enantiomer of **170** and the chiral bis(oxazoline) **102c** match in a fashion that allows the attack of benzoylchloride **172**, a transition state of type **E** is

formed (Figure 29, right). The benzoylated product **171** would result from such a transition state.

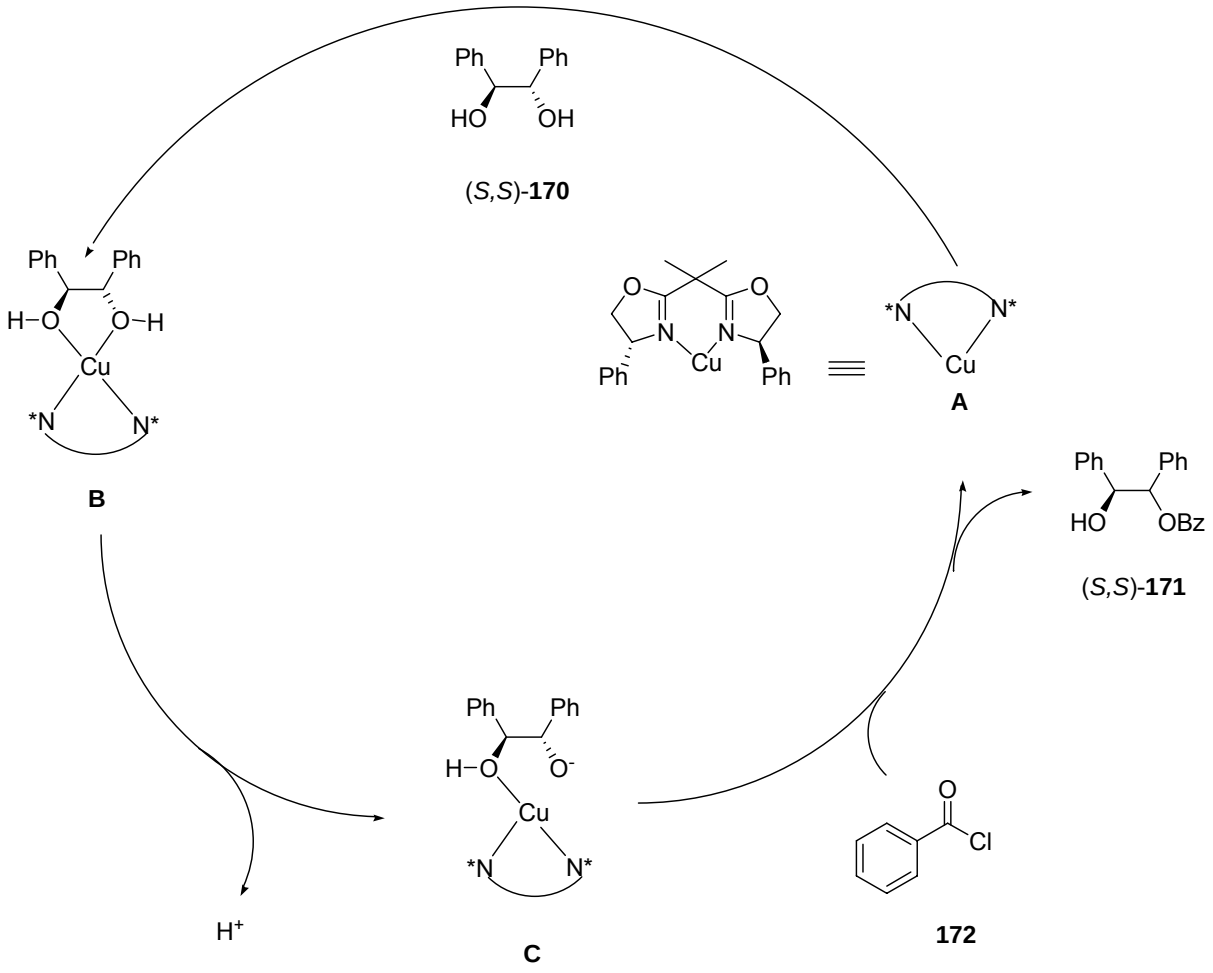

Scheme 62. Catalytic cycle as proposed by Matsumura et al.[8]

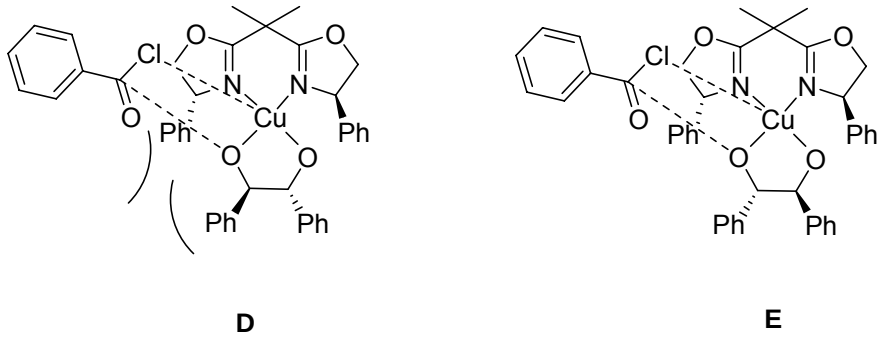

Figure 29. Schematic representation of unfavoured transition state **D** (left) and favoured transition state **E** (right).

1.2.1 Asymmetric monobenzoylation with homogeneous and polymer-supported azabis(oxazolines)

The concept discussed above was successfully coined on azabis(oxazolines).[9] Benzyl substituted AzaBOX **109d** had proven to be the most selective (entry 1, Table 3) in the asymmetric benzoylation of (±)-**170**. The isolated yield of 49% thus obtained was close to the maximum yield attainable in the desymmetrization of the 1,2-diol and could be achieved even at an extremely low catalyst concentration (0.5 mol%). Whereas methylation of the central nitrogen bridge was required for excellent selectivities, a triazole moiety has proven to be less favourable in this position, leading to diminished ee values for the homogeneous ligand **173** (entry 2). The slightly detrimental effect of the triazole has to be accepted when a copper(I)-catalyzed azide/alkyne cycloaddition is used as tagging method for polymeric supports. However, the drop in selectivity and activity for polymer supported catalysts **174** and **175** was much more severe.[10] The poor performance of polystyrene grafted AzaBOX **174** can be explained to some extent with the reaction temperature. Since it was not feasible to stir the reaction mixture at 0°C, mechanical agitation at room temperature was applied instead. However, the decrease in enantioselectivity is that more grave compared to selectivities observed for the homogeneous derivative **173**, thus it was reasoned that the slightly detrimental effect of the triazole is not the primary cause for this drop. More likely, uncomplexed coppersalt was retained in the polymer backbone from either the copper(I)-catalyzed azide/alkyne cycloaddition or the complexation reaction. Both polymers were subjected to several extraction cycles with aqueous EDTA-solution after the CuAAC-reaction, therefore any free coppersalt might more likely derive from uncomplexed $CuCl_2$. For the soluble MeOPEG supported catalyst **175**, copper(II)chloride was filtered off after stirring for one hour at room temperature and the catalyst was recovered by recrystallization from Et_2O. In the case of the heterogeneous catalyst supported on Merrifield resin **174**, coppersalt was removed by copious washing with methanol. However, selectivities faded for both polymer supported catalysts **174** and **175** upon recycling already in the second run (entries 3-6, Table 3).

Table 3. Cu(II)-catalyzed benzoylation of (±)-**170** in the presence of various immobilized and non-immobilized azabis(oxazoline) ligands.[a]

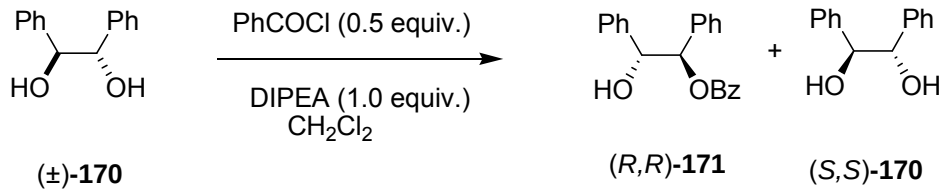

(±)-**170** (*R*,*R*)-**171** (*S*,*S*)-**170**

entry	catalyst (mol%)	run	yield (%)[b]	ee (%)[c]	s[d]
1[e]	**109d**·$CuCl_2$ (0.5)	1	49	>99	>751
2	**173**·$CuCl_2$ (1.0)	1	47	93	71
3[f], [g]	**174**·$CuCl_2$ (5.0)	1	31	67	7
4[f], [g]	**174**·$CuCl_2$ (5.0)	2	35	56	5
5[f], [h]	**175**·$CuCl_2$ (5.0)	1	36	82	16
6[f], [h]	**175**·$CuCl_2$ (5.0)	2	43	62	7

[a] Reagents and conditions: dl-Diol (1 mmol), benzoylchloride (0.5 mmol), DIPEA (1 mmol), 0°C, 3 h, CH_2Cl_2. [b] Yield of isolated product **171**. [c] Determined by chiral HPLC. [d] Ref.[11] [e] Taken from Ref.[9] [f] Taken from Ref.[10] [g] 6h, 25°C. [h] 6h.

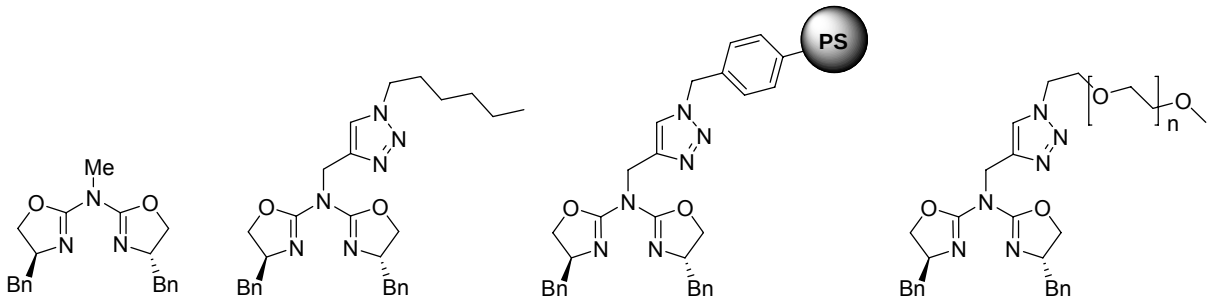

109d **173** **174** **175**

Figure 30. Immobilized and non-immobilized azabis(oxazoline) ligands **109d** and **173-175** used in the Cu(II)-catalyzed monobenzoylation.

1.2.2 Asymmetric monobenzoylation with azabis(oxazolines) supported on magnetite@silica-nanoparticles

1.2.2.1 In-situ prepared Fe_3O_4@SiO_2@AzaBOX·$Cu(OTf)_2$-catalyst

Uncomplexed Cu(II) is potentially the biggest disturbing factor in this reaction, hence complexation of magnetite@silica supported azabis(oxazolines) **144** and **146** was carried out with 2.0 equivalents of $Cu(OTf)_2$ in respect to azabis(oxazoline) as a copper source being soluble in dichloromethane. After stirring at ambient temperature, the excess of $Cu(OTf)_2$ in the supernatant can be easily eliminated via repeated magnetic decantation. $CuCl_2$ is insoluble in CH_2Cl_2 and uncomplexed coppersalt therefore more difficult to separate. In a heterogeneous dispersion of nanopowder, the removal of insoluble metalsalt is naturally less feasible than in the case of a soluble support such as MeOPEG. Washing with a coordinating solvent like MeOH, as applied for polystyrene supported catalyst **174**, appears to be suboptimal having the catalytic results in mind (entries 3 and 4, Table 3). On the other hand, coordination of surface silanol groups to coppersalt is not expected to give any problems due to the TMS-postcapping.[12] Indeed, selectivities of in-situ prepared catalysts **144**·$Cu(OTf)_2$ and **146**·$Cu(OTf)_2$ exceeded those obtained with their polymeric counterparts by far and were even able to measure up with enantioselectivities achieved with homogeneous catalysts **109d**·$CuCl_2$ and **173**·$CuCl_2$ (entries 1 and 2, Table 3). The fact, that the enantioselectivities of **144**·$Cu(OTf)_2$ and **146**·$Cu(OTf)_2$ were superior when compared to their triazole bearing homogeneous counterpart **173**·$CuCl_2$ might give hint that the detrimental coordination of the triazole moiety to copper centers is hampered by its proximity to the silica surface and therefore less predominant.

144·$Cu(OTf)_2$, which was synthesized and functionalized via a post-grafting route, performed slightly worse than **146**·$Cu(OTf)_2$ in means of selectivity. Moreover, **146**·$Cu(OTf)_2$ maintained its high activity and selectivity for at least 3 runs, which is clearly superior to the recycling ability provided by Merrifield resin and MeOPEG. (entries 2-4, Table 4).

Table 4. Cu(II)-catalyzed monobenzoylation of (±)**-170** using azabis(oxazolines) immobilized on magnetite@silica nanoparticles.[a]

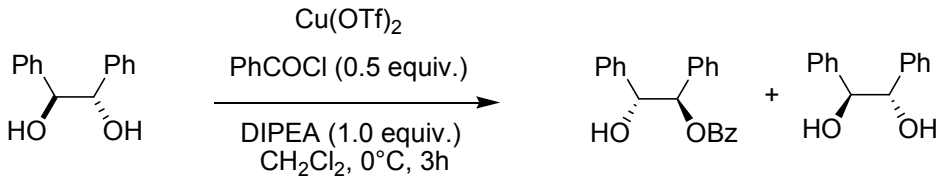

(±)**-170** (*R*,*R*)**-171** (*S*,*S*)**-170**

entry	ligand	run	yield (%)[b]	ee (%)[c]	s[d]
1	**144**	1	38	91	37
2	**146**	1	46	94	80
3	**146**	2	43	98	221
4	**146**	3	45	96	118

[a] Reagents and conditions: dl-Diol (1 mmol), benzoylchloride (0.5 mmol), DIPEA (1 mmol), 0°C, 3 h, CH_2Cl_2, catalyst (1 mol%). [b] Yield of isolated product **171**. [c] Determined by chiral HPLC. [d] Ref.[11]

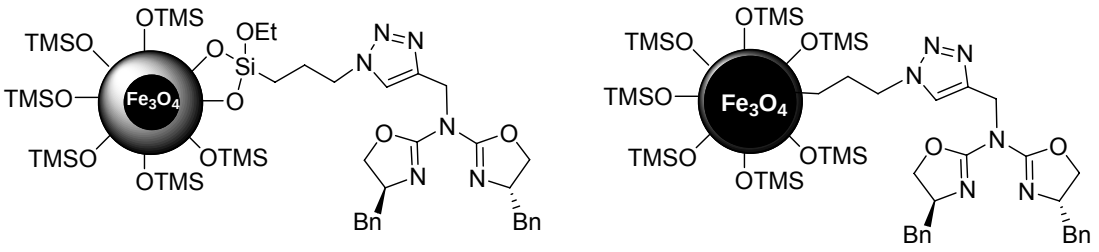

144 **146**

Figure 31. Different magnetite@silica immobilized azabis(oxazolines).

The recycling was carried out by applying an external magnet to the reaction vessel. Separation of the superparamagnetic ironoxide particles was achieved within seconds and the supernatant containing the product was decanted (Figure 32).

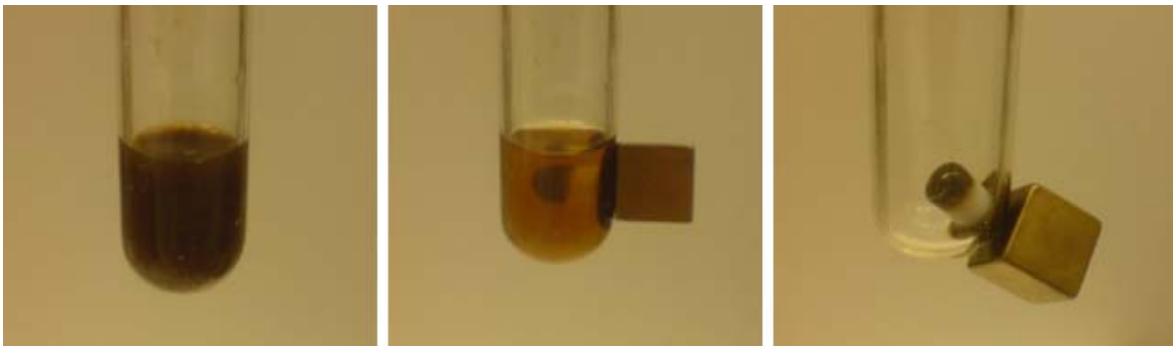

Figure 32. Dispersion of the magnetite@silica nanoparticle immobilized catalyst **146**·$Cu(OTf)_2$ during the asymmetric benzoylation of (±)**-170** (left). Recycling of the catalyst through magnetic decantation (right).

For maximum yield it was required to redisperse the catalyst in dichloromethane and repeat the magnetic decantation twice. The nanopowder could be reused for the next cycle without further activation. Due to this very efficient recycling mode virtually no loss of catalyst was observed.

1.2.2.2 Preformed Fe_3O_4@SiO_2@AzaBOX·$CuCl_2$-catalyst

The application of the preformed azabis(oxazoline)-$CuCl_2$ complex **147** for immobilization on magnetite@silica allowed to circumvent the obstacles caused by the use of a heterogeneous copper source in an in-situ protocol, e.g. above mentioned purification problems. Furthermore, $CuCl_2$ is the most efficient promoter for the asymmetric benzoylation, hence, its application highly desired. Moreover, an in-situ immobilization strategy which would rule out the most valuable copper source for this reaction appears suboptimal.

Selectivity levels with the novel catalyst **147** (Table 5) exceeded not only those obtained with immobilized catalysts **174**·$CuCl_2$ and **175**·$CuCl_2$ but also of triazole modified azabis(oxazoline) **173**·$CuCl_2$ (entries 2-6, Table 1). At least four runs were possible with the novel nanocatalyst **147** without evident drop in yield or enantioselectivity. Thus, the concise grafting of preformed azabis(oxazoline)-copper-complexes delivered as selective catalysts as accessed via an in-situ route but without any restrictions for the choice of the copper source.

Table 5. Cu(II)-catalyzed benzoylation of (±)-**170**: Recycling experiment using azabis(oxazolines) immobilized on magnetite@silica nanoparticles.[a]

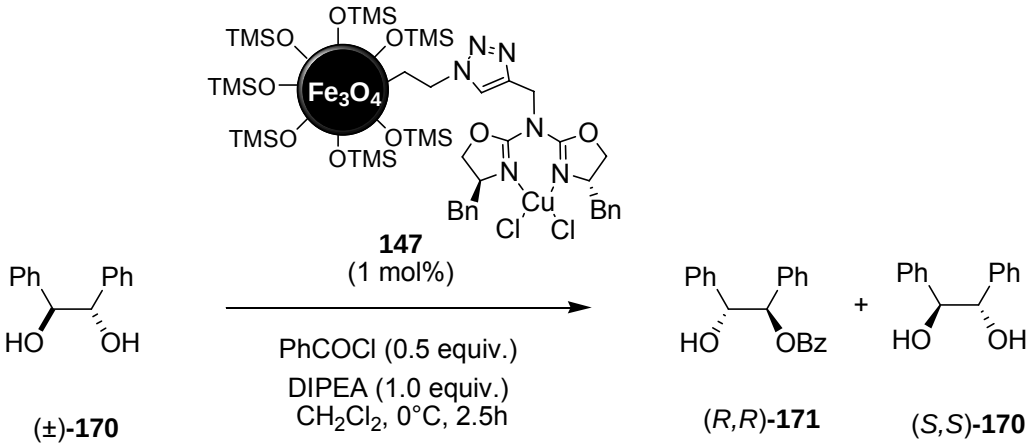

entry	run	yield (%)[b]	ee (%)[c]	s[d]
1	1	46	95	98
2	2	49	96	163
3	3	43	96	107
4	4	48	98	311

[a] Reagents and conditions: dl-Diol (1 mmol), benzoylchloride (0.5 mmol), DIPEA (1 mmol), 0°C, 2.5h, CH_2Cl_2. [b] Yield of isolated product **171**. [c] Determined by chiral HPLC. [d] Ref.[11]

Efforts to broaden the scope of the magnetite@silica immobilized catalyst **147** were limited by the efficacy of the ligand rather than restrictions due to the support. Racemic cyclohexane- and cycloheptane-diols **176a** and **176b** respectively were subjected to the kinetic resolution, giving, in general, good yields but lower selectivities (Table 6). However, at least for **177a** selectivities were equal to those obtained with **109d**· $CuCl_2$.

Table 6. Cu(II)-catalyzed benzoylation of aliphatic cyclic diols in the presence of magnetite@silica supported and non-immobilized azabis(oxazoline) ligands.[a]

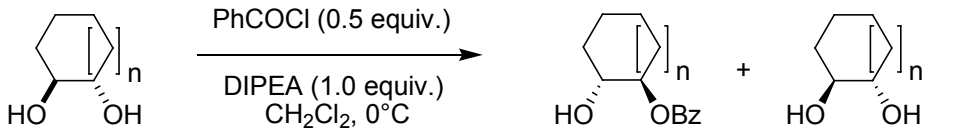

(±)-**176a** (n=1)
(±)-**176b** (n=2)

(*R,R*)-**177a** (n=1)
(*R,R*)-**177b** (n=2)

(*S,S*)-**176a** (n=1)
(*S,S*)-**176b** (n=2)

entry	diol	catalyst (mol%)	yield (%)[b]	ee (%)[c]	s[d]
1[e]	**176a**	**109d**·$CuCl_2$ (5.0)	45	73	11
2	**176a**	**147** (1.0)	39	79	14
3[e]	**176b**	**109d**·$CuCl_2$ (5.0)	41	80	16
4	**176b**	**147** (1.0)	47	59	6

[a] Reagents and conditions: dl-Diol (1 mmol), benzoylchloride (0.5 mmol), DIPEA (1 mmol), 0°C, 3h, CH_2Cl_2. [b] Yield of isolated product **177**. [c] Determined by chiral HPLC. [d] Ref.[11] [e] Ref.[9]

1.2.3 Asymmetric monobenzoylation with azabis(oxazolines) supported on Co/C-nanoparticles

1.2.3.1 Catalysis under batch conditions

Preformed azabis(oxazoline)-copper(II)chloride complexes, which were immobilized on carbon coated cobalt-nanoparticles, proved to be highly efficient catalysts for the asymmetric monobenzoylation of racemic diol **170**. However, stirring the highly ferromagnetic particles in order to create well-dispersed solutions had to be ruled out since the attraction of the nanobeads to the stir bar is too strong. The use of an ultrasound bath allowed the nanopowder to be dispersed efficiently though cooling remained a challenging issue. Maybe the most promising solution is provided by the immanent magnetism of the particles which caused selfsame problem: The cobalt cores bear the capacity to act as their own stirrers in a magnetic field strong enough. To this end, a Schlenk flask containing Co/C-immobilized catalyst **161** in the reaction mixture was placed between adjacent parallel flanks of two magnetic stirrers which were operated in a cooling chamber. Under these conditions, the asymmetric monobenzoylation of (±) diol **170** succeeded in very good yields and selectivities

(Table 7). Enantioselectivities increased even slightly after the first three cycles (entries 4 and 5).

Table 7. Cu(II)-catalyzed monobenzoylation of (±)-**170**: Recycling experiment using azabis(oxazoline)-$CuCl_2$-complexes immobilized on Co/C-nanoparticles.[a]

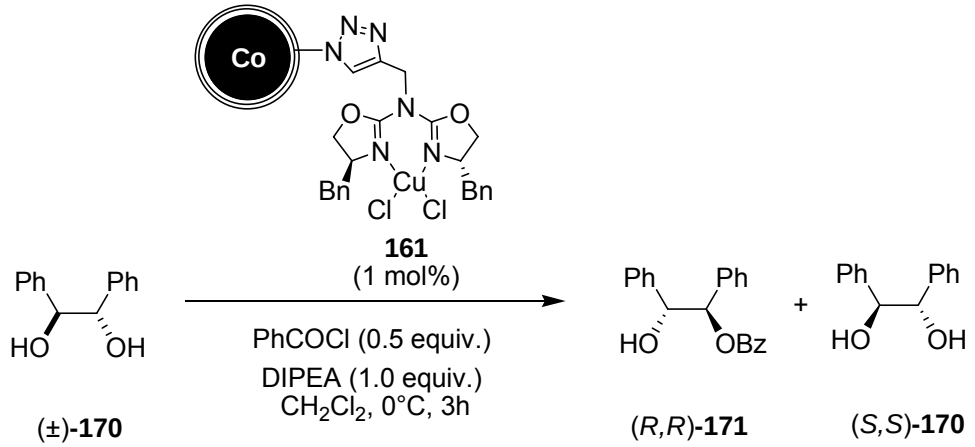

entry	run	yield (%)[b]	ee (%)[c]	s[d]
1	1	47	97	183
2	2	43	96	100
3	3	49	97	227
4	4	48	99	645
5	5	46	99	536

[a] Reagents and conditions: dl-Diol (1 mmol), benzoylchloride (0.5 mmol), DIPEA (1 mmol), 0°C, 3h, CH_2Cl_2. [b] Yield of isolated product **171**. [c] Determined by chiral HPLC. [d] Ref.[11]

Recycling of the catalyst via magnetic decantation was facilitated by the high saturation magnetization of the Co/C-nanocomposite, which allowed its separation from the reaction mixture within seconds. The recovered material maintained its high activity for at least five iterative runs.

1.2.3.2 Catalysis under continuous-flow conditions

An interesting option represented the application of the supported catalyst system in a continuous-flow process. The eminent low catalyst concentration (< 1 mol%), which is sufficient for high conversions within reasonable reaction times (entry 1, Table 3), additionally qualifies the title reaction for a process with inherent limited catalyst

package. A continuous-flow setup offers a number of potential advantages over batch techniques.[13] The reaction conditions (flow rate, stoichiometry and pressure) can be independently varied and precisely controlled. Flow processes are readily scalable by employing multichannel or parallel reactors (number-up vs. scale-up). Some interesting approaches were recently reported for continuous asymmetric processes using either organic or inorganic supports.[14] However, some of these systems suffered from uncontrollable fluid dynamics since catalysts packed as random fixed-bed reactors may lead to stagnation zones, hot-spot formations and large residence time distributions.[15] Additional drawbacks might arise from polymer-specific issues such as the necessity of swelling,[14e] limited accessibility of catalytic sites and clogging of the frit by polymerization byproducts.[14c]

The use of a magnetic nanoparticle supported catalyst was foreseen to allow a novel reactor design, which might be able to overcome several restrictions related to conventional fixed-bed reactors. Agitation of the nanomagnets in a rotating external magnetic field might have beneficial influence on the fluid dynamics. Moreover, due to the pronounced ferromagnetism of carbon coated cobalt particles, the free-floating nanocatalyst might be magnetically retained in the reactor, thus making the application of membranes for nanofiltration dispensable. This would provide an especially interesting feature since the nanoparticles tend to aggregate and block membranes because of their magnetic remanence, thus inevitably provoking a flow-collapse.

To this end, a glass column (Omnifit, 10 cm length, 3.4 mL volume) was charged with the recycled Co/C-immobilized catalyst **161** and placed vertically between adjacent parallel flanks of two magnetic stir motors (Heidolph) with a distance of 4 cm to each other (Figure 33). The glass column was equipped with adequate joints to be connected to a piston pump that allowed the reactor to be floated with anhydrous CH_2Cl_2. A PE frit (25 μm pore size) was mounted into the lower thread of the glass column to prevent excessive sedimentation of the particles to the piston pump after shutdown.

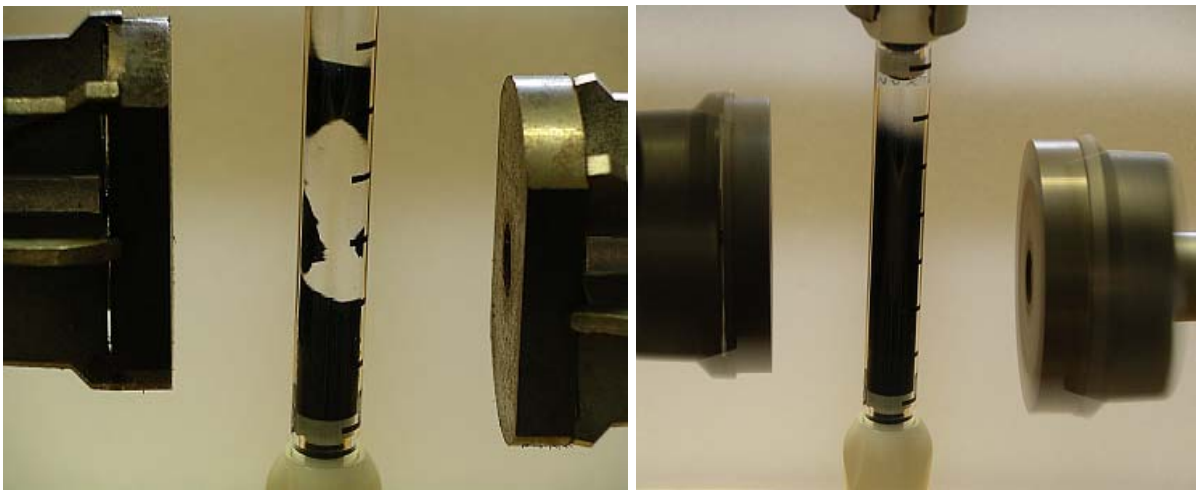

Figure 33. Co/C supported catalyst **161** in a jointed glass column contained by an external magnetic field (left). The nanomagnets were agitated in the rotating magnetic field while CH_2Cl_2 was passed through the reactor (right).

Because of the small flow rates required in these experiments, a diaphragm metering pump (KNF STEPDOS 03-RC) was chosen as the delivery assembly for reactants and reagents. Residence times of the reactants in the flow reactor were not sufficient to enable satisfying conversion of the racemic diol into the enantioenriched monobenzoylated product even at very low flow-rates (< 0.1 mL/min). Hence, adopting recirculation seemed more feasible than further reduction of flow rate in order to achieve high rates in a single pass. Nevertheless, a flow of 0.2 mL/min was maintained in order to avoid leaching of Co/C-nanoparticles.

In principle, for a given amount of catalyst, reaction rates in a continuous-flow reactor depend on the feed composition, mean residence time and reaction temperature. However, raising the temperature in order to increase rates up to a level adequate for a single pass is severely limited for an enantioselective process.

In order to control the temperature, the whole setup was operated in a cooling chamber (4°C), which was envisaged to secure an isothermal reaction rather than applying a column jacket with a circulating cooling fluid, for instance. Furthermore, a column jacket would demand space, which was required by the stir motors for the effective containment of the particles.

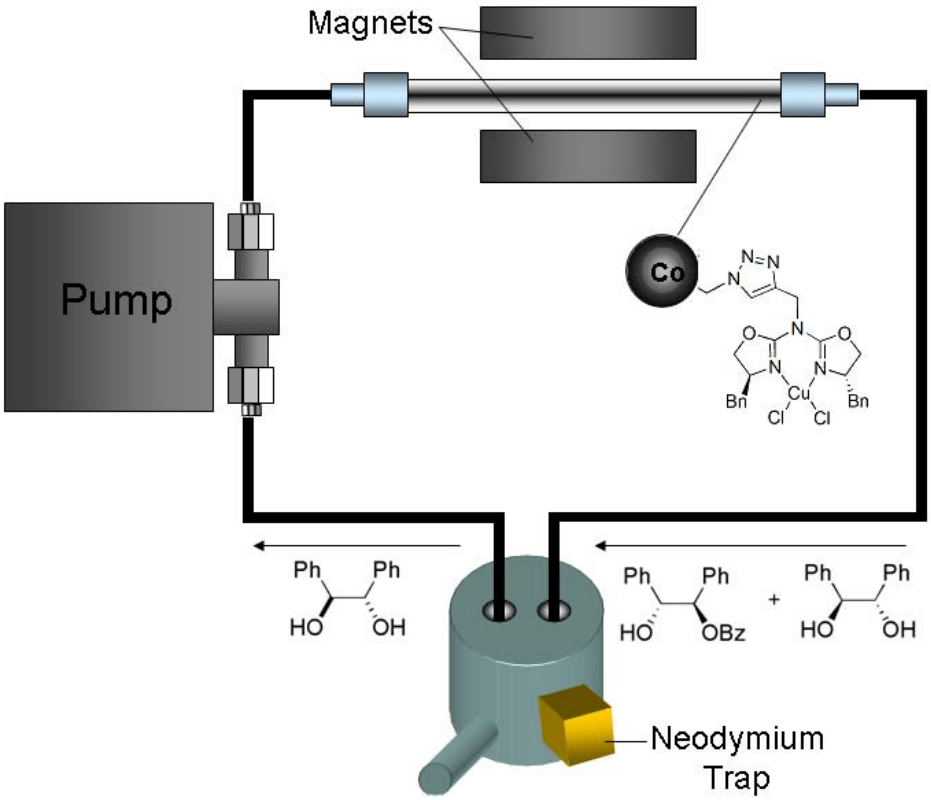

Figure 34. Representation of a closed circuit type reactor for the asymmetric monobenzoylation of racemic diol **170**

Charging of the closed circuit type reactor with solvents and reagents was carried out without sophisticated techniques, e.g. an inert atmosphere box. A nitrogen filled balloon was applied to create an inert atmosphere in the septum-sealed vessel containing the dissolved reactants. In addition, the flask was equipped with an external neodymium based magnet that would trap any catalyst leached from the reactor along with the circulating reactants (Figure 34).

In the case of the magnetite@silica-supported catalyst, excessive leaching occurred already at moderate flow-rates, thus, SPIO-nanoparticles with their comparatively low saturation magnetization appear ineligible under continuous-flow conditions. Co/C-nanoparticles instead, were retained at such a flow rate, showing only negligible catalyst leaching.

Considering the solvent volume of the whole system (8 mL) and the flow-rate applied, the total volume of the reaction mixture in the vessel would be circulated within 40 min. Four successive batches of a solution of **170** in anhydrous CH_2Cl_2 were thus fed with intermediate washing of the charged column using dry CH_2Cl_2.

The contact of the catalyst with adventitious air during the washing procedure had no mentionable effect on the catalyst efficiency in the next run.

By this procedure, overall 4 mmol of **170** were effectively resolved using catalyst **161**, which had been recovered from the batch reactions (Table 7). The immobilized azabis(oxazoline)-copper(II) complex **161** delivered essentially unchanged enantioselectivities in **171** within the first three runs (Table 8). A gradual decrease in yield was observed subsequent to the second run, followed by an explicit decline in enantioselectivity in the fourth run (entries 3 and 4).

Table 8. Cu(II)-catalyzed monobenzoylation of (±)**-170** catalyzed by azabis(oxazoline)-$CuCl_2$-complexes immobilized on Co/C-nanoparticles in a closed circuit type reactor.[a]

entry	batch	yield (%)[b]	ee (%)[c]	s[d]	catalyst-leaching (%)[e]
1	1	43	99	449	< 1
2	2	47	98	282	< 1
3	3	39	99	383	< 1
4	4	32	76	10	< 1

[a] Reagents and conditions: dl-Diol (1 mmol), benzoylchloride (0.5 mmol), DIPEA (1 mmol), catalyst **161** (5 mol%) 4°C, 20h, CH_2Cl_2. [b] Yield of isolated product **171**. [c] Determined by chiral HPLC. [d] Ref.[11] [e] Amount of supported catalyst **161** which was extruded from the reaction chamber during the denoted reaction time and collected in the neodymium magnet trap.

The drop in activity after the third run might be attributed to leaching of copper from the immobilized ligand rather than to the insignificant amount of immobilized catalyst leached from the reaction chamber. Hence, the containment and agitation of the nanomagnets in a microreactor via an external magnetic field provides an interesting alternative to fixed-bed reactors which necessitate a membrane that bears the danger of obstruction.

1.3 Asymmetric Michael-addition of indole to benzylidene malonates

Since the enantioselectivity in many asymmetric catalyses is improved by a slight surplus of ligand,[2-6] whereas the stereoelectronic outcome of the asymmetric monobenzoylation of 1,2-diols is affected by neither excess of copper(II) nor bis(oxazoline) ligands,[1b] the question arises if catalyses might even be negatively influenced in their optical yields by ligand excess. Indeed, such a detrimental effect was observed in the enantioselective Michael-addition of indole (**178**) to benzylidene malonates **179**.[1] A similar effect was reported shortly after by Chan et al. for the copper(I)-catalyzed alkynylation of α-amino ester with arylacetylenes, which responds to any excess of pybox with a significant decrease in enantiofacial selection to the point that even a reversal of enantioselectivity could be achieved.[16] Obtaining a deeper understanding of this unprecedented effect is crucial in order to develop strategies which allow the successful application of immobilized catalysts in such a reaction.

1.3.1 Catalysis with homogeneous azabis(oxazolines)

The Friedel-Crafts reaction is one of the most powerful methods for the formation of carbon-carbon bonds[17] and has therefore gained a lot of attention during the past decades including the development of enantioselective variants.[18] The copper(II) catalyzed 1,4-addition of indole (**178**) to benzylidene malonate **179** is known to proceed in the presence of bis(oxazoline) **102b** with moderate selectivities (up to 69% ee) under standard reaction conditions (ligand/copper ratio 1.1-1.2) as reported by Jørgensen et al. (Table 9).[19]

Table 9. Enantioselective Friedel-Crafts Alkylation of indoles with alkylidene malonates.[19]

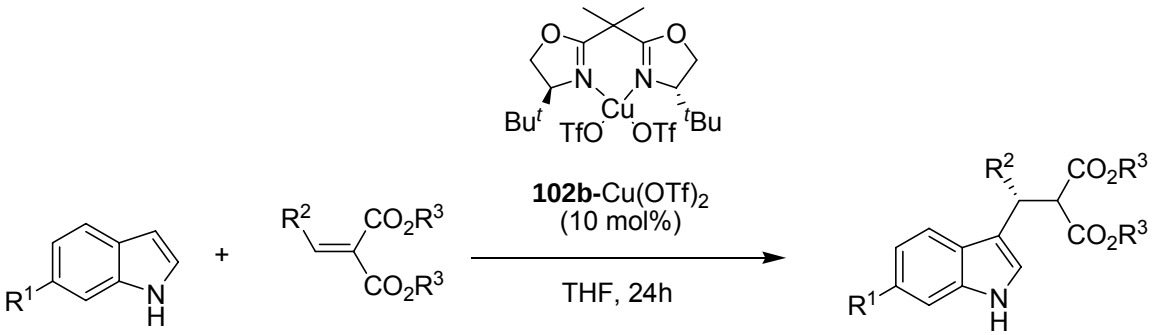

178 **179** **180**

entry	R^1	R^2	R^3	T(°C)	yield (%)	ee (%)
1	H	Ph	Et	0	73	60
2	H	Ph	Me	0	95	50
3	H	4-Br-Ph	Et	0	45	50
4	H	2-Cl-Ph	Et	30	87	69
5	OMe	4-NO_2-Ph	Me	20	99	58

Although some improvement was achieved by Tang et al.[20] (up to 82% ee) they reasoned that simple C_2-symmetric bis(oxazolines) were unsuitable ligands to form a highly stereodiscriminating environment for the copper complex, a prerequisite to achieve high enantioselectivities. An elegant alternative was proposed with the development of tris(oxazoline) ligand **181** which is able to coordinate in a tridentate fashion to the copper center.

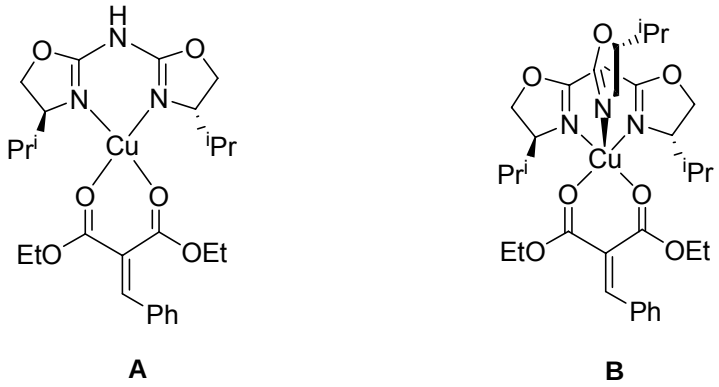

A **B**

Figure 35. Different binding modes of bidentate azabis(oxazoline) (left) and tridentate tris(oxazoline) (right) in a copper-benzylidene malonate complex.

A pentacoordinated complex of type **B** (Figure 35, right), in which one oxazoline moiety necessarily has to be in apical position, was postulated to account for enhanced stereochemical induction. Indeed, employing **181** resulted in highly improved selectivities up to 94% ee for the adduct **180a**.[21]

Table 10. Enantioselective Friedel-Crafts Alkylation of indole (**178**) with benzylidene malonate **179a** catalyzed with a tris(oxazoline)-copper complex.[21b]

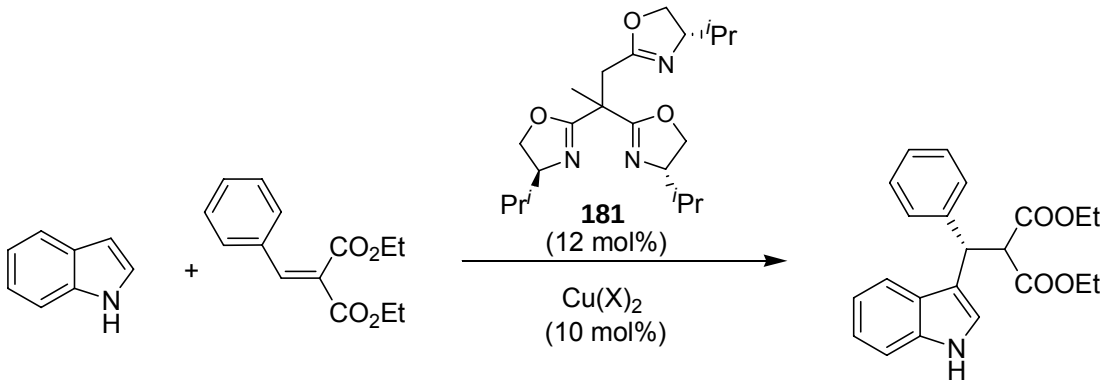

178 **179a** **180a**

entry	solvent	$Cu(X)_2$	T(°C)	yield (%)	ee (%)
1	acetone/ether	$Cu(ClO_4)_2\ 6H_2O$	0	50	85
2	EtOH	$Cu(ClO_4)_2\ 6H_2O$	15	100	82
3	TTCE	$Cu(OTf)_2$	15	76	65
4[a]	^{i}BuOH	$Cu(OTf)_2$	15	99	81
5	^{i}BuOH	$Cu(OTf)_2$	- 25	99	94

[a] **181**/$Cu(OTf)_2$ = 1.0/1.5.

Moreover, changing the solvent from apolar to polar protic ones resulted in greatly enhanced reactivity. Especially bulky alcohols, e.g. ^{i}BuOH, were capable of improving selectivities, thus indicating coordination of solvent to the metal center in the active species. Taking these observations and previous studies by Evans[22] into account, Tang et al. proposed a plausible mechanism for the catalytic cycle (Scheme 63).

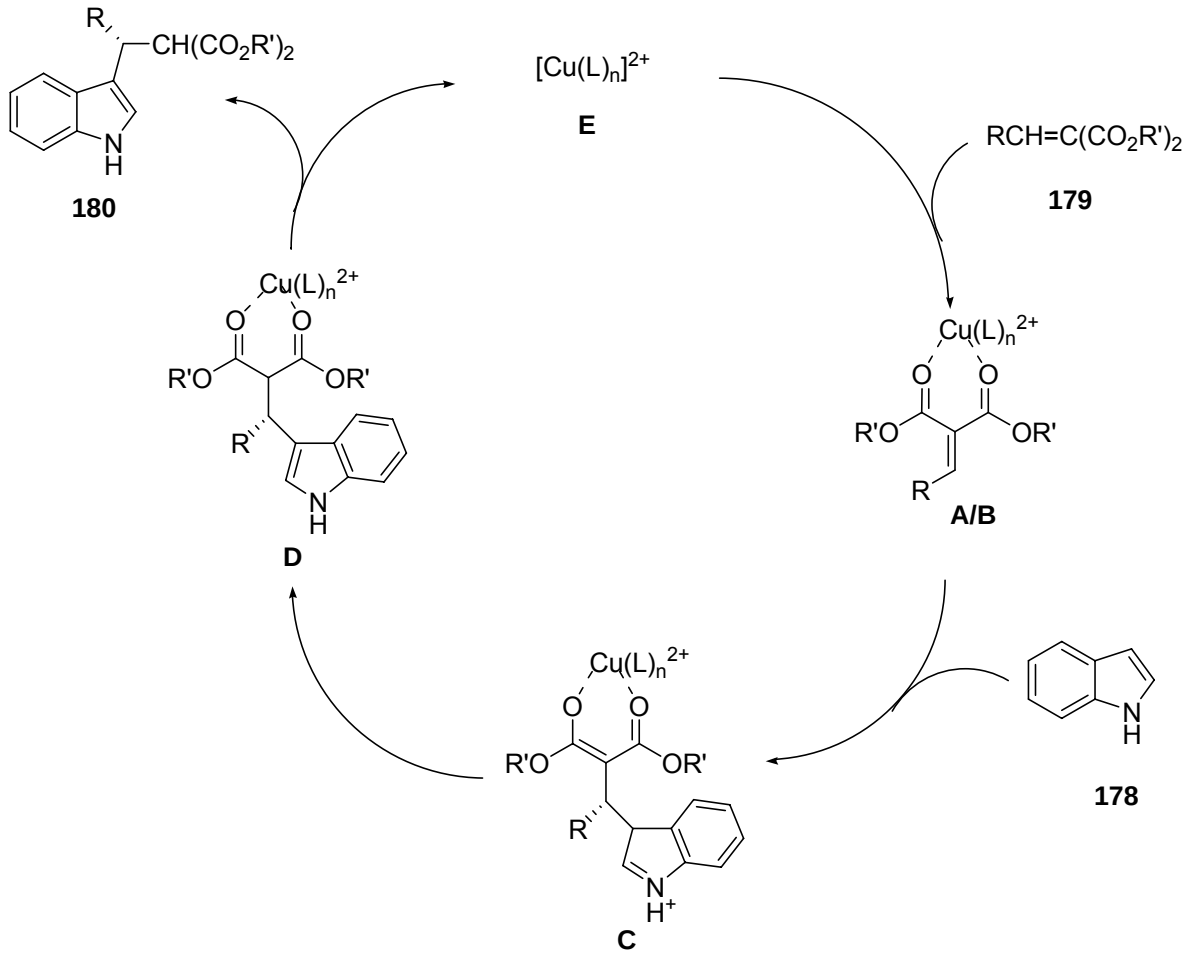

Scheme 63. Catalytic cycle as proposed by Tang et al.[21b]

Chelation of the malonate to the copper center affords the activated substrate-catalyst complex, which undergoes nucleophilic addition to provide the Cu(II)-alkylation adduct. Subsequent solvent assisted H-transfer, followed by decomplexation, gives the product and concomitantly regenerates the catalyst **E.**

However, it was found that a species of type **B** (Figure 35) might not necessarily be required in order to create highly stereoselective complexes. Seemingly inferior bidentate azabis(oxazolines) **103** were found to be applicable for the highly enantioselective addition of indole (**178**) to benzylidene malonate **179**.[1] If any excess of ligand is avoided and the ligand/copper ratio carefully adjusted to 1.04, excellent enantioselectivities (>99% ee) were obtained using both, bis(oxazoline) **102a** or azabis(oxazoline)[23] **103a**, the latter resulting in somewhat higher yields (entry 3, Table 11). Even if the **103a**/copper-ratio was shifted towards a slight excess of copper (entry 5, Table 11) the selectivity remained respectable and clearly superior to the one obtained if selfsame ligand surplus was employed (entry 2).

Table 11.[1] Dependence of enantioselectivity on ligand/metal-ratio in the asymmetric 1,4-addition of indole (**178**) to benzylidene malonate **179a**.[a]

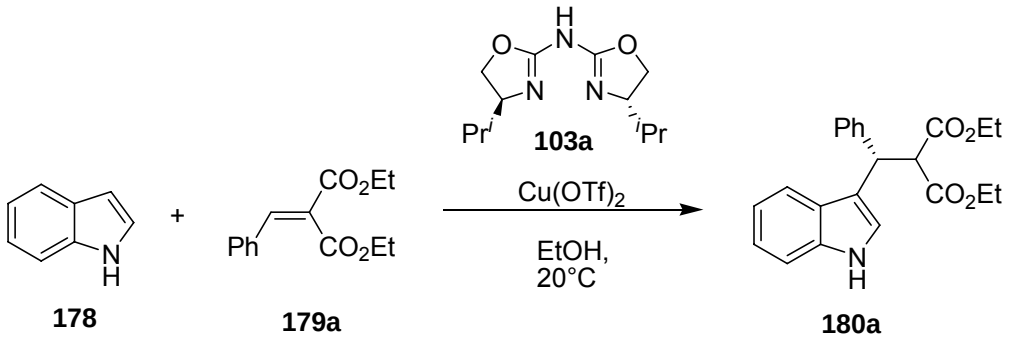

178 **179a** **180a**

entry	ligand/metal-ratio	yield (%)	ee (%)[b]
1	1.3/1.0	98	81
2	1.1/1.0	93	85
3	1.04/1.0	97	>99
4	1.0/1.0	90	98
5	1.0/1.1	96	98
6	1.0/1.3	95	91

[a] Reagents and conditions: 1.2 mmol Indole, 1.0 mmol malonate, 5 mol% **103a**, $Cu(OTf)_2$ according to metal/ligand ratio, 20°C, 8h, solvent: 4 mL EtOH. [b] Determined by HPLC.

This was quite in contrast to the usual observation in asymmetric catalysis that an excess of chiral ligand is beneficial in order to avoid background reactions by uncomplexed metal. A square-planar species of type **A** was assumed to give the same high enantioselectivity as its five-membered counterpart **B** if bis(oxazoline) ligands **102** or **103** are employed (Figure 35). A resting state of the catalyst might be entered by coordination of a third oxazoline moiety to copper, as suggested by Gade et al.,[24] if an excess of ligand is provided. To reach an active species one of the nitrogen moieties has to leave the coordination sphere, which should be the apical oxazoline if ligand **181** is employed. An excess of *external* ligand might however compete for an equatorial position, which could result in low enantioselectivity.

The use of indole (**178**) as nucleophile seems to be crucial for the performance of the Michael addition since other heteroaromatic compounds like pyrrole (**182**) or even substituted indoles[19] pale in comparison with indole (**178**) (Scheme 64).

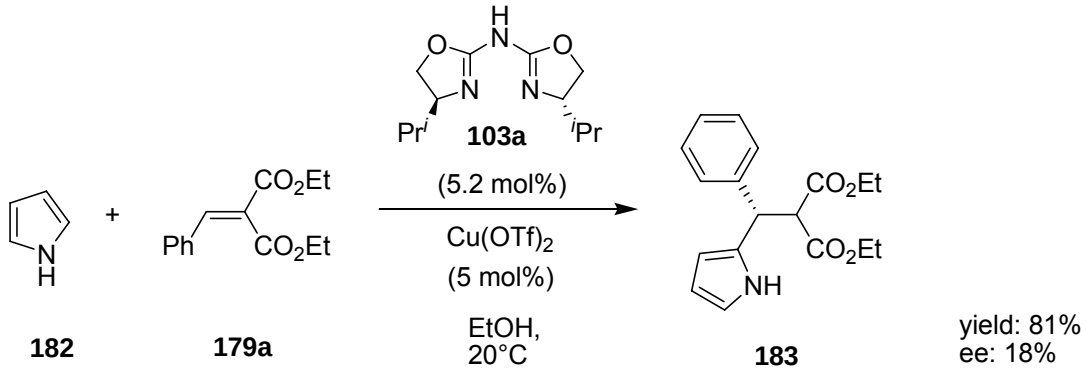

Scheme 64. Asymmetric 1,4-addition of pyrrole (**182**) to benzylidene malonate **179a**.

When a number of substituted benzylidene malonates was examined for the reaction with indole (**178**) at ligand/metal ratios of 1.05 and 1.3 a surprising dependence of the latter with the electronic nature of the substituent was revealed. It was found that comparatively electron rich compounds, especially **179a** and **179b** (entries 1 and 4, Table 12) were forming adducts with indole (**178**) in high optical yields if any excess of ligand is prevented. On the contrary, the strongly electron deficient 4-nitro-derivative **179g** paled in this respect (entry 13). Surprisingly, very good enantioselectivities were achieved for **179g** if excess of ligand (**103a**/copper ratio 1.3) was applied (entry 14) - selfsame excess which was found to be highly disadvantageous for the electron rich counterparts (entry 2). In addition, it was observed that the sensitivity of enantioselectivity towards ligand excess vanished with decreasing inductive contribution of the substituent until it was reversed in its contrary: Best results for compounds **179c** and **179d** were still found at nearly equimolar ratios of ligand and copper (entries 5-8), although both, selectivities and ligand dependence were somewhat lower compared to **179a** and **179b**. Whereas the 2-bromo-derivative **179e** appeared to be rather insensitive to the influence of ligand/copper ratio, 4-bromo-benzylidene malonate **179f** marked the turnaround, showing maximum ee at a ligand/metal ratio of 1.3 (entries 9-12). As mentioned above, the reversed sensitivity towards ligand excess culminated for 4-nitro-derivative **179g**. Further rise in the ligand/metal ratio did not increase the selectivity. Strongly electron donating substituents such as the dimethylamino-group oppressed the reactivity of the substrate completely (entry 15).

Table 12. Dependence of enantioselectivity on ligand/metal ratio in the 1,4-addition of indole (**178**) to substituted benzylidene malonates (**179a-h**): Electronic effects of different malonates.[a]

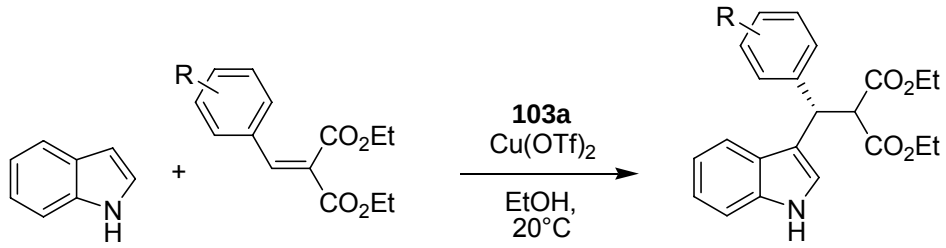

178 **179a-h** **180a-h**

entry	ligand/metal-ratio	R	yield (%)	ee (%)[b]
1[c]	1.04/1.0	H (**179a**)	97	>99[d]
2	1.3/1.0	H (**179a**)	98	81[d]
3[c]	1.04/1.0	4-Me (**179b**)	80	93
4	1.3/1.0	4-Me (**179b**)	78	76
5	1.05/1.0	4-OMe (**179c**)	75	84
6	1.3/1.0	4-OMe (**179c**)	69	70
7	1.05/1.0	4-CF_3 (**179d**)	95	90
8	1.3/1.0	4-CF_3 (**179d**)	93	81
9	1.05/1.0	2-Br (**179e**)	89	85
10	1.3/1.0	2-Br (**179e**)	86	86
11	1.05/1.0	4-Br (**179f**)	97	75
12	1.3/1.0	4-Br (**179f**)	95	82
13	1.05/1.0	4-NO_2 (**179g**)	92	82[d]
14	1.3/1.0	4-NO_2 (**179g**)	83	94[d]
15	1.05/1.0	4-NMe_2 (**179h**)	-	-

[a] Reagents and conditions: 1.2 mmol Indole, 1.0 mmol malonate, 5 mol% **103a**, 20°C, 8h, solvent: 4 mL EtOH. [b] Determined by HPLC. [c] Ref.[1b] [d] Obtained in at least two independent runs.

Hence, this different behavior might be associated with the different electronic parameters of the derivatives **179a-g**. A semi-logarithmic plot of optical yields at the two different ligand/metal ratios (1.05 and 1.3) versus the σ_I values[25] of all *para*-substituted benzylidene malonates, gave a sigmoid trajectory (Figure 36).

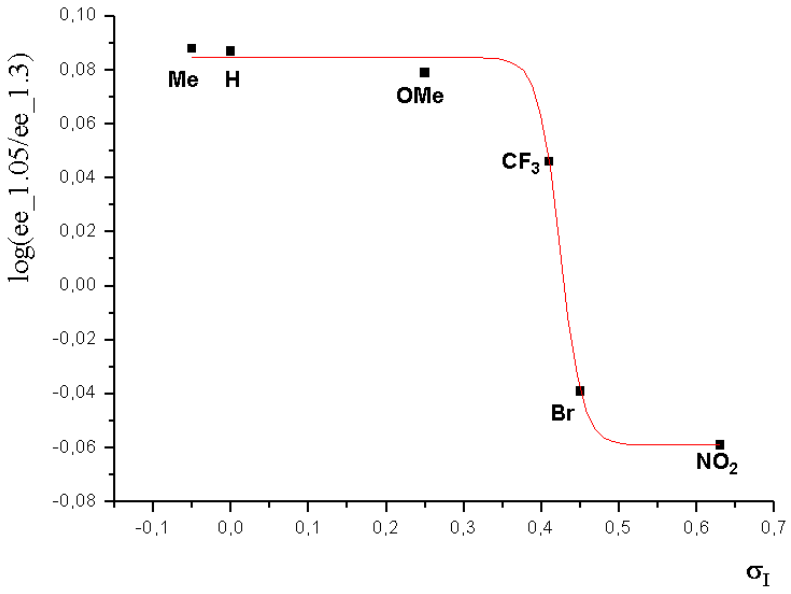

Figure 36. Semi-logarithmic correlation of optical yield ratio versus σ_I values of *para*-substituents in the reaction of indole (**4**) and substituted benzylidene-malonates **179a-d, f, g**.

In order to obtain a deeper insight into the proposed interplay of tetra- and pentacoordinated copper-oxazoline complexes, the use of lithium triflate for the title reaction was investigated, an additive that was supposed to have an influence on the enantioselectivity by coordination of triflate on the copper center in apical position.[21b] It is possible that a pentacoordinated complex of type **F** might be less affected by ligand excess (Scheme 65). In contrast to the likewise square-pyramidal species **B**, no additional stereochemical information is provided by coordination of the triflate counterion.

Table 13. Dependence of enantioselectivity on ligand/metal-ratio in the 1,4-addition of indole (**178**) to benzylidene malonates **179a,e,g**: Influence of triflate as additive.[a]

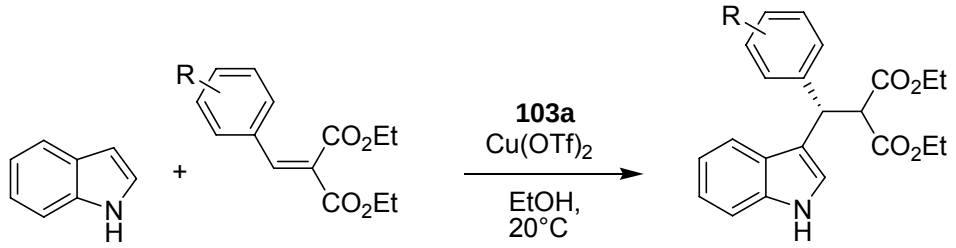

178 **179a,e,g** **180a,e,g**

entry	ligand/metal-ratio	R	Li(OTf)/103a	yield (%)	ee (%)[b]
1[c]	1.04/1.0	H (**179a**)	-	97	>99[d]
2	1.05/1.0	H (**179a**)	5	90	93
3	1.3/1.0	H (**179a**)	-	98	81[d]
4	1.3/1.0	H (**179a**)	5	97	96
5[c]	1.04/1.0	2-Br (**179e**)	-	89	85
6	1.05/1.0	2-Br (**179e**)	5	84	82
7	1.3/1.0	2-Br (**179e**)	-	86	86
8	1.3/1.0	2-Br (**179e**)	5	78	85
9	1.05/1.0	4-NO_2 (**179g**)	-	92	82[d]
10	1.05/1.0	4-NO_2 (**179g**)	5	89	96
11	1.3/1.0	4-NO_2 (**179g**)	-	83	94[d]
12	1.3/1.0	4-NO_2 (**179g**)	5	73	93

[a] Reagents and conditions: 1.2 mmol Indole, 1.0 mmol malonate, 5 mol% **103a**, 20°C, 8h, solvent: 4 mL EtOH. [b] Determined by HPLC. [c] Ref.[1b] [d] Obtained in at least two independent runs.

Studies were carried out at different **103a**/copper ratios and with benzylidene malonates **179a**, **179e** and **179g**, each representing a varied inductive contribution and therefore different sensitivity towards ligand excess. Changing the amount of indole (**178**) in the reaction with **179a** from 1.2 to 5.0 mmol at a ligand/metal ratio of 1.04 had no influence on neither enantioselectivity nor yield (entry 1, Table 13), thus indicating a subordinate role played by indole (**178**) in that regard. An addition of 25 mol% (= 5 equiv. with respect to the copper-azabis(oxazoline) complexes) of lithiumtriflate to the already highly selective reaction of indole (**178**) with **179a** in the absence of additives at a ligand/metal ratio of 1.04 had some negative effect on

enantioselectivity, whereas the same amount of additive at the disadvantageous **103a**/copper ratio of 1.3 annihilated the negative influence of ligand excess to a large part. The enantioselectivity thus obtained was almost comparable to the one at a meticulously adjusted ligand/metal ratio (entries 1-4, Table 13).

This observation might be explained if a five-membered square-pyramidal complex is taken into consideration, which is widely accepted to persist additionally to the distorted square-planar complex of type **A** during catalysis with bis(oxazoline) complexes,[26] whereas the catalytic activity of such intermediates remains an unsettled issue. This square-pyramidal complex offers two possible modes for the coordination of the benzylidene malonate: It might be bound in the plain of the oxazolines with either both carboxyl moieties or with one in equatorial and the other in apical position. The latter binding fashion is most popular for pybox[27] but was also discussed for bis(oxazolines).[26b,28] With an excess of ligand present competing with benzylidene malonate for coordination space, the benzylidene malonate might be driven in the less enantioselective binding mode **G** (Scheme 65), thus providing the sterically more demanding oxazoline surplus with an equatorial position.

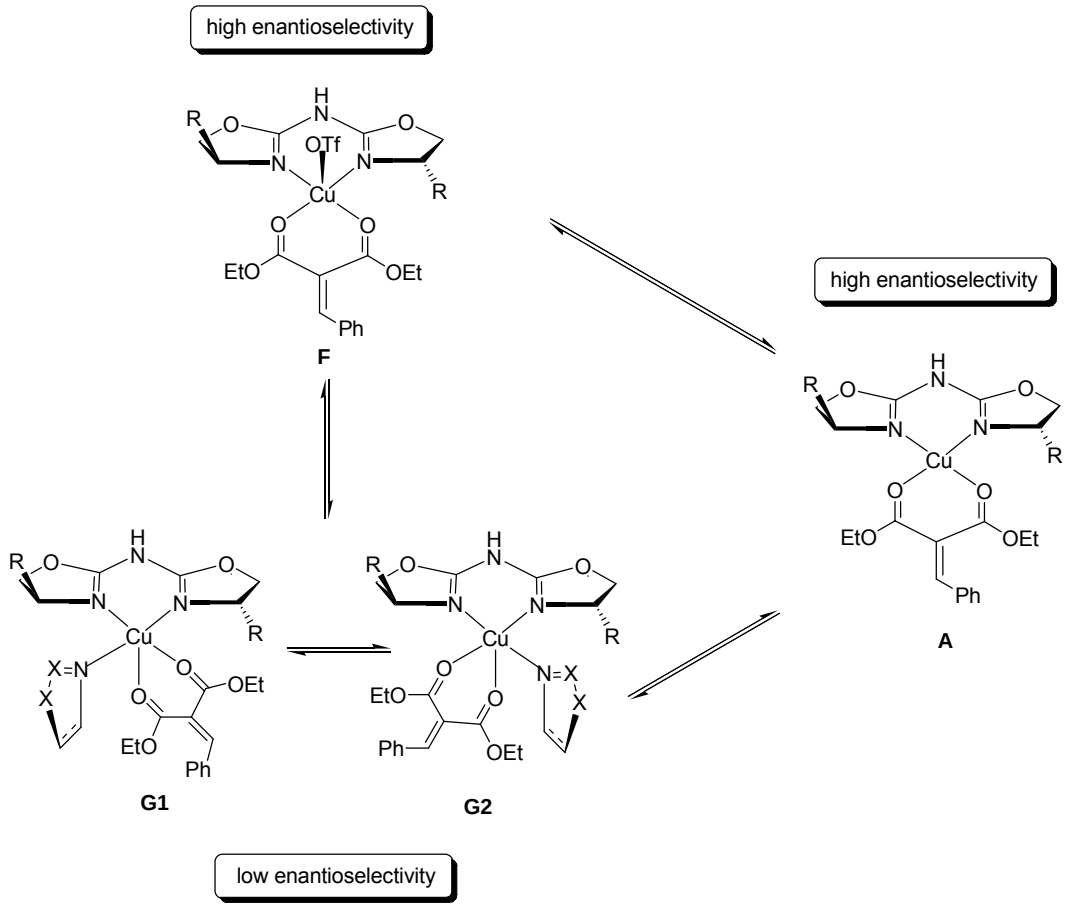

Scheme 65. Mechanistic model for the asymmetric 1,4-addition of benzylidene malonate **179a**.

In this case non-identical alternatives for coordination in equatorial position would probably arise, accounting for the drop in selectivity. In fact, there are hints that triazole moieties, although sterically less demanding than their oxazoline counterparts, are bound in a square-pyramidal copper-complex in equatorial rather than in apical position (Figure 37). With a considerable excess of triflate applied (5 equivalents in respect of **103a**), competing with a rather small ligand surplus for the fifth coordination site, triflate might cover this position due to plain spill-over. However, it is unlikely in means of steric and electronic demand that triflate would occupy an equatorial position rather than benzylidene malonate. Moreover, structures of type **F** in which triflate is bound in apical position were disclosed before.[21b,26c] Such a complex geometry would provide the same high enantioselectivity as the four-membered species **A** (Scheme 65). After all, a mechanistic model involving a five-membered intermediate is capable of explaining both, the effect of ligand excess and effects caused by the addition of triflate. However, coordination of a third oxazoline moiety would in this model not result in a deactivation of the complex due to reduced Lewis acidity as proposed by Gade et al.,[24] but in less enantioselective 19e$^-$-species **G1** and **G2**. Pentacoordinated copper-bis(oxazoline) complexes with equatorial/apical coordinated α-ketoesters[29] or (benzyloxy) acetaldehyde[26a] as electrophilic substrates have been proposed as catalytically relevant species before.

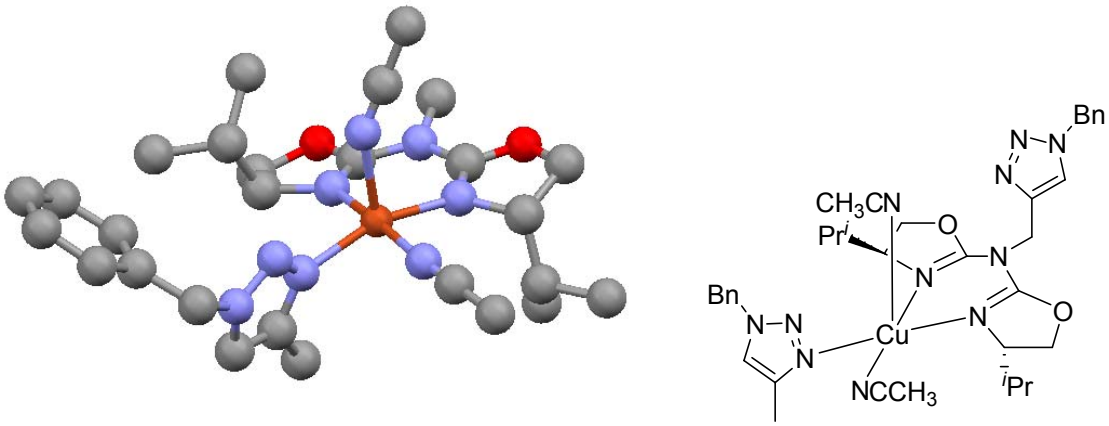

Figure 37. X-ray structure of a polymeric ligand structure bridged by copper atom: Triazole moieties are coordinated in equatorial position.[1]

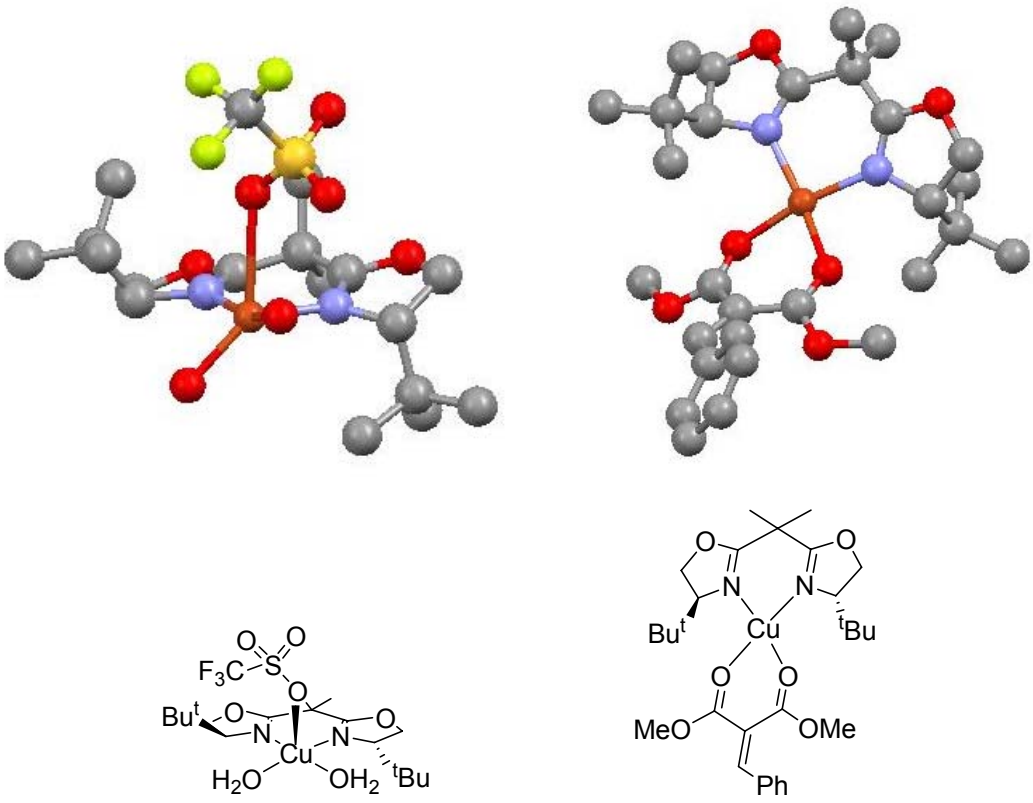

Figure 38. X-ray structure of [Cu-**102b**$(H_2O)_2$] $(OTf)_2$[26c] (left) and [Cu-**102b**$(Ph(CH)_2(CO_2Me)_2)$] $(SbF_6)_2$[26d] (right); non-coordinating counterions omitted for clarity.

As expected, the addition of triflate did not increase the selectivity if the reaction itself is insensitive towards ligand/copper ratio, as it is the case for the alkylation of indole (**178**) with **179e** (entries 5-7, Table 13). The enantioselectivity obtained with the 4-nitro-derivative **179g** at optimum reaction conditions, i.e. at a **103a**/copper ratio of 1.3, was likewise indiscernible from the result without additive. However, when the disfavored ligand/metal ratio was applied for substrate **179g**, its detrimental influence vanished after addition of triflate, leading in this case to the highest enantioselectivities ever obtained for **180g**, either using bis- or tris(oxazoline) ligands (entries 9-11).[21a] Lithiumtriflate seems to act as a decoupling agent for the ligand/metal ratio by stabilizing a pentacoordinated complex of type **F**, which is supposed to be less susceptible to this effect.

1.3.2 Catalysis with nanoparticle-supported azabis(oxazolines)

The promising results using Li(OTf), an agent which might make meticulous adjustment of the ligand/metal-ratio unnecessary, motivated the application of magnetite@silica-immobilized azabis(oxazolines) **144**, **146** and **184**, as well as Co/C immobilized ligand **161** in this reaction. The catalysts were prepared in analogy to those used for the monobenzoylation of 1,2-diols. Briefly, the nanomagnets were dispersed in dichloromethane containing 2.0 equiv. of $Cu(OTf)_2$, agitated for 3 h at ambient temperature and copiously washed via magnetic decantation. The magnetite@silica-particles enabled the use of a magnetic stir bar, whereas this option was ruled out for **161** because of the high ferromagnetism of the cobalt cores. In the latter case, it was not feasible to remove the nanomagnets quantitatively from the stir bar. Hence, agitation of the Co/C-nanopowder was accomplished in an external magnetic field provided by two stir motors. The use of malonates **179a** and **179g** was expected to be especially interesting since they represent the two counterpoints in the dependence of this reaction from the ligand/metal-ratio. The results, however, were mediocre (Table 14).

Table 14. Asymmetric 1,4-addition of indole (**178**) to benzylidene malonates (**179a,g**) using different homogeneous and heterogeneous azabis(oxazolines).[a]

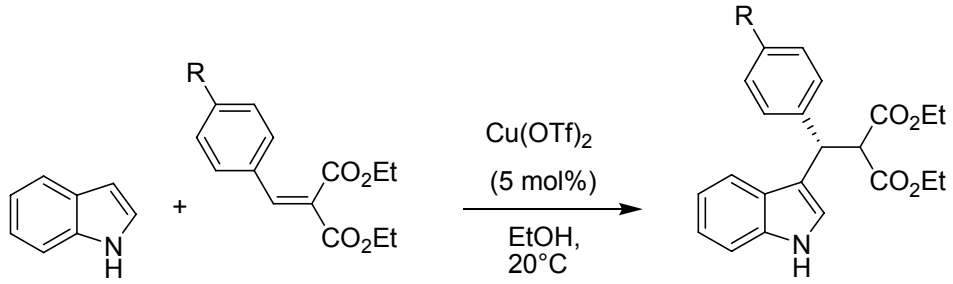

178 **179a,g** **180a,e,g**

entry	run	ligand (mol%)	time (h)	R	yield (%)	ee (%)[b]
1[c]	1	**103a** (5.2)	8	H	97	99
2	1	**103a** (6.5)	8	NO_2	73	93
3	1	**146** (5.0)	8	H	traces	n.d.
4	1	**146** (5.0)	8	NO_2	traces	n.d.
5	1	**146** (10)	48	H	32	66
6	2	**146** (10)	48	H	traces	n.d.
7	1	**182** (10)	48	H	18	n.d.
8	2	**184** (10)	48	H	traces	n.d.
9	1	**144** (10)	48	H	traces	n.d.
10	1	**161** (10)	48	H	traces	n.d.

[a] Reagents and conditions: 1.2 mmol Indole, 1.0 mmol malonate, 20°C, 8h, solvent: 4 mL EtOH.
[b] Determined by chiral HPLC. [c] Ref.[1b]

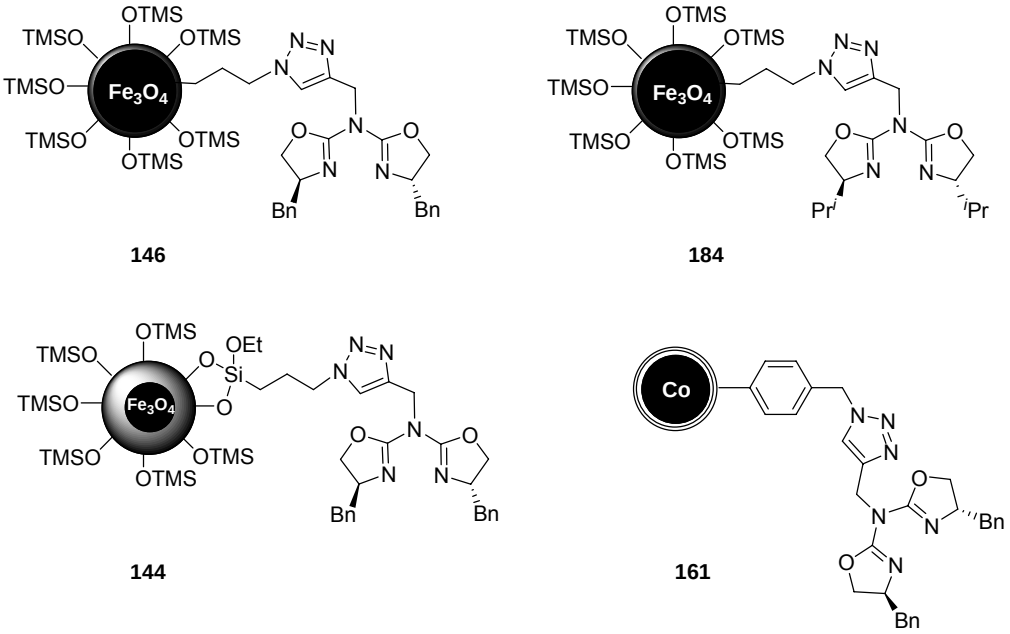

Figure 39. Different magnetite@silica and Co/C-immobilized azabis(oxazolines).

For both, magnetite- and cobalt-supported catalysts, virtually no conversion was observed, even after prolonged reaction times (up to 48 h) and at higher catalyst concentrations (up to 10 mol%). Immobilized ligand **146** delivered the best result in this regard, affording 32% yield and 66% ee in product **180a** (entry 5). The recovered $Cu(OTf)_2$-**146** complex was unable to promote the reaction in a second cycle (entry 6). This finding might be explained with leaching of copper during product isolation/catalyst recycling. In a polar solvent like EtOH, the complex might be especially susceptible to this effect. However, the poor performance of all immobilized catalysts remains an issue. Insufficient spacer length might contribute to the suppressed reactivity, although this is seemingly no problem in the monobenzoylation of 1,2-diols. A negative influence of the triazole linker can be ruled out since it is known that triazole additives have a beneficial effect in this reaction, if any.[1b]

1.4 Asymmetric Michael-addition of indole to nitroalkenes

Whereas asymmetric Friedel-Crafts alkylations that proceed via 1,4- or 1,5-chelating complexes with β,γ-unsaturated α-ketoesters[30] and alkylidene malonates[19,20] respectively have been studied extensively, reports on 1,3-metal bonding species with chiral Lewis acids are scarce. Especially nitroalkenes serve as excellent Michael

acceptors.[31] Hence, Zhou et al.[32] developed a $Zn(OTf)_2$-bis(oxazoline) catalyst for the asymmetric addition of indole (**178**) to *trans*-β-nitrostyrene **185** (Scheme 66).

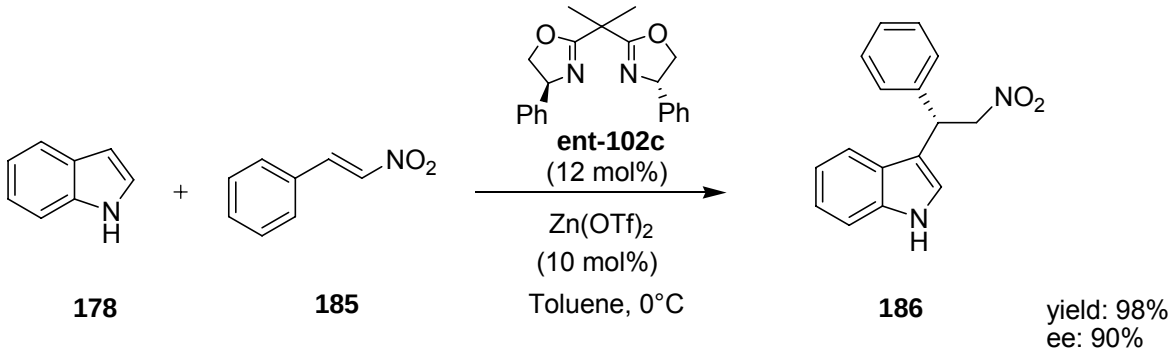

Scheme 66. Asymmetric Friedel-Crafts alkylation of indole (**178**) with *trans*-β-nitrostyrene **182**.

The proposed reaction mechanism is similar to the one provided in Scheme 63. The nitroalkene is activated by chelating to Zn(II) to form a four-membered intermediate, which undergoes a nucleophilic addition of indole (**178**) to provide the Friedel-Crafts alkylation adduct. Subsequently, the H-transfer, followed by dissociation of the product, affords **186** and regenerates the Zn(II)-bis(oxazoline) catalyst **A** (Scheme 67).

This reaction was considered to be interesting under two aspects: On the one hand, the Michael-addition of indole (**178**) to nitroalkene **185** might show the same sensitivity towards ligand excess which was observed for the Michael-addition with benzylidene malonates **179**. Tuning the ligand/metal-ratio to 1.05 might therefore result in improved enantioselectivities for **186**. On the other hand, the optimized reaction was envisaged to be a suitable target for the application of immobilized azabis(oxazolines).

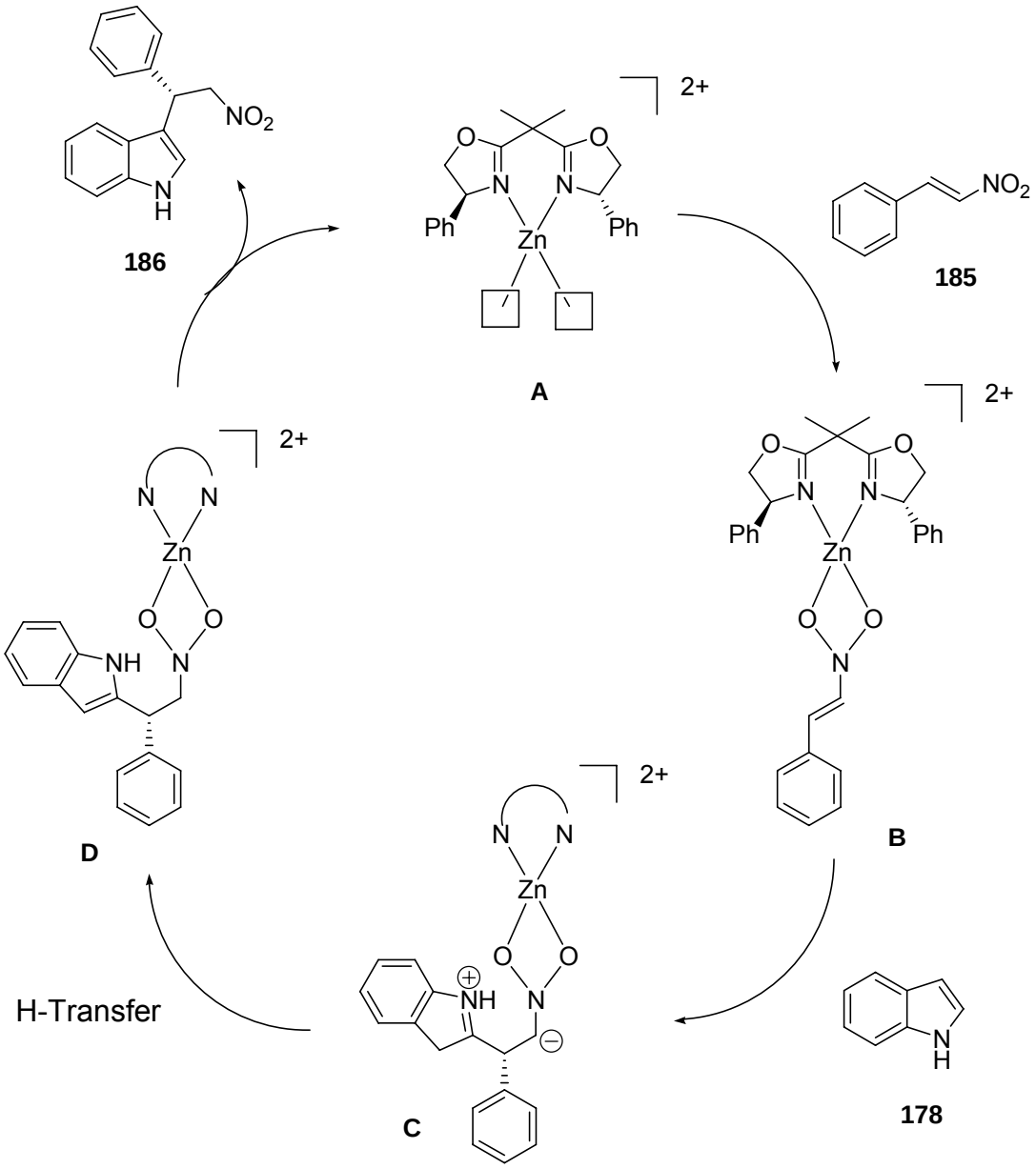

Scheme 67. Proposed catalytic cycle for the alkylation of indole (**178**) with *trans*-β-nitroalkene **185**.

First, a couple of azabis(oxazoline)-ligands and metal salts was screened under conditions that were found to be ideal for the bis(oxazoline)-system (Table 15).

Table 15. Asymmetric Friedel-Crafts alkylation of indole (**178**) with *trans*-β-nitrostyrene **185** using different azabis(oxazolines) and metalsalts.[a]

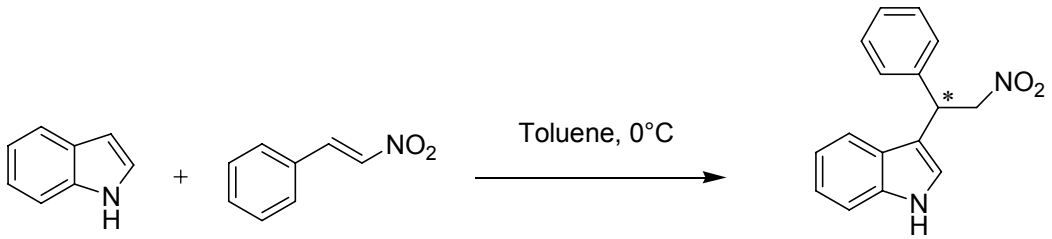

178 **185** **186**

entry	ligand	metalsalt	time (h)	yield (%)	ee (%)[b]
1	**109a**	$Ni(OTf)_2$	96	98	58
2	**109b**	$Ni(OTf)_2$	96	99	71
3	**109c**	$Ni(OTf)_2$	72	75	69
4	**109d**	$Ni(OTf)_2$	96	95	55
5	**103c**	$Ni(OTf)_2$	96	99	65
6	**187**	$Ni(OTf)_2$	72	56	35
7	**103c**	$Cu(OTf)_2$	72	24	69
8	**187**	$Cu(OTf)_2$	72	23	28
9	**109a**	$Zn(OTf)_2$	72	66	rac
10	**109b**	$Zn(OTf)_2$	72	96	17
11	**109c**	$Zn(OTf)_2$	72	92	65
12	**109d**	$Zn(OTf)_2$	72	77	13
13	**103c**	$Zn(OTf)_2$	72	95	34
14	**187**	$Zn(OTf)_2$	72	80	39

[a] Reagents and conditions: 1.0 mmol Indole, 2.0 mmol β-nitrostyrene, 10 mol% $M(OTf)_2$, 10.5 mol% ligand, toluene, 0 °C; [b] Determined by chiral HPLC.

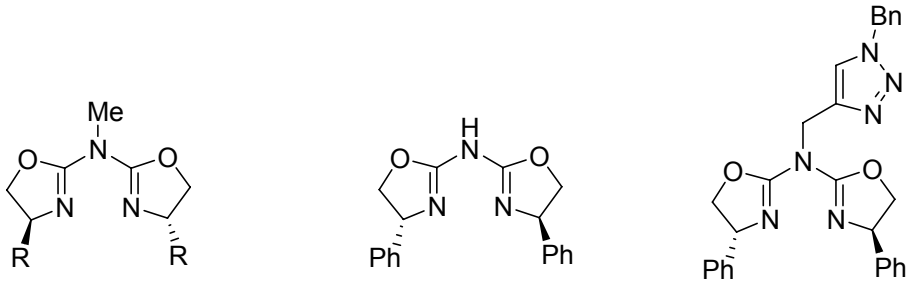

109a: R = ^{i}Pr
109b: R = ^{t}Bu
ent-109c: R = Ph
109d: R = Bn

103c

187

Figure 40. Azabis(oxazolines) for the asymmetric Friedel-Crafts alkylation of indole (**178**) with *trans*-β-nitrostyrene **185**.

The most relevant conclusion that could be drawn out of the results from Table 15 was that no azabis(oxazoline) ligand is able to reach levels of enantioselectivity provided by bis(oxazoline) **102c**. Moreover, reaction times ranging from 72-96 h were necessary to access yields comparable to those obtained with bis(oxazoline) **102c** within 15 h. However, ^{t}Bu-AzaBOX **109b** and Ph-AzaBOX **109c** performed with equal levels of activity and selectivity (entries 2 and 3, Table 15) when $Ni(OTf)_2$ was used. The catalyst had to be prepared in-situ by adding Ag(OTf) to the corresponding $NiBr_2$-derivative because of the hygroscopic nature of $Ni(OTf)_2$-complexes. Since this procedure is pretentious and prone to nonconformities, further studies were carried out with $Zn(OTf)_2$ which delivered comparable yields and selectivities when complexed with Ph-AzaBOX **109c** (entry 11). Using $Cu(OTf)_2$ resulted in as high enantioselectivities but considerably lower yield (entry 7). The unmethylated central nitrogen bridge in **103c** is detrimental when $Zn(OTf)_2$ is used but has only a negligible effect in the case of $Ni(OTf)_2$ (entries 5 and 13, Table 15). Possessing a triazole moiety on the same position is advantageous in neither case, causing a harsh drop in selectivity (entries 6, 8 and 14).

In order to improve rates and selectivities, different counterions and solvents were screened using the most successful ligand **109c**.

Table 16. Asymmetric Friedel-Crafts alkylation of indole (**178**) with *trans*-β-nitrostyrene **185** using different solvents and metalsalts.[a]

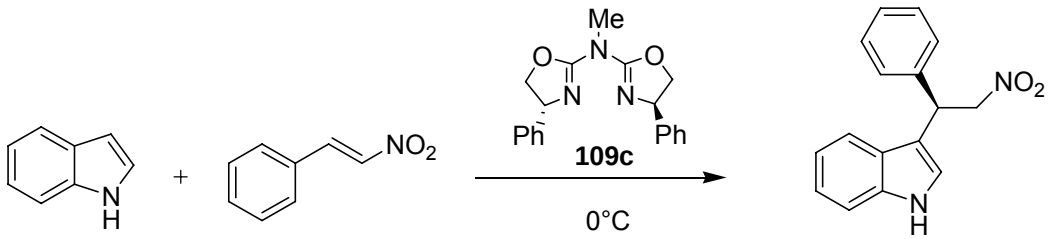

178 **185** **186**

entry	solvent	metalsalt	time (h)	yield (%)	ee (%)[b]
1	Toluene	$Zn(OTf)_2$	72	92	65
2	Toluene	$Ni(ClO_4)_2\ 6H_2O$	72	-	-
3	Toluene/EtOH 4 :1	$Ni(ClO_4)_2\ 6H_2O$	72	76	36
4	Toluene/EtOH 4:1	$Co(ClO_4)_2\ 6H_2O$	72	86	29
5	Toluene/EtOH 4:1	$Cu(ClO_4)_2\ 6H_2O$	72	17	42
6	Toluene	$CuCl_2$	72	-	-
7	Toluene/CH_2Cl_2 4:1	$Zn(OTf)_2$	60	98	61
8	Et_2O	$Zn(OTf)_2$	72	73	60
9	CH_2Cl_2	$Zn(OTf)_2$	48	95	35
10	EtOH	$Zn(OTf)_2$	96	44	rac

[a] Reagents and conditions: 1.0 mmol Indole, 2.0 mmol β-nitrostyrene, 10 mol% $M(OTf)_2$, 10.5 mol% ligand, toluene, 0 °C; [b] Determined by chiral HPLC.

Perchlorates have the disadvantage of being insoluble in apolar solvents, thus no conversion was achieved in toluene (entry 2, Table 16). Only if the perchlorates were solubilised in EtOH prior to the addition of toluene, moderate yields were obtained in general but only modest selectivities (entries 3-5). Strongly coordinating counterions such as chloride oppressed the reactivity of the complex completely (entry 6). In means of enantioselectivity $Zn(OTf)_2$ complexes in toluene remained superior. When CH_2Cl_2 was used as the solvent, reaction rates increased but this lead also to diminished ee values (entry 9). Consequently, the use of dichloromethane as

cosolvent in a 1:4 mixture with toluene accelerated the reaction, but was accompanied by a slight decrease in selectivity (entry 7, Table 16).

Table 17. Asymmetric Friedel-Crafts alkylation of indole (**178**) with *trans*-β-nitrostyrene **185** at different reaction temperatures.[a]

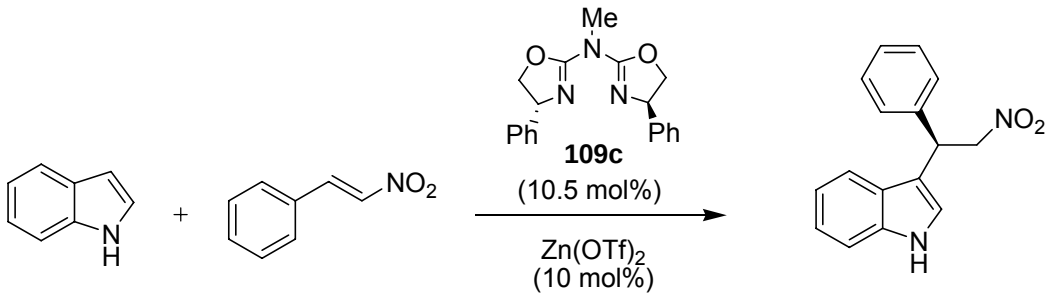

178 **185** **186**

entry	T(°C)	time (h)	yield (%)	ee (%)[b]
1	15	60	81	56
2	0	72	90	65
3	-15	96	99	63

[a] Reagents and conditions: 1.0 mmol Indole, 2.0 mmol β-nitrostyrene, 10 mol% $Zn(OTf)_2$, 10.5 mol% ligand, toluene; [b] Determined by chiral HPLC.

Decreasing the temperature down to -15°C had no beneficial effect on the chiral induction. On the other hand, increasing the temperature did not allow considerable shortening of reaction times either.

Table 18. Asymmetric Friedel-Crafts alkylation of indole (**178**) with *trans*-β-nitrostyrene **185** at different ligand/metal-ratios.[a]

entry	ligand/metal-ratio	yield (%)	ee (%)[b]
1	1.2/1.0	99	61
2	1.05/1.0	99	65
3	1.0/1.0	98	67
4	0.9/1.0	99	65

[a] Reagents and conditions: 1.0 mmol Indole, 2.0 mmol β-nitrostyrene, toluene, 96 h, 0°C, 10 mol% $Zn(OTf)_2$; [b] Determined by chiral HPLC.

Tuning of the ligand/metal ratio had no positive effect on enantioselectivities. In conclusion, results obtained do not indicate that azabis(oxazolines) are suitable ligands for this reaction. Moreover, the asymmetric Friedel-Crafts-reaction of indole (**178**) with trans-β-nitroalkene **185** did not exhibit the same sensitivity towards ligand excess as the analogous reaction with benzylidene malonate **179**, albeit the proposed mechanistic models are alike (Scheme 63 vs. Scheme 67). Since the complex geometry on the metal center was discussed to account for the impact of the ligand/metal-ratio on the optical yields of certain reactions, the different behaviour of the two reactions might be explained with the different metal source used. Hence, copper(II)-catalyzed reactions were considered to be more versatile for further studies on the influence of the ligand/metal-ratio.

1.5 Asymmetric intramolecular Cannizarro reaction

The copper(II)-catalyzed conversion of phenyl glyoxal hydrate **188** to isopropyl mandelate was envisaged to be especially worthwhile for studying effects of ligand/metal-ratio. Morken and coworkers[33] reported on such a enantioselective reaction using an in-situ created $Cu(OTf)_2$-bis(oxazoline) complex, which afforded **189** in 57% yield and 28% ee (Scheme 68).

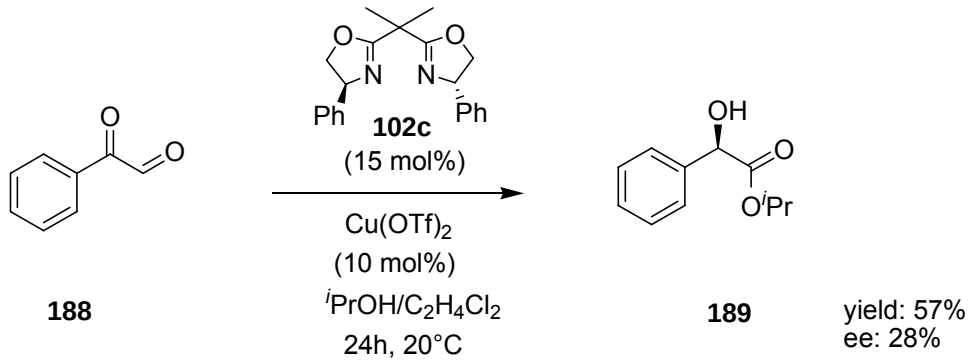

Scheme 68. Cu(II)-Ph-BOX catalyzed asymmetric Cannizarro Reaction.

The reaction took place in a 2-propanol/dichloroethane (2:1) mixture, in which 2-propanol reacts with the arylglyoxal **188** to form hemiacetal **189**. The authors suggested that coordination of **190** to the chiral Lewis-acid catalyst gives rise to an intramolecular hydride transfer. A transition state of type **B** would then coin the stereocenter in **189** (Scheme 69). A ligand/metal-ratio of 1.5/1.0 was employed, which made this reaction appear quite interesting for studies concerning ligand/metal-ratio despite the low levels of enantioselectivities and moderate yields obtained.

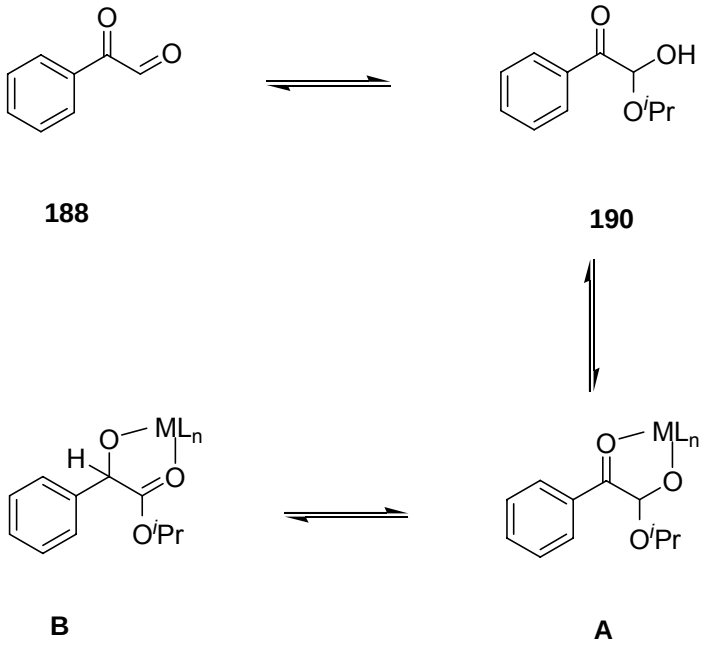

Scheme 69. Mechanistic model for the intramolecular copper(II)-catalyzed Cannizarro reaction as proposed by Morken et al.[33]

Table 19. Asymmetric Cannizarro reaction: Variation of ligand/metal-ratio and cosolvent.[a]

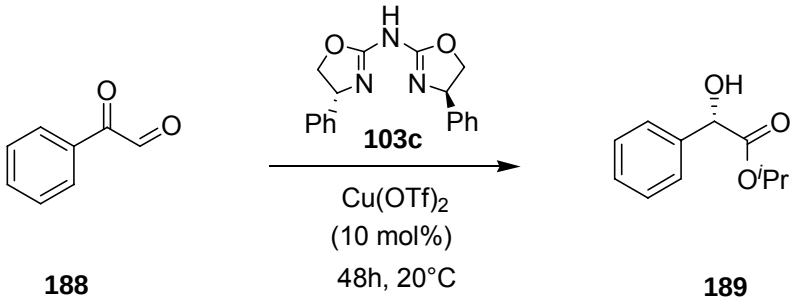

entry	solvent	ligand/metal-ratio	conversion (%)[b]	yield (%)	ee (%)[c]
1	$C_2H_4Cl_2$/ ^{i}PrOH 1 : 2	1.5/ 1.0	33	27	30
2	$C_2H_4Cl_2$/ ^{i}PrOH 1 : 2	1.05/ 1.0	99	97	41
3	Toluene/ ^{i}PrOH 1 : 2	1.05/ 1.0	64	60	35
4	CH_3CN/ ^{i}PrOH 1 : 2	1.05/ 1.0	70	65	36
5	^{i}PrOH	1.05/ 1.0	66	64	36

[a] Reagents and conditions: 5 mol % $Cu(OTf)_2$, 2 mL of solvent, 48 h, 20 °C; [b] Determined by GC; [c] Determined by HPLC.

It was evident from the studies of Morken et al. that phenyl-substituted bis(oxazoline) ligands are the most suitable ones for this type of reaction, hence no further ligand screening was carried out. Indeed, lowering the excess of ligand did increase selectivities noticeably (entry 2, Table 19) but the overall values are still moderate. Increased yields are only partly due to this effect since reaction times were extended considerably (48 h vs. 24 h). The use of cosolvents different from dichloroethane resulted in inferior conversions.

Table 20. Asymmetric Cannizarro reaction: Variation of ligand/metal-ratio and cosolvent.[a]

entry	Li(OTf)/Cu(OTf)$_2$	ligand/metal-ratio	conversion (%)[b]	yield (%)	ee (%)[c]
1	0	1.5/ 1.0	33	27	30
2	5	1.05/ 1.0	86	85	37
3	0	1.05/ 1.0	99	97	41
4	5	1.05/ 1.0	87	83	37

[a] Reagents and conditions: 5 mol % Cu(OTf)$_2$, 2 mL of solvent, 48 h, 20 °C; [b] Determined by GC; [c] Determined by HPLC.

The addition of 5 equiv. of Li(OTf), an agent which is possibly capable of diminishing the detrimental effect of ligand excess, gave the expected results, namely a slight increase in enantioselectivity of **189**. However, conclusions can hardly be drawn upon such marginal deviations.

2. Co/C-immobilized catalysts for oxidation reactions

2.1 TEMPO mediated oxidation of primary and secondary alcohols

The stable nitroxyl radical TEMPO, anchored on carbon coated cobalt nanoparticles, was used to promote the oxidation of benzylic and aliphatic alcohols using a modified Anelli protocol.[34] The active species is not the radical itself, but the oxoammonium cation **191** in which it disproportions (Scheme 70).[35]

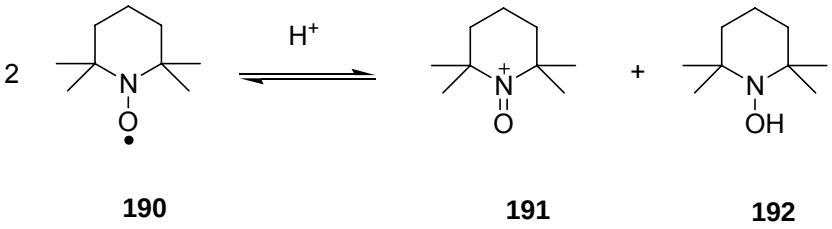

190 **191** **192**

Scheme 70. Disproportion of TEMPO **190** into oxoammonium cation **191** and TEMPOH **192**.

The catalytic cycle involves alternating oxidation of the alcohol by the oxoammonium cation which is regenerated with the primary oxidant hypochlorite. Bromide can be used as a promoter because it is assumed that hypobromite is more reactive towards TEMPO than hypochlorite.

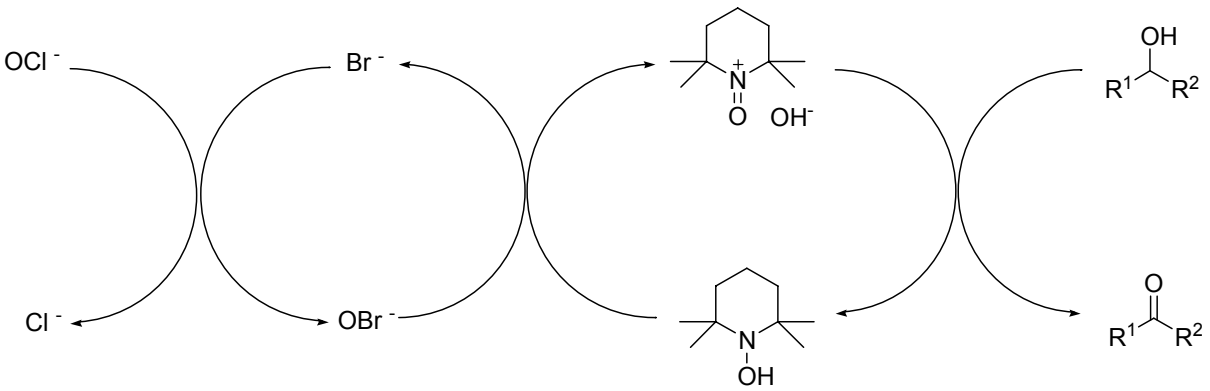

Scheme 71. Catalytic cycle for the TEMPO mediated oxidation of alcohols using hypochlorite as primary oxidant and bromide as promotor.[35]

The best turnover is achieved in a CH_2Cl_2/water system at pH 9 and at a reaction temperature of 0°C. Since the disproportion equilibrium is temperature dependent, an increase in temperature has consequently a detrimental effect on the reactivity.

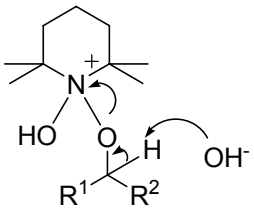

Figure 41. Proposed transition state in the oxidation of alcohol by oxoammonium cation **191**.[35]

2.5 mol% of CoNP-TEMPO **164** were used along with 1.25 equivalents of sodium hypochlorite as primary oxidant and together with 30 mol% potassium bromide. Under these conditions, complete and chemoselective conversion of 4-methylbenzylic alcohol **193** into the corresponding aldehyde **194** was achieved within 1 h (Scheme 72). No overoxidation to the corresponding carboxylic acid was observed.

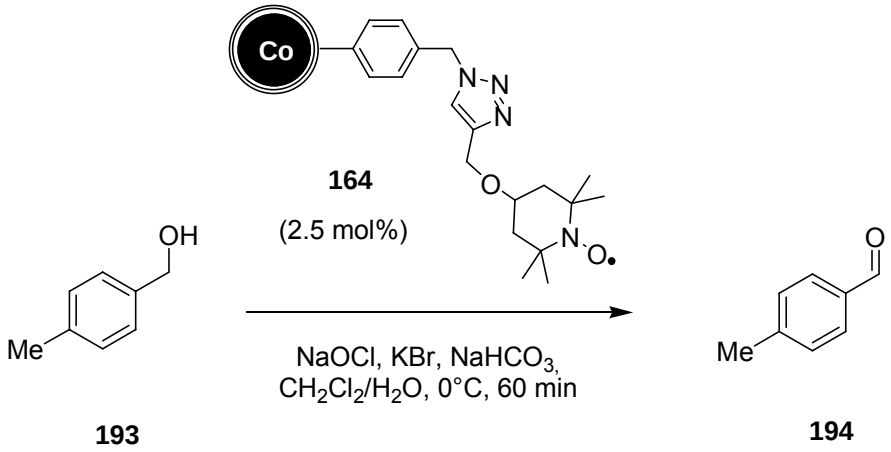

Scheme 72. CoNP-TEMPO **164** mediated oxidation of 4-methylbenzylic alcohol **193**.

This reaction was repeated five times with the recycled catalyst **163** (Table 21). After each iterative oxidation reaction, the nanocomposite was recovered via magnetic decantation and reused in the next run. The activity of the catalyst did not decrease significantly after six runs.

Table 21. Recycling experiment in the CoNP-TEMPO **164** mediated oxidation of 4-methylbenzyl alcohol **193**.[a]

entry	run	conversion (%)[b]	yield (%)[c]	purity (%)[b]
1	1	> 98	89	> 98
2	2	> 96	92	> 96
3	3	> 98	95	> 98
4	4	> 98	87	> 98
5	5	> 93	90	> 93
6	6	> 98	96	> 98

[a] 4-Methylbenzyl alcohol **193** (3 mmol), CH_2Cl_2 (6 mL), KBr (1 mmol), CoNP-TEMPO **164** (2.5 mol%), NaOCl (3.8 mmol), $NaHCO_3$ (0.6 mmol), 0°C, 60 min; [b] Determined by ^1H and ^{13}C NMR; [c] Isolated yield.

Moreover, the carbon coated cobalt particles endured the oxidative stress without significant morphologic alteration as determined by transmission electron micrography analyses of Co/C-particles before and after the oxidation reactions (Figure 42).

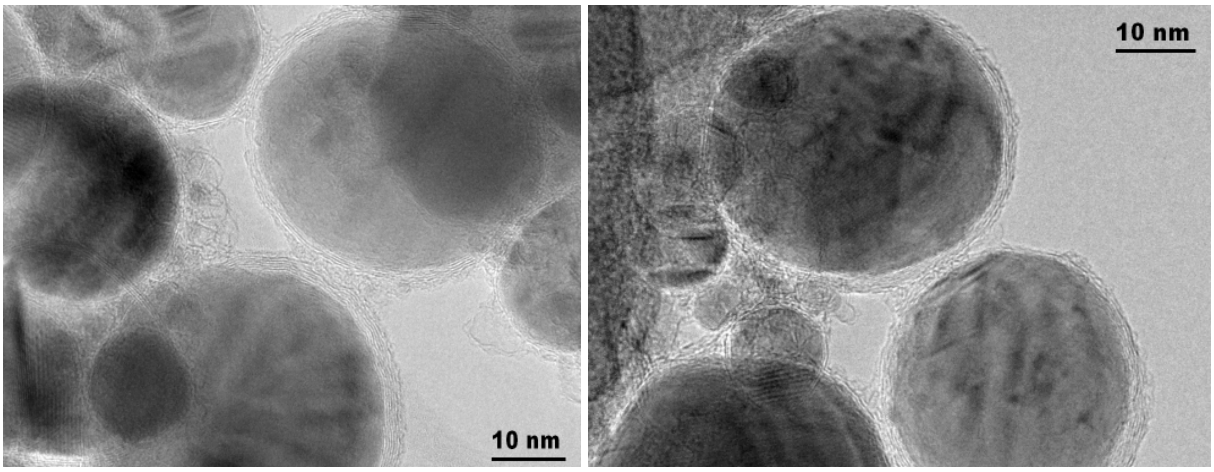

Figure 42. TEM images of CoNP-TEMPO **164** before (left) and after (right) the 5 recycling experiments: The structure of the nanoparticles is not affected by iterative oxidation reactions.

Consequently, recycled catalyst was used for all subsequent oxidations (Table 22). Again, quantitative recovery was achieved after each run. 2-Phenylethanol showed diminished reaction rates allowing no complete conversion within 60 minutes (entry 5, Table 22). However, applying 5 mol% of CoNP-TEMPO **164** afforded 2-phenylacetaldehyde in very good yield and purity. Furthermore, catalyst **164**

demonstrated its efficacy in the oxidation of aliphatic alcohols (entry 6 and 7, Table 2). A peculiarity of TEMPO-mediated oxidations is the different activity towards primary and secondary alcohols, the latter being oxidized much slower. Indeed, the secondary alcohol proved to be oxidized significantly slower, demanding a reaction time of 3 h at an elevated hypochlorite concentration to reach quantitative conversion (entry 8, Table 22).

Table 22. CoNP-TEMPO **164** mediated oxidation of different alcohols to aldehydes. The catalyst was recycled after each iterative run and reused.[a]

entry	alcohol	conversion (%)[b]	yield (%)[c]	purity (%)[b]
1	4-methylbenzyl alcohol	> 98	89	> 98
2	4-bromobenzyl alcohol	> 98	92	> 98
3	4-methoxybenzyl alcohol	> 98	96	> 98
4	benzyl alcohol	> 98	85	> 98
5	2-phenylethanol	> 83 (>98)[d]	77 (94)[d]	> 83 (>98)[d]
6[d]	1-octanol	> 98	87	> 98
7[d]	1-dodecanol	> 98	92	> 98
8[e]	cyclohexanol	> 98	96	> 98

[a] Alcohol (3 mmol), CH_2Cl_2 (6 mL), KBr (1 mmol), CoNP-TEMPO **164** (2.5 mol%), NaOCl (3.8 mmol), $NaHCO_3$ (0.6 mmol), 0°C, 60 min; [b] Determined by ^1H and ^{13}C NMR; [c] Isolated yield; [d] 5 mol% CoNP-TEMPO **164**; [e] 5 mol% CoNP-TEMPO **164**, 7.5 mmol NaOCl, 3 h.

2.2 Co(II)-Schiff base catalyzed oxidations with molecular oxygen

Co(II)-Schiff base complexes are known to bind molecular oxygen in the presence of an axial ligand, whereas the corresponding four-coordinated complexes are very poor acceptors for oxygen at ambient pressure.[36] Aliphatic aldehydes and cyclic ketones can act as such ligands, resulting in Co(III)-dioxygen complexes of type **B** (Scheme 73).[37] In the case of 2-methylpropanal (**195**) as reducing agent, an intramolecular oxygen transfer to the aldehyde via dioxygen complex **B** provides isobutyric acid **196** and species **C**. Cobalt complex **C** is capable of oxidizing diverse substrates. Because of the high reactivity of the radical complex, a mixture of different oxidation products is often obtained. However, the oxidation of e.g. alcohols to the corresponding carbonyls regenerates catalyst **A** to complete the cycle (Scheme 73).

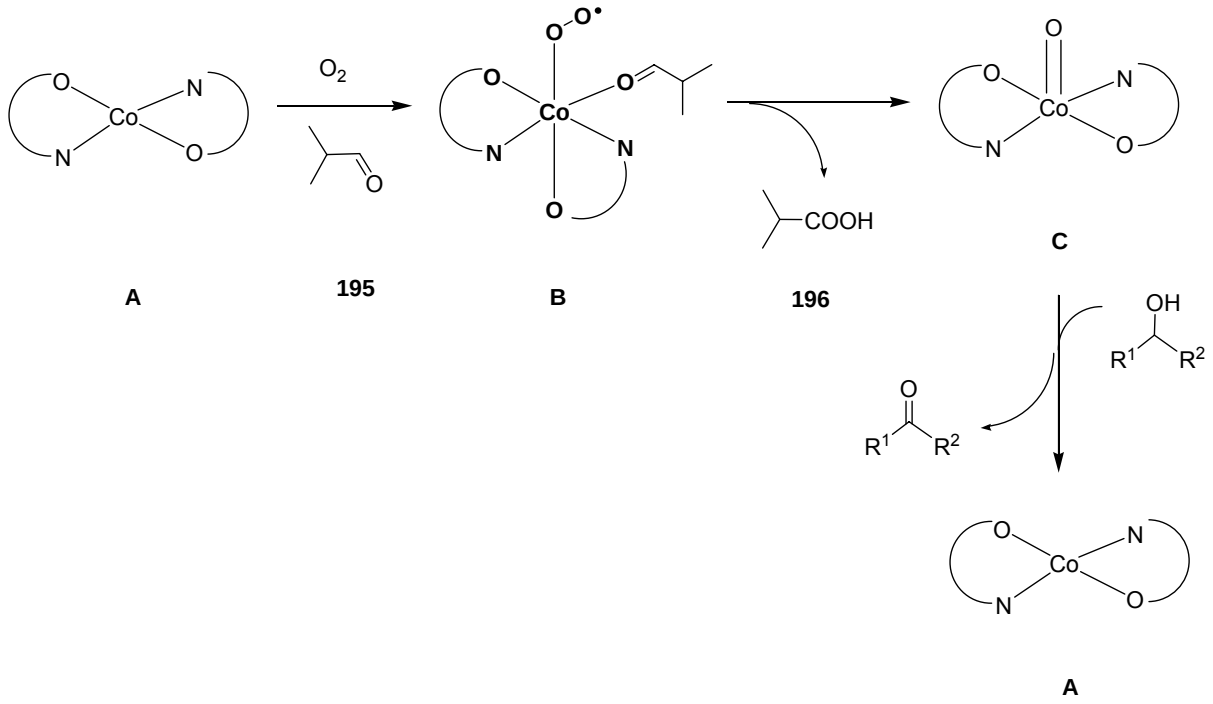

Scheme 73. 2-Methylpropanal mediated oxidation of alcohols with Co(III)-dioxygen complexes.

Using ethyl-2-oxocyclopentanecarboxylate (**197**) instead of 2-methylpropanal (**195**) results likewise in the initial formation of a cobalt(III)-superoxo complex **C** and oxygen atom transfer to the carbonyl compound, which is initiated by an intramolecular hydrogen transfer from ketoester **197** to the terminal oxygen of the complex bound dioxygen. The resulting cobalt enolate **E** can undergo an intramolecular hydroxylation to give the tertiary alcohol **198** and highly reactive cobalt(IV)-oxo intermediate **C**. The latter species can transfer oxygen to an arbitrary substrate.

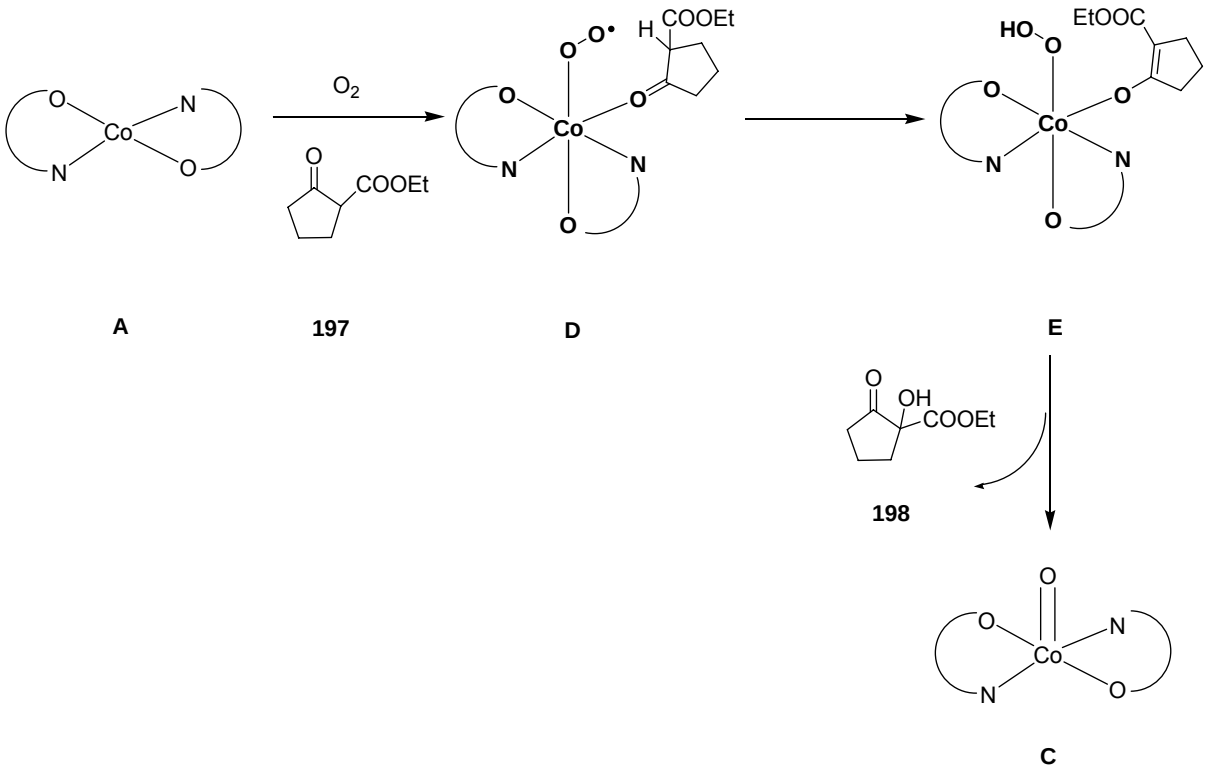

Scheme 74. Ethyl-2-oxocyclopentanecarboxylate (**197**) assisted formation of Co(IV)-oxo complex **C**.

The oxidation of secondary alcohols to the ketones was chosen as a model reaction to examine the catalytic power of the nanoparticles supported catalyst **168**. To this end, Co(II)-Schiff base complex, immobilized on carbon coated cobalt particles, was placed in a glass vessel (8 cm length, 10 mL volume), equipped with a column jacket for the controlled heating of the reaction chamber via a thermostat. The bottom of the reactor was sealed with a G3-frit, which enabled bubbling of oxygen through a jointed gas inlet. The outlet of the glass tube was connected to a reflux condenser in order to reduce the evaporation of solvent due to heating and the constant oxygen streaming. The whole apparatus was placed vertically between adjacent parallel flanks of two magnetic stir motors with a distance of 5 cm to each other, thus allowing the Co/C-nanoparticles to be agitated in the field created by the two rotating magnets (Figures 43 and 44).

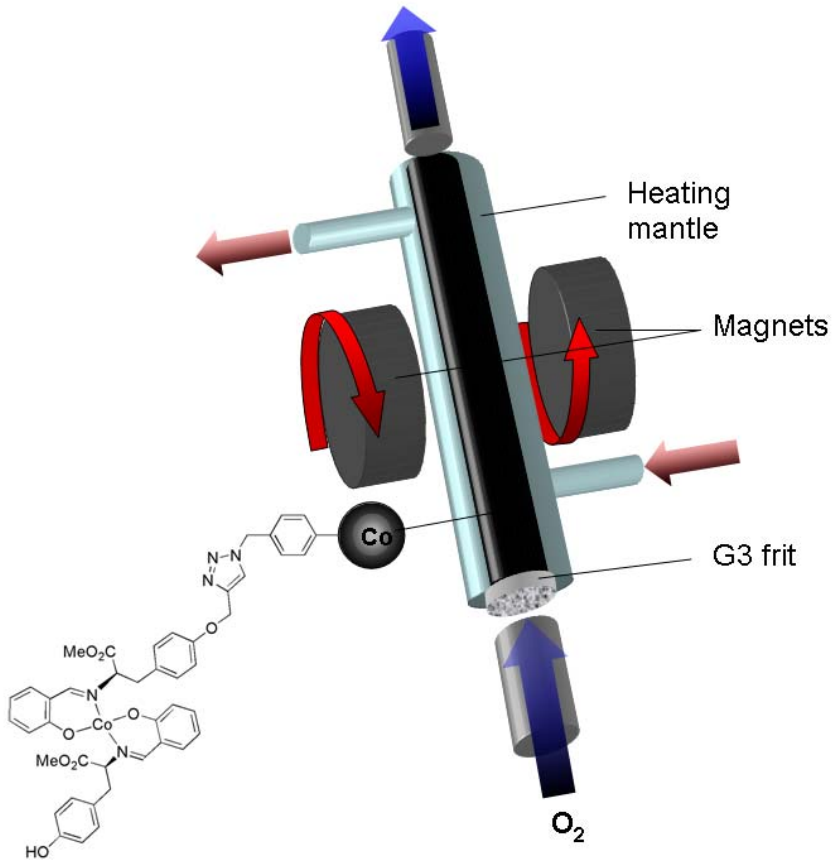

Figure 43. Schematic representation of the setup used for the Co(II)-Schiff base catalyzed oxidation with molecular oxygen.

Figure 44. Glass reactor containing Co/C-nanoparticle supported Co(II)-Schiff base complex **168** between adjacent parallel flanks of two magnetic stir motors at rest (left) and in motion (right).

In a preliminary experiment, the reaction chamber was charged with 1.5 equivalents of the reductant 2-methylpropanal (**195**) with reference to the oxidizable substrate, dissolved in dry acetonitrile. A catalyst concentration of 5 mol% was applied and a reaction temperature of 50°C established before oxygen was bubbled through the reaction mixture, containing molecular sieves (3 Å). Under these conditions, the oxidation of diphenylmethanol (**199**) to benzophenone **200** succeeded rather slowly. After 3 h, only 28% of the alcohol had been converted into the ketone (entry 2, Table 23). Since salicylaldehyde **195** exhibits a rather high vapour pressure, parts might have been volatilized through the oxygen bubbling. Decreasing the reaction temperature, prolonging reaction times or increasing the amount of 2-methylpropanal (**195**) could not improve results considerably (entries 3-5). However, when the cyclopentanone derivative **197** was used as reductant, conversions were significantly improved, especially when a continuous oxygen flow was applied (entries 6 and 7).

Table 23. Consecutive oxidations of diphenylmethanol (**199**) with Co/C-supported Co(II)-Schiff Base complex **164**.[a] The catalyst was recovered and reused after each run.

entry	reductant (equiv.)	T (°C)	time (h)	conversion (%)[b]
1	**195** (1.5)	25	3	26
2	**195** (1.5)	50	3	28
3[c]	**195** (1.5)	50	3	57
4	**195** (1.5)	50	6	34
5	**195** (3.0)	50	3	53
6[c]	**197** (1.5)	50	3	46
7	**197** (1.5)	50	3	> 98
8	**197** (1.5)	50	3	92
9	**197** (1.5)	50	3	> 95
10	**197** (1.5)	50	3	> 98
11	**197** (1.5)	50	3	> 98

[a] Diphenylmethanol (**199**) (184 mg, 1 mmol), reductant (1.5 mmol), catalyst **168** (5 mol%), acetonitrile (10 mL), O_2-flow; [b] Determined by ^1H and ^{13}C NMR; [c] O_2 (1 atm.).

Under these conditions, complete conversion of the model substrate diphenylmethanol (**199**) to the corresponding ketone was achieved. The reaction mixture containing the crude product was extracted into the bottom glass tube by suction from the reaction chamber through the mounted G3 frit. To this end, vacuum was applied at the oxygen inlet. Due to their high magnetic remanence, the Co/C-nanoparticles form comparatively large aggregates if not dispersed in an external magnetic field. This procedure allowed the efficient separation of the nanocomposite via filtration. Small quantities of nanoparticles withdrawn in the waters were eliminated through magnetic decantation. The remaining nanomagnets were washed with dry acetonitrile thrice and reused for the following run. Heterogeneous catalyst **168** remained its activity in at least five iterative oxidations (entries 7-11, Table 23).

To demonstrate the scope of the immobilized Co(II)-Schiff base complex **168** in oxidations with molecular oxygen, a number of substrates was screened (Table 24). The catalyst was recycled after each run as described above. Secondary benzylic alcohols **199**, **201** and **203** underwent oxidation to the carbonyl compounds in excellent yields within 3 h (entries 1-3, Table 24). Benzylic oxidations required in general longer reaction times (6 h) and a higher concentration of reductant **197** (2 equivalents) (entries 4-6). Finally, the oxidation of diphenylmethanol (**199**) was repeated in order to re-evaluate an eventual loss in activity of the recovered material over the several consecutive reactions. The corresponding ketone **200** was formed once more in excellent yield, thus indicating that no significant drop in the catalyst efficacy occurred over the indicated period.

In conclusion, Co(II)-Schiff base complexes immobilized on carbon coated cobalt nanoparticles can be considered highly versatile and recyclable heterogeneous catalysts for the oxidation of diverse substrates with molecular oxygen.

Table 24. Consecutive oxidations with Co/C-supported Co(II)-Schiff base complex **168**.[a] The catalyst was recovered and reused after each run.

entry	substrate	product	conversion (%)[b]	yield (%)[c]
1	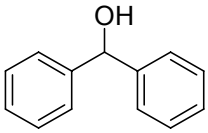 **199**	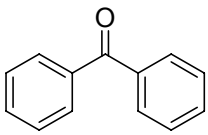 **200**	> 98	96
2	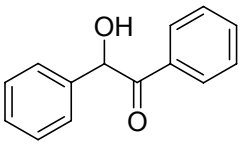 **201**	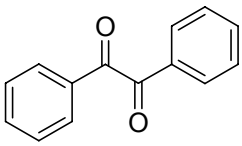 **202**	> 98	95
3	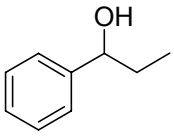 **203**	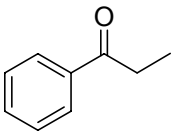 **204**	85	79
4[d]	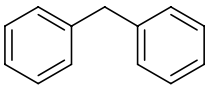 **205**	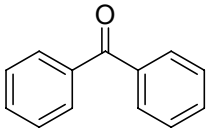 **200**	91	88
5[d]	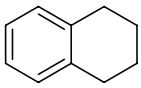 **206**	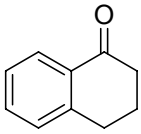 **207**	74	70
6[d]	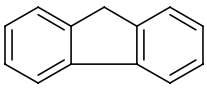 **208**	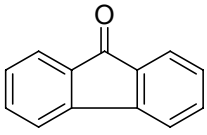 **209**	> 98	97
7	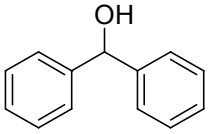 **199**	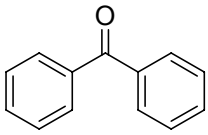 **200**	> 98	91

[a] Substrate (1 mmol), ethyl-2-cyclopentanone-carboxylate (**197**) (1.5 mmol), catalyst **168** (5 mol%), acetonitrile (10 mL), O_2-flow, 50°C, 3h; [b] Determined by ^1H and ^{13}C NMR; [c] Isolated yield; [d] 6 h, 2 mmol **197**.

3. References

1 a) A. Schätz, R. Rasappan, M. Hager, A. Gissibl, O. Reiser, *Chem. Eur. J.* **2008**, *14*, 7259; b) R. Rasappan, M. Hager, A. Gissibl, O. Reiser, *Org. Lett.* **2006**, *8*, 6099.

2 a) H. Brunner, U. Obermann, *Chem. Ber.* **1989**, *122*, 499; b) G. Eblavoine, J.C. Clinet, I. Lellouche, *Tetrahedron Lett*. **1989**, *30*, 5141; c) H. Brunner, P. Brandl, *Tetrahedron: Asymmetry* **1991**, *2*, 919.

3 H. Brunner, U. Obermann, P. Wimmer, *Organometallics*, **1989**, *8*, 821.

4 D. A. Evans, K. A. Woerpel, M. M. Hinman, M. M. Faul, *J. Am. Chem. Soc*. **1991**, *113*, 726.

5 a) H. Fritschi, U. Leutenegger, A. Pfaltz, *Helv. Chim. Acta*. **1988**, *71*, 1553; b) U. Leutenegger, G. Umbricht, P. Fahrni, P. von Matt, A. Pfaltz, *Tetrahedron* **1992**, *48*, 2143.

6 a) A. Gissibl, M. G. Finn, O. Reiser, *Org. Lett.* **2005**, *7*, 2325; b) A. Gissibl, C. Padie, M. Hager, F. Jaroschik, R. Rasappan, E. Cuevas-Yanez, C.-O. Turrin, A.-M. Caminade, J.-P. Majoral, O. Reiser, *Org. Lett.* **2007**, *9*, 2895.

7 *Enzyme Catalysis in Organic Synthesis: A Comprehensive Handbook*, K. Drauz, H. Waldmann, Eds. Wiley-VCH, Weinheim, **2002**; Vols. I-III.

8 a) Y. Matsumura, T. Maki, S. Murakami, O. Onomura, *J. Am. Chem. Soc.* **2003**, *125*, 2052; b) Y. Matsumura, T. Maki, K. Tsurumaki, O. Onomura, *Tetrahedron Lett.* **2004**, *45*, 9131; c) C. Mazet, V. Köhler, A. Pfaltz, *Angew. Chem., Int. Ed.* **2005**, *44*, 4888; d) C. Mazet, S. Roseblade, V. Köhler, A. Pfaltz, *Org. Lett.* **2006**, *8*, 1879.

9 A. Gissibl, M. G. Finn, O. Reiser *Org. Lett.* **2005**, *7*, 2327.

10 M. Hager, master thesis, Regensburg, **2006**.

11 a) H. B. Kagan, J.-C. Fiaud, *Top. Stereochem.* **1988**, *18*, 249; b) C. J. Sih, S. H. Wu, *Top. Stereochem*. **1989**, *19*, 63; c) H. B. Kagan, *Tetrahedron* **2001**, *57*, 2449; d) J. M. Keith, J. F. Larrow, E. N. Jacobsen, *Adv. Synth. Catal.* **2001**, *343*, 5.

12 J. Lim, S. N. Riduan, S. S. Lee, J. Y. Ying, *Adv. Synth. Catal.* **2008**, *350*, 1295.

13 a) P. Hodge, P. *Curr. Opin. Chem. Biol.* **2003**, *7*, 362; b) U. Jas, A. Kirschning, *Chem. Eur. J.* **2003**, *9*, 5708; c) P. Hodge, *Ind. Eng. Chem. Res.* **2005**, *44*, 8542; d) A. Kirschning, W. Solodenko, K. Mennecke, *Chem. Eur. J.* **2006**, *12*, 5972.

14 a) D. A. Annis, E. N. Jacobsen, *J. Am. Chem. Soc.* **1999**, *121*, 4147; b) A. J. Sandee, D. G. I. Petra, J. N. H. Reek, P. C. J. Kamer, P. W. N. M. van Leeuwen, *Chem. Eur. J.* **2001**, *7*, 1202; b) C. Jonsonn, S. Lundgren, S. J. Haswell, C. Morberg, *Tetrahedron* **2004**, *60*, 10515; c) A. Mandoli, S. Orlandi, D. Pini, P. Salvadori, *Tetrahedron: Asymmetry* **2004**, *15*, 3233; d) M. I. Burgete, A. Cornejo, E. García-Verdugo, M. J. Gil, S. V. Luis, J. A. Mayoral, V. Martínez-Merino, M. Sokolova, *J. Org. Chem.* **2007**, *72*, 4344; e) M. A. Pericàs, C. I. Herrerías, L. Solá, *Adv. Synth. Catal.* **2008**, *350*, 927.

15 A. Cybulski, J. A. Moulijn, *Structured Catalysts and Reactors*; Marcel Dekker: New York, **1998**.

16 Z. Shao, J. Wang, K. Ding, A. Chan, *Adv. Synth. Catal.* **2007**, *349*, 2375.

17 a) G. A. Olah, R. Krishnamurti, G. K. S. Prakash, *Comprehensive Organic Synthesis*, Pergamon Press, Oxford, **1991**; b) G. R. Meima, G. S. Lee, J. M. Garces, *Friedel-Crafts Alkylation*, Wiley-VCH, New York, **2001**.

18 Review: K. A. Jørgensen, *Synthesis*, **2003**, 1117.

19 W. Zhuang, T. Hansen, K. A. Jørgensen, *Chem. Commun*. **2001**, 347.

20 J. Zhou, Y. Tang, *Chem. Commun.* **2004**, 432.

21 a) J. Zhou, Y. Tang, *J. Am. Chem. Soc.* **2002**, *124*, 9030; b) J. Zhou, J.; M.-C. Ye, Z.-Z. Huang, Y. Tang, *J. Org. Chem.* **2004**, *69*, 1309; c) J. Zhou, M.-C. Ye, Y. Tang, *J. Comb. Chem.* **2004**, *6*, 301; d) M.-C. Ye, B. Li, J. Zhou, X.-L. Sun, Y. Tang, *J. Org. Chem.* **2005**, *70*, 6108.

22 a) D. A. Evans, T. Rovis, M. C. Kozlowski, J. S. Tedrow, *J. Am. Chem. Soc*., **1999**, *121*, 1994; b) D. A. Evans, T. Rovis, M. C. Kozlowski, C. W. Dowey, J. S. Tedrow, *J. Am. Chem. Soc*. **2000**, *122*, 9134.

23 a) H. Werner, R. Vicha, A. Gissibl, O. Reiser, *J. Org. Chem.* **2003**, *68*, 10166; b) M. Glos, O. Reiser, *Org. Lett.* **2000**, *2*, 2045.

24 a) C. Foltz, M. Enders, S. Bellemin-Laponnaz, H. Wadepohl, L. H. Gade, *Chem. Eur. J.* **2007**, *13*, 5994; b) C. Dro, S. Bellemin-Laponnaz, R. Welter, L. H. Gade, *Angew. Chem. Int. Ed. Engl.* **2004**, *34*, 4479; c) C. Foltz, B. Stecker, G. Marconi, S. Bellemin-Laponnaz, H. Wadepohl, L. H. Gade, *Chem. Commun.* **2005**, 5115; d) B. D. Ward, S. Bellemin-Laponnaz, L.-H. Gade, *Angew. Chem. Int. Ed.* **2005**, *44*, 1668.

25 R. W. Taft, I. C. Lewis, *J. Am. Chem. Soc.* **1957**, *80*, 2436.

26 a) D. A. Evans, M. C. Kozlowski, J. A. Murry, C. S. Burgey, K. R. Campos, B. T. Connell, R. J. Staples, *J. Am. Chem. Soc*. **1999**, *121*, 669; b) D. A. Evans, S. J. Miller, T. Lectka, P. von Matt, *J. Am. Chem. Soc*. **1999**, *121*, 7559; c) D. A. Evans, E. J. Olhava, J. S. Johnson, J. M. Janey, *Angew. Chem. Int. Ed*. **1998**, *37*, 3372.

27 G. Desimoni, G. Faita, P. Quadrelli, *Chem. Rev*. **2003**, *103*, 3119.

28 a) J. Thorhauge, M. Roberson, R. G. Hazell, K. A. Jørgensen, *Chem. Eur. J.* **2002**, *8*, 1888; b) D. A. Evans, T. Rovis, J. S. Johnson, *Pure Appl. Chem.* **1999**, *71*, 1407.

29 C. Christensen, K. Juhl, R. G. Hazell, K. A. Jørgensen, *J. Org. Chem.* **2002**, *67*, 4875.

30 K. B. Jensen, J. Thorauge, R.-G. Mazell, K. A. Jørgensen, *Angew. Chem. Int. Ed.* **2001**, *69*, 7511.

31 a) H. Schäfer, D. Seebach, *Tetrahedron* **1995**, *51*, 2305; b) A. Alexakis, C. Benhaim, *Org. Lett.* **2000**, *2*, 2579; c) A. Duursma, A. J. Minnaard, B. L. Feringa, *J. Am. Chem. Soc.* **2003**, *125*, 3700; d) N. Sewald, *Angew. Chem., Int. Ed.* **2003**, *42*, 5794; e) H. Choi, Z. Hua, I. Ojima, *Org. Lett.* **2004**, *6*, 2689; f) D. M. Mampreian, A. H. Hoveyda, *Org. Lett.* **2004**, *6*, 2829; g) T. Hayashi, T. Senda, M. Ogasawara, *J. Am. Chem. Soc.* **2000**, *122*, 10716; h) J.-G. Ji, D. M. Barnes, J. Zhang, S. A. King, S. J. Wittenberger, H. E. Morton, *J. Am. Chem. Soc.* **1999**, *121*, 10215; i) T. Okino, Y. Hoashi, Y. Takemoto, *J. Am. Chem. Soc.* **2003**, *125*, 12672; j) M. Watanabe, A. Ikagawa, H. Wang, K. Murata, T. Ikariya, *J. Am. Chem. Soc.* **2004**, *126*, 11148; k) H. Li, Y. Wang, L. Tang, L. Deng, *J. Am. Chem. Soc.* **2004**, *126*, 9906; m) C. Czekelius, E. M. Carreira, *Angew. Chem. Int. Ed.* **2003**, *42*, 4793.

32 Y.-X. Jia, S.-F. Zhu, Y. Yang, Q.-L. Zhou, *J. Org. Chem.* **2006**, *71*, 75.

33 A. E. Russel, S. P. Miller, J. P. Morken, *J. Org. Chem.* **2000**, *65*, 8381.

34 P. L. Anelli, S. Banfi, F. Montanari, S. Quici, *J. Org. Chem*. **1989**, *54*, 2970.

35 R. A. Sheldon, I. W. C. E. Arends, *Adv. Synth. Catal.* **2004**, *346*, 1051.

36 L. D. Jones, D. A. Sommerville, F. Basolo, *Chem. Rev.* **1979**, *79,* 139.

37 a) T. Punniyamurthy, J. Iqbal, *Tetrahedron Lett.* **1994**, *35*, 4003; b) S. J. S. Singh Kaira, T. Punniyamurthy, J. Iqbal, *Tetrahedron Lett.* **1994**, *35*, 4847.

C. Summary

It was the aim of this work to develop a generally applicable strategy for the immobilization of catalysts on different nanoparticles with particular interest in the "heterogenization" of chiral azabis(oxazolines),[1] which represent a predestined class of ligands for the grafting on solid supports due to their central nitrogen atom. To this end, a copper(I)-catalyzed[2] azide/alkyne cycloaddition[3] (CuAAC) reaction was envisaged to be the most versatile tagging method, allowing even the use of preformed transition-metal complexes after according derivatization with an alkyne moiety. Such a route was expected to provide distinct advantages over the in-situ complexation by adding the equivalent amount of metalsalt to the immobilized ligand, since the exact determination of ligand loading is challenging. This issue was aggravated by recent investigations from Reiser et al.,[4] indicating that not only an excess of transition metal has a detrimental effect on the optical yields attained, but also a ligand surplus is capable of diminishing the level of enantioselectivity in certain reactions.[4,5] Whereas the negative influence of uncomplexed metal centers on the ee-values obtained is apparent, since no stereodiscriminating environment is coined to the catalytic center by a chiral ligand, the elucidation of the mechanism of the unprecedented effect of ligand surplus was considered highly relevant for immobilized ligands on any type of support. Thus, preliminary investigations focused on the understanding of this effect with the aim to develop strategies, which could help circumventing the negative influence of ligand excess in the reactions affected.

1. Significance of ligand/metal-ratio

The stereoelectronic outcome of the asymmetric copper(II)-catalyzed Michael-addition of indole (**178**) to benzylidene malonates **179** was found to be highly dependent from the azabis(oxazoline)/copper-ratio applied (Scheme 75). Enantioselectivities up to >99% were obtained under the prerequisite that the ligand/metal ratio was tuned meticulously.[4]

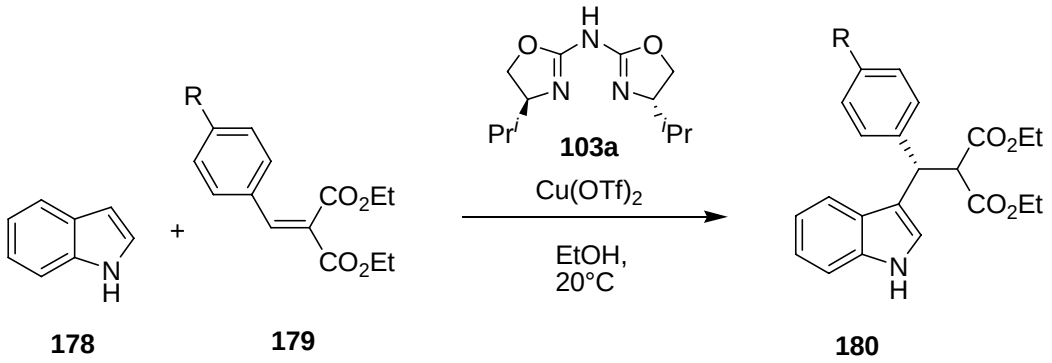

Scheme 75. Enantioselective Friedel-Crafts Alkylation of indole (**178**) with benzylidene malonates **179** catalyzed by azabis(oxazoline)/copper(II) complexes.

Explicit attention had to be paid to the electronic parameters of the malonate derivatives **179**. If comparatively electron rich benzylidene malonates were used, any excess of ligand had to be avoided to reach high enantioselectivities, a fact which is in contradiction to a common paradigm in asymmetric catalysis that calls for excess of ligand in order to suppress a background reaction promoted by metal centers in a ligand-free, i.e. achiral environment. It was found that the sensitivity of enantioselectivity towards ligand excess vanished with decreasing inductive contribution of the substituent. This trend was even reversed for strong electron acceptors, which required an excess of ligand for maximum ee. A semi-logarithmic plot of optical yields at two different ligand/metal ratios versus the σ_I values[6] of the substituted benzylidene malonates **179** resulted in a sigmoid trajectory (Figure 45).

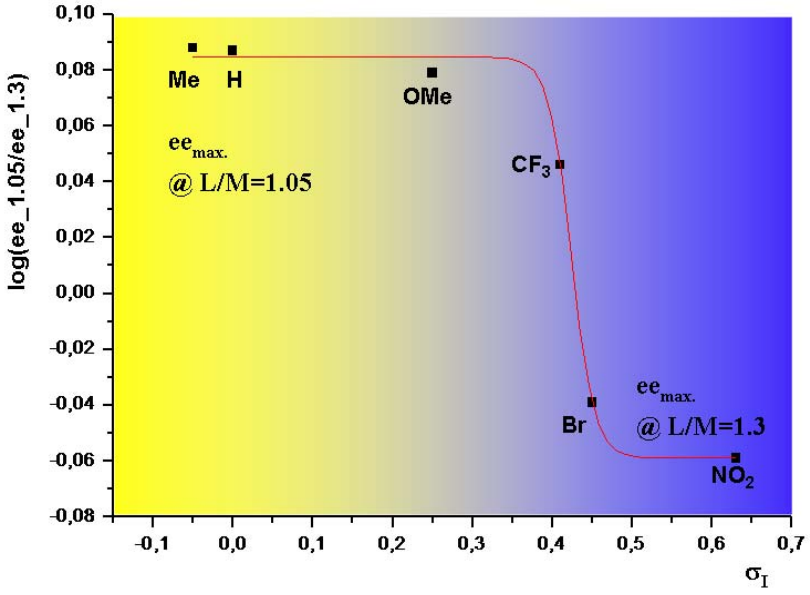

Figure 45. Semi-logarithmic correlation of optical yield ratio versus σ_I values of *para*-substituents in the reaction of indole (**178**) with different substituted benzylidene-malonates **179.**

More strikingly, the significance of the ligand/metal ratio vanished in the presence of an excess of lithiumtriflate, giving rise to equal or even superior enantioselectivities at any ligand/metal ratio employed (Table 25).

Table 25. Dependence of enantioselectivity on ligand/metal-ratio in the 1,4-addition of indole (**178**) to benzylidene malonates (**179a,e,g**): Influence of triflate as additive.[a]

entry	ligand/metal-ratio	R	Li(OTf)/X	yield (%)	ee (%)[b]
1[c]	1.04/1.0	H (**179a**)	-	97	>99[d]
2	1.05/1.0	H (**179a**)	5	90	93
3	1.3/1.0	H (**179a**)	-	98	81[d]
4	1.3/1.0	H (**179a**)	5	97	96
9[c]	1.05/1.0	4-NO_2 (**179g**)	-	92	82[d]
10	1.05/1.0	4-NO_2 (**179g**)	5	89	96
11	1.3/1.0	4-NO_2 (**179g**)	-	83	94[d]
12	1.3/1.0	4-NO_2 (**179g**)	5	73	93

[a] Reagents and conditions: 1.2 mmol Indole, 1.0 mmol malonate, 5 mol% **103a**, 20°C, 8h, solvent: 4 mL EtOH. [b] Determined by HPLC; [c] Ref.[4b] [d] Obtained in at least two independent runs.

It was reasoned that a five-membered square-pyramidal complex, having triflate in apical position, might be less prone to the effect of ligand/metal-ratio. Thus, applying an excess of triflate was foreseen to be a convenient strategy to overcome the difficult adjustment of the ligand/metal-ratio with nanoparticle-supported azabis(oxazolines).

2. Azabis(oxazolines) immobilized on nanoparticles

Azabis(oxazoline) ligands and azabis(oxazoline)-copper(II) complexes respectively were successfully immobilized on superparamagnetic magnetite@silica- and ferromagnetic carbon coated cobalt-nanoparticles[7] using a concise "click" protocol. The application of selfsame protocol was not feasible using monolayer-protected gold nanoparticles of the Brust-type,[8] since mandatory copper(I) caused disintegration of the thiolate shell followed by the irreversible aggregation of the Au cores. Moreover, the oxazoline-moieties of the azabis(oxazolines) were not stable against an attack of thiols, thus making the immobilization of this type of ligand in an environment of

thiolate-SAMs appear disadvantageous. However, different azide-functionalized magnetic nanobeads were not affected by such incompatibilities, thus resulting in azabis(oxazoline)-ligands and -copper(II) complexes respectively, grafted on magnetic nanoparticles via a triazole-linker (Figure 46). Propargylated azabis(oxazoline)-ligands and Cu(II)-complexes were equally active in the CuAAC reaction with the azide functionalized core/shell materials, resulting in quantitative conversion of the azide moieties. The material thus obtained, proved to be highly active and selective in the asymmetric monobenzoylation of racemic 1,2-diols. Magnetite@silica-nanoparticle supported catalysts could be recycled via magnetic decantation (Figure 47) after each run and proved to be active in at least five consecutive batch reactions without any significant drop in selectivity (Scheme 76).

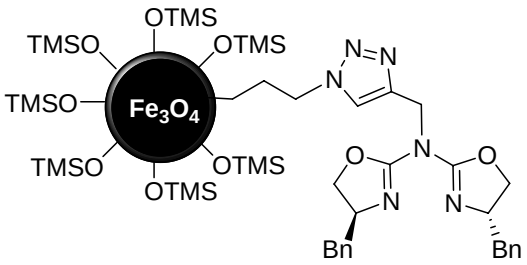

146

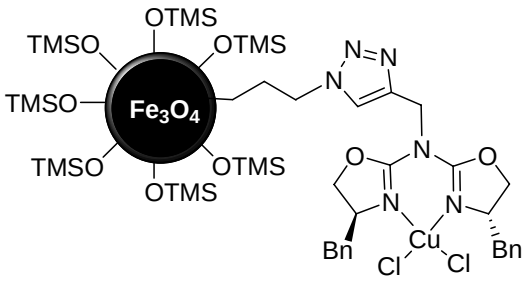

147

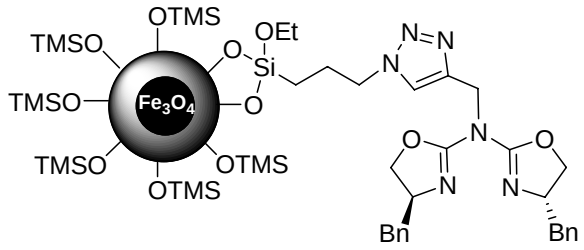

144

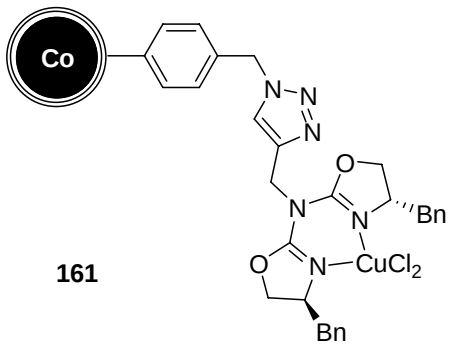

161

Figure 46. Different magnetite@silica and Co/C-immobilized azabis(oxazolines) and azabis(oxazoline)-copper(II) complexes.

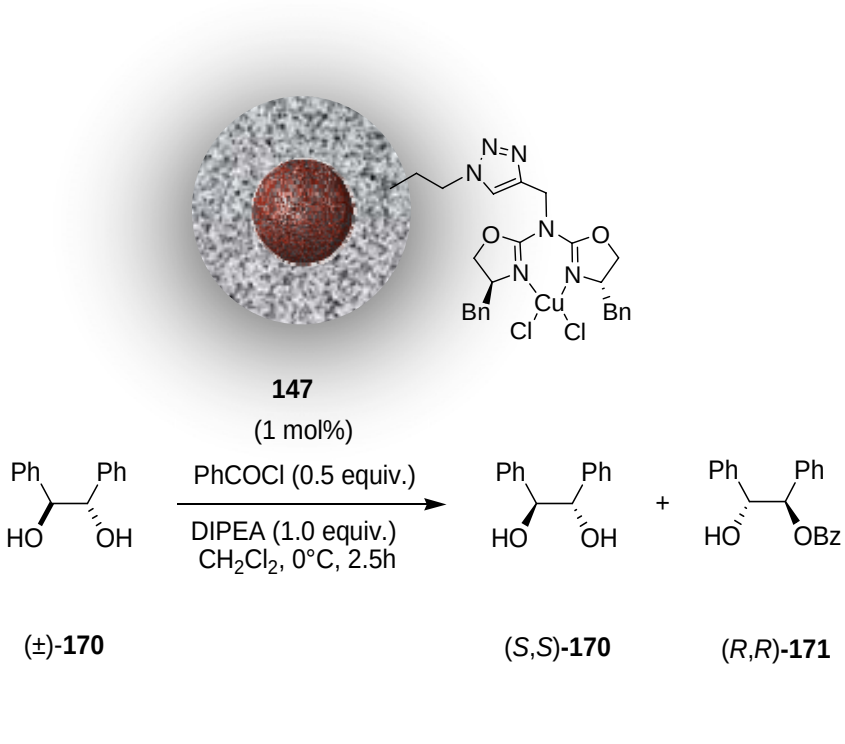

Scheme 76. Cu(II) catalyzed monobenzoylation of (±)**-170**: Recycling experiment using azabis(oxazoline)-$CuCl_2$ complexes immobilized on magnetite@silica-nanoparticles.

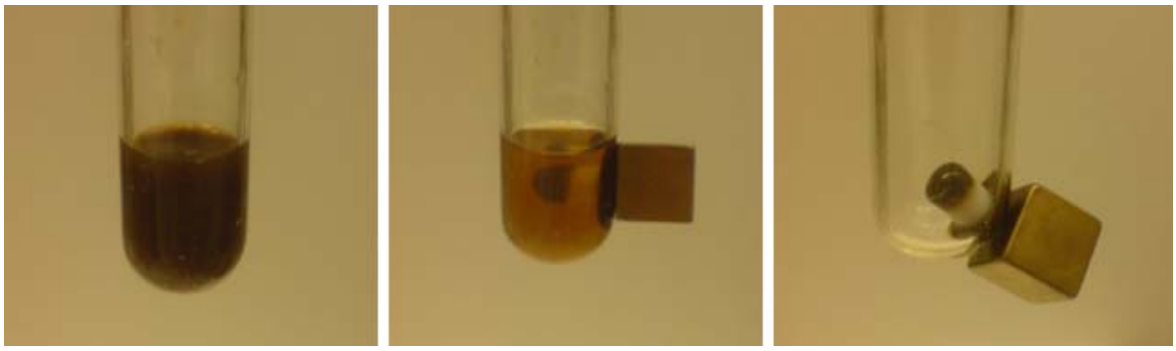

Figure 47. Dispersion of the magnetite@silica nanoparticle immobilized catalyst **146**·$Cu(OTf)_2$ during the asymmetric benzoylation of (±)**-170** (left). Recycling of the catalyst through magnetic decantation (right).

Co/C-nanoparticle supported catalyst **161** was as active in 5 iterative runs at batch conditions and allowed the implementation of the nanomagnets in a closed circuit-type reactor under continuous-flow conditions. The high saturation magnetization of the ferromagnetic cobalt cores allowed those particles to act as their own nanosized stirrers in a microreactor that was operated vertically between adjacent parallel flanks of two magnetic stir motors (Figure 48).

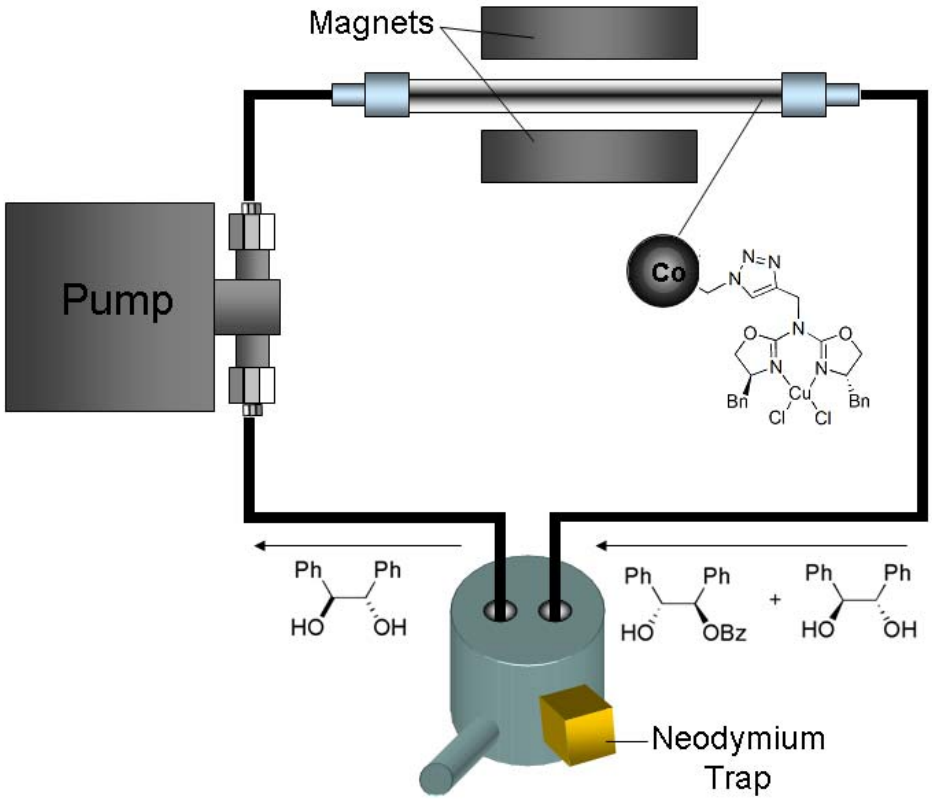

Figure 48. Representation of a closed circuit-type reactor for the asymmetric monobenzoylation of racemic diol **170**.

In addition, the cobalt nanoparticles were contained in the magnetic field. Hence, a membrane on the outlet of the microreactor was unnecessary, thus preventing a flow-collapse which would inevitably arise from a blocked membrane.

The asymmetric monobenzoylation of 1,2-diols is known to be indifferent towards the influence of the ligand/metal-ratio.[4b] However, nanoparticle supported azabis(oxazolines) gave only very poor yields and enantioselectivities in the asymmetric Michael-addition of indole (**178**) to benzylidene malonates **179**, thus limiting the scope for further investigations concerning ligand/metal-ratio and the application of lithiumtriflate in this regard.

3. Oxidation catalysts immobilized on carbon coated cobalt nanoparticles

Azabis(oxazoline)-copper(II) complexes were the first example of a catalyst immobilized on carbon coated cobalt nanoparticles by then. In general, core/shell structures that possess a ferromagnetic metal core bear the disadvantage of being willingly oxidized. In contrast to the magnetite particles, that would be oxidized to the

likewise ferrimagnetic maghemite, cobaltoxide is antiferromagnetic, thus implicating a potential loss of magnetizability of the nanobeads. Hence, the impermeability of the carbon coating against oxidants during several iterative reactions was expected to set a benchmark for immanent limitations on the stability of this material. To this end, the stable nitroxyl-radical TEMPO[9] was immobilized on Co/C-nanoparticles, resulting in a highly active and recyclable heterogeneous organocatalyst, which was capable of oxidizing primary alcohols chemoselectively into the corresponding aldehydes (Scheme 77).

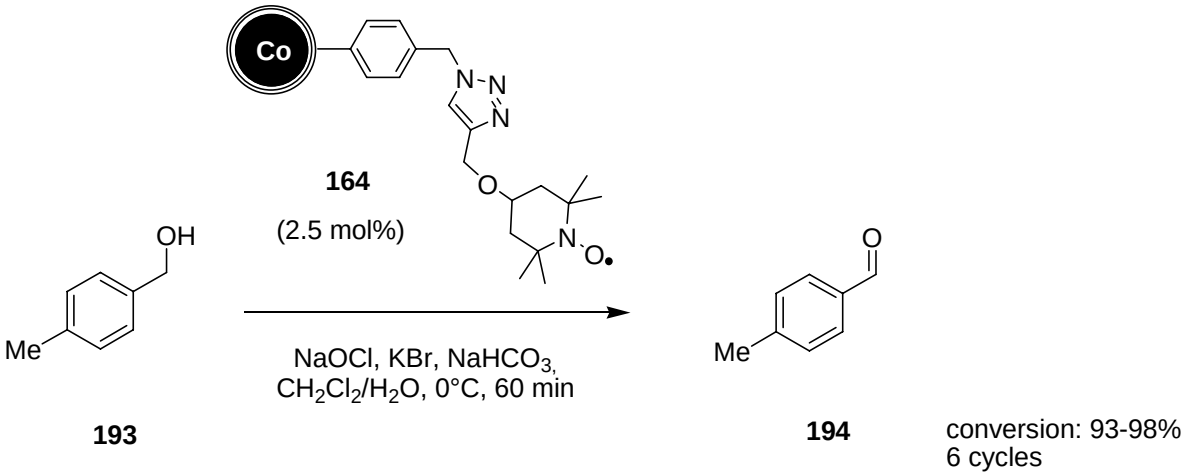

Scheme 77. CoNP-TEMPO **164** mediated oxidation of 4-methylbenzylic alcohol **193**.

No morphologic alterations were observed in the TEM analyses of the recovered catalyst. Next, Co(II)-Schiff base complexes[10] were tethered to Co/C-nanoparticles, forming a catalyst that was able to bind and activate molecular oxygen for the oxidation of e.g. secondary alcohols. A setup similar to the one applied for the monobenzoylation of 1,2-diols under continuous-flow conditions was used to agitate the nanomagnets while oxygen was purged through the reactor. The nanocomposite was retained after the reaction was finished, thus allowing the catalyst to be reused without further treatment.

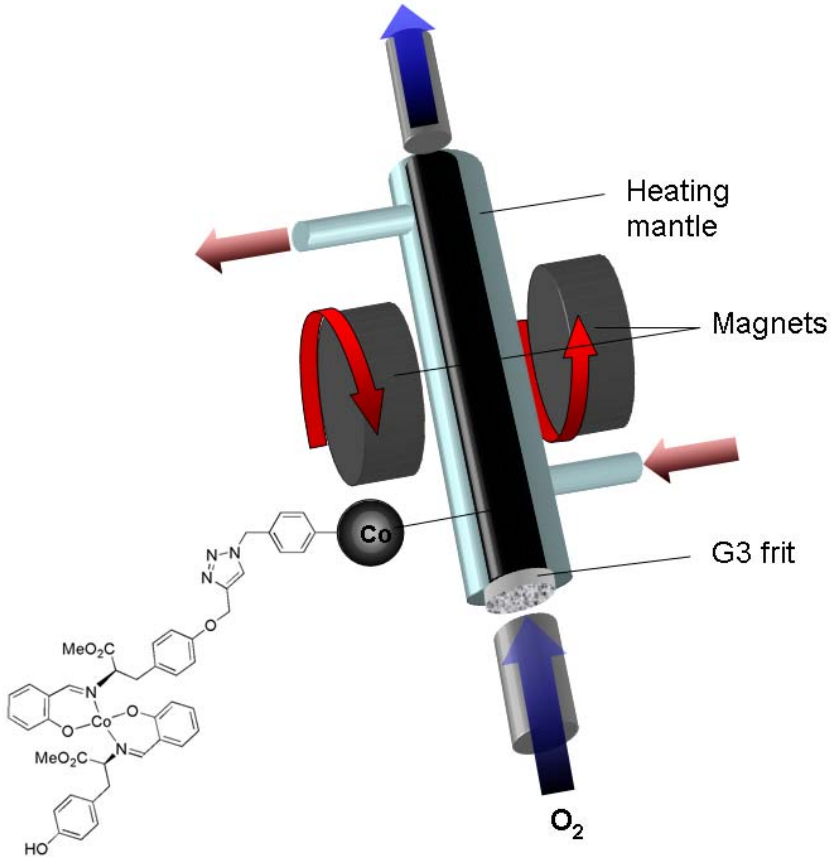

Figure 49. Schematic representation of the setup used for the Co(II)-Schiff base catalyzed oxidation with molecular oxygen.

In summary, novel carbon coated cobalt nanoparticles,[7] which had not been tagged with homogeneous catalysts hitherto, turned out to be an extremely stable support that allowed rapid recycling due to the inherent ferromagnetism of the cobalt cores.

4. References

1 a) M. Glos, O. Reiser, *Org. Lett.* **2000**, *14*, 2045; b) H. Werner, R. Vicha, A. Gissibl, O. Reiser, *J. Org.Chem.* **2003**, *68*, 10166.

2 a) C. W. Tornøe, M. Meldal, *In American Peptide Symposium;* M. Lebl, R. A. Houghten, Eds, American Peptide Society and Kluwer Academic Publishers: San Diego, CA, **2001**, p 263; b) V. V. Rostovtsev, L. G. Green, V. V. Fokin, K. B. Sharpless, *Angew. Chem. Int. Ed*. **2002**, *41*, 2596; c) C. W. Tornøe, C. Christensen, M. Meldal, *J. Org. Chem*. **2002**, *67*, 3057.

3 R. Huisgen, *Pure Appl. Chem.* **1989**, *61*, 613.

4 a) A. Schätz, R. Rasappan, M. Hager, A. Gissibl, O. Reiser, *Chem. Eur. J.* **2008**, *14*, 7259; b) R. Rasappan, M. Hager, A. Gissibl, O. Reiser, *Org. Lett.* **2006**, *8*, 6099.

5 Z. Shao, J. Wang, K. Ding, A. Chan, *Adv. Synth. Catal.* **2007**, *349*, 2375.

6 R. W. Taft, I. C. Lewis, *J. Am. Chem. Soc.* **1957**, *80*, 2436.

7 R. N. Grass, E. K. Athanassiou, W. J. Stark, *Angew. Chem.* **2007**, *119*, 4996.

8 a) M. Brust, A. Walker, D. Bethell, D. J. Schiffrin, R. Whyman, *J. Chem. Soc., Chem. Commun.* **1994**, 801; b) M. Brust, J. Fink, D. Bethell, D. J. Schiffrin, C. J. Kiely, *Chem. Commun*. **1995**, 1655.

9 a) P. L. Anelli, C. Biffi, F. Montanari, S. Quici, *J. Org. Chem*. **1987**, *52*, 2559; b) P. L. Anelli, S. Banfi, F. Montanari, S. Quici, *J. Org. Chem*. **1989**, *54*, 2970; c) P. L. Anelli, F. Montanari, S. Quici, *Org. Synth*. **1990**, *69*, 212.

10 a) T. Yamada, T. Mukaiyama, *Chem. Lett.* **1989**, 519; b) K. Kato, T. Yamada, T. Takai, S. Inoki, S. Isayama, *Bull. Chem. Soc. Jpn.* **1990**, *63*, 179; c) S. Inoki, T. Mukaiyama, *Chem. Lett.* **1990**, 67.

D. Experimental

1. General comments

All reactions were carried out in oven dried glassware under an atmosphere of dry nitrogen unless otherwise indicated. Commercially available reagents were used as received. Carbon coated cobalt nanoparticles were donated from Prof. W. J. Stark (ETH Zürich). Magnetic nanobeads were dispersed with the aid of an ultrasound bath (Sonorex RK 255 H-R, Bandelin) and recovered with the aid of a neodymium based magnet (N48, W-12-N, Webcraft GmbH, side length 12 mm) unless stated otherwise. The following solvents and reagents were purified prior to use:

Dichloromethane (CH_2Cl_2) was distilled from calciumhydride. Ethanol (EtOH) and methanol (MeOH) were distilled from magnesium and stored over molecular sieves (3 A). Tetrahydrofurane (THF) was distilled from sodium wire. Toluene and Xylene were dried with CaH_2, distilled and stored over sodium wire. Ethylacetate (EE) and hexanes (PE) for chromatographic separations were distilled before use.

Benzaldehyde, benzoylchloride, 2-methylpropanal (**195**), ethyl-2-cyclohexanone-carboxylate (**197**) and *N,N*-diisopropylethylamine (DIPEA) were distilled prior to use. $CoCl_2 \cdot 6H_2O$ was dried at 110°C for 4 h.

Analytical thin layer chromatography was performed on Merck TLC aluminium sheets silica gel 60 F_{254}. Visualization was accomplished with UV light and vaniline solution followed by heating. Liquid chromatography was performed using Merck silica gel 60 (70-230 mesh ASTM).

NMR spectroscopy

^1H (300 MHz) NMR spectra were recorded on a Bruker AC 300 spectrometer at ambient temperature. Data are as follows: Chemical shift in ppm from internal $CHCl_3$ (7.27 ppm) as standard on the δ scale, multiplicity (b = broad, s = singlet, d = doublet, t = triplet, q = quartet, dd = doublet of doublet and m = multiplet), integration and coupling constant (Hz). ^{13}C (75.5 MHz) NMR spectra were recorded on a Bruker AC 300 spectrometer at ambient temperature. Chemical shifts are reported in ppm from internal $CHCl_3$ (77 ppm) as standard on the δ scale.

HPLC

High performance liquid chromatography was carried out using a HPLC 335 detector on a 325 system by Kontron Instruments. Chiralcel OD/OD-H, OJ and AS respectively served as chiral stationary phase.

GC

Gas chromatography was performed on a Fisons GC 8000.

Melting points

The melting points were meassured on a Büchi SMP-20 apparatus in a silicon oilbath. Values thus obtained were not corrected.

Alpha

The optical rotation was determined in a Perkin Elmer 241 polarimeter at 589 nm wavelength (sodium-d-line) in a 1.0 dm measuring cell of 2 mL volume.

Mass spectrometry

Mass spectrometry was performed using a Finnigan ThermoQuest TSQ 7000 at the Central Analytical Laboratory (Universität Regensburg).

IR spectroscopy

ATR-IR spectroscopy was carried out on a Biorad Excalibur FTS 3000 spectrometer, equipped with a Specac Golden Gate Diamond Single Reflection ATR-System.

Elemental microanalysis

Elemental microanalysis was performed on a LECO CHN-900 at the ETH Zürich.

TEM

Transmission electron microscopy was carried out with a Philips CM30 ST equipped with a LaB_6 cathode and operated at 300kV point resolution (~ 4 Å) at the ETH Zürich.

2. Syntheses of literature-known compounds

The following compounds were prepared according to literature synthesis: (4*S*)-(1-Methylethyl)-2-oxazolidinone (**106a**);[1] (4*S*)-(1,1-Dimethylethyl)-2-oxazolidinone (**106b**);[1] (4*R*)-Phenyl-2-oxazolidinone (**106c**);[1] (4*S*)-Benzyl-2-oxazolidinone (**106d**);[2] 2-Amino-4,5-dihydro-(4*S*)-(1-methylethyl)-1,3-oxazole (**108a**);[1] 2-Amino-4,5-dihydro-(4S)-(1,1-dimethylethyl)-1,3-oxazole (**108b**);[1] 2-Amino-4,5-dihydro-(4*R*)-(phenyl)-1,3-oxazole (**108c**);[1] 2-Amino-4,5-dihydro-(4*S*)-(benzyl)-1,3-oxazole (**108d**);[2] 2-Ethoxy-(4*S*)-(1-methylethyl)-4,5-dihydro-oxazole (**107a**);[1] 2-Ethoxy-(4*S*)-(1,1-dimethylethyl)-4,5-dihydro-oxazole (**107b**);[1] 2-Ethoxy-(4*R*)-phenyl-4,5-dihydro-oxazole (**107c**);[1] 2-Ethoxy (4*S*)-Benzyl-4,5-dihydro-oxazole (**107d**);[2] Bis[4,5-dihydro-(4*S*)-(1-methylethyl)-1,3-oxazol-2-yl]-amine (**103a**);[1] Bis[4,5-dihydro-(4*S*)-(1,1-dimethylethyl)-1,3-oxazol-2-yl]-amine (**103b**);[1] Bis[4,5-dihydro-(4*R*)-(phenyl)-1,3-oxazol-2-yl]-amine (**103c**);[1] Bis[4,5-dihydro-(4*S*)-(benzyl)-1,3-oxazol-2-yl]-amine (**103d**);[2] Bis-[4,5-dihydro-(4*S*)-(1-methylethyl)-1,3-oxazol-2-yl]-methylamine (**109a**);[1] Bis-[4,5-dihydro-(4*S*)-(1,1-dimethylethyl)-1,3-oxazol-2-yl]-methylamine (**109b**);[1] Bis-[4,5-dihydro-(4*S*)-(phenyl)-1,3-oxazol-2-yl]-methylamine (**109c**);[1] Bis-[4,5-dihydro-(4*S*)-(benzyl)-1,3-oxazol-2-yl]-methylamine (**109d**);[1] Bis-[4,5-dihydro-(4*S*)-(1-methylethyl)-1,3-oxazol-2-yl]-prop-2-ynyl-amine (**120a**);[1] L-3-(4-Propargyloxyphenyl)-2-aminopropionic acid methyl ester (**166b**);[3] 1-(Nitrophenyl)-2-propyn-1-one (**142**);[4] 12-Bromododecanethanethioate (**132**);[5] 3-Azidopropyl-triethoxysilane;[6] Diethyl-2-benzylidene malonate;[7] Diethyl-2-(4-methylbenzylidene) malonate;[7] Diethyl-2-(4-methoxybenzylidene) malonate;[7] Diethyl-2-(4-trifluoromethylbenzylidene) malonate;[7] Diethyl-2-(2-bromobenzylidene) malonate;[7] Diethyl 2-(4-bromobenzylidene) malonate;[7] Diethyl 2-(4-nitrobenzylidene) malonate;[7] Diethyl 2-(4-dimethylaminobenzylidene) malonate.[7]

3. Syntheses of novel compounds

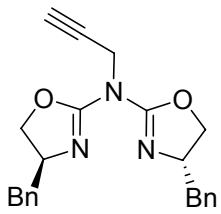

Bis-[4,5-dihydro-(4*S*)-(benzyl)-1,3-oxazol-2-yl]-prop-2-ynyl-amine (120b):

336 mg (1.0 mmol) of azabis(oxazoline) **103d** was dissolved in anhydrous THF (8 mL) and the solution was cooled down to -78°C under nitrogen atmosphere. *n*-Butyllithium (0.66 mL; 1.6 N in hexane, 1.1 mmol) was added dropwise. Upon addition, the solution changed its colour from to a bright orange. The reaction mixture was stirred for further 15 min before propargylbromide (440 µL; 80% (w/w) in toluene, 4 mmol) was injected through a septum. The solution was allowed to reach ambient temperature while stirring continued for further 12 h. A saturated solution of Na_2CO_3 was added and the mixture was concentrated. The aqueous layer was extracted thrice with CH_2Cl_2 and the combined organic layers were dried over $MgSO_4$. After removing the solvent under vacuum, 360 mg (0.96 mmol, 96%) of **120b** were obtained as brown oil.

^{1}H-NMR (300 MHz, $CDCl_3$): δ = 2.29 (s, 1 H), 2.62 (dd, *J* = 8.3, 13.2 Hz, 2 H), 3.21 (dd, *J* = 5.0, 13.8 Hz, 2 H), 4.2 (dd, *J* = 6.3, 7.8 Hz, 2 H), 4.28-4.46 (m, 4 H), 4.6 (d, *J* = 1.4 Hz, 2 H), 7.12-7.35 (m, 10 H); ^{13}C-NMR (75.5 MHz, $CDCl_3$): δ = 169.4, 136.1, 128.1, 127.2, 70.7, 65.2, 40.1, 38.5; IR (ν/cm^{-1}): 2959, 1700, 1632, 1545, 1407, 1383, 1326, 1261, 1240, 1092, 1051, 1025, 969, 935, 796, 722, 573; MS (CI): m/z (%) = 374 (MH^+, 100), 233 (2), 215 (4), 195 (18).

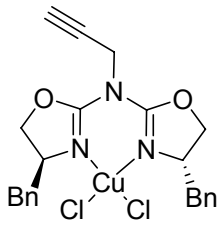

Copper(II)chloride-[Bis-(4-benzyl-4,5-dihydro-oxazol-2-yl)-prop-2-ynyl-amine]:
Propargylated azabis(oxazoline) **120b** (373.5 mg, 1.0 mmol) was stirred in CH_2Cl_2 (5 mL) at ambient temperature together with $CuCl_2$ (121 mg, 0.9 mmol) for 3 h. The solvent was evaporated to yield 494 mg of a green solid (99%).
IR (ν/cm^{-1}): 3229, 1678, 1588, 1489, 1460, 1248, 1096, 952, 705, 668, 512.

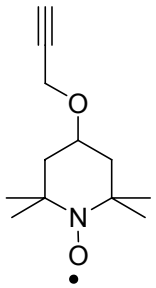

2,2,6,6-Tetramethyl-4-(prop-2-ynyloxy)piperidine-1-oxyl (163):
To a stirred suspension of NaH (60% in mineral oil, 850 mg, 22.0 mmol) in dry DMF (50 mL) was added 4-hydroxy-TEMPO **162** (3.0 g, 17.4 mmol) in portions at 0°C and stirred for 30 min. Propargylbromide (2.4 mL, 22.0 mmol) was added dropwise at 0°C and the resulting mixture was allowed to warm to room temperature while stirring continued for further 3 h. Water (80 mL) was added and the solution was extracted five times with EE (80 mL). The combined organic layers were dried over $MgSO_4$, filtered, evaporated under reduced pressure and purified by column chromatography (PE/EE = 3/1) to afford 3.1 g of compound **163** as a ruby-red solid (85%).
m.p. 57–59°C; IR (ν/cm^{-1}): 3230, 2974, 2937, 2111, 1719, 1313, 1243, 1176, 1083, 1022, 938, 734, 691, 594, 554; MS (EI-MS, 70 eV): m/z = 210 (M^+, 44).

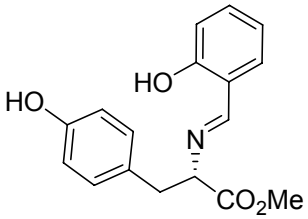

(*S*,E)-Methyl-2-(2-hydroxybenzylideneamino)-3-(4-hydroxyphenyl)propanoate (167a):

Salicylaldehyde (2.44 g, 20 mmol) was added to a stirred solution of L-tyrosine methyl ester (3.9 g, 20 mmol) and molecular sieves (3 A) in anhydrous methanol (25 mL) and the reaction mixture was stirred at ambient temperature for 24 h. The molecular sieves were filtered off and the solution was concentrated in vacuo down to 10 mL volume. The Schiff base precipitated over night at 4°C from the solution and could be separated by filtration to afford **167a**, which was sufficiently pure to be used without further purification (3.59 g, 60%).

^{1}H-NMR (300 Hz, DMSO): δ = 2.93-2.99 (m, 1 H), 3.12-3.18 (m, 1 H), 3.70 (s, 3 H), 4.35 (dd, *J* = 5.3, 8.19 Hz, 1 H), 6.62-6.67 (m, 2 H), 6.86-6.99 (m, 4 H), 7.31-7.38 (m, 2 H), 8.33 (s, 1 H), 9.24 (s, 1 H) 13.1 (s, 1 H); ^{13}C-NMR (DMSO): δ = 171.1, 167.5, 160.1, 155.8, 132.6, 131.7, 130.2, 126.6, 118.6, 118.3, 116.3, 114.9, 71.4, 51.9; IR (ν/cm^{-1}): 2571, 1739, 1637, 1610, 1519, 1442, 1371, 1341, 1238, 1154, 1107, 873, 829, 763, 527; MS (CI): m/z (%) = 300 (MH^+, 100), 196 (1).

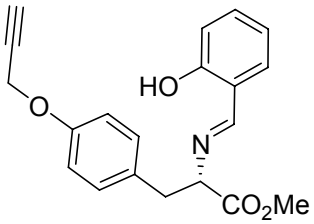

(*S*,E)-Methyl-2-(2-hydroxybenzylideneamino)-3-(4-(prop-2-ynyloxy)phenyl) propanoate (165b):

Salicylaldehyde (2.44 g, 20 mmol) was added to a stirred solution of *L*-(4-propargyloxy)tyrosine methyl ester (4.66 g, 20 mmol) in anhydrous methanol (25 mL) and the reaction mixture was stirred at ambient temperature for 12 h. The Schiff base

precipitated in the course of the reaction and was subsequently separated from the supernatant by filtration to afford **165b**, which was sufficiently pure to be used without further purification (5.40 g, 81%).

^{1}H-NMR (300 Hz, $CDCl_3$): δ = 2.48 (t, *J* = 2.37 Hz, 1 H), 3.09 (dd, *J* = 9.0, 13.73 Hz, 1 H), 3.32 (dd, *J* = 4.69, 13.73 Hz, 1 H), 3.76 (s, 3 H), 4.11 (dd, *J* = 4.7, 8.97 Hz, 1 H), 4.63 (d, *J* = 2.38 Hz, 2 H), 6.81-6.89 (m, 3 H), 6.98 (d, *J* = 8.2 Hz, 1 H), 7.06-7.15 (m, 3 H) 7.29-7.36 (m, 1 H), 7.97 (s, 1 H), 12.96 (s, 1 H); ^{13}C-NMR ($CDCl_3$): δ = 171.3, 166.9, 160.9, 156.4, 132.8, 131.7, 130.6, 129.7, 118.7, 118.4, 117.1, 114.9, 78.5, 75.4, 73.3, 55.8, 52.4, 39.1; IR (ν/cm^{-1}): 3270, 1732, 1633, 1579, 1513, 1407, 1281, 1242, 1196, 1172, 1114, 1033, 983, 873, 834, 771, 656, 599; MS (CI): m/z (%) = 338 (MH^+, 100).

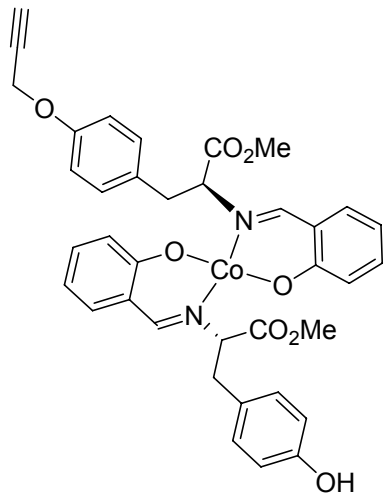

[Co((*S*,*E*)-methyl 2-(2-hydroxybenzylideneamino)-3-(4-(prop-2-ynyloxy) phenyl) propanoate) ((*S*,*E*)-methyl 3-(4-((1-benzyl-1H-1,2,3-triazol-4-yl)methoxy)phenyl)-2-(2-hydroxybenzylideneamino)propanoate)] (169):

Schiff base **165a** (1.49 g, 5 mmol) and **165b** (1.68 g, 5 mmol) were dissolved in acetonitrile (25 mL) containing anhydrous cobalt(II)chloride (mg, 2.5 mmol) and stirred for 20 h at ambient temperature under nitrogen atmosphere. Removal of the solvent yielded 3.46 g (99%) of **169** as a green soild.

IR (ν/cm^{-1}): 3274, 1744, 1600, 1511, 1448, 1223, 1015, 762, 667, 537, 454.

4. Nanoparticle syntheses

4.1 Synthesis of monolayer-protected gold clusters

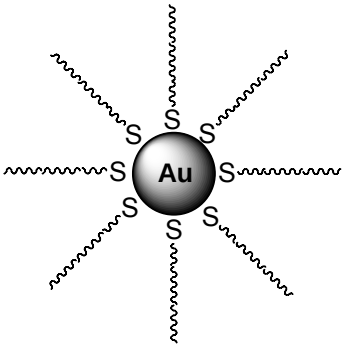

Dodecanthiol-protected gold cluster (101):

0.31 g of $HAuCl_4$ (1.1 mmol) in 25 mL of water (milipore) was transferred into 80 mL of toluene using 1.5 g of tetraoctylammonium bromide (7 mmol). The organic phase was isolated, and 0.45 g of dodecanethiol (2.2 mmol) was added. The solution was cooled to 0°C and stirred for 10 min, after which 25 mL of a freshly prepared, aqueous $NaBH_4$-solution (0.38 g, 10 mmol) was added within 15 min. The slurry was allowed to stir further 30 min at 0°C and an additional 3 h at room temperature before the organic layer was separated and evaporated (< 50°C), producing a black, waxy solid. The product was suspended in 30 mL of ethanol, briefly sonicated to ensure complete dissolution of byproducts, collected on a glass filtration frit, and washed with at thrice with 80 mL of ethanol and twice with 150 mL of acetone.

The as-prepared AuMPCs were further purified via Soxhlet extraction. The nanoparticles were dissolved in toluene (50 mg/mL) and then placed into a Soxhlet thimble. 250 mL of acetone was used as the cleansing solvent. The product was recovered by dissolving the particles held within the thimble in toluene, affording 260 mg of **101**.

IR (ν/cm^{-1}): 2915, 2848, 1469, 718.

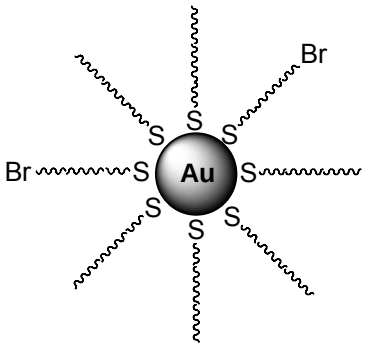

12-bromododecanthiol/dodecanthiol-protected gold cluster (135):

500 mg 12-bromododecanthiol (1.8 mmol) was dissolved in 220 mL anhydrous and degassed dichloromethane together with 800 mg of the alkanethiolate-protected gold cluster **101**. The reaction mixture was stirred for 30 h at room temperature. After this, the solvent removed under vacuum and the resulting precipitate was collected by filtration and washed thrice with 50 mL of absolute EtOH and twice with 50 mL anhydrous acetonitrile to give 780 mg of a black, waxy solid which was processed without further purification.

IR (ν/cm^{-1}): 2955, 2820, 1742, 1460, 717.

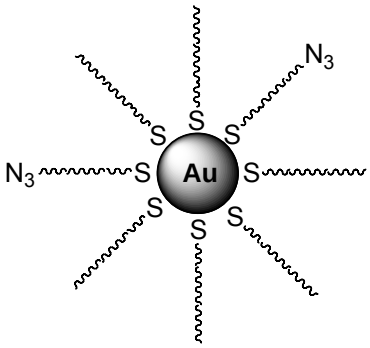

12-azidododecanthiol/dodecanthiol-protected gold cluster (134):

500 mg of 12-bromododecanthiol/dodecanthiol-protected gold clusters **135** were dissolved in CH_2Cl_2 (200 mL) together with tetrabutylammoniumazide (640 mg, 2.25 mmol). The solution was stirred for 12 h at ambient temperature. After this, the solvent was removed under vacuum and the resulting precipitate was collected by filtration and washed five times with 50 mL of EtOH to yield 440 mg of a black, waxy solid.

IR (ν/cm^{-1}): 2923, 2850, 2097, 1472, 720.

4.2 Syntheses of magnetite@silica-nanoparticles

General procedure for the synthesis of magnetite@silica nanoparticles:
Sodiumdodecylbenzenesulfonate (1.75 g, 5 mmol) was dissolved in 15 mL of xylene. To this emulsion was added a solution of $FeCl_2 \cdot 4H_2O$ (199 mg, 1 mmol) $Fe(NO_3)_3 \cdot 9H_2O$ (808 mg, 2 mmol) in 0.9 mL of deionized water under vigorous stirring and the resulting mixture was kept at ambient temperature for 12 h. The solution was heated to 90°C within 1 h under continuous N_2 flow before 1 mL aqueous hydrazine solution (34 wt%) was added. The reaction mixture was kept at this temperature for 3 h and subsequently cooled to 40°C within 1 h. Tetraethyl orthosilicate (TEOS) and a 1:1 mixture of TEOS and 3-azidopropyl triethoxysilane respectively were injected to form the silica coated magnetite particles which were then removed from the reaction mixture with the aid of an external neodymium based magnet, repeatedly redispersed in and recovered from EtOH by magnetic decantation.

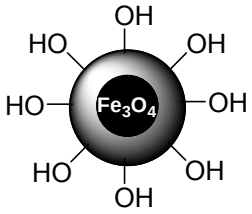

Magnetite@silica nanoparticles (138):
Synthesized according to the aforementioned protocol using 2 mL of TEOS.
Yield: 852 mg.
IR (ν/cm^{-1}): 3292, 2938, 1630, 1576, 1500, 1055, 1003, 797, 603, 565.

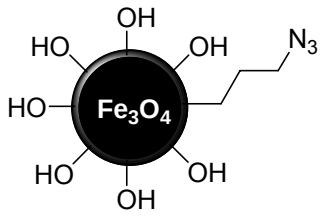

Magnetite@silica-N_3 nanoparticles (140):

Synthesized according to the aforementioned protocol using 1 mL of TEOS and 1 mL of 3-azidopropyl triethoxysilane. Yield: 600 mg.

IR (ν/cm^{-1}): 3435, 3200, 2923, 2853, 2094, 1626, 1454, 1409, 1179, 1068, 1035, 830, 789, 669, 578.

Magnetite@silica-N_3 nanoparticles through post-grafting (139):

138 (250 mg) was dispersed in a solution of 3-azidopropyl triethoxysilane (200 mg, 0.8 mmol) in THF and stirred for 48 h at ambient temperature under N_2 atmosphere. The particles were removed from the reaction mixture with the aid of an external magnet, repeatedly redispersed in THF and recovered by magnetic decantation. The material thus obtained was subjected to TMS endcapping as described below to afford 224 mg of **139**.

General procedure for TMS endcapping of magnetite@silica-N_3 139 and 141:

Magnetite@silica-N_3 nanoparticles (400 mg) were degassed in vacuo at 50°C overnight. The flask was cooled down using liquid N_2 and excess of HMDS (2 mL) was injected under vacuum. The vessel was slowly warmed to room temperature and subsequently heated to 75°C for 3 h. After this time, the excess of HMDS was removed under vacuum to afford **139** and **141** respectively in quantitative yield.

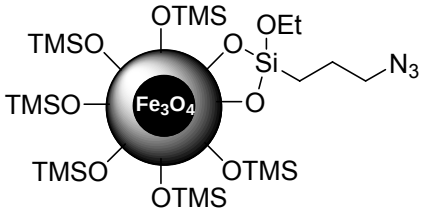

139: IR (ν/cm^{-1}): 1633, 1059, 795, 565; elemental microanalysis (%): C, 3.24; N, 1.35; H, 0.83.

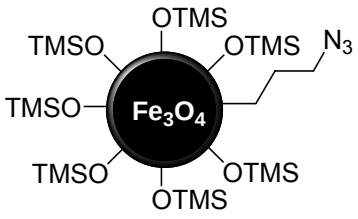

141: IR (ν/cm^{-1}): 2926, 2099, 1629, 1456, 1039, 844, 791, 576; elemental microanalysis (%): C, 9.53; N, 1.97; H, 4.15.

General procedure for 4-nitrophenyl-1-benzyl-1H-1,2,3-triazole-4-carboxylate functionalized magnetite@silica nanoparticles:

The azide-functionalized magnetite@silica particles were suspended in degassed dioxane (2 mL) before 1-(nitrophenyl)-2-propyn-1-one (**142**) and CuI were added. The resulting dispersion was stirred for 48 h at ambient temperature. The nanoparticles were recovered from the reaction mixture with the aid of a magnet and washed with dioxane (5x 5 mL) as described above.

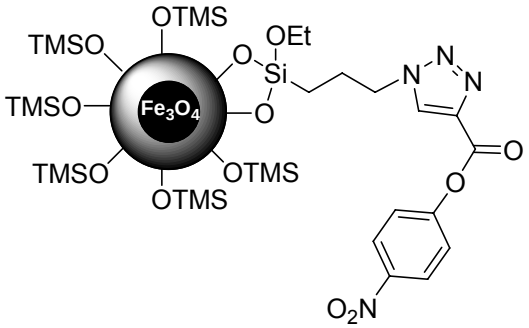

4-Nitrophenyl-1-benzyl-1H-1,2,3-triazole-4-carboxylate functionalized magnetite@silica nanoparticles (143):

Synthesized according to the aforementioned protocol, using 200 mg (0.3 mmol/g azide) of **139**, 20 mg (0.15 mmol) of **142** and CuI (1 mg) affording 196 mg of **143**.

IR (ν/cm^{-1}): 1736, 1618, 1055, 797, 561.

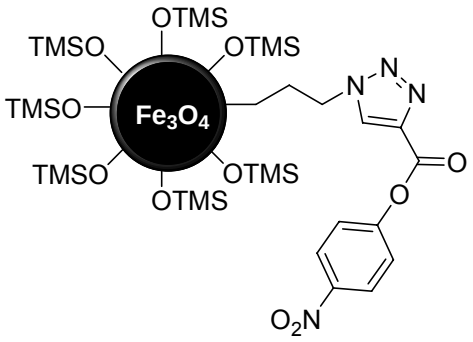

4-Nitrophenyl-1-benzyl-1H-1,2,3-triazole-4-carboxylate functionalized magnetite@silica nanoparticles (145):

Synthesized according to the aforementioned protocol, using 240 mg (0.5 mmol/g azide) of **141**, 115 mg (0.6 mmol) of **142** and CuI (3 mg, 0.01 mmol), to afford 267 mg of **145**.

IR (ν/cm^{-1}): 3294, 2960, 2102, 1630, 1577, 1500, 1255, 1055, 844, 804, 756, 559.

General procedure for azabis(oxazoline)-functionalized magnetite@silica nanoparticles:

The azide-functionalized magnetite@silica particles were dispersed in degassed CH_2Cl_2 (5 mL) before propargylated azabis(oxazoline) **120**, NEt_3 and CuI were added. The reaction mixture was stirred for 48 h at ambient temperature. The nanoparticles were recovered from the reaction mixture with the aid of a magnet and washed with CH_2Cl_2 (5x 5 mL) as described above.

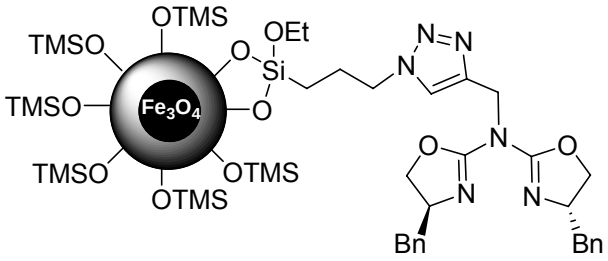

(4*S*)-4-benzyl-N-((1-propyl-1*H*-1,2,3-triazol-4-yl)methyl)-N-((*S*)-4-benzyl-4,5-dihydrooxazol-2-yl)-4,5-dihydrooxazol-2-amine functionalized magnetite@silica nanoparticles (144):

Synthesized according to the aforementioned protocol using 550 mg (0.3 mmol/g azide) of **139**, 140 mg (0.38 mmol) of **120b**, NEt_3 (21 μL, 0.15 mmol) and CuI (4 mg, 0.02 mmol) affording 536 mg of **144**.

IR (ν/cm^{-1}): 1632, 1052, 772, 558;

elemental microanalysis (%): C, 6.65; N, 1.73; H, 2.22.

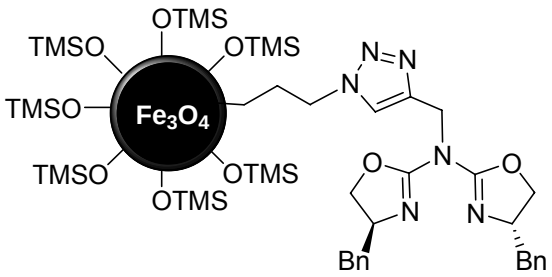

(4*S*)-4-benzyl-N-((1-propyl-1*H*-1,2,3-triazol-4-yl)methyl)-N-((*S*)-4-benzyl-4,5-dihydrooxazol-2-yl)-4,5-dihydrooxazol-2-amine functionalized magnetite@silica nanoparticles (146):

Synthesized according to the aforementioned protocol using 510 mg (0.5 mmol/g azide) of **141**, 480 mg (1.3 mmol) of **120b**, NEt_3 (65 μL, 0.5 mmol) and CuI (6 mg, 0.03 mmol) affording 554 mg of **146**.

IR (ν/cm^{-1}): 2100, 1672, 1641, 1490, 1451, 1265, 1049, 843, 732, 701, 582;

elemental microanalysis (%): C, 18.53; N, 2.58; H, 5.47.

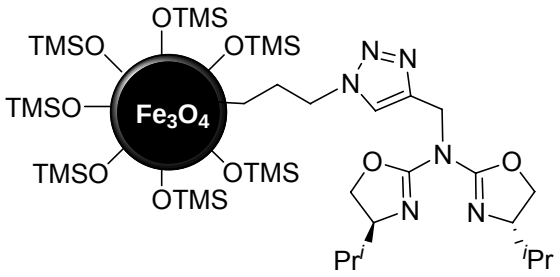

(4*S*)-4-isopropyl-N-((1-propyl-1*H*-1,2,3-triazol-4-yl)methyl)-N-((*S*)-4-isopropyl-4,5-dihydrooxazol-2-yl)-4,5-dihydrooxazol-2-amine functionalized magnetite@silica nanoparticles (184):

Synthesized according to the aforementioned protocol using 620 mg (0.5 mmol/g azide) of **141**, 220 mg (0.8 mmol) of **120a**, NEt_3 (45 μL, 0.3 mmol) and CuI (6 mg, 0.03 mmol) affording 598 mg of **184**.

IR (ν/cm^{-1}): 2098, 1700, 1642, 1490, 1460, 1271, 1050, 840, 732.

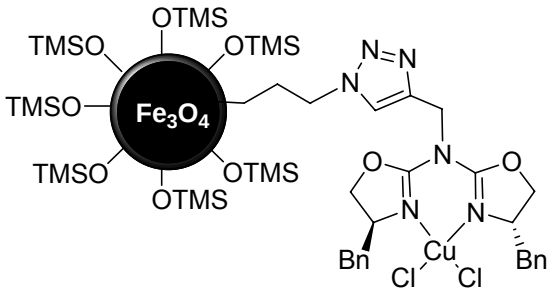

[$CuCl_2$((4*S*)-4-benzyl-N-((1-propyl-1*H*-1,2,3-triazol-4-yl)methyl)-N-((*S*)-4-benzyl-4,5-dihydrooxazol-2-yl)-4,5-dihydrooxazol-2-amine)] functionalized magnetite@silica nanoparticles (147):

Azide-functionalized magnetite@silica particles **141** (500 mg, 0.5 mmol/g azide loading) were dispersed in degassed CH_2Cl_2 (5 mL) before propargylated azabis(oxazoline)-$CuCl_2$ complex (317 mg, 0.625 mmol), NEt_3 (35 μL, 0.25 mmol) and CuI (4 mg, 0.02 mmol) were added. The reaction mixture was stirred for 48 h at ambient temperature. The nanoparticles (503 mg) were recovered from the reaction mixture with the aid of a magnet and washed with CH_2Cl_2 (5x 5 mL) as described above.

IR (ν/cm^{-1}): 3354, 2960, 2105, 1681, 1491, 1047, 796, 572.

4.3 Syntheses of carbon coated cobalt-nanoparticles

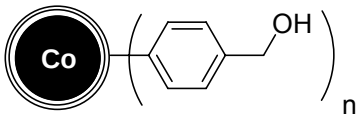

Phenylmethanol functionalized carbon coated cobalt nanoparticles (156):
Carbon coated cobalt nanobeads **150** (1 g) were suspended in milipore water (5 mL) by the use of an ultrasonic bath (Sonorex RK 255 H-R, Bandelin). 4-aminobenzyl alcohol **155** was transformed into the corresponding diazonium salt in-situ by adding a cooled solution of sodium nitrite (2.3 mmol, 160 mg in 12 mL H_2O) to a mixture of the alcohol **155** (1.5 mmol, 185 mg), HCl (0.6 mL, concentrated) and H_2O (20 mL) in an ice bath. After addition of the carbon coated nanoparticles, the reaction mixture was sonicated for 30 minutes. The nanobeads were recovered from the reaction mixture with the aid of a neodymium based magnet (N48, W-12-N, Webcraft GmbH, side length 12 mm) and washed with water (3x 5 mL) and acetone (6x 5 mL). Each washing step consisted of suspending the particles in the solvent, ultrasonication (5 min) and retracting the particles from the solvent by the aid of the magnet. After the last washing step the particles were dried in vacuo to afford 972 mg of **156**.
IR (ν/cm^{-1}): 2916, 2850, 1698, 1599, 1398, 1276, 1214, 1178, 1015, 835, 681; elemental microanalysis (%): C, 8.75; N, 0.24; H, 0.2.

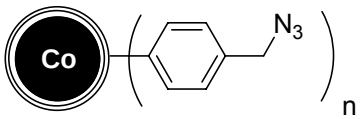

(azidomethyl)Benzene functionalized carbon coated cobalt nanoparticles (157):
The functionalized cobalt particles **156** (900 mg) were suspended in toluene$_{abs.}$ (5 mL) by sonication (10 min) before PPh_3 (0.3 mmol, 80 mg), freshly prepared HN_3 (0.3 mmol, 1M solution in toluene) and diethylazodicarboxylate (0.3 mmol, 40% in toluene) were added. The resulting slurry was sonicated for 24 h at ambient temperature. The nanoparticles were recovered from the reaction mixture with the aid of a magnet and washed with toluene (3x 5 mL) and acetone (3x 5 mL) as described above. After the last washing step the particles were dried in vacuo to afford 897 mg of **157**.

IR (ν/cm^{-1}): 2922, 2854, 2100, 1699, 1599, 1539, 1386, 1217, 1115, 1015, 830, 781, 723, 693; elemental microanalysis (%): C, 8.9; N, 0.77; H, 0.26.

General procedure for the CuAAC-reaction on azide-functionalized Co/C-NPs with propargylated compounds:

The azide-functionalized cobalt particles **157** (1 g) were suspended in degassed solvent (5 mL) by sonication (10 min) before propargylated catalyst (0.5 mmol), NEt_3 (0.5 mmol, 70 μL) and catalytic amounts of CuI were added. The resulting slurry was either sonicated or magnetically agitated for 36 h at ambient temperature. The nanoparticles were recovered quantitatively from the reaction mixture with the aid of a magnet and washed copiously with the appropriate solvent.

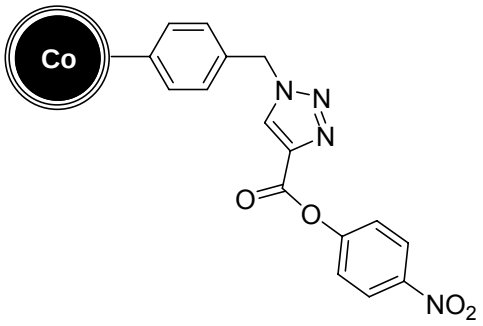

4-Nitrophenyl-1-benzyl-1*H*-1,2,3-triazole-4-carboxylate functionalized carbon coated cobalt nanoparticles (158):

The azide-functionalized cobalt particles **157** (0.5 g) were suspended in degassed dioxane (4 mL) by sonication (10 min) before 1-(nitrophenyl)-2-propyn-1-one (**142**) (0.25 mmol, 48 mg) and CuI (0.025 mmol, 5 mg) were added. The resulting slurry was sonicated for 36 h at ambient temperature. Two additional portions of CuI (0.013 mmol, 3 mg) were added after 12 and 24 h. The nanoparticles were recovered from the reaction mixture with the aid of a magnet and washed with dioxane (3x 5 mL) and acetone (5x 5 mL) as described above to yield 504 mg of **158**.

IR (ν/cm^{-1}): 2852, 1751, 1699, 1594, 1524, 1346, 1208, 1111, 1014, 861, 831, 746, 682; elemental microanalysis (%): C, 9.27; N, 0.87; H, 0.33.

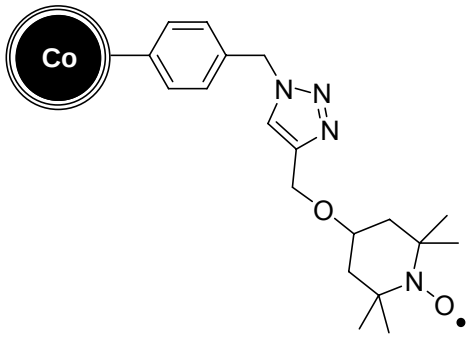

4-(1-Benzyl-1*H*-1,2,3- triazol-4- yloxy)-2,2,6,6- tetramethylpiperidine-1- oxyl functionalized carbon coated cobalt nanoparticles (164):

The azide-functionalized cobalt particles **157** (1 g) were suspended in degassed toluene (5 mL) by sonication (10 min) before propargyl ether TEMPO **163** (0.5 mmol, 95 mg), NEt_3 (0.5 mmol, 70 μL) and CuI (0.05 mmol, 10 mg) were added. The resulting slurry was sonicated for 36 h at ambient temperature. Two additional portions of CuI (0.025 mmol, 5 mg) were added after 12 and 24 h. The nanoparticles were recovered from the reaction mixture with the aid of a magnet and washed with toluene (3x 5 mL) and acetone (5x 5 mL) as described above to afford 936 mg of **164**.

IR (ν/cm^{-1}): 2974, 2935, 1700, 1600, 1541, 1507, 1379, 1363, 1242, 1218, 1177, 1083, 1015, 833, 679; elemental microanalysis (%): C, 10; N, 0.97; H, 0.5.

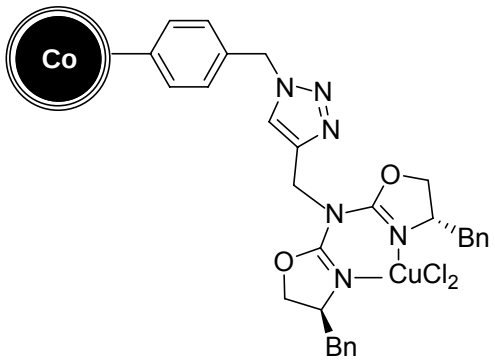

[$CuCl_2${(4*S*)-4-benzyl-N-((1-benzyl-1H-1,2,3-triazol-4-yl)methyl)-N-((*S*)-4-benzyl-4,5-dihydrooxazol-2-yl)-4,5-dihydrooxazol-2-amine}] functionalized carbon coated cobalt nanoparticles (161):

The azide-functionalized cobalt particles **157** (1 g) were suspended in degassed CH_2Cl_2 (5 mL) by sonication (10 min) before propargylated azabis(oxazoline)-copper

complex (0.5 mmol, 250 mg), NEt_3 (0.5 mmol, 70 μL) and CuI (0.05 mmol, 10 mg) were added to the Schlenk tube. The vessel was placed between two opposing magnetic stirrers (Heidolph) operating at 1100 rpm for 36 h at ambient temperature. Two additional portions of CuI (0.025 mmol, 5 mg) were added after 12 and 24 h. The nanoparticles were recovered from the reaction mixture with the aid of a magnet and washed with CH_2Cl_2 (10x 5 mL) as described above to yield 1.08 g of **161**.
IR (ν/cm^{-1}): 1671, 1596, 1489, 1376, 1217, 1091, 1014, 836, 701, 631, 531; elemental microanalysis (%): C, 12.07; N, 1.0; H, 0.56.

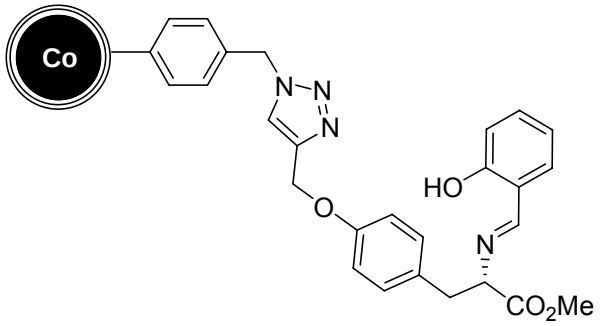

(*S*,*E*)-methyl 3-(4-((1-benzyl-1H-1,2,3-triazol-4-yl)methoxy)phenyl)-2-(2-hydroxybenzylideneamino)propanoate functionalized carbon coated cobalt nanoparticles (166):

The azide-functionalized cobalt particles **157** (1 g) were suspended in degassed acetonitrile (5 mL) by sonication (10 min) before propargylated Schiff-base **165b** (0.5 mmol, 170 mg), NEt_3 (0.5 mmol, 70 μL) and CuI (0.05 mmol, 10 mg) were added to the Schlenk tube. The vessel was placed between two opposing magnetic stirrers (Heidolph) operating at 1100 rpm for 36 h at ambient temperature. Two additional portions of CuI (0.025 mmol, 5 mg) were added after 12 and 24 h. The nanoparticles were recovered from the reaction mixture with the aid of a magnet and washed with acetonitrile (10x 5 mL) as described above to yield 0.998 g of **166**.
IR (ν/cm^{-1}): 3300, 2925, 1663, 1599, 1508, 1392, 1213, 1170, 1003, 834, 762; elemental microanalysis (%): C, 14.07; N, 1.2; H, 0.8.

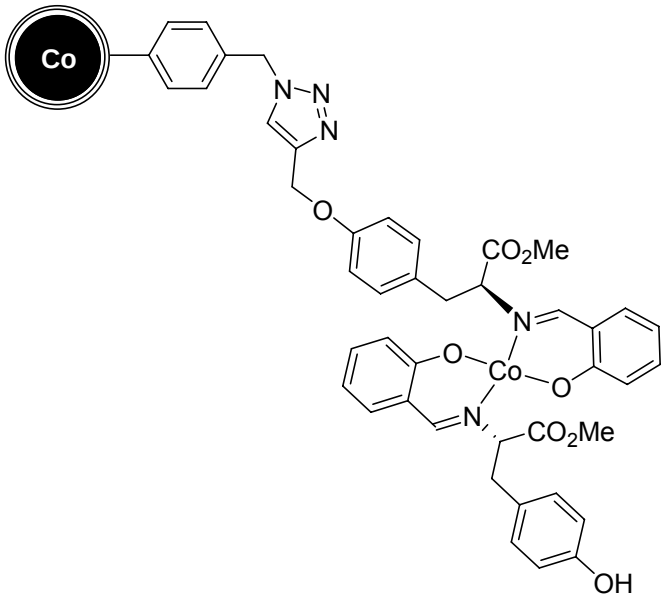

[Co((*S*,*E*)-methyl 2-(2-hydroxybenzylideneamino)-3-(4-hydroxyphenyl) propanoate) ((*S*,*E*)-methyl 3-(4-((1-benzyl-1H-1,2,3-triazol-4-yl)methoxy)phenyl)-2-(2-hydroxybenzylideneamino)propanoate)] functionalized carbon coated cobalt nanoparticles (168):

The azide-functionalized cobalt particles **157** (1 g) were suspended in degassed acetonitrile (5 mL) by sonication (10 min) before propargylated Co(II)-Schiff base complex **169** (0.5 mmol, 350 mg), NEt_3 (0.5 mmol, 70 μL) and CuI (0.05 mmol, 10 mg) were added to the Schlenk tube. The vessel was placed between two opposing magnetic stirrers (Heidolph) operating at 1100 rpm for 36 h at ambient temperature. Two additional portions of CuI (0.025 mmol, 5 mg) were added after 12 and 24 h. The nanoparticles were recovered from the reaction mixture with the aid of a magnet and washed with acetonitrile (10x 5 mL) as described above to afford 1.02 g of **168**.

IR (ν/cm^{-1}): 3300, 2925, 1601, 1510, 1444, 1400, 1225, 1176, 1017, 758, 536; elemental microanalysis (%): C, 14.99; N, 1.4; H, 0.92.

5. Catalysis

General procedure for the asymmetric benzoylation with azabis(oxazoline)-copper complexes:

Azabis(oxazoline) **109d** (17.5 mg, 0.05 mmol) and $CuCl_2$ (6.7 mg, 0.05 mmol) were allowed to stir for 1 h in dry CH_2Cl_2 (2 mL) at room temperature under nitrogen atmosphere. The solution was diluted up to 5 mL with dry CH_2Cl_2 and the vessel subsequently charged with 1,2 diol **170** (214 mg, 1.0 mmol) and diisopropylethylamine (DIPEA, 170 μL, 1.0 mmol) before the reaction mixture was cooled to 0°C. Benzoylchloride **172** (58 μL, 0.5 mmol) was added and stirring continued at 0°C until the acid chloride disappeared (TLC). The reaction mixture was diluted with water (5 mL) and extracted three times with CH_2Cl_2 (5 mL). The combined organic layers were dried over magnesium sulfate, concentrated under reduced pressure and the residue was purified on silica. Optical yields were determined by chiral HPLC.

General procedure for the catalytic asymmetric benzoylation with magnetite@silica nanoparticle supported azabis(oxazolines):

1,2 Diol **170** (214 mg, 1.0 mmol), diisopropylethylamine (DIPEA, 170 μL, 1.0 mmol) and typically 0.01 mmol of the immobilized catalyst were dissolved in dry CH_2Cl_2 (5 mL) and cooled to 0°C. Benzoylchloride **172** (58 μL, 0.5 mmol) was added and the mixture was stirred at 0°C until the benzoylchloride **172** disappeared (TLC). Immobilized catalyst was recovered from the reaction mixture with the aid of an external neodymium based magnet, three times redispersed in and recovered from CH_2Cl_2 by magnetic decantation. The reaction mixture was diluted with water and extracted three times with CH_2Cl_2. The combined organic layers were dried over magnesium sulfate, concentrated under reduced pressure and the residue was purified on silica. Optical yields were determined by chiral HPLC.

General procedure for the catalytic asymmetric benzoylation with Co/C nanoparticle supported azabis(oxazolines) under batch conditions:

1,2 Diol **170** (214 mg, 1.0 mmol), diisopropylethylamine (DIPEA, 170 μL, 1.0 mmol) and typically 0.01 mmol of the immobilized catalyst **161** were dispersed in dry CH_2Cl_2 (5 mL). The Schlenk tube containing the reaction mixture was placed vertically between adjacent parallel flanks of two magnetic stir motors (Heidolph) with a distance of 4 cm to each other, operating at 1100 rpm in a cooling chamber (4°C). Benzoylchloride (58 μL, 0.5 mmol) was added and the mixture was stirred at 4°C until the acid chloride **172** disappeared (TLC). Immobilized catalyst was recovered from the reaction mixture with the aid of an external neodymium based magnet, which was then redispersed in and recovered from CH_2Cl_2 by magnetic decantation three times. The separated reaction mixture was concentrated under reduced pressure and the residue was purified on silica. Optical yields were determined by chiral HPLC.

General procedure for the catalytic asymmetric benzoylation with Co/C nanoparticle supported azabis(oxazolines) under continuous flow conditions:

A glass column (Omnifit, 10 cm length, 3.4 mL volume) was charged with 0.05 mmol of the Co/C-immobilized catalyst **161** and placed vertically between adjacent parallel flanks of two magnetic stir motors (Heidolph, 1100 rpm) with a distance of 4 cm to each other. The lower thread was mounted with a PE frit (25 μm pore size) and the glass column subsequently connected to a piston pump (KNF STEPDOS 03-RC) via the lower joint and a septum-sealed Schlenk tube containing 1,2 diol **170** (214 mg, 1.0 mmol), diisopropylethylamine (DIPEA, 170 μL, 1.0 mmol) and benzoylchloride **172** (58 μL, 0.5 mmol) dissolved in dry CH_2Cl_2 (5 mL) under a nitrogen filled balloon. The whole setup was operated in a cooling chamber (4°C). The Schlenk tube, equipped with a neodymium based magnet, was likewise connected to the piston pump and the reaction mixture moved through the reactor in a circular course at a constant flow rate (0.2 mL/min) until the benzoylchloride **172** disappeared (TLC). The crude product was extruded from the glass column by floating the apparatus with dry CH_2Cl_2 (20 mL) and the separated reaction mixture concentrated under reduced pressure. The residue was purified on silica. Optical yields were determined by chiral HPLC.

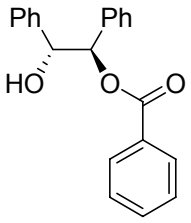

(*R*,*R*)-Benzoic acid 2-hydroxy-1,2-diphenyl-ethyl ester (171):

Prepared according to the general procedure and purified by column chromatography (PE/EE 3:1) to obtain the pure product as a white solid.

m.p. 145-146°C; ^{1}H-NMR (300 MHz, $CDCl_3$): δ = 2.61 (d, 1 H, *J* = 3.4 Hz), 5.09 (d, 1 H, *J* = 7.4 Hz), 6.11 (d, 1 H, *J* = 7.4 Hz), 7.17-7.27 (m, 10 H), 7.45-7.50 (m, 2 H), 7.57-7.63 (m, 1 H), 8.07-8.15 (m, 2H); ^{13}C-NMR (75.5 MHz, $CDCl_3$): δ = 164.7, 137.9, 135.7, 132.2, 128.9, 128.7, 127.4, 127.2, 127.2, 127.1, 127.1, 126.2, 126.1, 79.5; IR (ν/cm^{-1}): 3494, 3387, 2895, 1699, 1452, 1276, 1116, 695; HPLC: OJ column, *n*-heptane : isopropanol = 80 : 20, detection wavelength: 254 nm, flow rate: 0.5 mL/min, t_r (minor) = 19.8 min, t_r (major) = 35.6 min, >99% ee; $[\alpha]_D^{20}$ = -66 (50 mg/2mL, $CHCl_3$).

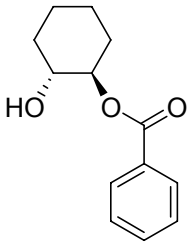

(*R*,*R*)-Benzoic acid 2-hydroxy-cyclohexyl ester (177a):

Prepared according to the general procedure and purified by column chromatography (PE/EE 3:1) to obtain the pure product as a white solid.

m.p. 92-94°C; ^{1}H-NMR (300 MHz, $CDCl_3$): δ = 1.26-1.53 (m, 4 H), 1.70-1.82 (m, 2 H), 2.06-2.20 (m, 2 H), 3.67-3.81 (m, 1 H), 4.80-4.89 (m, 2 H), 7.42-7.48 (m, 2 H), 7.53-7.61 (m, 1 H), 8.04-8-08 (m, 2 H); ^{13}C-NMR (75.5 MHz, $CDCl_3$): δ = 166.7, 133.1, 129.6, 128.4, 78.8, 72.9, 33.1, 30.1, 23.9, 23.8; IR (ν/cm^{-1}): 3526, 2935, 2861, 1686, 1273, 1115, 716; HPLC: OJ column, *n*-heptane : isopropanol = 95 : 5, detection wavelength: 254 nm, flow rate: 0.5 mL/min, t_r (minor) = 25.9 min, t_r (major) = 26.8 min, 79 % ee, $[\alpha]_D^{20}$ = -59 (50 mg/2mL, $CHCl_3$).

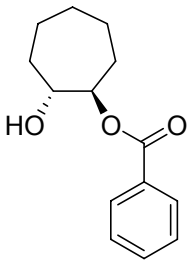

(*R,R*)-Benzoic acid 2-hydroxy-cycloheptyl ester (177b):

Prepared according to the general procedure and purified by column chromatography (PE/EE 3:1) to obtain the pure product as a white solid.

m.p. 72-74°C; ^{1}H-NMR (300 MHz, $CDCl_3$): δ = 1.43-1.99 (m, 10 H), 2.84 (s, 1 H), 3.89-3.92 (bs, 1 H), 4.91-5.01 (m, 1 H), 7.42-7.47 (m, 2 H), 7.54-7.56 (m 1 H), 8.03-8.06 (m, 2 H); ^{13}C-NMR (75.5 MHz, $CDCl_3$): δ = 167.0, 133.1, 130.3, 129.7, 128.4, 82.7, 76.1, 32.7, 30.4, 28.3, 23.1, 23.0; IR (ν/cm^{-1}): 3535, 2932, 1688, 1454, 1275, 709; HPLC: OD/OD-H, *n*-heptane : isopropanol = 95:5, detection wavelength: 254 nm, flow rate 0.3 mL/min, t_r (minor) = 29.2 min, t_r (major) = 33.2 min, 59% ee, $[\alpha]_D^{20}$ = –29.3 (50 mg/2mL, $CHCl_3$).

General procedure for the catalytic asymmetric Michael-additions with azabis(oxazoline)-copper complexes:

To a Schlenk tube were added catalyst **103a** (12.0 mg, 0.05 mmol) and $Cu(OTf)_2$ (18.1 mg, 0.05 mmol) under ambient atmosphere. Ethanol (2 mL) was added and the mixture was stirred for 1 h at room temperature (20-25°C). To the resulting blue-green solution benzylidene malonate **179** (1 mmol) in EtOH (2 mL) was added and stirring continued for 20 min before the indole (**178**) (140 mg, 1.2 mmol) was added. After stirring for 8 h at room temperature, the solution was concentrated under reduced pressure and the crude product purified by column chromatography (performed with PE/CH_2Cl_2 1:1, followed by CH_2Cl_2).

General procedure for the catalytic asymmetric Michael-additions with nanoparticle supported catalyst:

In a typical procedure, to a Schlenk tube were added immobilized azabis(oxazoline) copper complex (0.1 mmol) under ambient atmosphere. Benzylidene malonate **179** (1 mmol) in EtOH (4 mL) was added and the dispersion was allowed to stir at room temperature for 20 min before indole (**178**) (140 mg, 1.2 mmol) was added. In the case of Co/C-immobilized catalyst **161**, magnetic agitation of the particles was applied instead of stirring. After agitation for 8 h at room temperature, the catalyst was recovered from the reaction mixture with the aid of an external neodymium based magnet, three times redispersed in and recovered from EtOH by magnetic decantation. The combined waters were concentrated under reduced pressure and the crude product purified by column chromatography (performed with PE/CH_2Cl_2 1:1, followed by CH_2Cl_2).

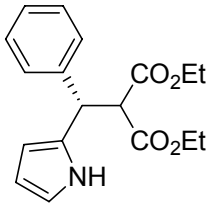

(*S*)–Ethyl2–ethoxycarbonyl–3–(2–pyrrolyl)–3–(phenyl)propanoate (183):

Prepared according to the general procedure and purified by column chromatography (performed with PE/CH_2Cl_2 1:1, followed by CH_2Cl_2) to obtain the pure product as a white solid.

m.p. 104-106°C; ^{1}H NMR (300 MHz, $CDCl_3$): δ = 0.97 (t, *J* = 7.14 Hz, 3 H), 1.19 (t, *J* = 7.14 Hz, 3 H), 3.92 (q, *J* = 7.12 Hz, 2 H), 4.14 (d, *J* = 10.6 Hz, 1 H), 4.16 (q, *J* = 7.12 Hz, 2 H) 4.78 (d, *J* = 10.5 Hz, 1 H), 5.94 (brs, 1 H), 6.07 (m, 1 H), 6.65 (m, 1 H), 7.20–7.31 (m, 5 H), 8.48 (brs, 1 H); ^{13}C NMR (75 MHz, $CDCl_3$): δ = 168.8, 167.6, 139.8, 130.9, 128.5, 128.3, 127.2, 117.6, 108.1, 106.6, 61.9, 61.5, 58.1, 44.4, 14.1, 13.8; IR (ν/cm^{-1}): 3383, 2983, 1741, 1456, 1368, 1311, 1258, 1145, 1094, 1025, 861, 732, 697, 551; MS (CI): m/z (%) = 333 (MNH_4^+, 2), 316 (MH^+, 100), 178 (4), 156 (18); HPLC: OD/OD-H, *n*-heptane : isopropanol = 90:10, detection wavelength: 254 nm, flow rate 0.5 mL/min, t_r (major) = 15.76 min, t_r (minor) = 18.57 min, 18 % ee, $[\alpha]_D^{20}$ = +2.4 (20 mg/2 mL, CH_2Cl_2).

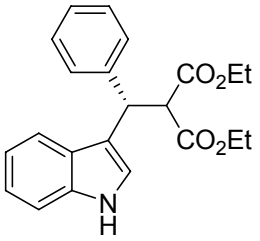

(*S*)–Ethyl2–ethoxycarbonyl–3–(3–indolyl)–3–phenylpropanoate (180a):

Prepared according to the general procedure and purified by column chromatography (performed with PE/CH_2Cl_2 1:1, followed by CH_2Cl_2) to obtain the pure product as a white solid.

m.p. 174-176°C; ^{1}H-NMR (300 MHz, $CDCl_3$): δ = 0.93-1.06 (m, 6 H), 3.93-4.06 (m, 4 H), 4.30 (d, *J* = 11.8 Hz, 1 H), 5.09 (d, *J* = 11.8 Hz, 1 H), 7.00-7.07 (m, 1 H), 7.09-7.31 (m, 6 H), 7.37 (d, *J* = 7.4 Hz, 2 H), 7.56 (d, *J* = 8.0 Hz, 1 H), 8.07 (brs, 1 H); ^{13}C-NMR (75 MHz, $CDCl_3$): δ = 168.1, 167.9, 141.4, 136.2, 128.4, 128.2, 126.8, 126.7, 122.3, 120.9, 119.5, 119.4, 117.0, 111.0, 61.5, 61.4, 58.4, 42.9, 13.8, 13.8; IR (ν/cm^{-1}): 3401, 2983, 1741, 1457, 1368, 1307, 1268, 1149, 1104, 1026, 851, 740, 701, 584; MS (CI): m/z (%) = 383 (MNH_4^+, 89), 366 (MH^+, 3), 206 (100), 178 (5); HPLC: OD/OD-H, *n*-heptane : isopropanol = 90:10, detection wavelength: 254 nm, flow rate 0.5 mL/min, t_r (minor) = 26.67 min, t_r (major) = 31.40 min; >99% ee, $[\alpha]_D^{20}$ = +65.4 (20 mg/2 mL, CH_2Cl_2).

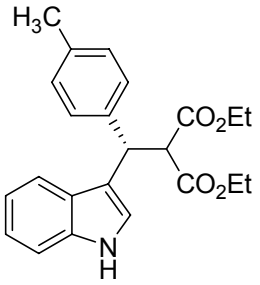

(*S*)–Ethyl2–ethoxycarbonyl–3–(3–indolyl)–3–(p-methylphenyl)propanoate (180b):

Prepared according to the general procedure and purified by column chromatography (performed with PE/CH_2Cl_2 1:1, followed by CH_2Cl_2) to obtain the pure product as a white solid.

m.p. 140-142°C; ^{1}H-NMR (300 MHz, $CDCl_3$): δ = 0.98 (t, *J* = 7.1 Hz, 3 H), 1.04 (t, *J* = 7.1 Hz, 3 H), 2.24 (s, 3 H), 3.94-4.05 (m, 4 H), 4.27 (d, *J* = 11.8 Hz, 1 H), 5.04 (d, *J* = 11.8 Hz, 1 H), 6.99-7.06 (m, 3 H), 7.08-7.18 (m, 2 H), 7.22-7.31 (m, 3 H), 7.55 (d, *J* = 8.0 Hz, 1 H), 7.99 (brs, 1 H); ^{13}C-NMR (75 MHz, $CDCl_3$): δ = 168.1, 167.9, 138.4, 136.2, 136.2, 129.0, 128.0, 126.7, 122.2, 120.8, 119.5, 119.5, 117.3, 110.9, 61.4, 61.4, 58.4, 42.4, 21.0, 13.8, 13.8; IR (ν/cm^{-1}): 3406, 2977, 1745, 1514, 1458, 1369, 1306, 1268, 1180, 1142, 1028, 829, 740, 641, 582, 531, 502; MS (CI): m/z (%) = 397 (MNH_4^+, 73), 379 (2), 220 (100), 178 (7); HPLC: OD/OD-H, *n*-heptane : isopropanol = 90:10, detection wavelength: 254 nm, flow rate 0.5 mL/min, t_r (major) = 22.12 min, t_r (minor) = 25.47 min, 94 % ee, $[\alpha]_D^{20}$ = +26.7 (10 mg/2 mL, CH_2Cl_2).

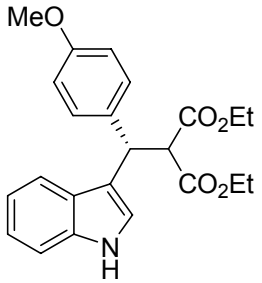

(*S*)–Ethyl2–ethoxycarbonyl–3–(3–indolyl)–3–(p-methyoxyphenyl)propanoate (180c):

Prepared according to the general procedure and purified by column chromatography (performed with PE/CH_2Cl_2 1:1, followed by CH_2Cl_2) to obtain the pure product as a white solid.

m.p. 168-170°C; ^{1}H-NMR (300 MHz, $CDCl_3$): δ = 0.97-1.07 (m, 6 H), 3.73 (s, 3 H), 3.95-4.04 (m, 4 H), 4.23 (d, *J* = 11.7 Hz, 1 H), 5.03 (d, *J* = 11.8 Hz, 1 H), 6.73-6.78 (m, 2 H), 6.98-7.31 (m, 6 H), 7.52 (d, *J* = 7.8 Hz, 1 H), 8.01 (brs, 1 H); ^{13}C-NMR (75 MHz, $CDCl_3$): δ = 167.9, 158.3, 136.3, 133.5, 129.2, 126.7, 122.3, 120.7, 119.5, 117.4, 113.7, 110.9, 61.4, 58.6, 55.3, 42.1, 13.8; IR (ν/cm^{-1}): 3408, 2980, 1744, 1610, 1512, 1458, 1371, 1338, 1244, 1177, 1145, 1097, 1033, 842, 808, 742, 584, 515; MS (CI): m/z (%) = 413 (MNH_4^+, 31), 395 (5), 236 (100), 178 (11); HPLC: OD/OD-H, *n*-heptane : isopropanol = 90:10, detection wavelength: 254 nm, flow rate 0.5 mL/min, t_r (minor) = 48.38 min, t_r (major) = 53.71 min, 84 % ee, $[\alpha]_D^{20}$ = +53.3 (20 mg/2 mL, CH_2Cl_2).

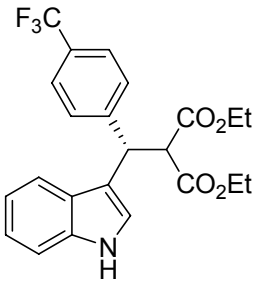

(*S*)–Ethyl2–ethoxycarbonyl–3–(3–indolyl)–3–(p-trifluoromethylphenyl)-propanoate (180d):

Prepared according to the general procedure and purified by column chromatography (performed with PE/CH_2Cl_2 1:1, followed by CH_2Cl_2) to obtain the pure product as a white solid.

m.p. 152-154°C; ^{1}H-NMR (300 MHz, $CDCl_3$): δ = 1.02 (m, 6 H), 3.95-4.05 (m, 4 H), 4.29 (d, *J* = 11.7 Hz, 1 H), 5.14 (d, *J* = 11.7 Hz, 1 H), 7.01-7.22 (m, 3 H), 7.29-7.33 (m, 1 H), 7.50-7.52 (m, 4 H), 8.05 (brs, 1 H); ^{13}C-NMR (75 MHz, $CDCl_3$): δ = 167.6, 167.5, 145.6, 136.2, 128.6, 126.4, 125.3, 122.6, 121.0, 119.1, 116.1, 111.1, 61.7, 61.6, 57.9, 42.5, 13.7; IR (ν/cm^{-1}): 3408, 2926, 1744, 1619, 1458, 1421, 1373, 1325, 1273, 1196, 1155, 1110, 1069, 1041, 857, 815, 741, 693, 652, 609, 518; MS (CI): m/z (%) = 451 (MNH_4^+, 100), 433 (12), 274 (78), 178 (9); HPLC: OD/OD-H, *n*-heptane : isopropanol = 90:10, detection wavelength: 254 nm, flow rate 0.5 mL/min, t_r (minor) = 40.78 min, t_r (major) = 47.98 min, 90 % ee, $[\alpha]_D^{20}$= +15.2 (10 mg/2 mL, CH_2Cl_2).

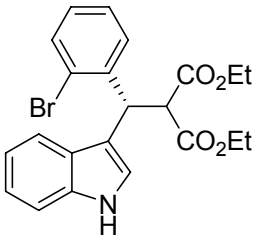

(*S*)–Ethyl2–ethoxycarbonyl–3–(3–indolyl)–3–(o-bromophenyl)propanoate (180e):

Prepared according to the general procedure and purified by column chromatography (performed with PE/CH_2Cl_2 1:1, followed by CH_2Cl_2) to obtain the pure product as a brown oil.

^{1}H-NMR (300 MHz, $CDCl_3$): δ = 0.96 (t, *J* = 7.1 Hz, 3 H), 1.03 (t, *J* = 7.1 Hz, 3 H), 3.92-4.07 (m, 4 H), 4.37 (d, *J* = 11.5 Hz, 1 H), 5.64 (d, *J* = 11.5 Hz, 1 H), 6.97-7.31 (m, 5 H), 7.41 (dd, *J* = 8.0, 1.6 Hz, 1 H), 7.53 (dd, *J* = 8.0, 1.4 Hz, 1 H), 7.72 (d, *J* = 7.7 Hz, 1 H), 8.08 (brs, 1 H); ^{13}C-NMR (75 MHz, $CDCl_3$): δ = 168.0, 167.7, 140.8, 136.1, 133.2, 129.1, 128.2, 127.6, 126.7, 124.9, 122.3, 122.2, 119.7, 115.6, 111.2, 61.6, 58.0, 41.8, 41.4, 14.1, 13.8, 13.7; IR (ν/cm^{-1}): 3396, 2981, 1725, 1467, 1369, 1301, 1244, 1148, 1095, 1024, 861, 741, 595; MS (CI): m/z (%) = 461 (MNH_4^+, 100), 444 (MH^+, 4), 284 (58), 206 (3), 178 (12); HPLC: OD/OD-H, *n*-heptane : isopropanol = 90:10, detection wavelength: 254 nm, flow rate 0.5 mL/min, t_r (minor) = 24.30 min, t_r (major) = 37.42 min, 85 % ee, $[\alpha]_D^{20}$= +48.5 (20 mg/2 mL, CH_2Cl_2).

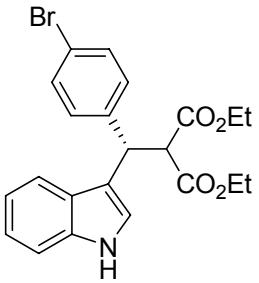

(*S*)–Ethyl2–ethoxycarbonyl–3–(3–indolyl)–3–(p-bromophenyl)propanoate (180f):

Prepared according to the general procedure and purified by column chromatography (performed with PE/CH_2Cl_2 1:1, followed by CH_2Cl_2) to obtain the pure product as a white solid.

m.p. 148-150°C; ^{1}H-NMR (300 MHz, $CDCl_3$): δ = 1.00 (t, *J* = 7.1 Hz, 3 H), 1.06 (t, *J* = 7.1 Hz, 3 H), 4.02 (m, *J* = 7.13 Hz, 4 H), 4.24 (d, *J* = 11.7 Hz, 1 H), 5.04 (d, *J* = 11.7 Hz, 1 H), 6.99-7.38 (m, 8 H), 7.49 (d, *J* = 7.9 Hz, 1H), 8.02 (brs, 1 H); ^{13}C-NMR (75 MHz, $CDCl_3$): δ = 167.7, 167.6, 140.5, 136.2, 131.4, 129.9, 126.5, 122.8, 120.6, 119.7, 119.2, 116.5, 111.0, 61.6, 58.0, 42.2, 13.8, 13.7; IR (ν/cm^{-1}): 3409, 2925, 2855, 1744, 1626, 1489, 1457, 1369, 1335, 1246, 1151, 1107, 1010, 741, 583, 517; MS (CI): m/z (%) = 461 (MNH_4^+, 66), 443 (9), 284 (100), 178 (7); HPLC: OD/OD-H, *n*-heptane : isopropanol = 90:10, detection wavelength: 254 nm, flow rate 0.5 mL/min, t_r (minor) = 29.17 min, t_r (major) = 31.86 min, 82 % ee, $[\alpha]_D^{20}$= +24.4 (20 mg/2 mL, CH_2Cl_2).

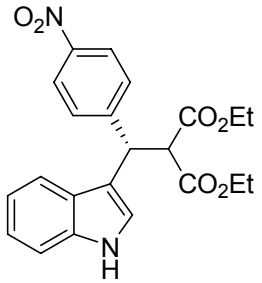

(*S*)–Ethyl2–ethoxycarbonyl–3–(3–indolyl)–3–(p-nitrophenyl)propanoate (180g):
Prepared according to the general procedure and purified by column chromatography (performed with PE/CH_2Cl_2 1:1, followed by CH_2Cl_2) to obtain the pure product as a yellow solid.

m.p. 105-107°C; ^{1}H-NMR (300 MHz, $CDCl_3$): δ = 1.01 (t, *J* = 7.1 Hz, 3 H), 1.07 (t, *J* =7.1 Hz, 3 H), 3.97-4.08 (m, 4 H), 4.32 (d, *J* = 11.8 Hz, 1 H), 5.20 (d, *J* = 11.5 Hz, 1 H), 7.05 (m, 1 H), 7.16 (m, 1 H), 7.21 (d, *J* = 2.5 Hz, 1 H), 7.32 (d, *J* = 8.2 Hz, 1 H), 7.47 (d, *J* = 8.0 Hz, 1 H), 7.55 (m, 2 H), 8.10 (m, 2 H), 8.15 (brs, 1 H); ^{13}C-NMR (75 MHz, $CDCl_3$): δ = 167.5, 167.4, 149.3, 146.7, 136.2, 129.2, 126.3, 123.7, 122.7, 121.3, 119.9, 118.9, 115.4, 111.3, 61.8, 57.7, 42.5, 13.9, 13.8; IR (ν/cm^{-1}): 3409, 2987, 1741, 1598, 1512, 1458, 1338, 1271, 1150, 1105, 1032, 857, 742, 697, 582, 519; MS (CI): m/z (%) = 428 (MNH_4^+, 100), 410 (2), 398 (7), 251 (25), 221 (22), 178 (11); HPLC: AS, *n*-heptane : isopropanol = 85:15, detection wavelength: 254 nm, flow rate 0.5 mL/min, t_r (minor) = 29.13 min, t_r (major) = 39.83 min, 96 % ee, $[\alpha]_D^{20}$= +8.3 (20 mg/2 mL, CH_2Cl_2);

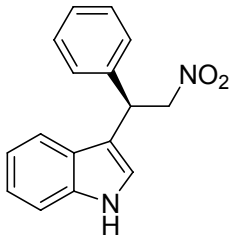

(*R*)-3-(2-nitro-1-phenylethyl)-1*H*-indole (186):

In a representative procedure, $Zn(OTf)_2$ (18.5 mg, 0.05 mmol) and azabis(oxazoline) **109c** (16.28 mg, 0.05 mmol) were added to a dried Schlenk tube under N_2 atmosphere, followed by addition of $toluene_{abs.}$ (5 mL). The solution was stirred at room temperature for 2 h before the *trans*- β-nitrostyrene (**185**) (149 mg, 1.0 mmol) was added. The mixture was cooled to 0°C and stirred for 10 min before the indole (**178**) (57 mg, 0.5 mmol) was added. After the reaction was complete (monitored by TLC), the solvent was removed under vacuum and the residue was chromatographically purified (EE/PE = 1:3) to afford **186**.

^{1}H-NMR (300 MHz, $CDCl_3$): δ = 4.94 (dd, *J* = 8.4, 12.4 Hz, 1 H), 5.06 (dd, *J* = 7.6, 12.4 Hz, 1 H), 5.2 (t, *J* = 8.0 Hz, 1 H), 7.0 (d, *J* = 2.2 Hz, 1 H), 7.07-7.13 (m, 1 H), 7.19-7.36 (m, 7 H), 7.48 (d, *J* = 7.9 Hz, 1 H), 8.07 (s, 1 H); ^{13}C-NMR (75 MHz, $CDCl_3$): δ = 139.2, 136.5, 128.9, 128.7, 127.8, 127.6, 126.1, 122.7, 121.7, 119.9, 118.9, 114.4, 111.5, 79.57, 41.59, 29.77, 14.21; IR (ν/cm^{-1}): MS (CI): m/z (%) = 266 (M^+, 49), 220 (43), 219 (100), 206 (60); HPLC: OD/OD-H, *n*-heptane : isopropanol = 90:10, detection wavelength: 254 nm, flow rate 0.5 mL/min, t_r (minor) = 54.28 min, t_r (major) = 64.66 min, 67 % ee, $[\alpha]_D^{20}$= +4.5 (20 mg/2 mL, CH_2Cl_2).

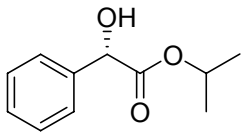

(*S*)-isopropyl 2-hydroxy-2-phenylacetate (189):

In a representative procedure, a 10 mL round bottom flask under N_2-atmosphere was charged with azabis(oxazoline) **103c** (8 mg, 0.026 mmol) and 9 mg $Cu(OTf)_2$ (0.025 mmol) before 720 μL of dichloroethane were poured in the flask to allow stirring at ambient temperature for 3 h. To the reaction mixture were added 50 mg phenylglyoxal **186** (0.37 mmol) followed by 1.4 mL isopropanol. The resulting slurry was stirred at room temperature for 24 h. The reaction was then poured into 50 mL of 2 N HCl and extracted thrice with dichloromethane. The organic layer was dried with $MgSO_4$, filtered and concentrated by rotary evaporation to crude product **189** which was further purified by flash chromatography. Conversion and optical purity were determined by chiral GC.

^{1}H-NMR (300 MHz, $CDCl_3$): δ = 1.09 (d, *J* = 6.26, Hz, 3 H); 1.27 (d, *J* = 6.28 Hz, 3 H); 3.53 (d, *J* = 5.95 Hz, 1 H); 5.05-5.13 (m, 1 H); 5.11 (d, *J* = 5.9 Hz, 1 H); 7.44-7.28 (m, 5 H); ^{13}C-NMR (75 MHz, $CDCl_3$): δ = 173.3, 138.6, 128.5, 128.3, 72.9, 70.2; IR (ν/cm^{-1}): 3306, 2973, 2890, 1728, 1105; MS (CI): m/z (%) = 212 (MNH_4^+, 100), 195 (MH^+, 5); GC: CP-Chirasil-Dex CB 25m x 0.25 mm D_i, 0.25 mm film, 250 °C detection temperature, 250°C injection temperature, t_r (major) = 5.21 min, t_r (minor) = 5.50 min, 41 % ee, $[\alpha]_D^{20}$= +39 (47 mg/2 mL, CH_2Cl_2).

General procedure for the CoNP-TEMPO mediated oxidation of alcohols:

4-Methylbenzyl alcohol **194** (3 mmol, 366 mg) in CH_2Cl_2 (6 mL), KBr (1.0 mmol, 120 mg) and CoNP-TEMPO **164** (0.1 mmol/g, 750 mg, 2.5 mol% TEMPO) were merged in a 50 mL round-bottom flask. The reaction mixture was sonicated at 0°C for 15 min using an ultrasonic bath filled with a tempered coolant solution (10% glycol in water) before 2.4 mL of a NaOCl solution (10%, Aldrich) and $NaHCO_3$ (120 mg, 50 mg/mL bleach) were added. The resulting suspension was sonicated at 0°C for 1 h. Then the reaction mixture was separated from catalyst **164** by decantation with the aid of a neodymium based magnet. The particles were suspended in CH_2Cl_2 (10 mL), subjected to ultrasound (5 min) and the supernatant was decanted once again after applying an external magnet. This procedure was repeated thrice before the solution was dried over $MgSO_4$, filtered and concentrated under vacuum to afford 4-methylbenzaldehyde **194**. CoNP-TEMPO **164** was washed as described above with water (3x 5 mL) and acetone (6x 5 mL), dried in vacuo and reused without further purification.

General procedure for CoNP-Co(II)-Schiff base complex catalyzed oxidations with molecular oxygen:

A glass column (8 cm, 10 mL volume) containing 0.05 mmol of the Co/C immobilized Co(II)-Schiff base complex **168** and 500 mg molecular sieves (3 Å) in dry acetonitrile (10 mL) was charged with benzhydrol **199** (184 mg, 1 mmol) and cyclohexanone-2-ethylcarboxylate **197** (220 μL, 1.5 mmol). The microreactor was equipped with a column jacket which allowed applying a temperature of 50°C in the reaction chamber via a thermostat. The bottom of the reactor was sealed with a G3-frit, which enabled bubbling of oxygen through a jointed gas inlet at a low flow rate. The outlet of the glass column was connected to a reflux condenser in order to reduce the evaporation of solvent due to heating and the constant oxygen streaming. The whole apparatus was placed vertically between adjacent parallel flanks of two magnetic stir motors with a distance of 5 cm to each other, thus allowing the Co/C-nanoparticles to be agitated in the field created by the two rotating magnets. The particles were agitated until the secondary alcohol disappeared (TLC). Subsequently, the oxygen inlet was disconnected and vacuum was applied in order to filter the reaction mixture through the jointed frit into the glass tube beneath the reaction chamber. The reaction chamber was floated repeatedly with dry acetonitrile (4 x 10 mL) under magnetic agitation of the particles to remove any residual crude product. The combined waters were concentrated in vacuo and subjected to column chromatography (PE/EE 5:1) to deliver benzophenone **200** in 96% yield.

6. References

1 a) H. Werner, R. Vicha, A. Gissibl, O.Reiser, *J. Org. Chem*., **2003**, *68*, 10166; b) H. Werner, C. I. Herrerias, M. Glos, A. Gissibl, J. M. Fraile, I. Pérez, J. A. Mayoral, O. Reiser, *Adv. Synth. Catal*., **2006**, *348*, 125; c) H. Werner, Dissertation, Regensburg, **2003**.

2 A. Gißibl, Dissertation, Regensburg, **2006**.

3 S. Jain, O. Reiser, *ChemSusChem* **2001**, *1*, 534.

4 D. A. Fleming, C. J. Thode, M. E. Williams, *Chem. Mater.* **2006**, *18*, 2327.

5 C. D. Bain, E. B. Troughton, Y. Tao, J. Evall, G. M. Whitesides, R. G. Nuzzo, *J. Am. Chem. Soc.* **1989**, *111*, 321.

6 M. Ortega-Muñoz, J. Lopez-Jaramillo, F. Hernandez-Mateo, F. Santoyo-Gonzalez, *Adv. Synth. Catal.* **2006**, *348*, 2410.

7 J. Zabicky, *J. Chem. Soc.* **1961**, 683.

E. Appendix

1. NMR-spectra

^{1}H-NMR (300 MHz, $CDCl_3$): -upper image

^{13}C-NMR (75 MHz, $CDCl_3$): -lower image

Solvent (if not stated otherwise): $CDCl_3$

Bis[4,5-dihydro-(4*S*)-(1-methylethyl)-1,3-oxazol-2-yl]-amine (103a):

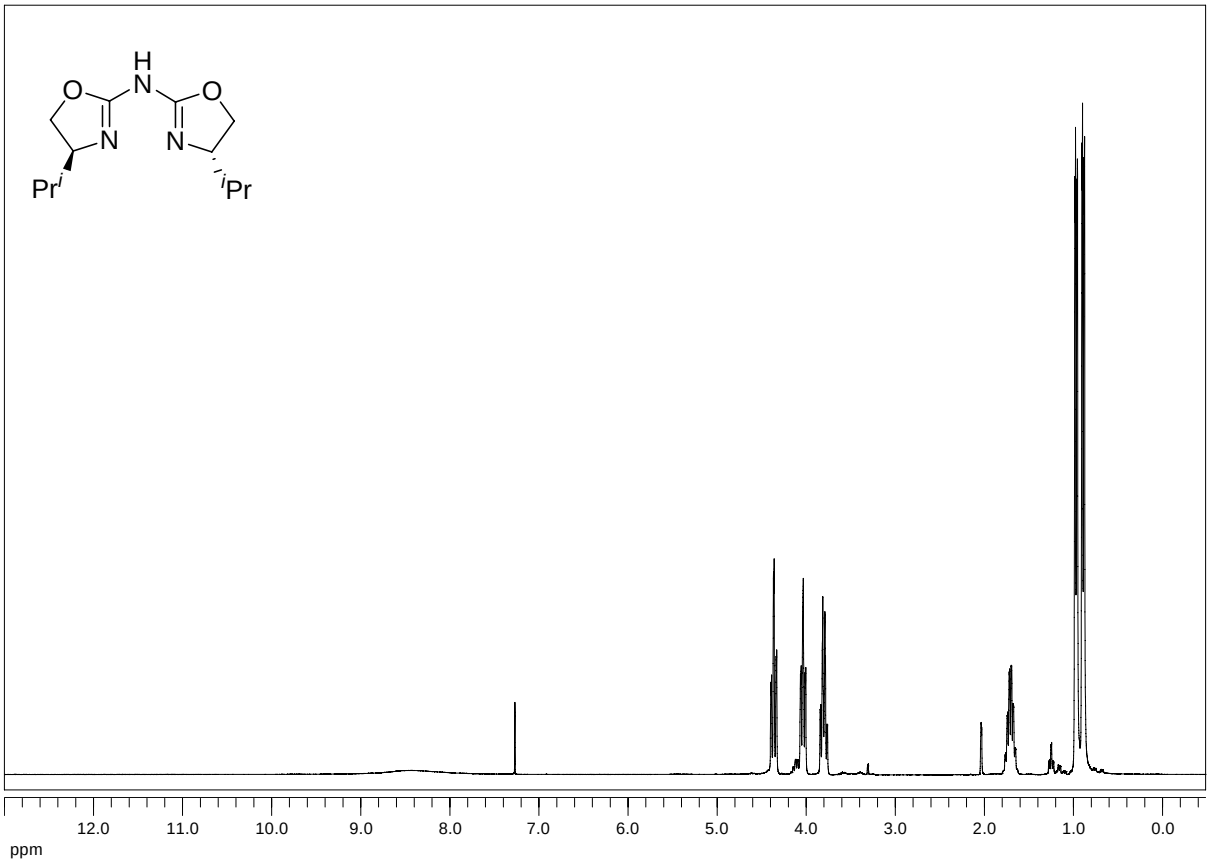

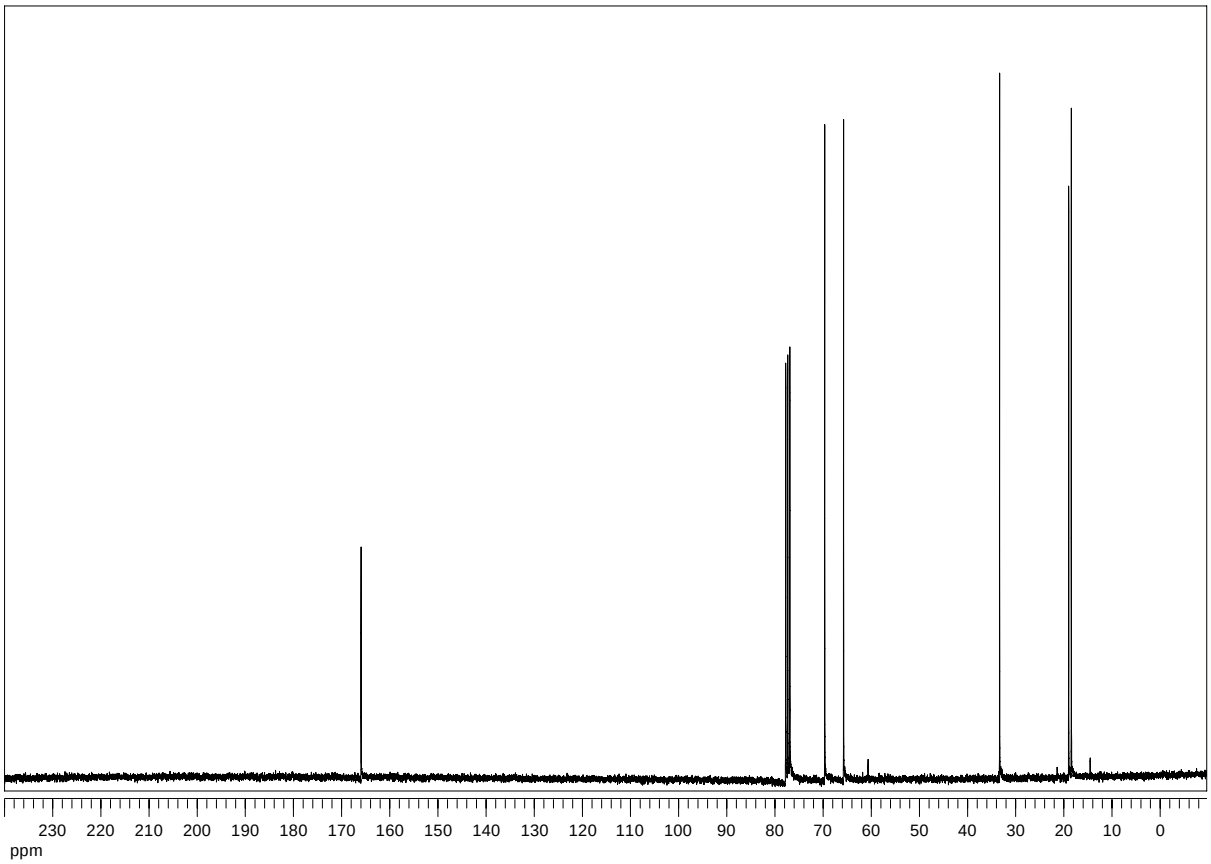

Bis-[4,5-dihydro-(4*S*)-(1-methylethyl)-1,3-oxazol-2-yl]-methylamine (109a):

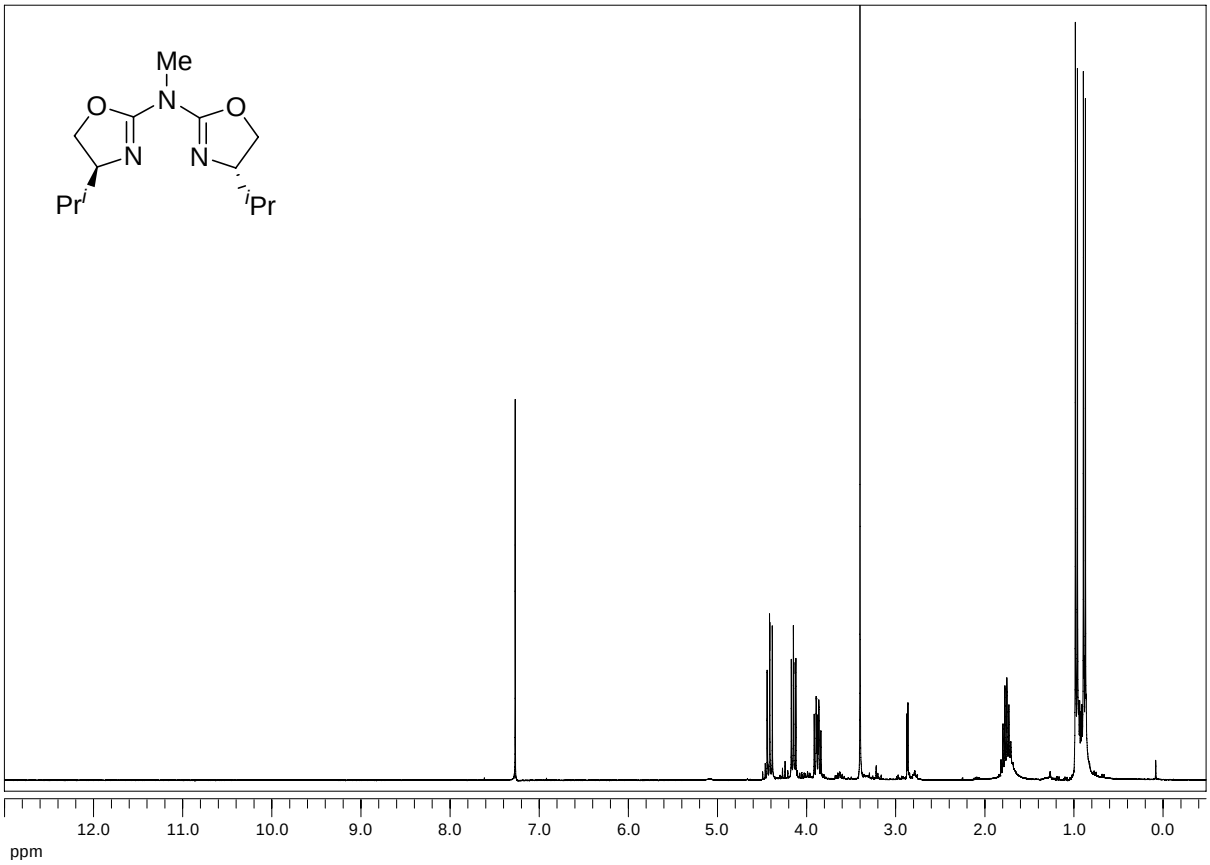

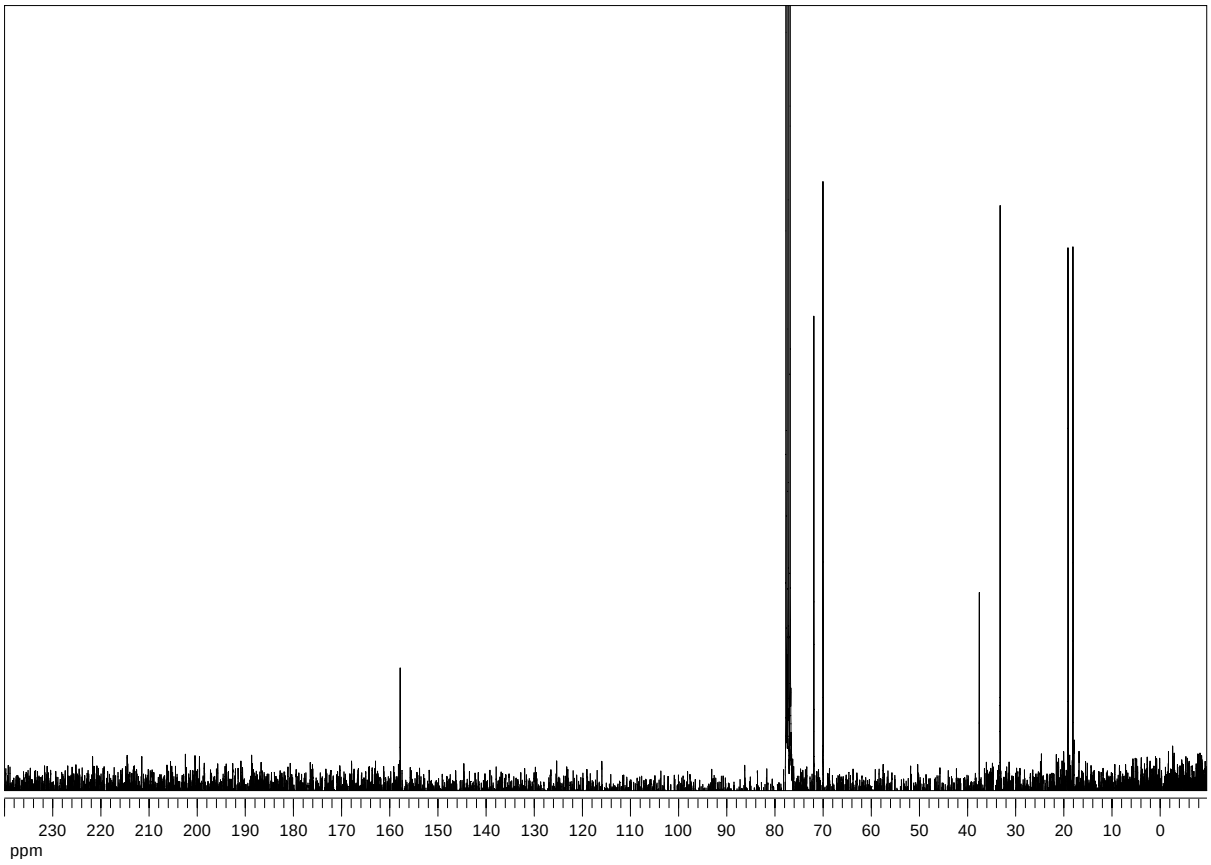

Bis[4,5-dihydro-(4*S*)-(1,1-dimethylethyl)-1,3-oxazol-2-yl]-amine (103b):

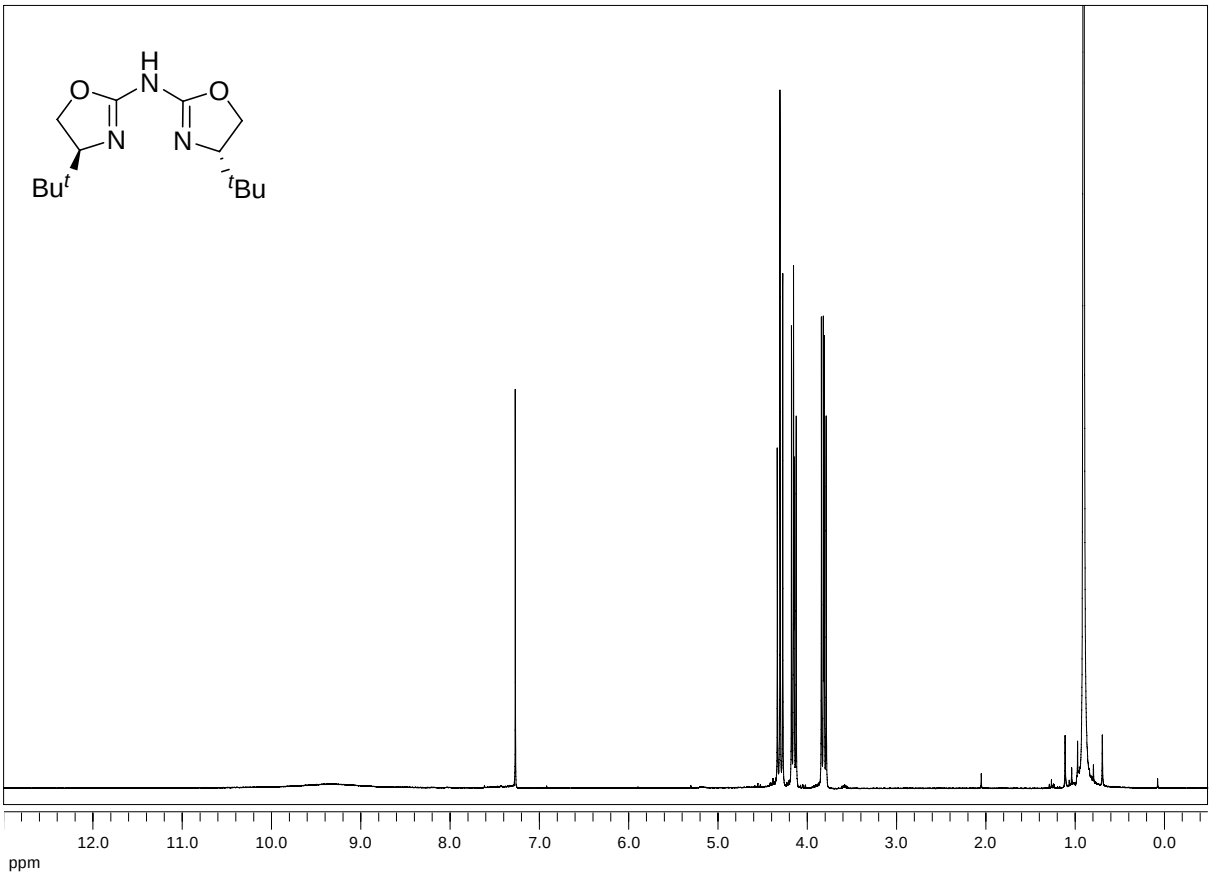

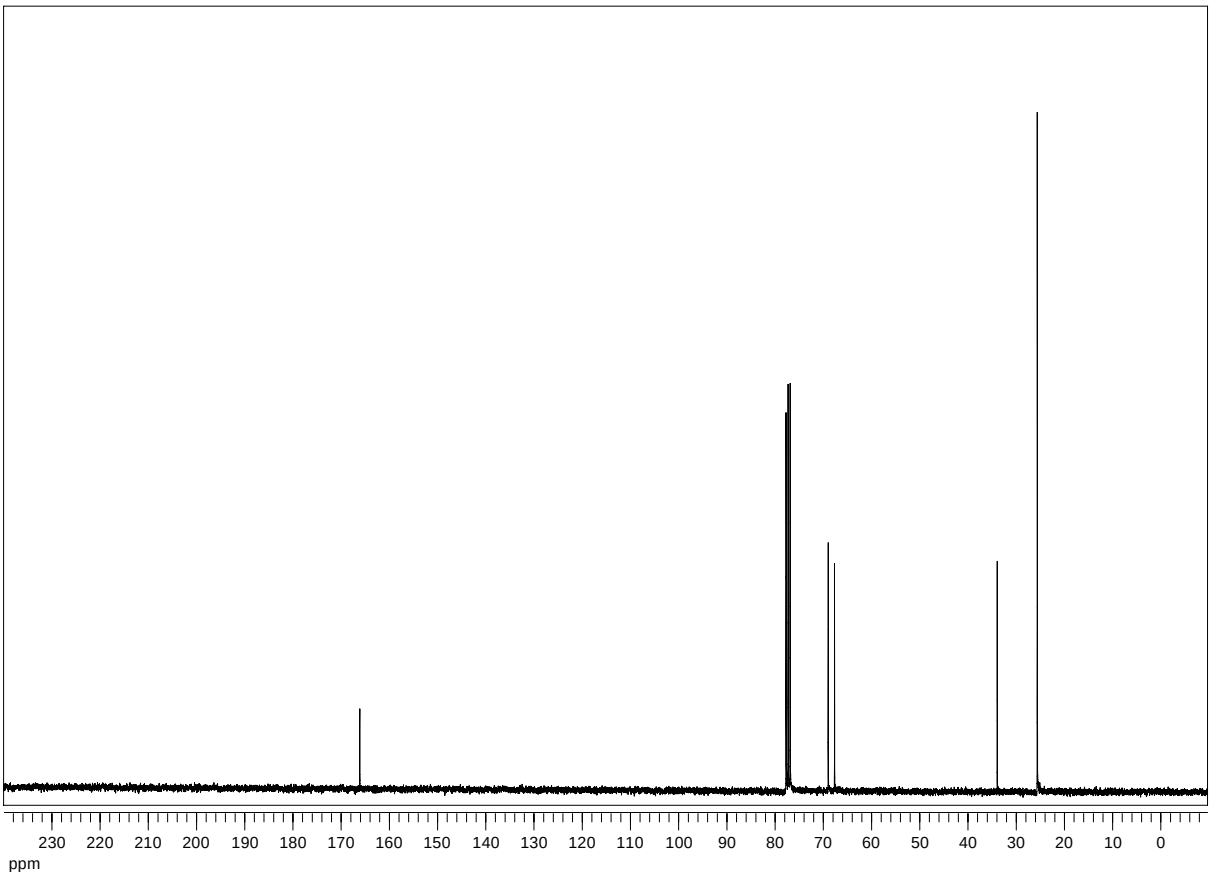

Bis[4,5-dihydro-(4*S*)-(1,1-dimethylethyl)-1,3-oxazol-2-yl]-methylamine (109d):

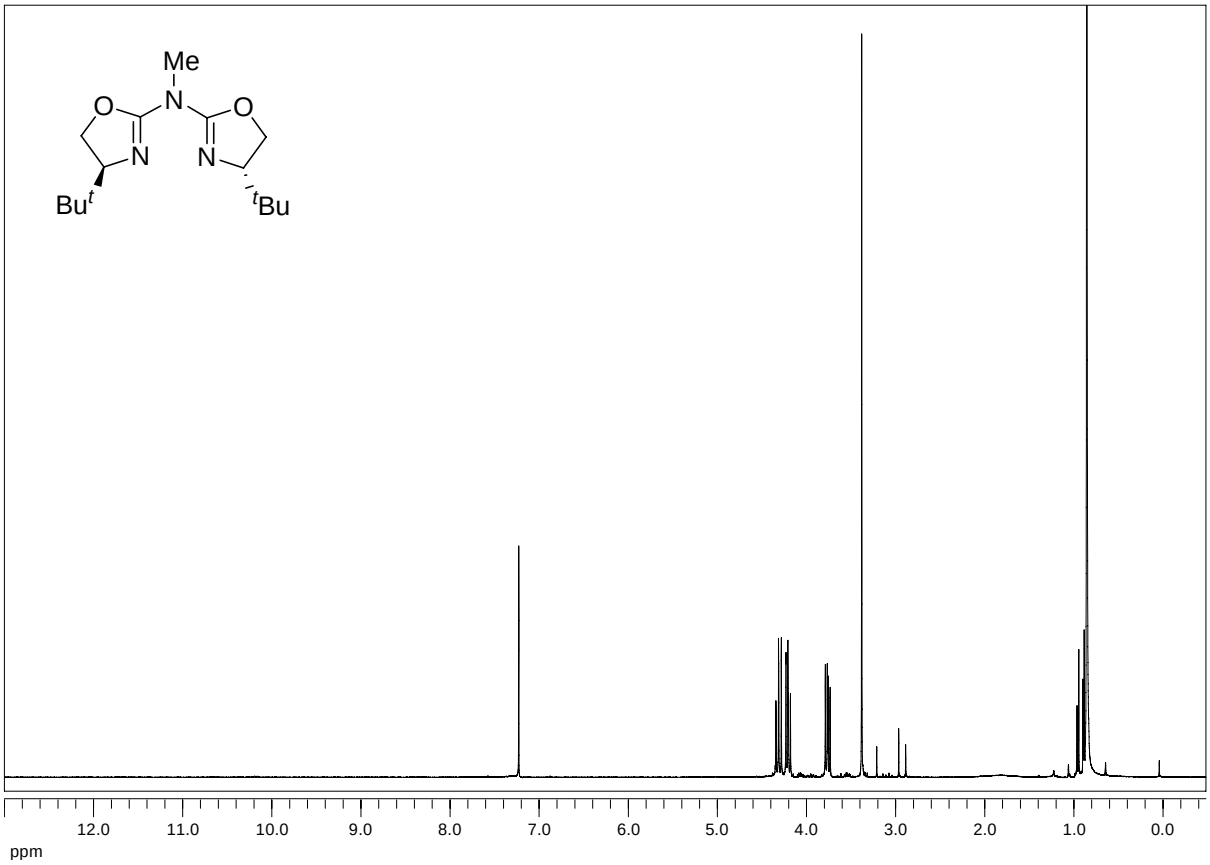

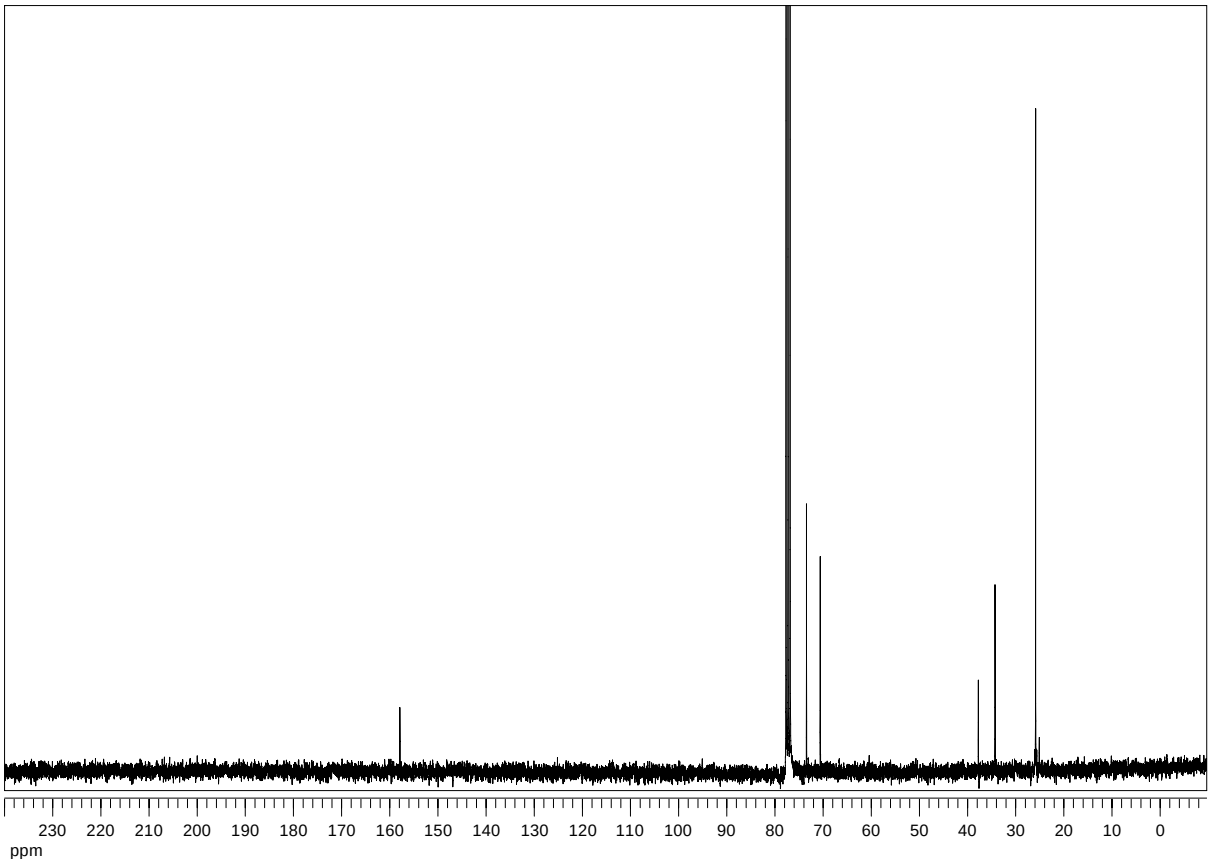

Bis[4,5-dihydro-(4*R*)-(phenyl)-1,3-oxazol-2-yl]-amine (103c):

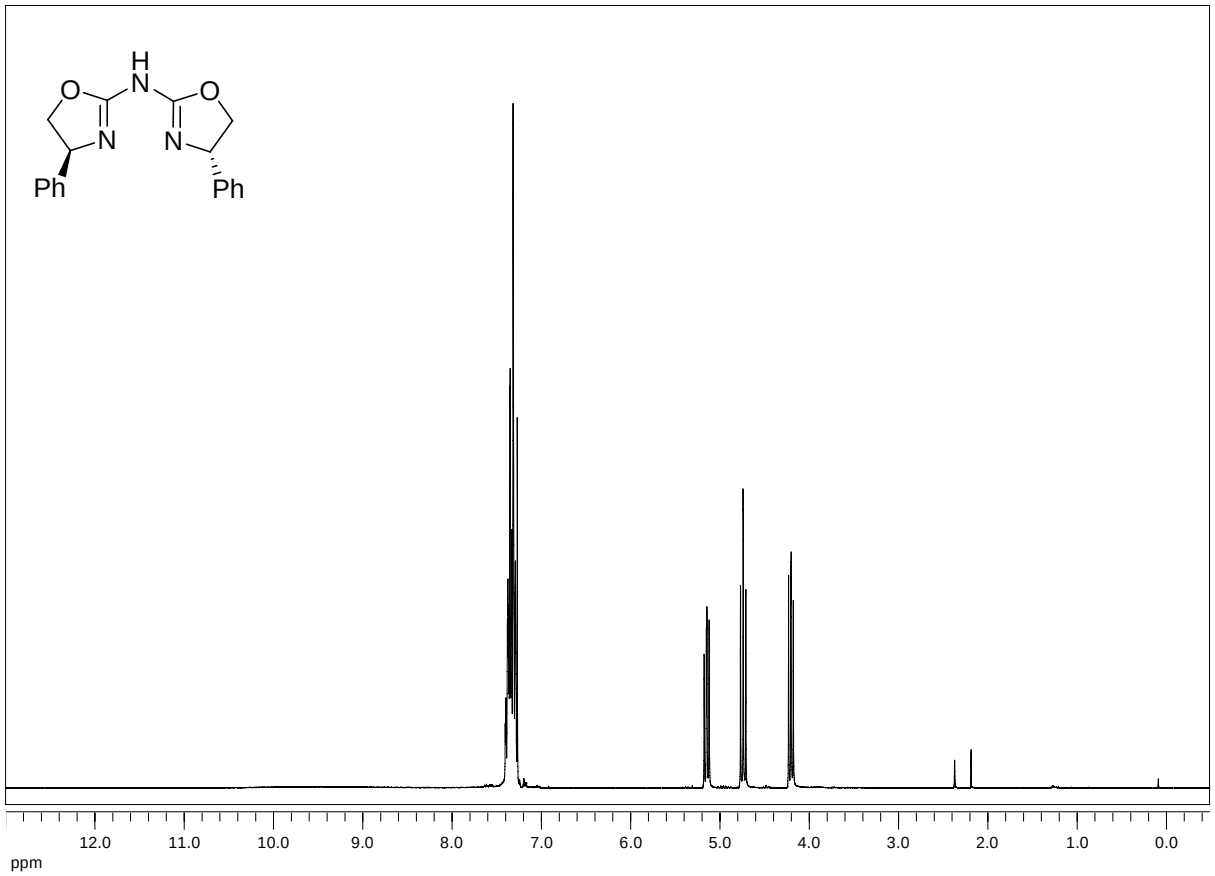

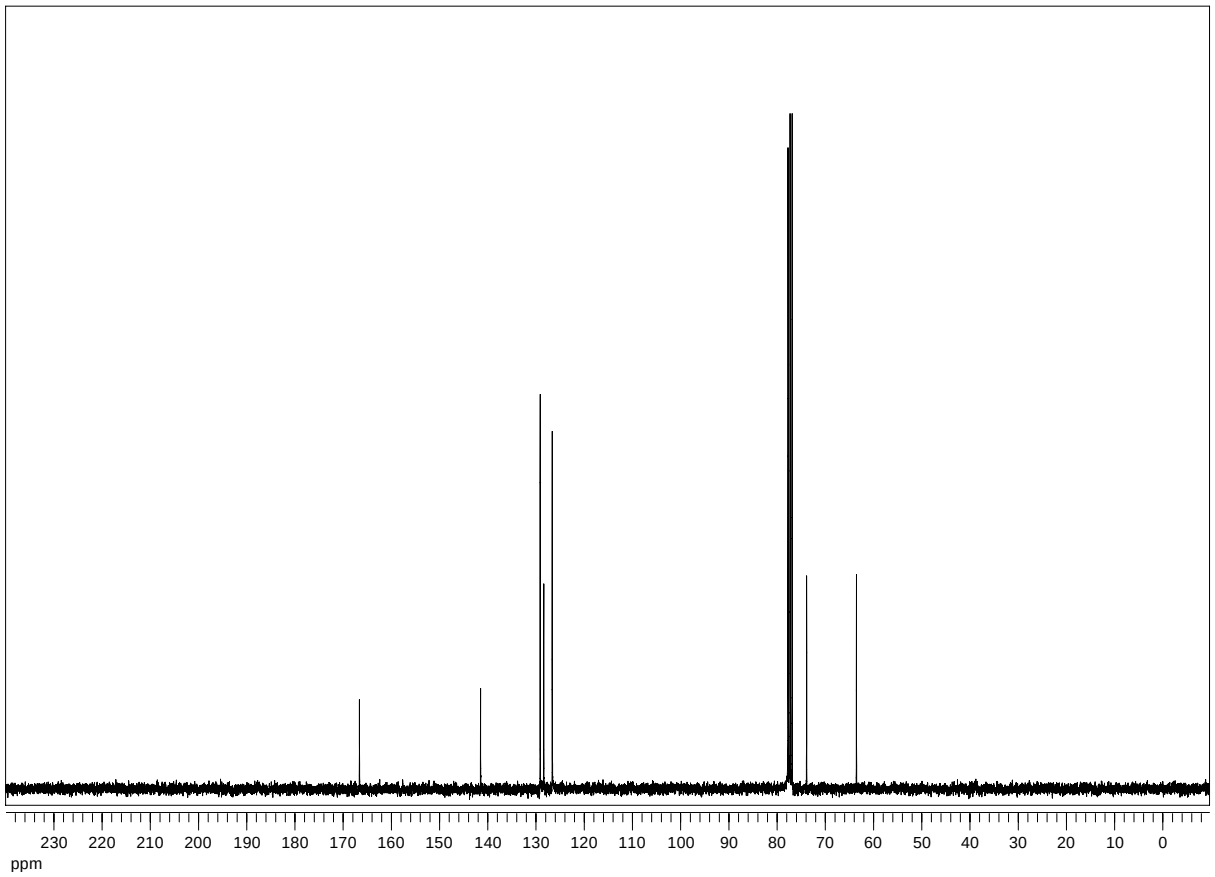

Bis[4,5-dihydro-(4*S*)-(benzyl)-1,3-oxazol-2-yl]-amine (103d):

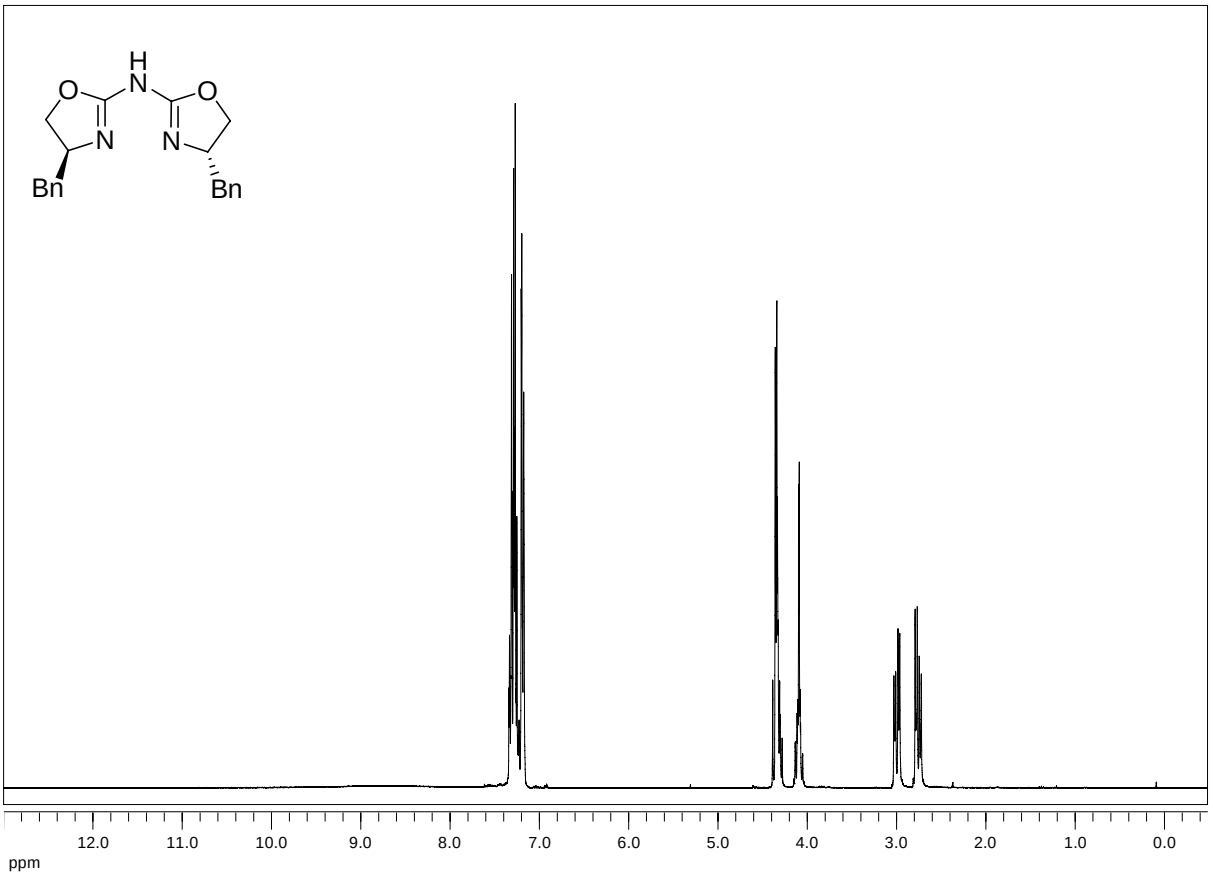

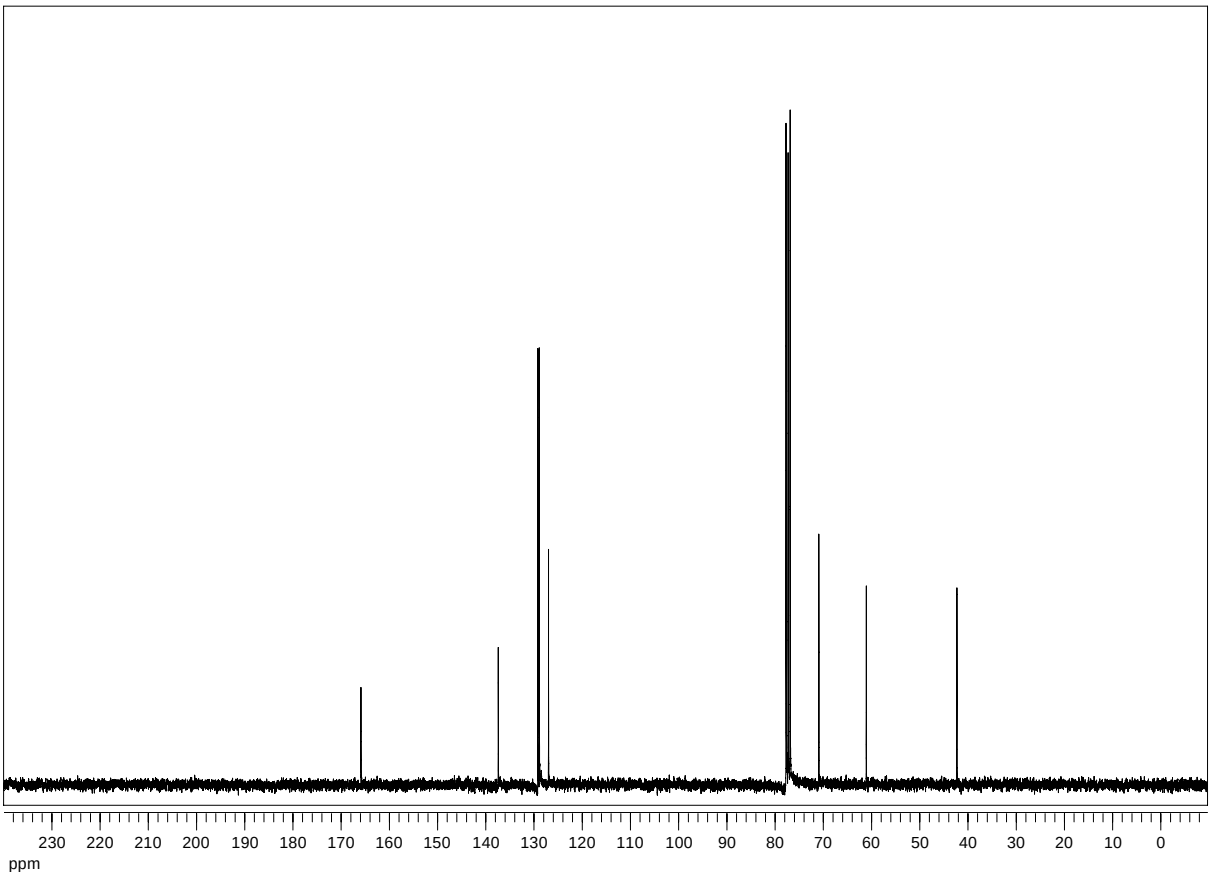

Bis[4,5-dihydro-(4*S*)-(benzyl)-1,3-oxazol-2-yl]-amine (109d):

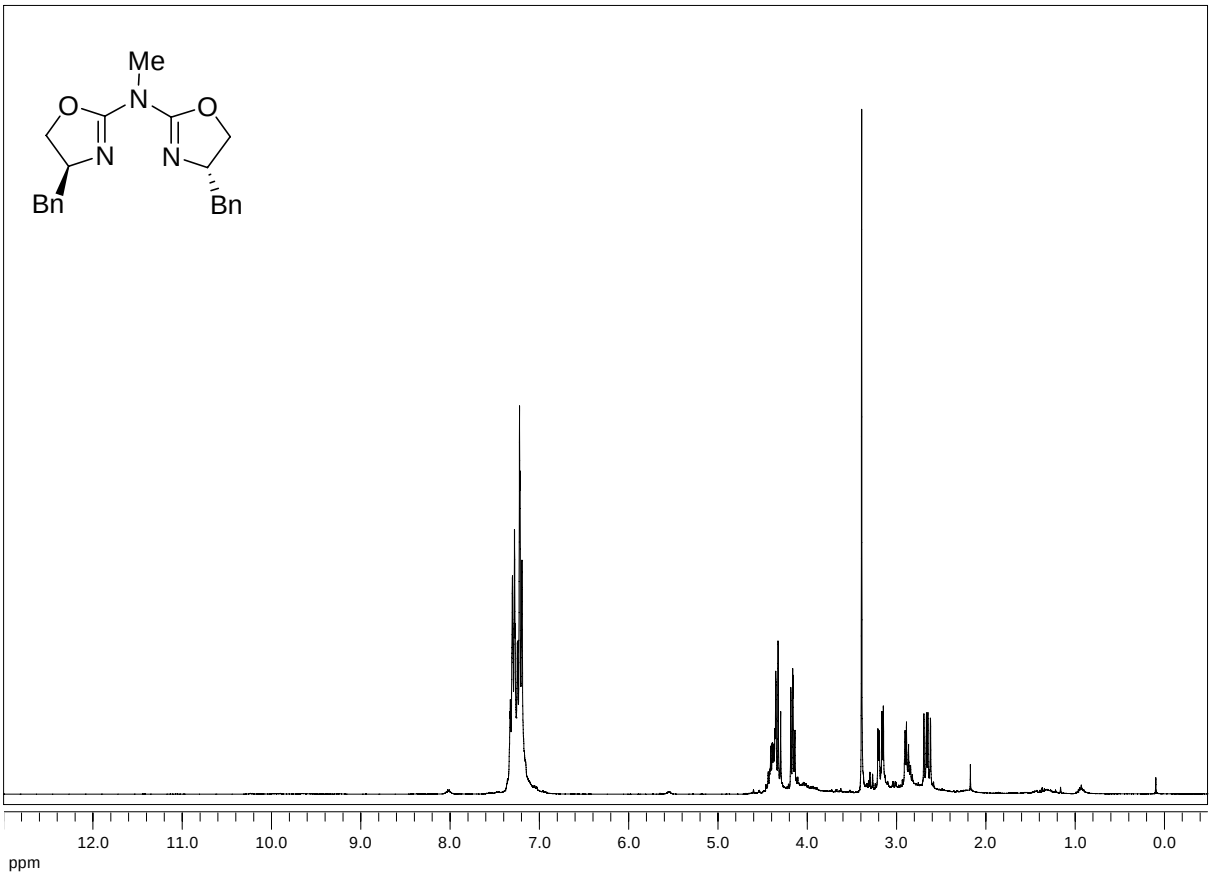

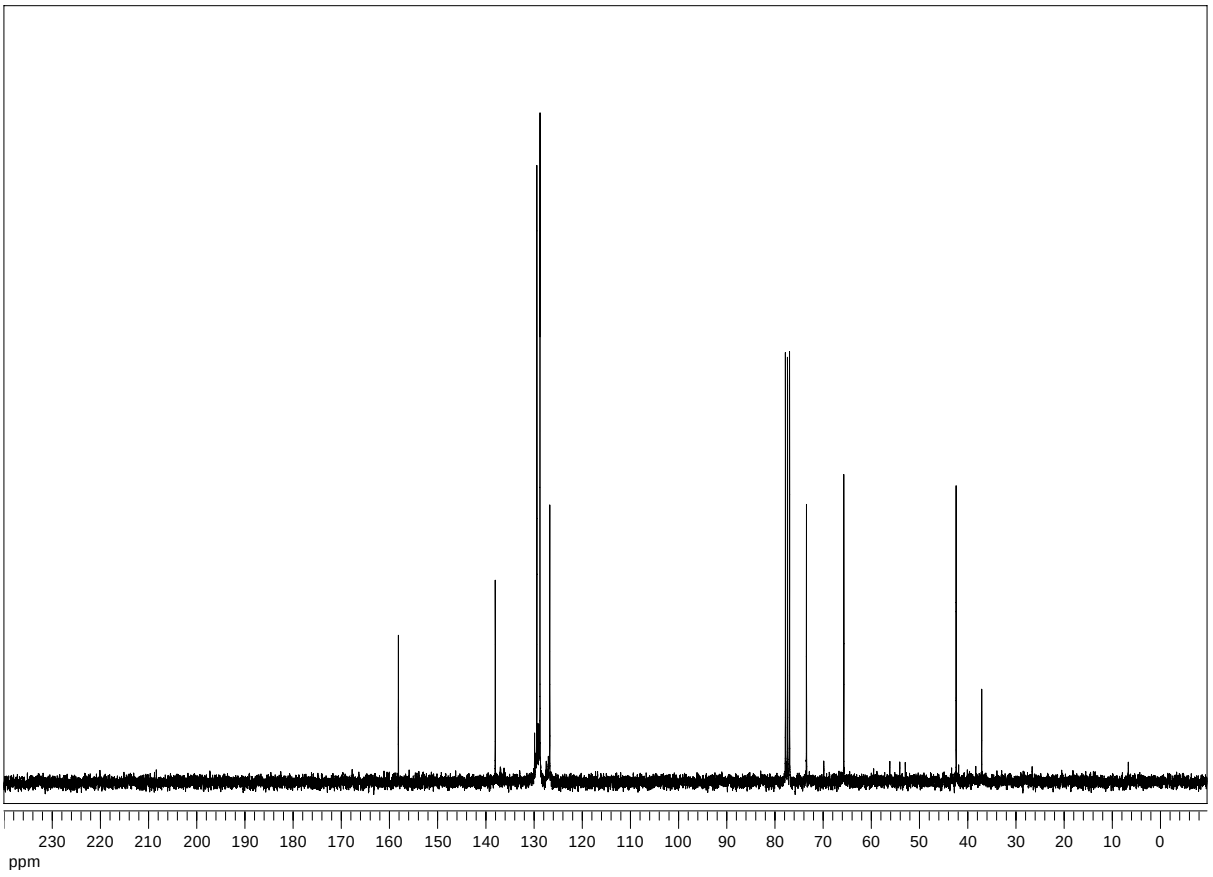

Bis-[4,5-dihydro-(4*S*)-(benzyl)-1,3-oxazol-2-yl]-prop-2-ynyl-amine (120b):

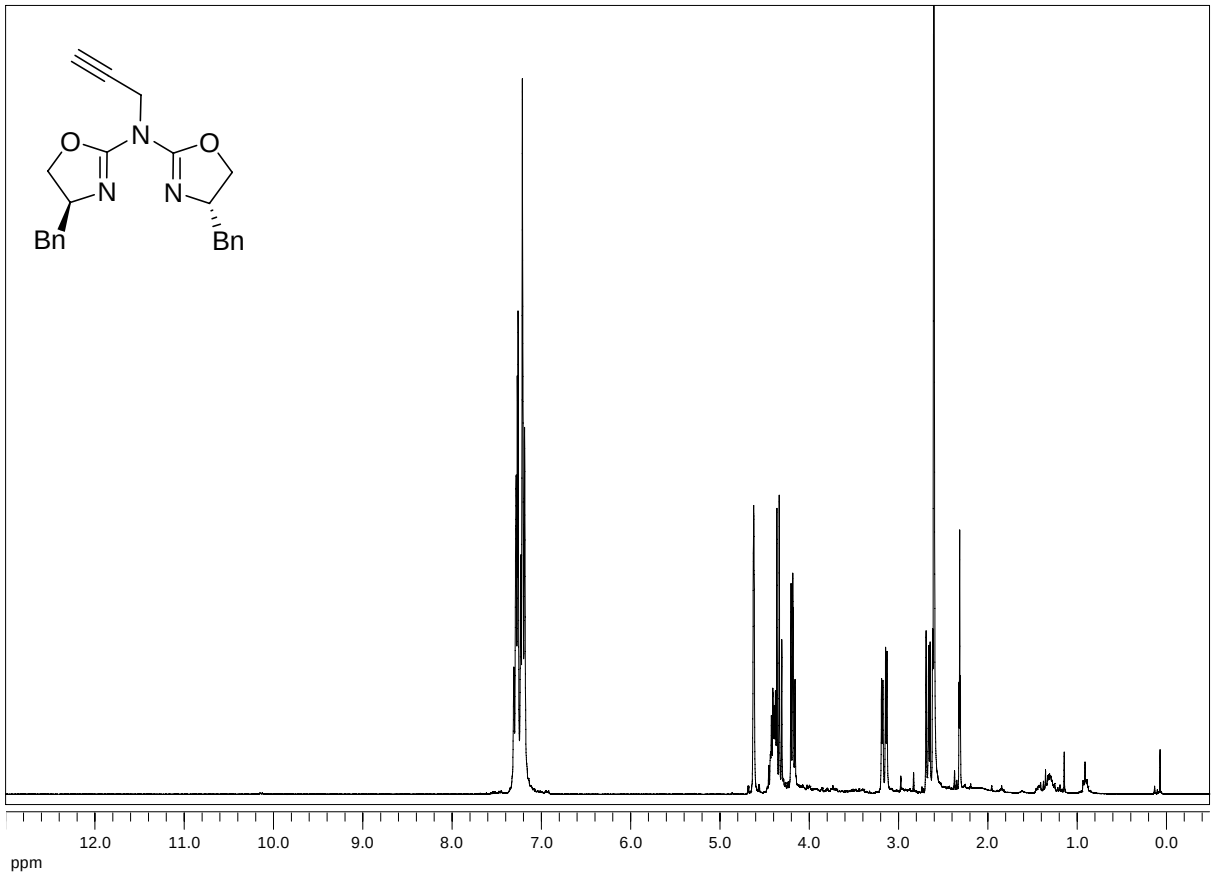

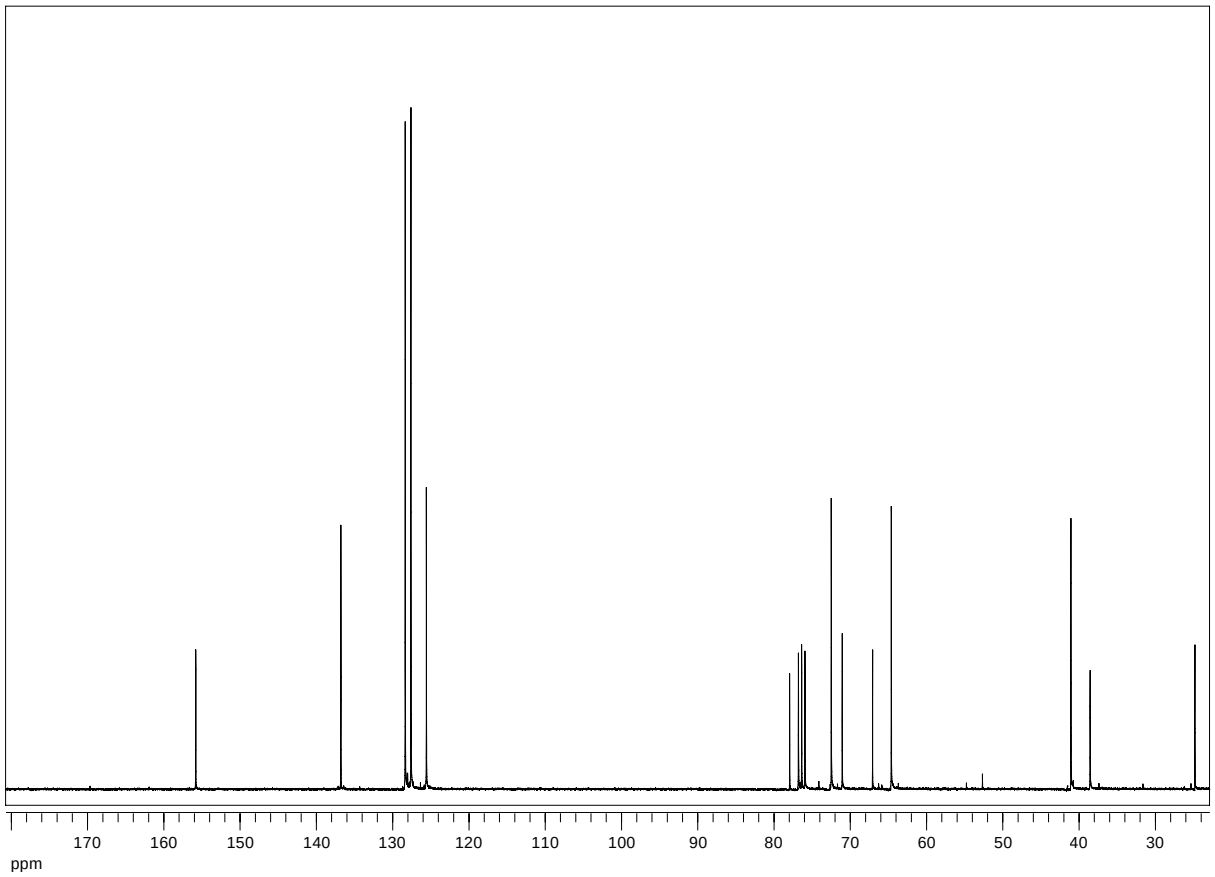

1-(Nitrophenyl)-2-propyn-1-one (142):

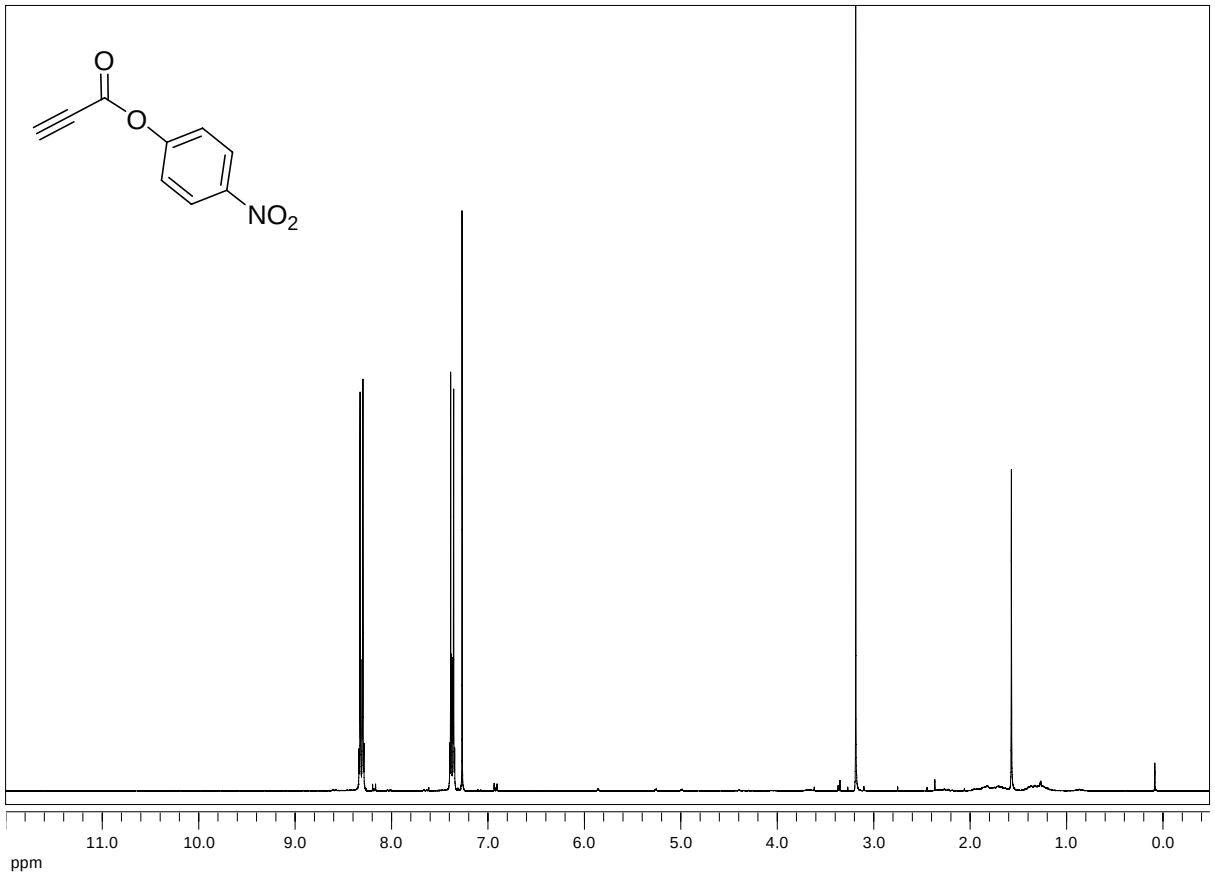

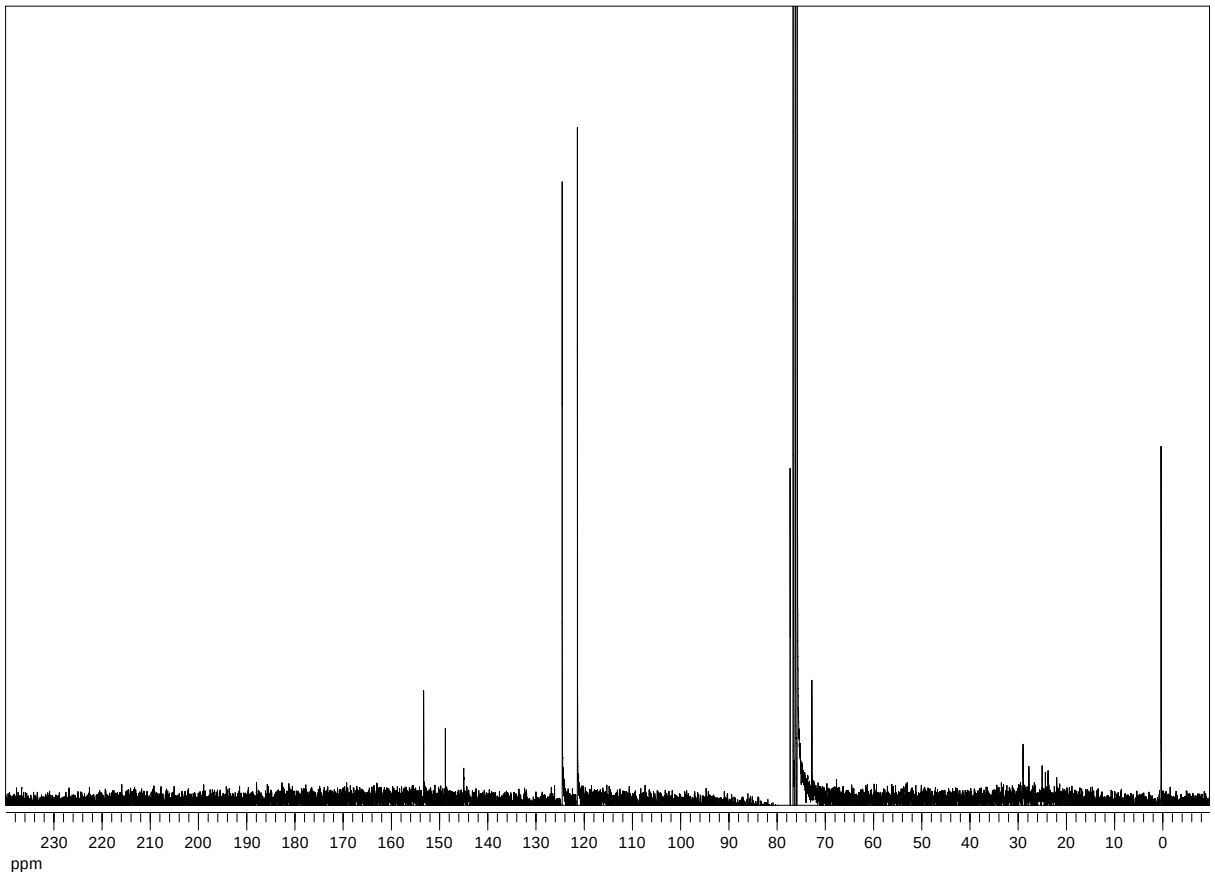

(*S*,E)-methyl2-(2-hydroxybenzylideneamino)-3-(4-hydroxyphenyl)propanoate (165a): Solvent: DMSO

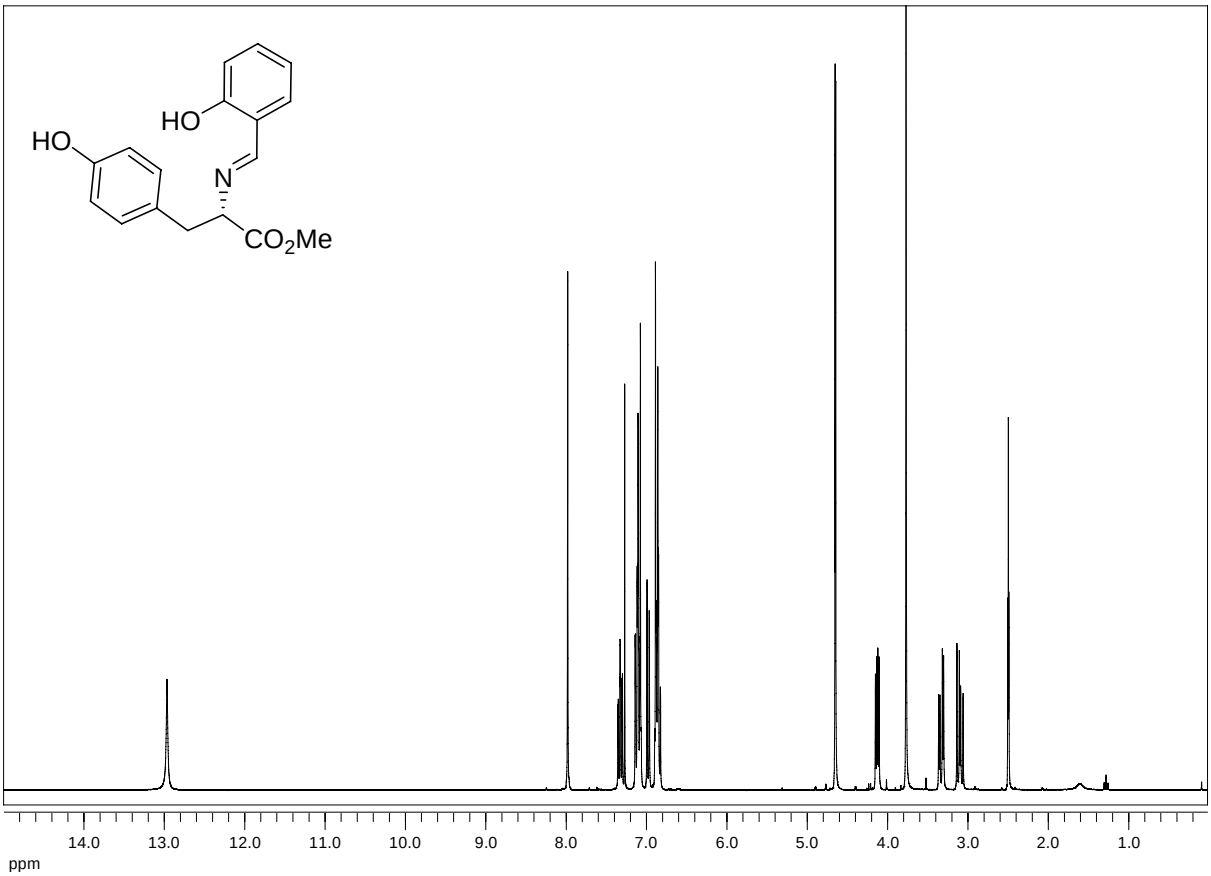

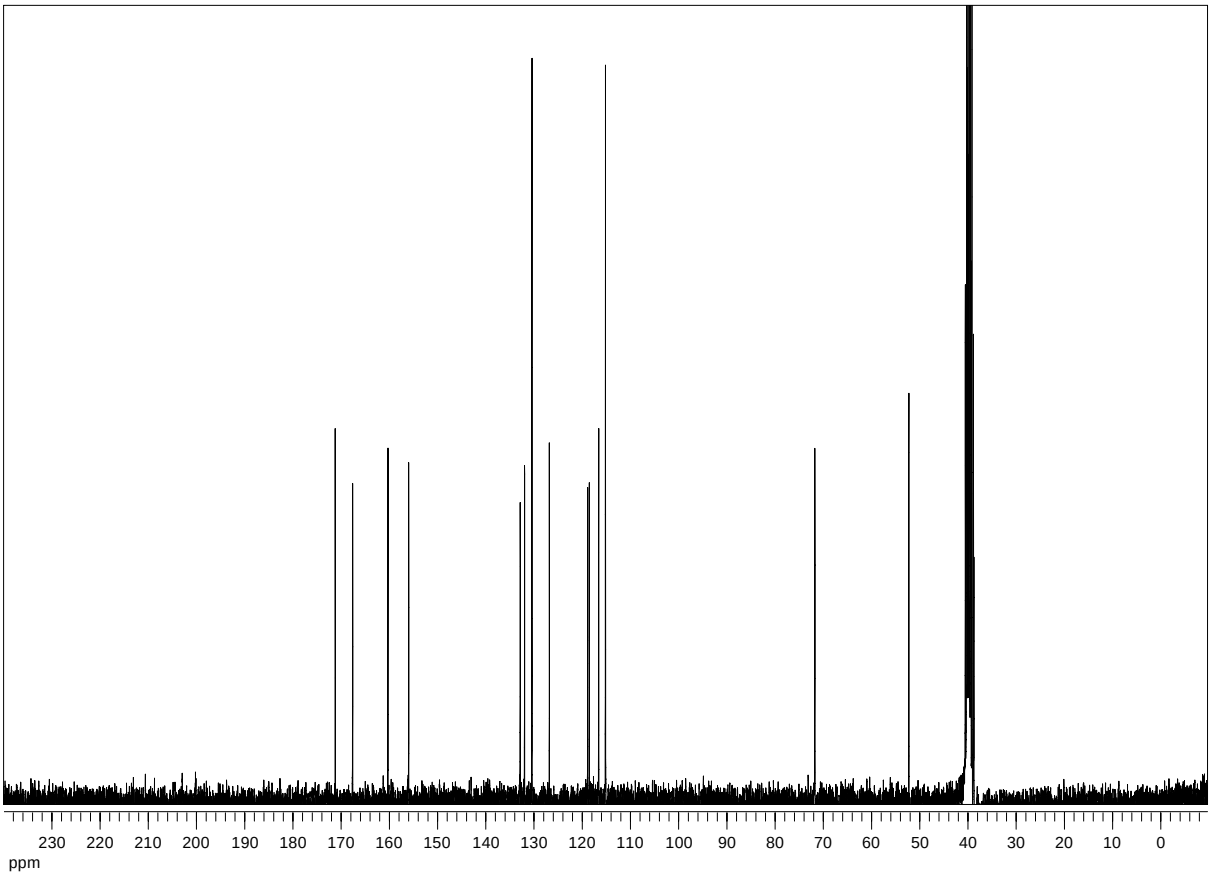

(*S*,E)-methyl-2-(2-hydroxybenzylideneamino)-3-(4-(prop-2-ynyloxy)phenyl) propanoate (165b):

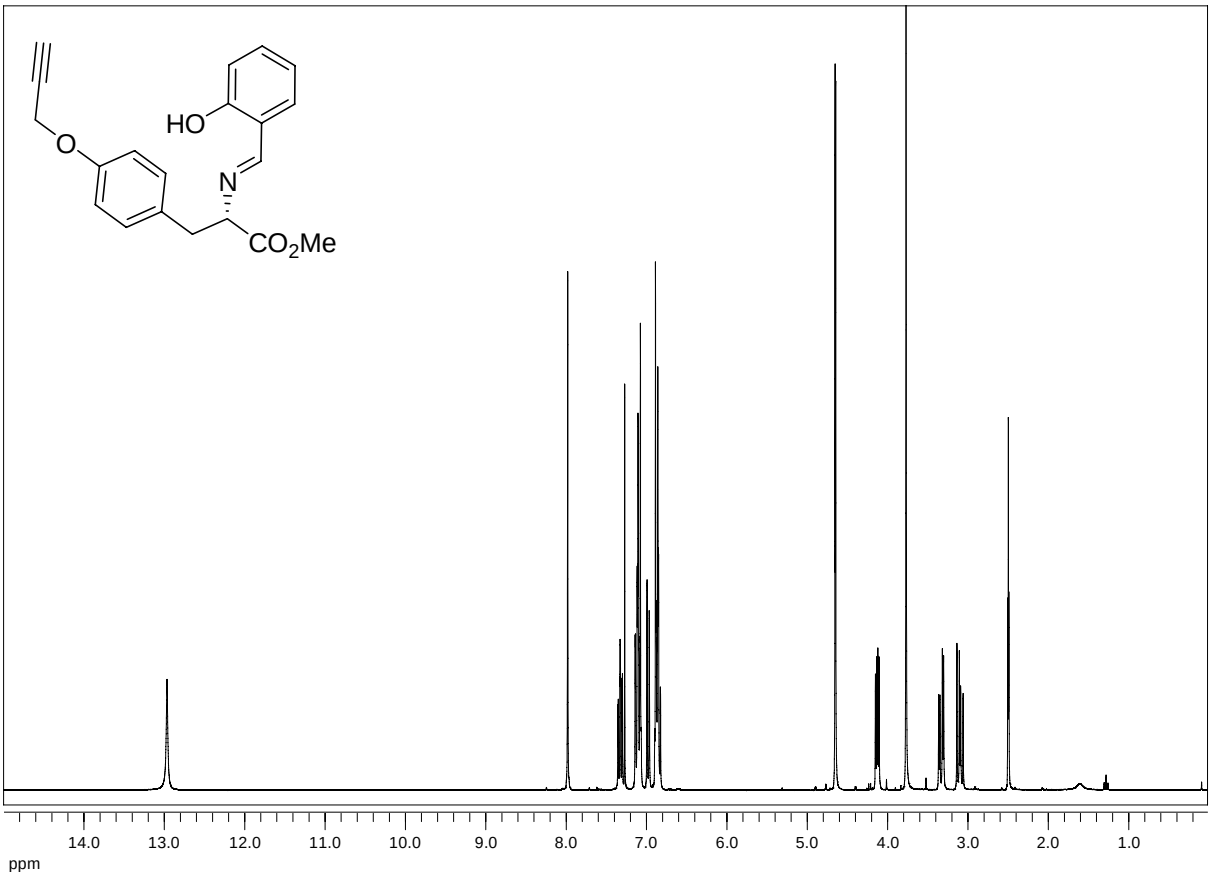

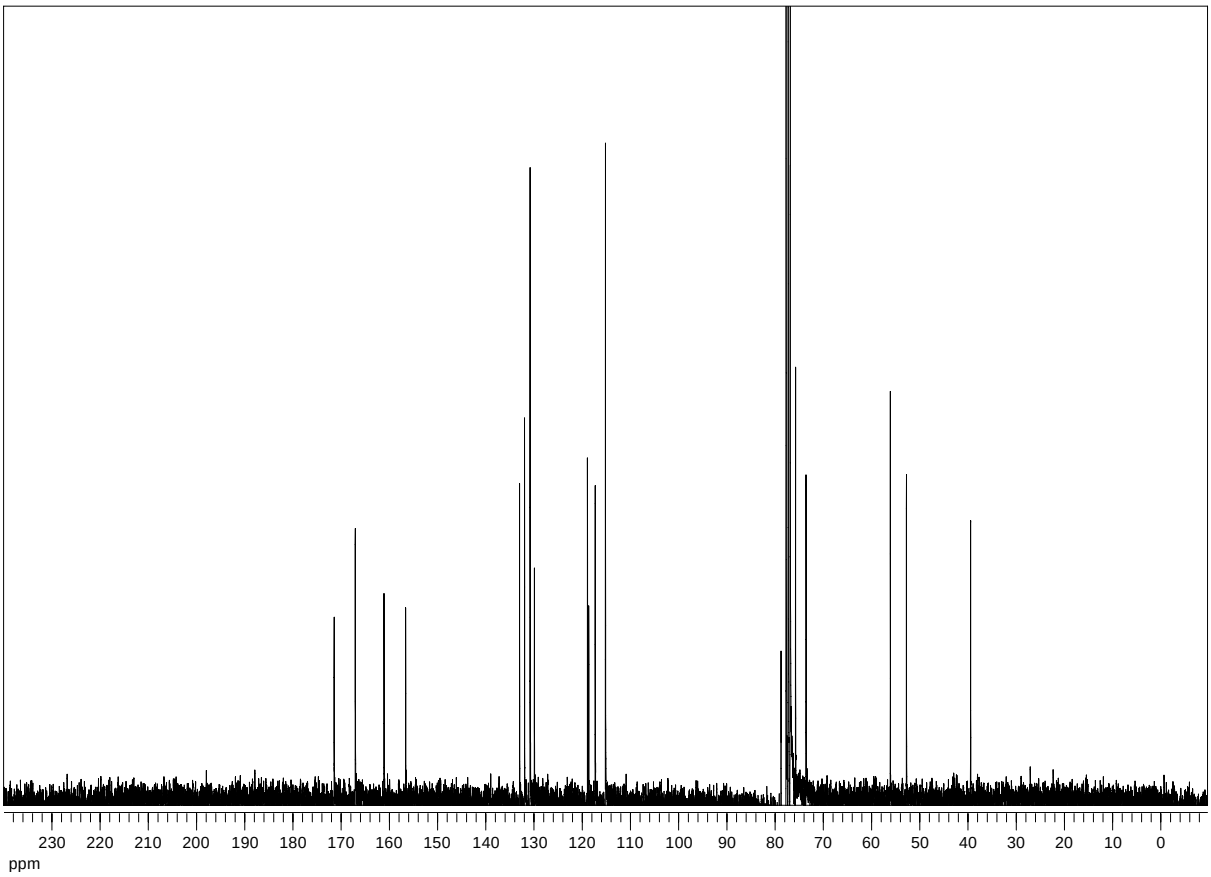

(*R*,*R*)-Benzoic acid 2-hydroxy-1,2-diphenyl-ethyl ester (171):

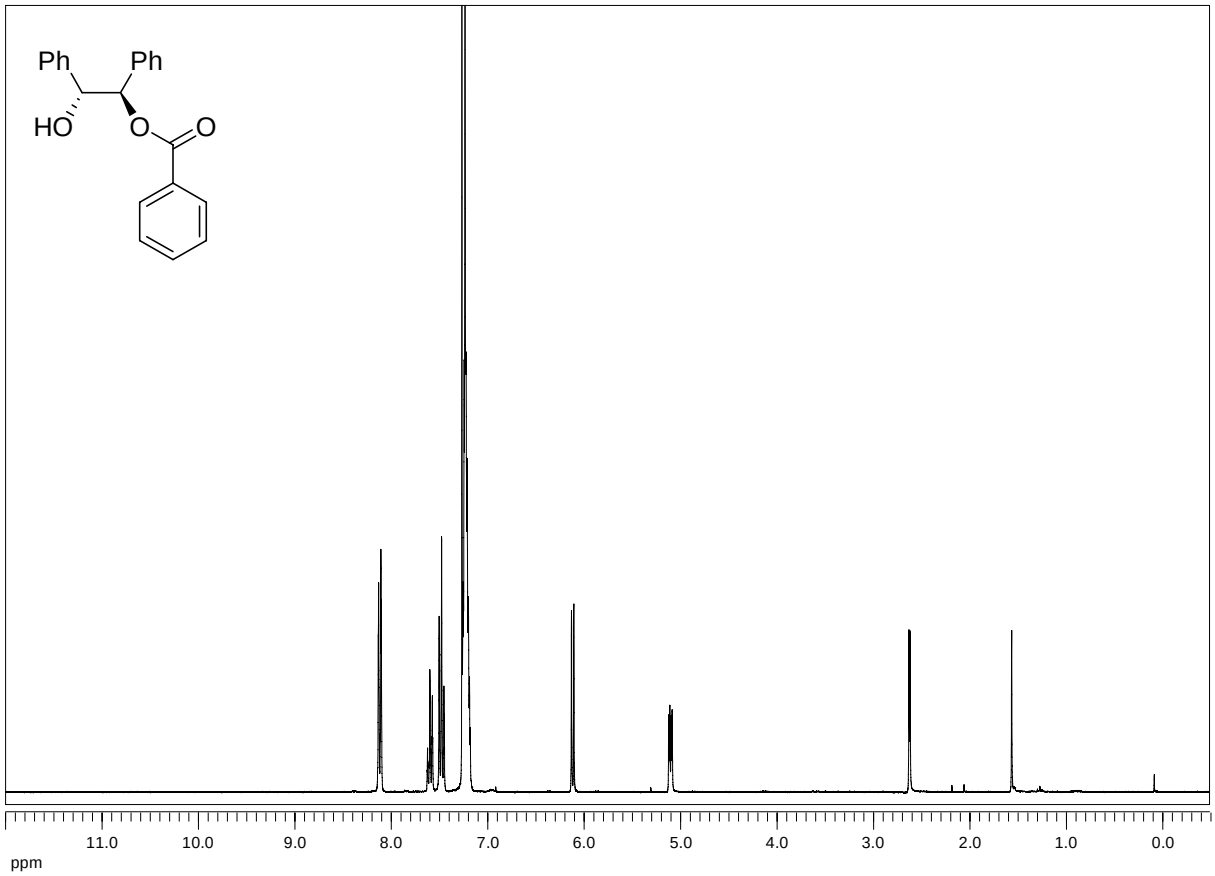

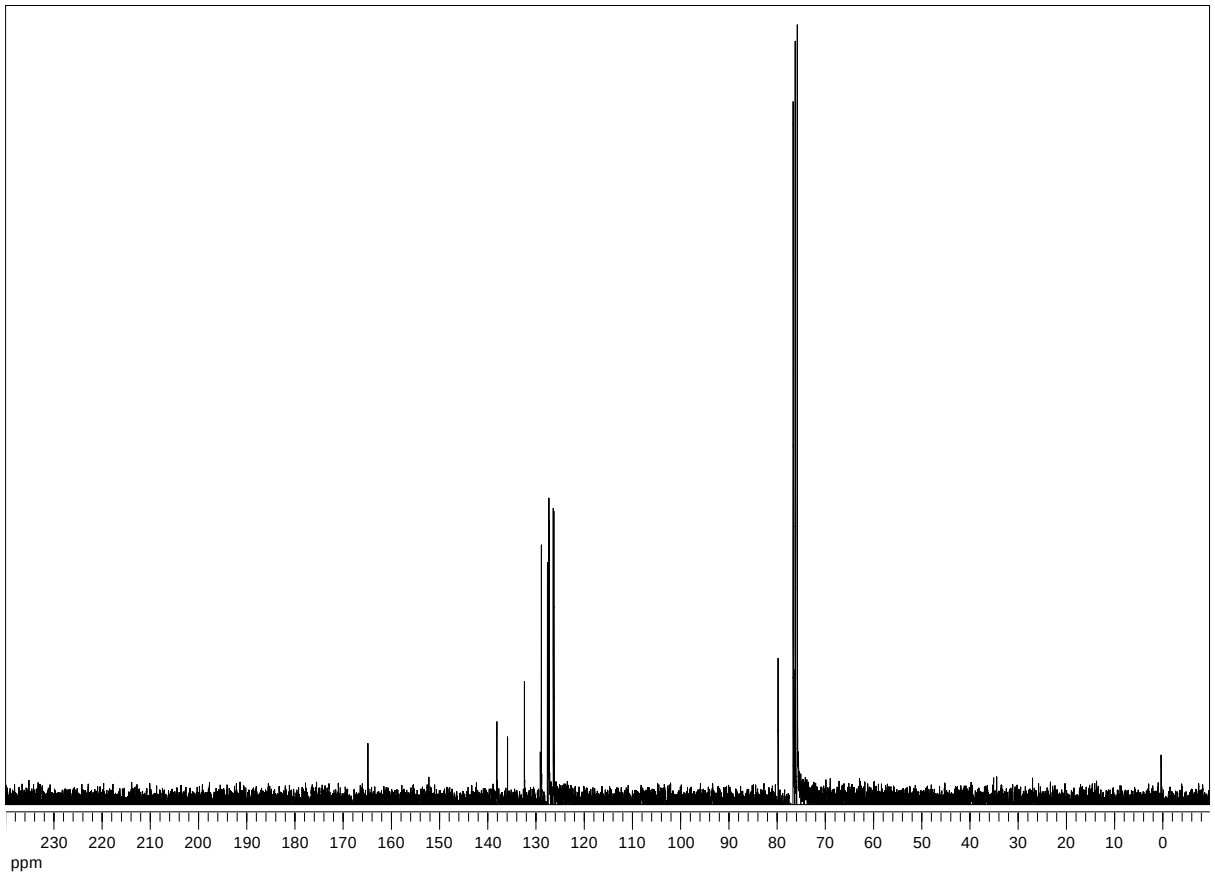

(*R,R*)-Benzoic acid 2-hydroxy-cyclohexyl ester (177a):

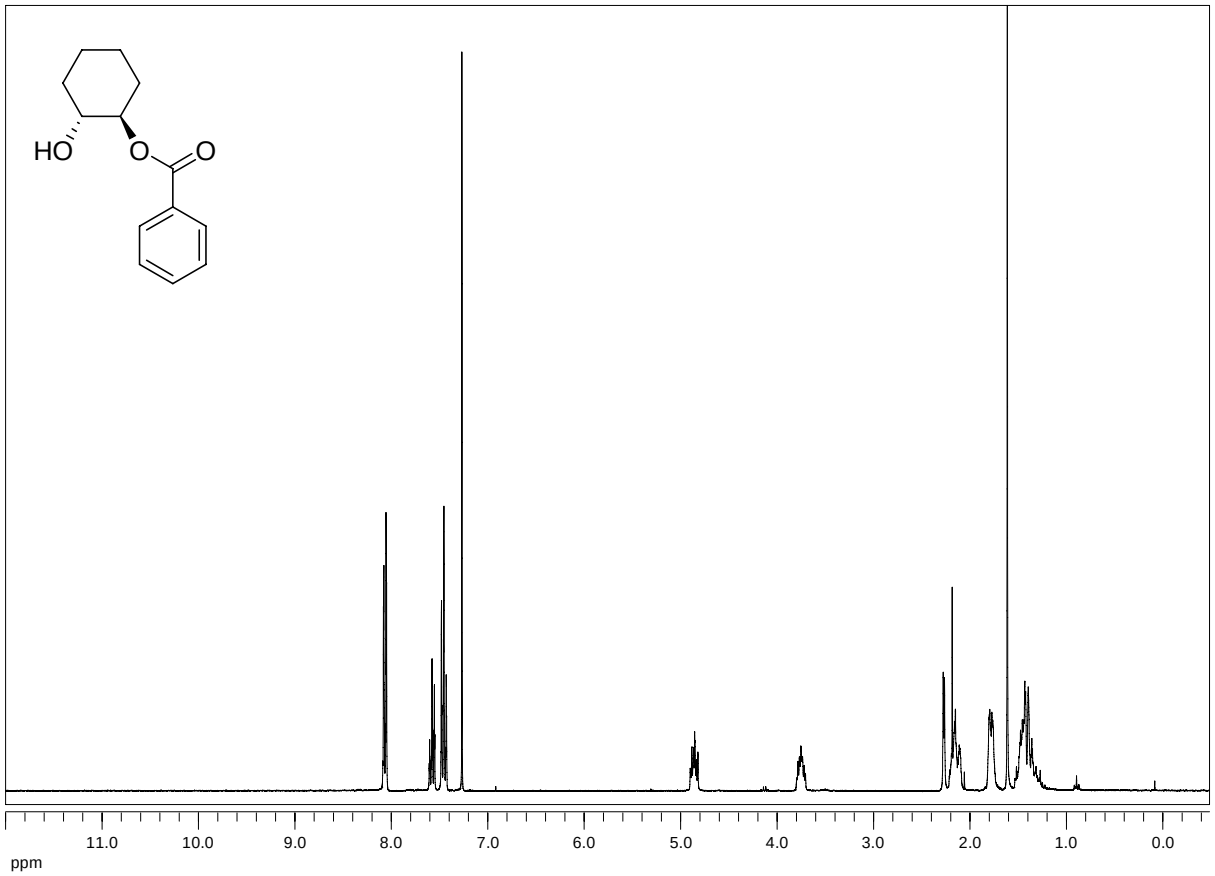

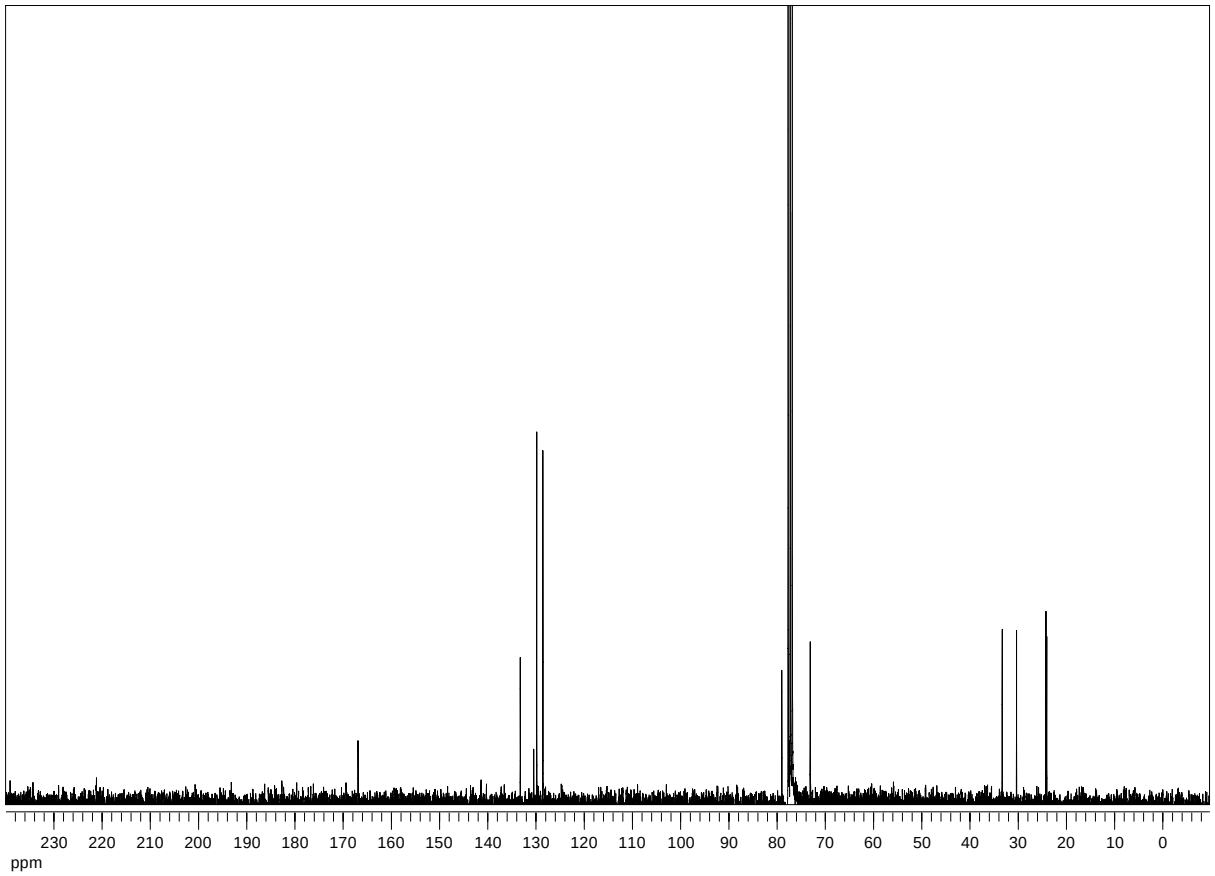

(*R*,*R*)-Benzoic acid 2-hydroxy-cycloheptyl ester (177b):

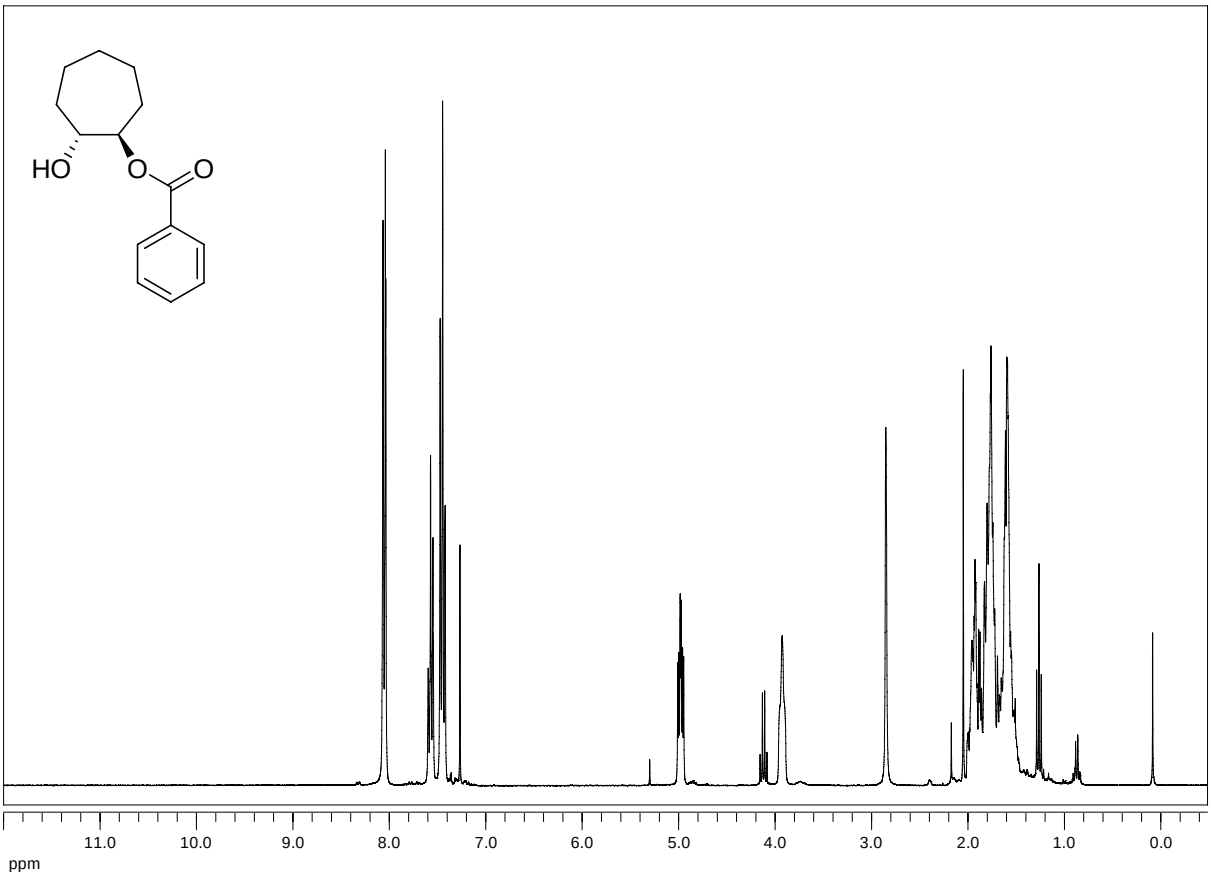

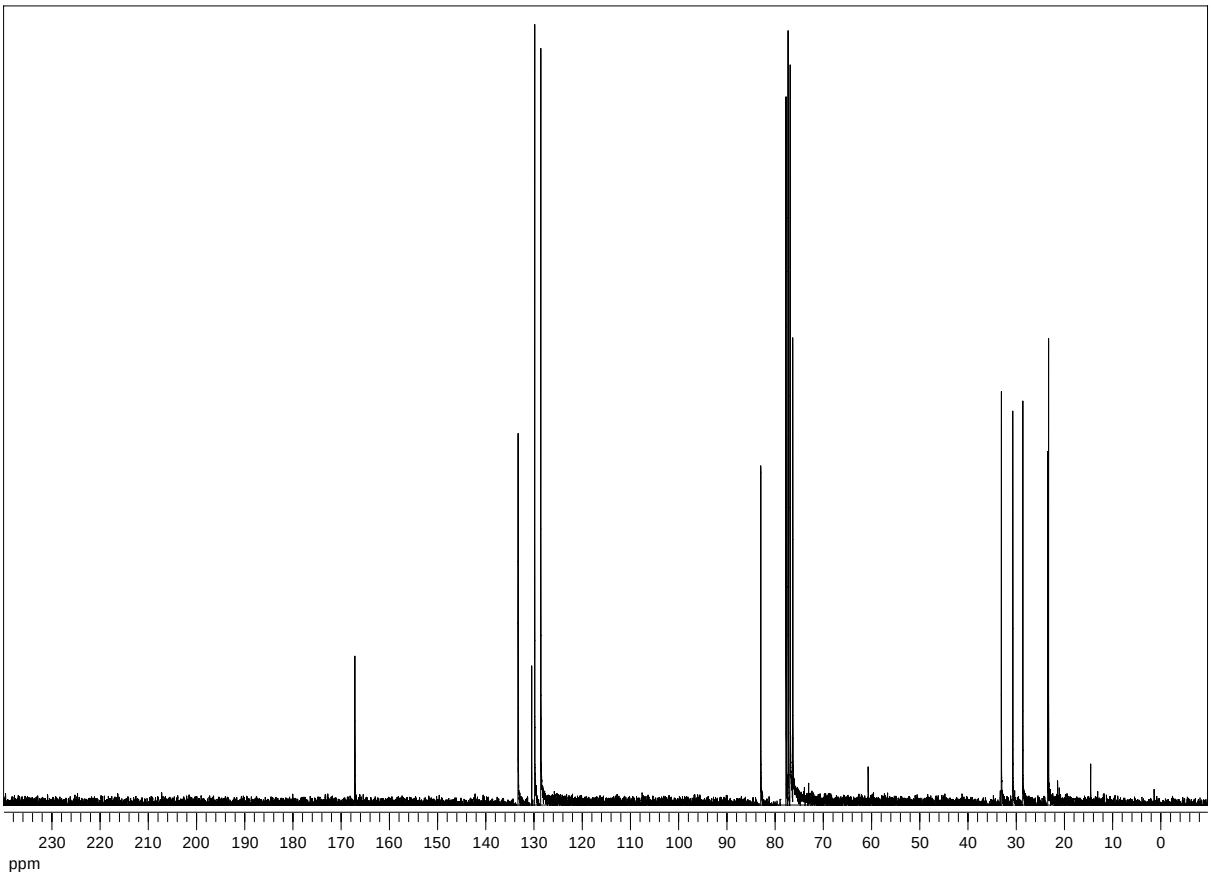

(*S*)–Ethyl2–ethoxycarbonyl–3–(3–indolyl)–3–(p-methyoxyphenyl)propanoate (183):

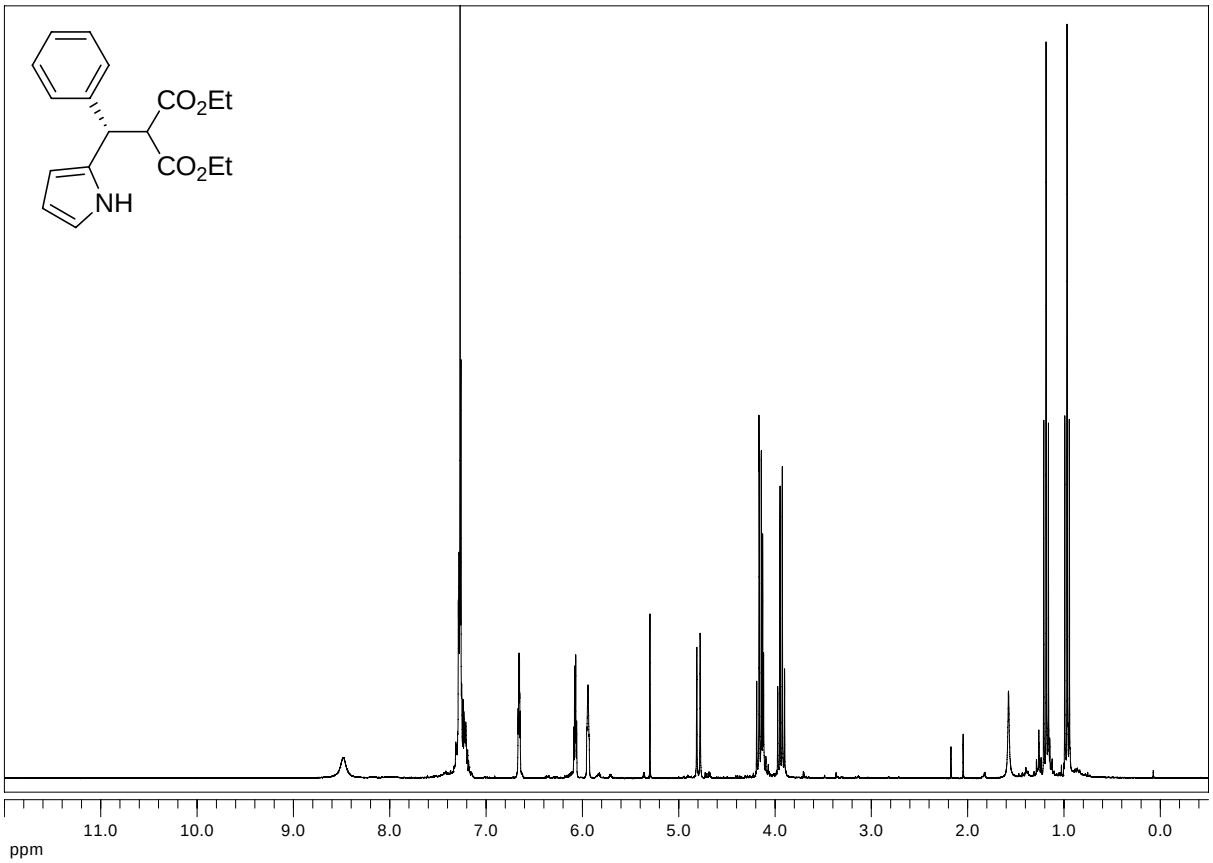

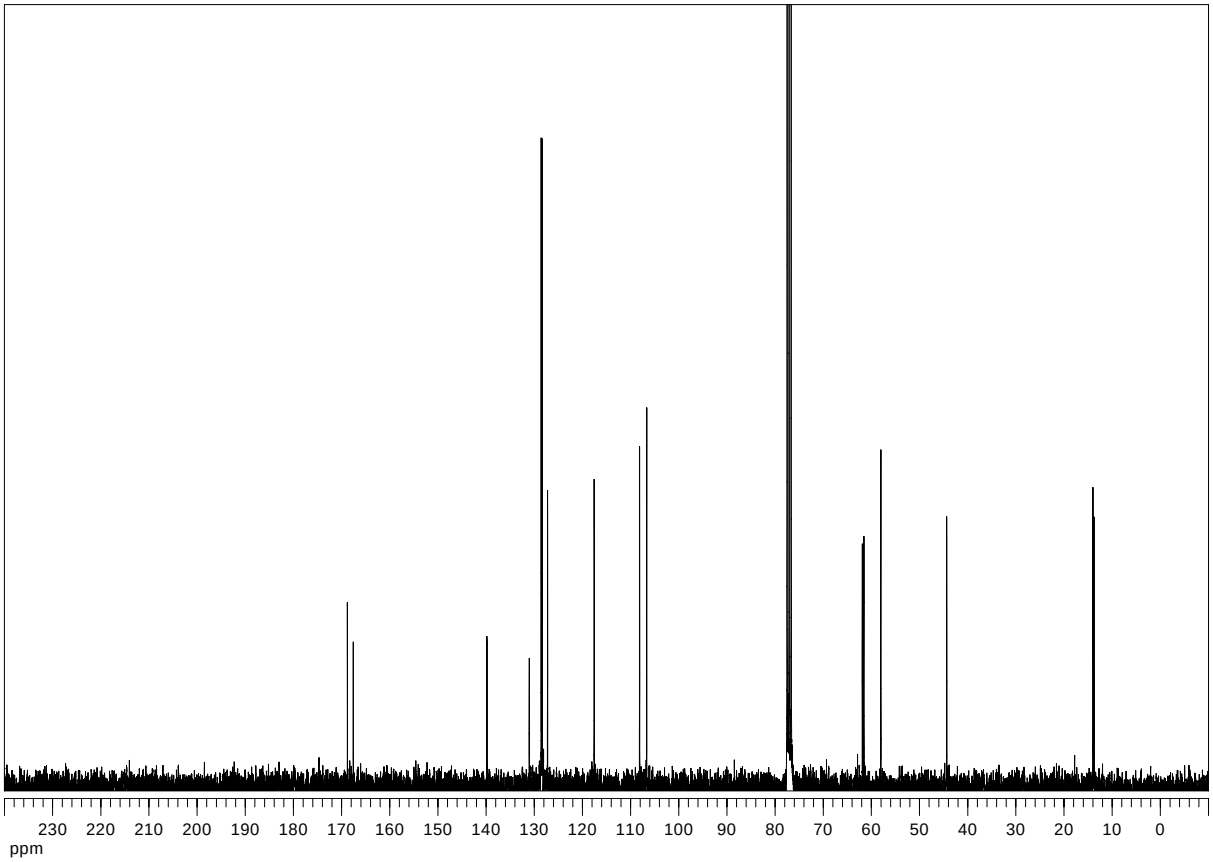

(*S*)–Ethyl2–ethoxycarbonyl–3–(3–indolyl)–3–phenylpropanoate (180a):

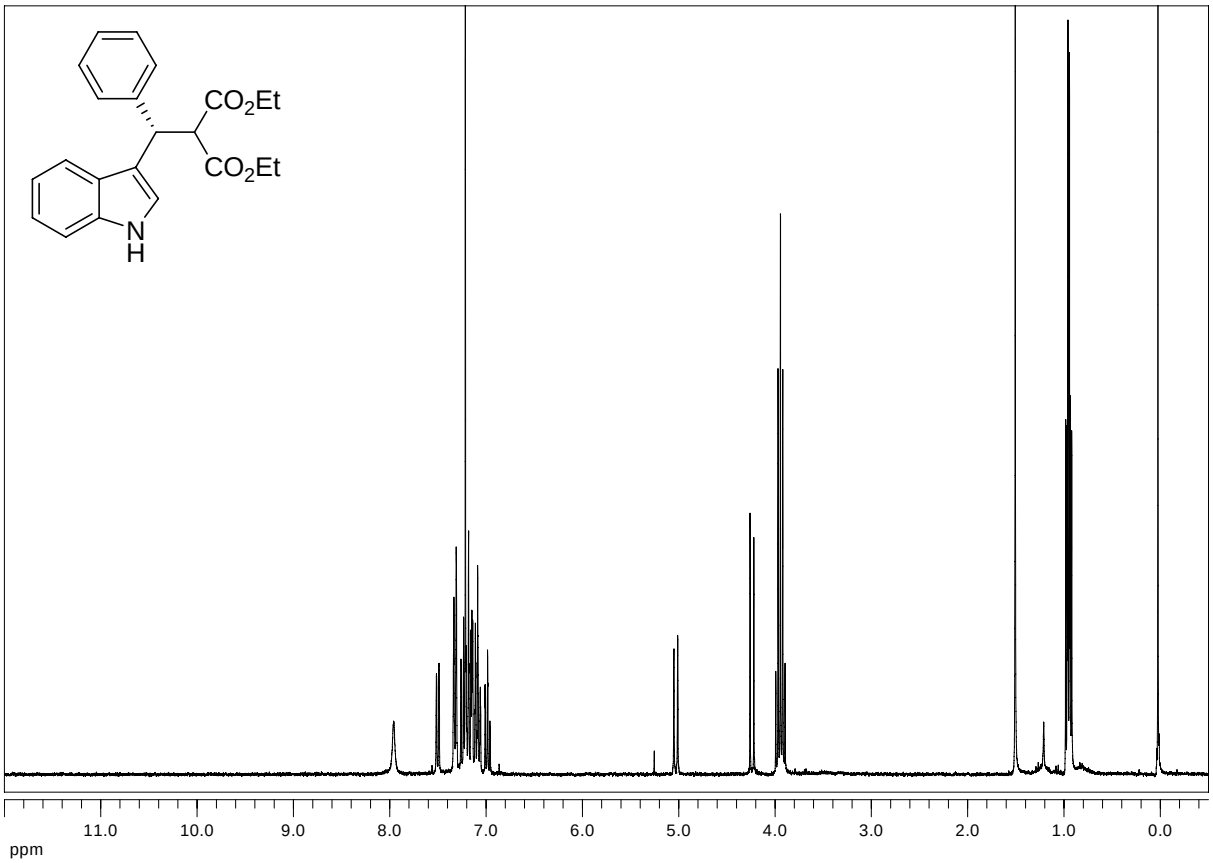

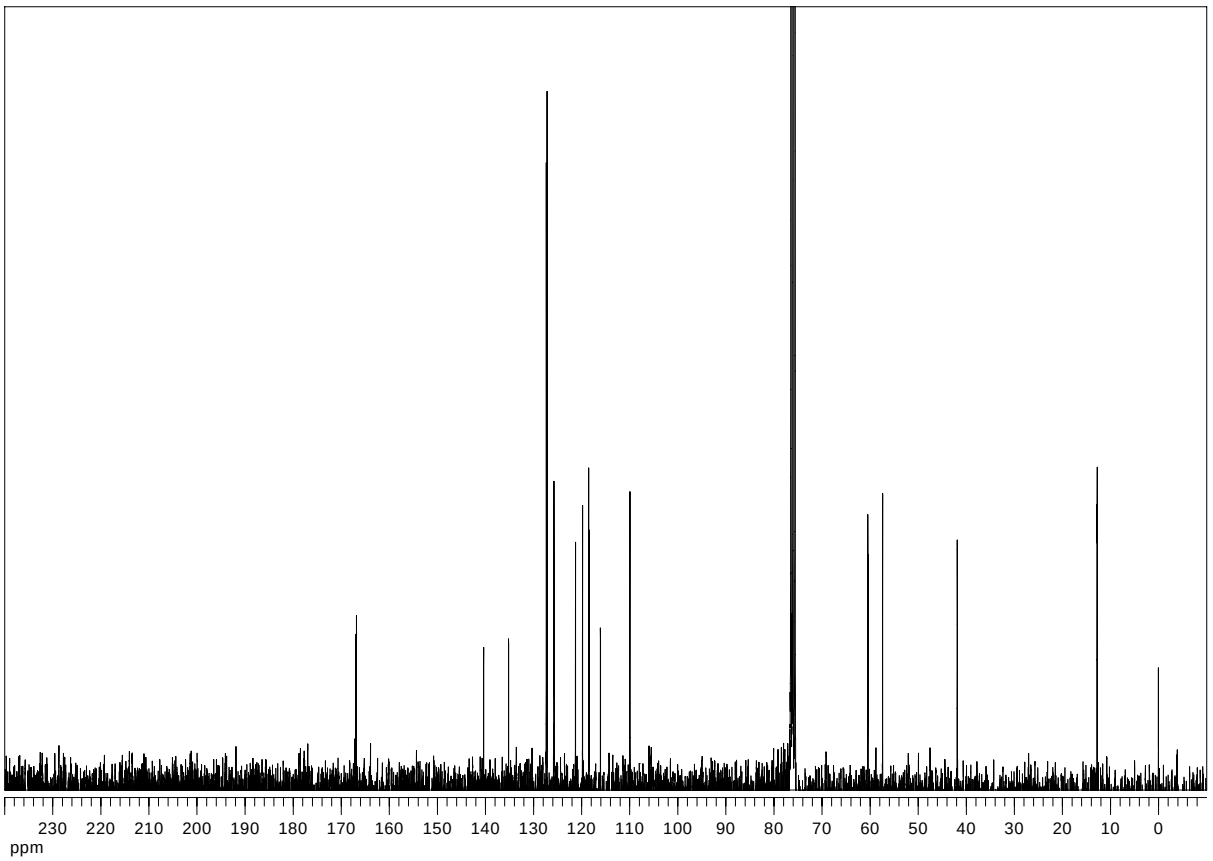

(*S*)–Ethyl2–ethoxycarbonyl–3–(3–indolyl)–3–(p-methylphenyl)propanoate (180b):

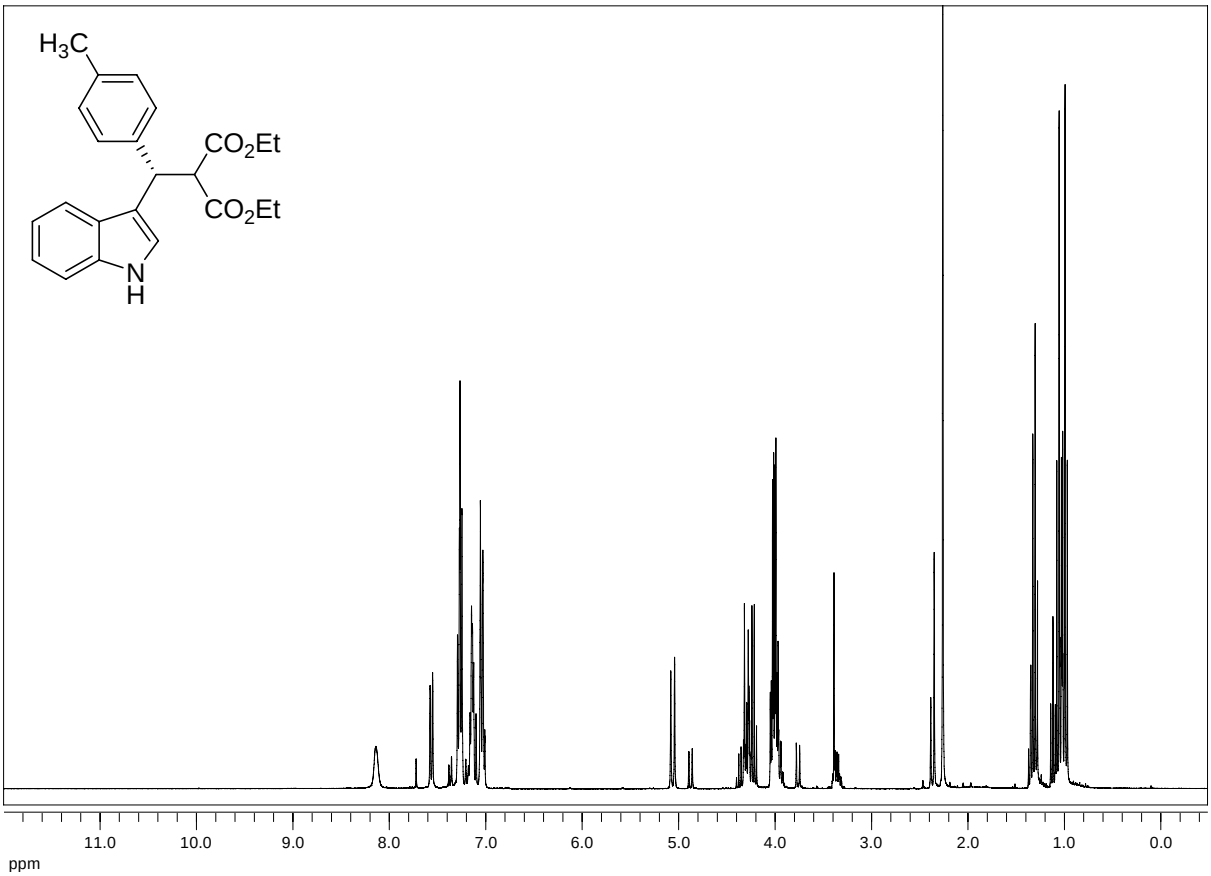

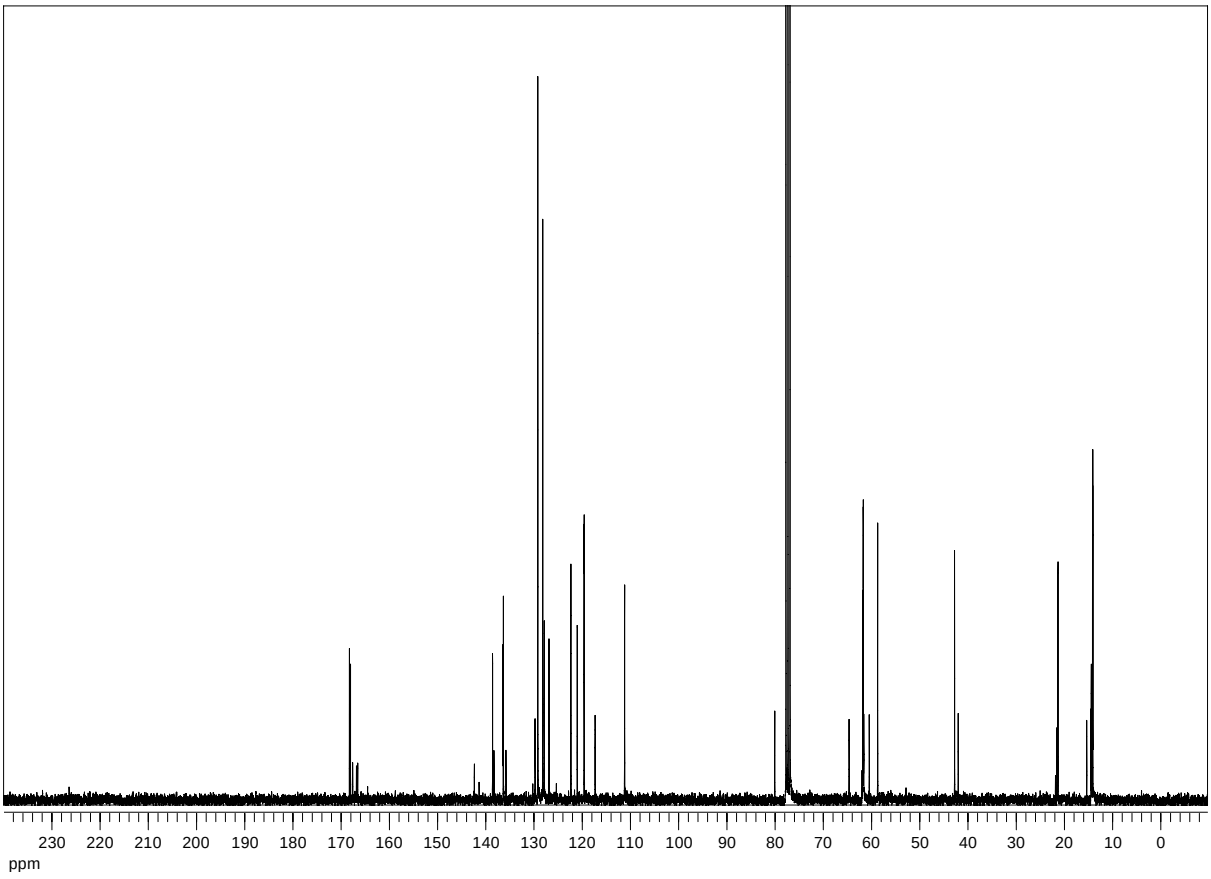

(*S*)–Ethyl2–ethoxycarbonyl–3–(3–indolyl)–3–(p-methyoxyphenyl)propanoate (180c):

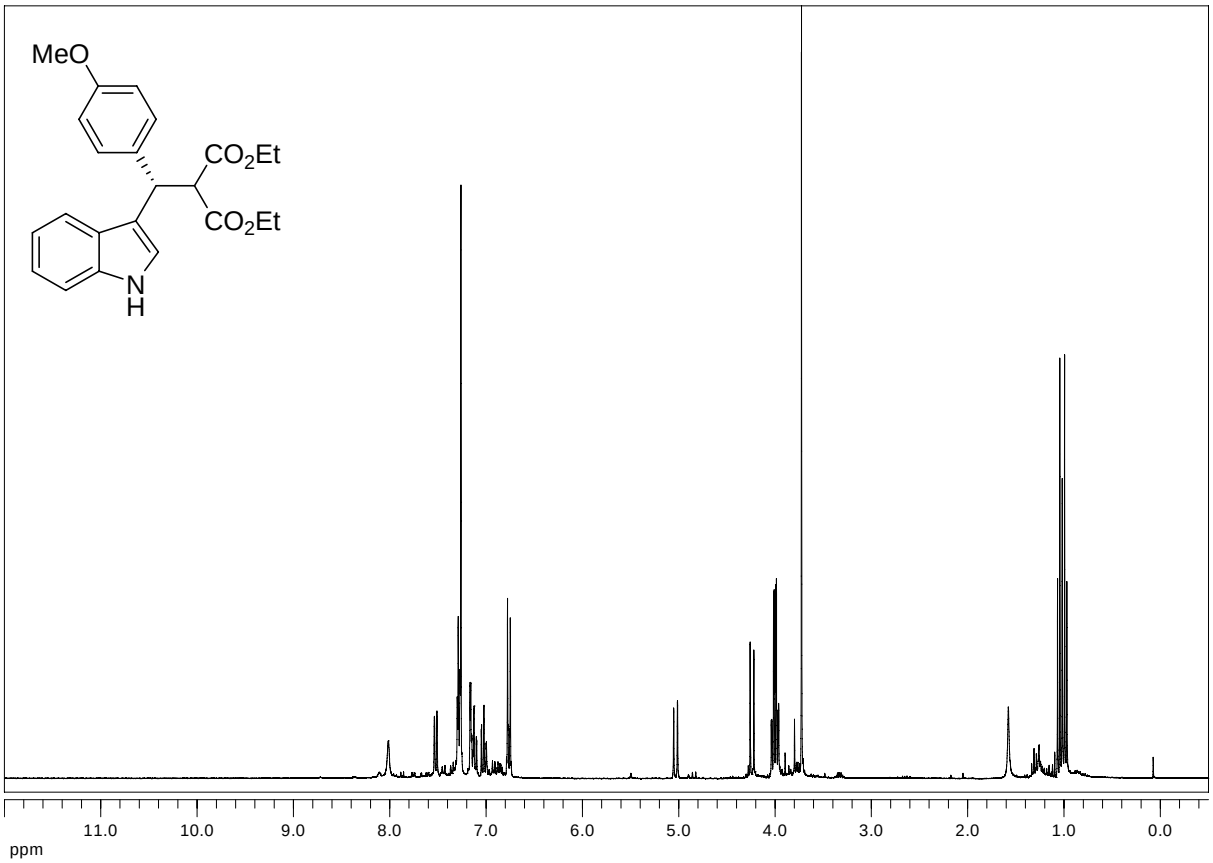

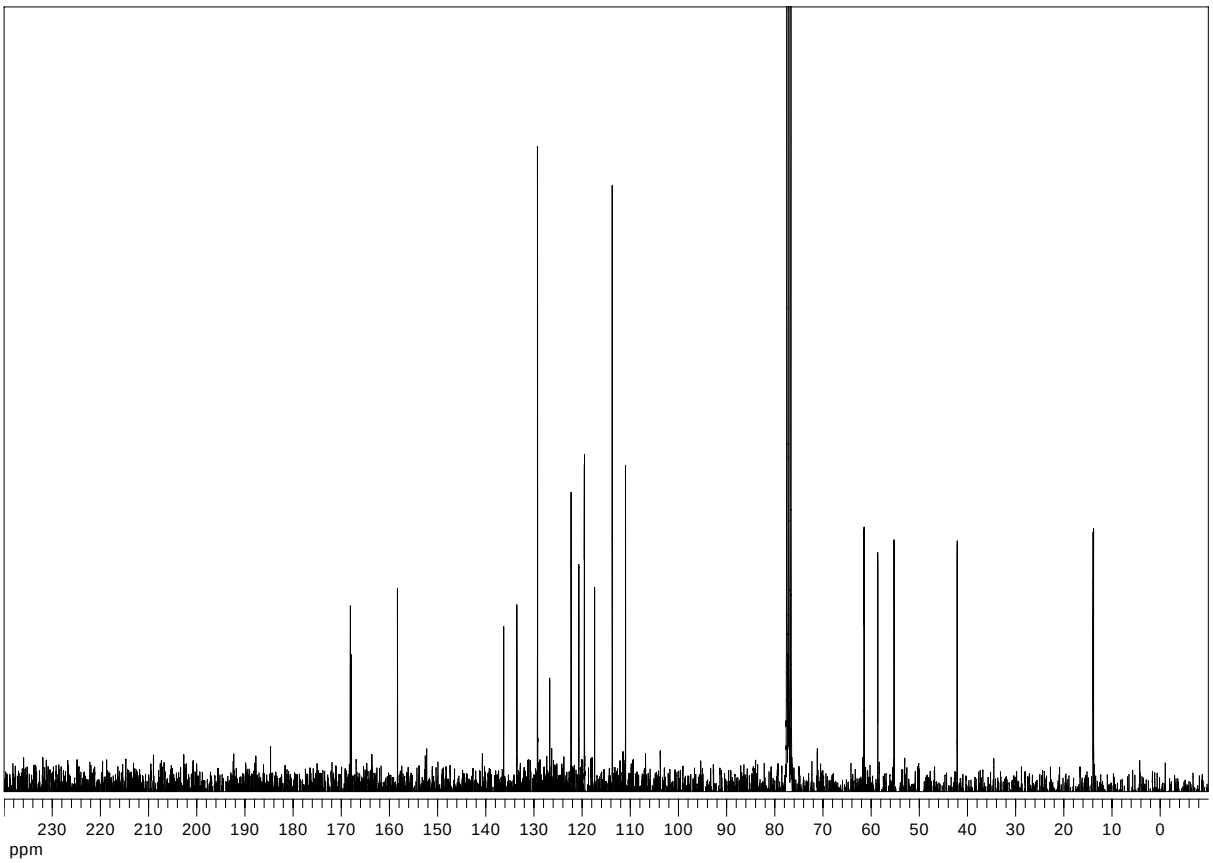

(*S*)–Ethyl2–ethoxycarbonyl–3–(3–indolyl)–3–(p-trifluoromethylphenyl)-propanoate (180d):

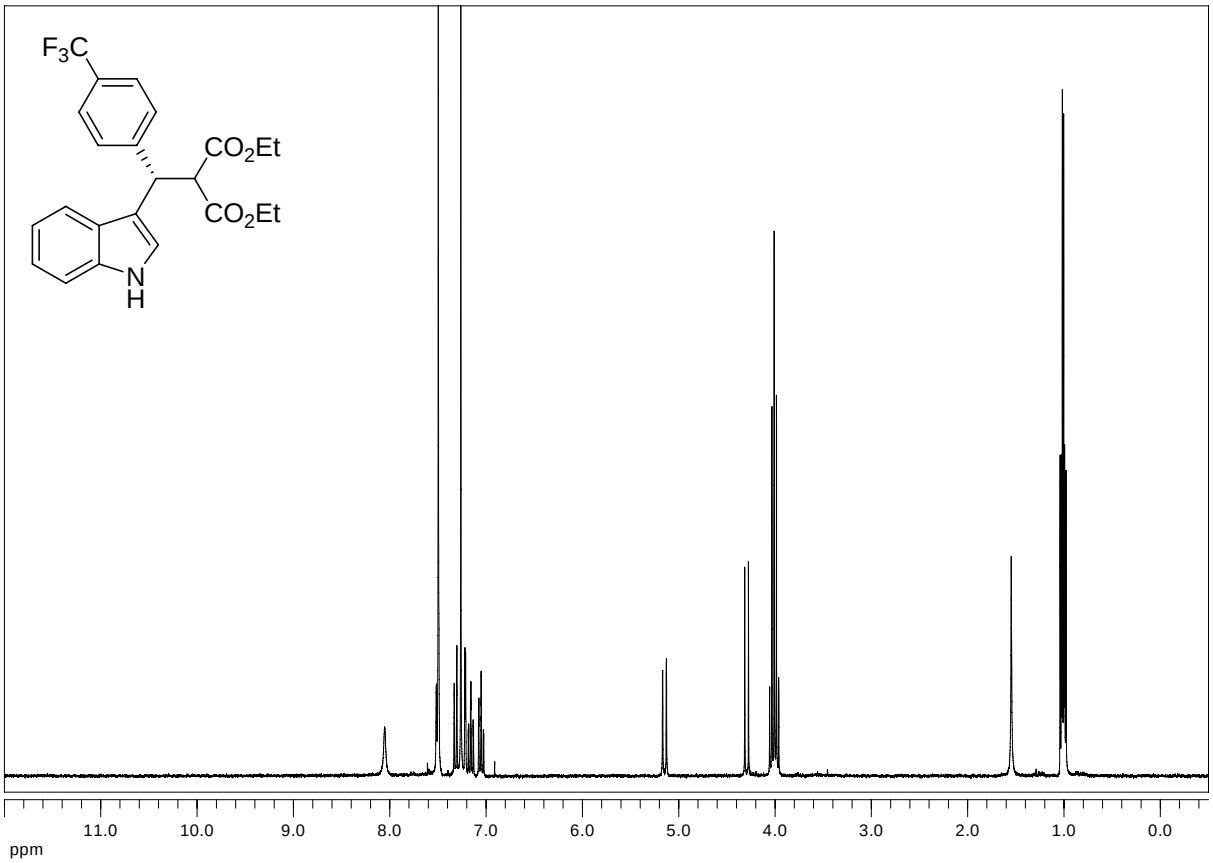

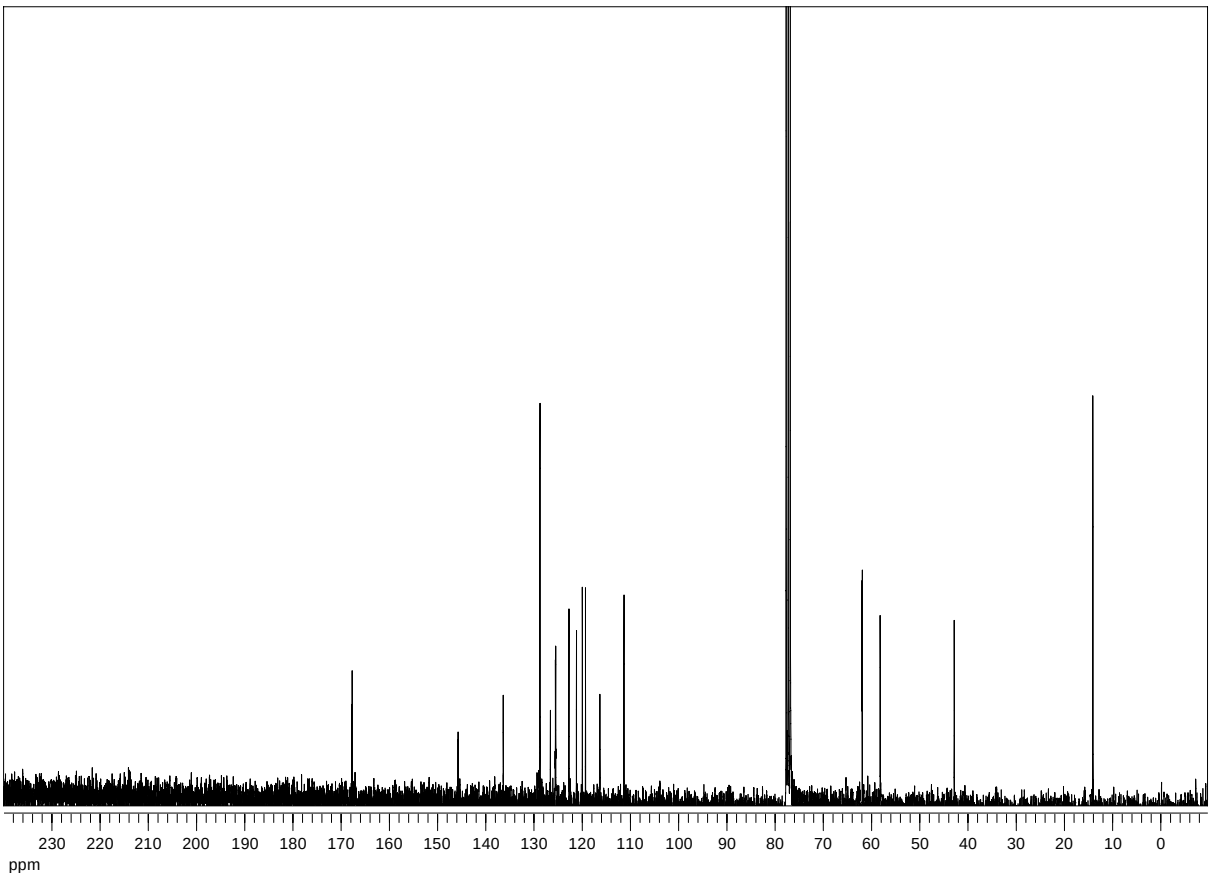

(*S*)–Ethyl2–ethoxycarbonyl–3–(3–indolyl)–3–(o-bromophenyl)propanoate (180e):

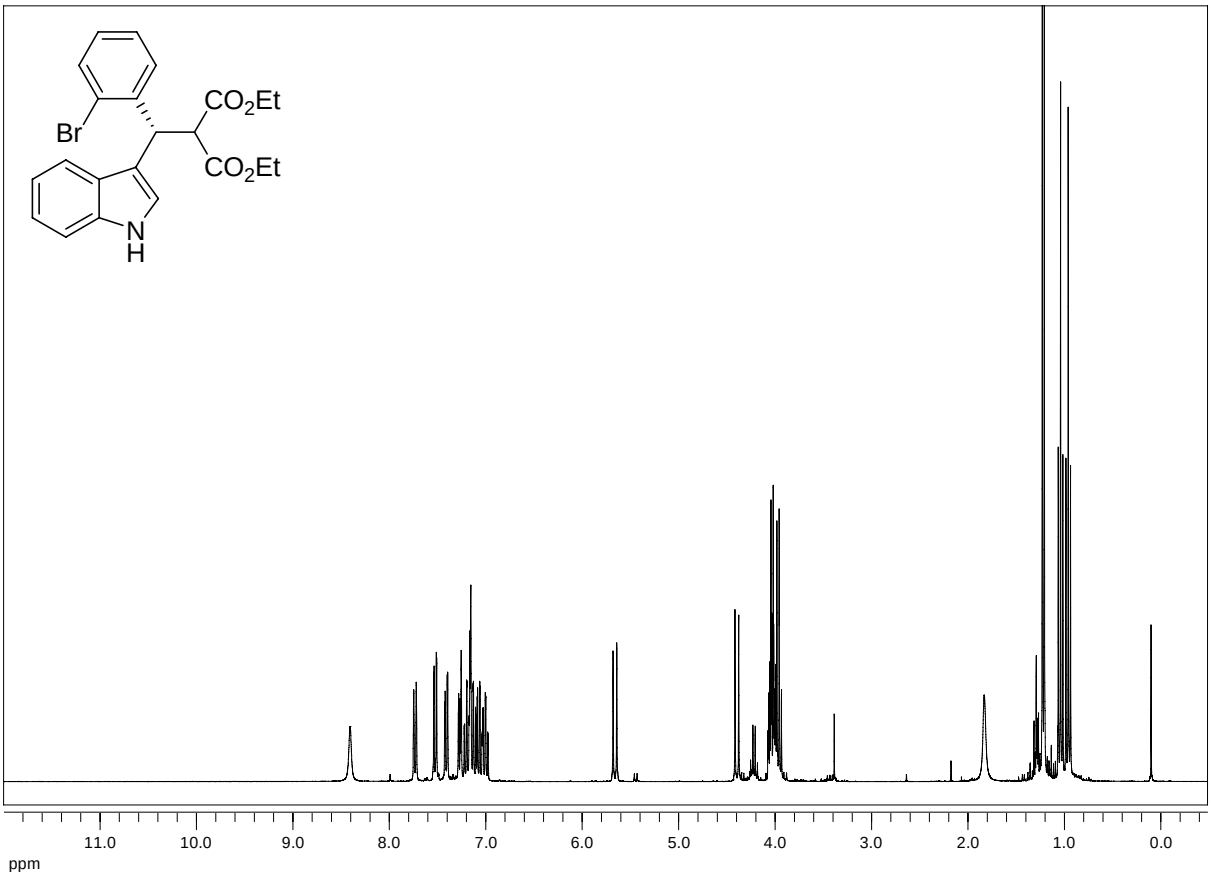

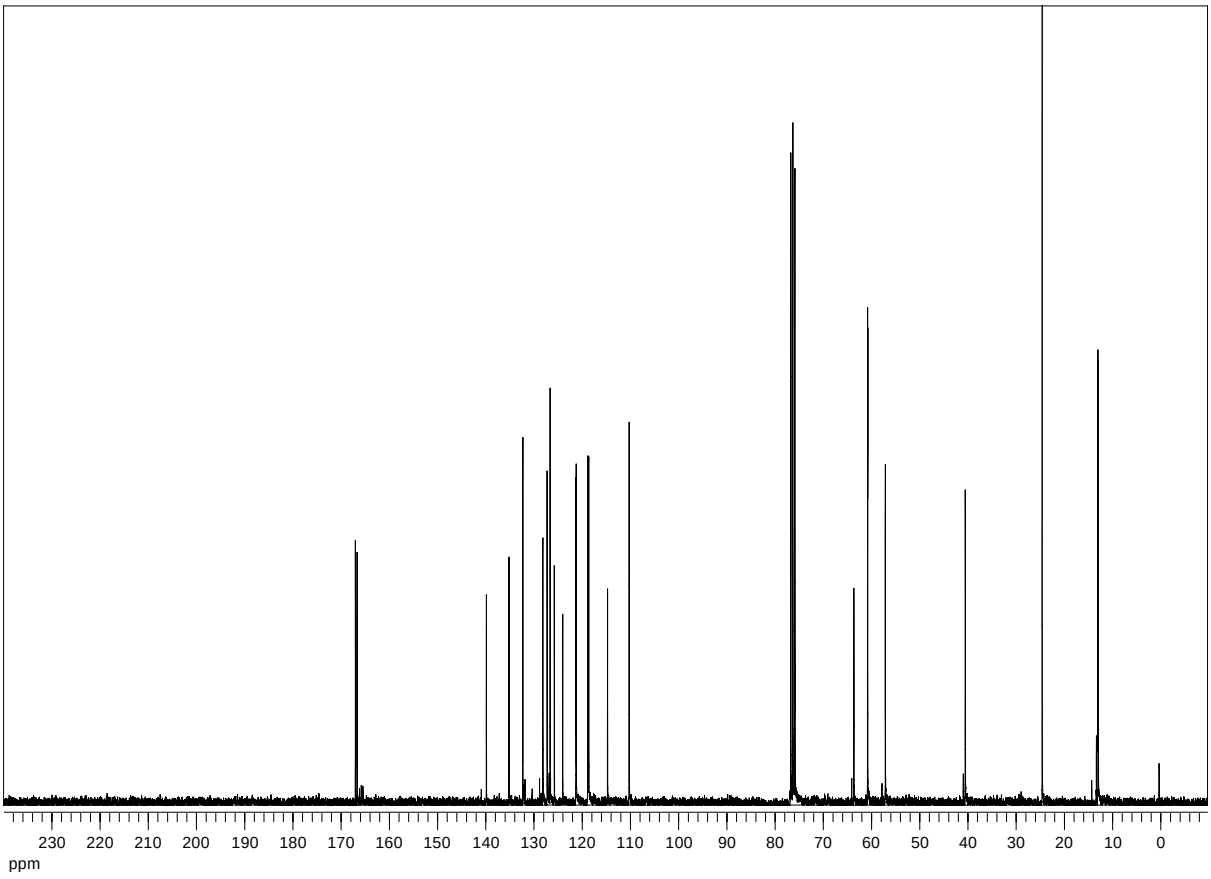

(*S*)–Ethyl2–ethoxycarbonyl–3–(3–indolyl)–3–(p-bromophenyl)propanoate (180f):

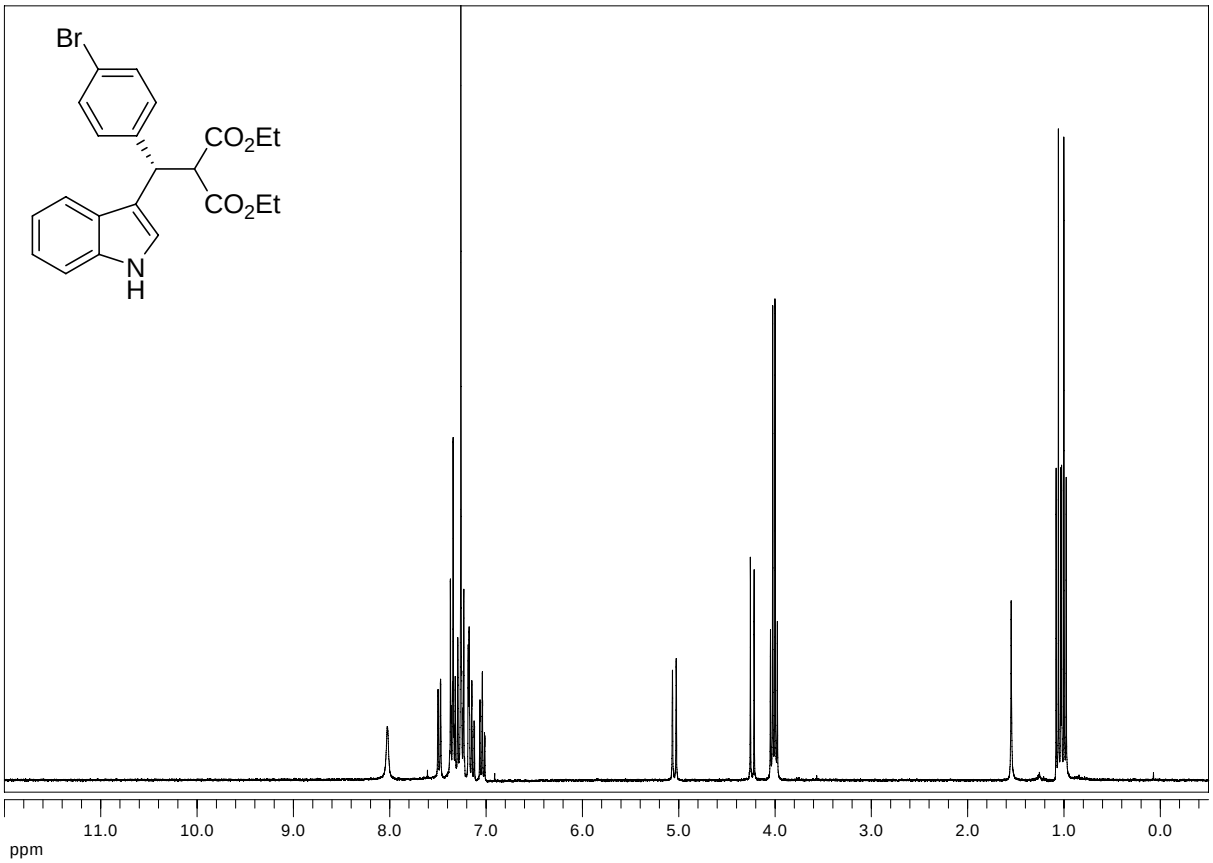

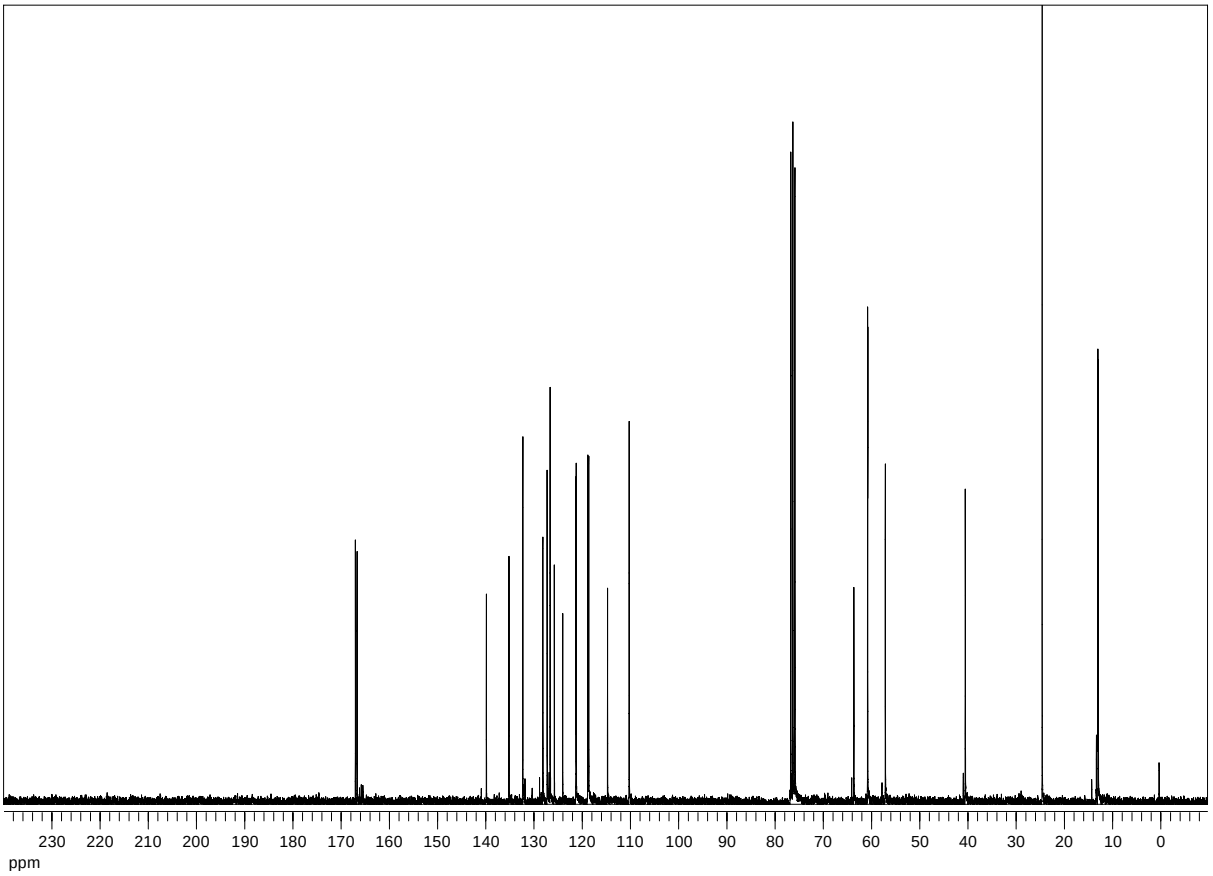

(*S*)–Ethyl2–ethoxycarbonyl–3–(3–indolyl)–3–(p-nitrophenyl)propanoate (180g):

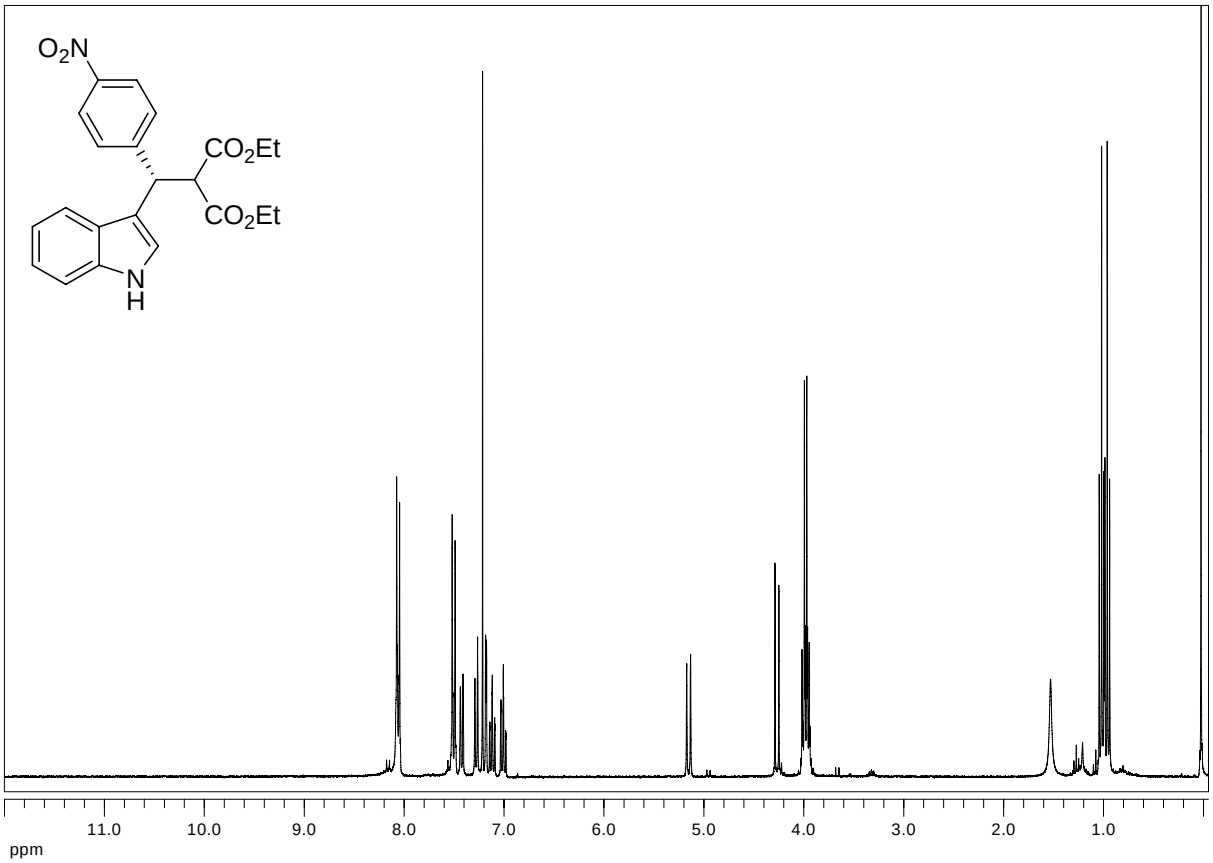

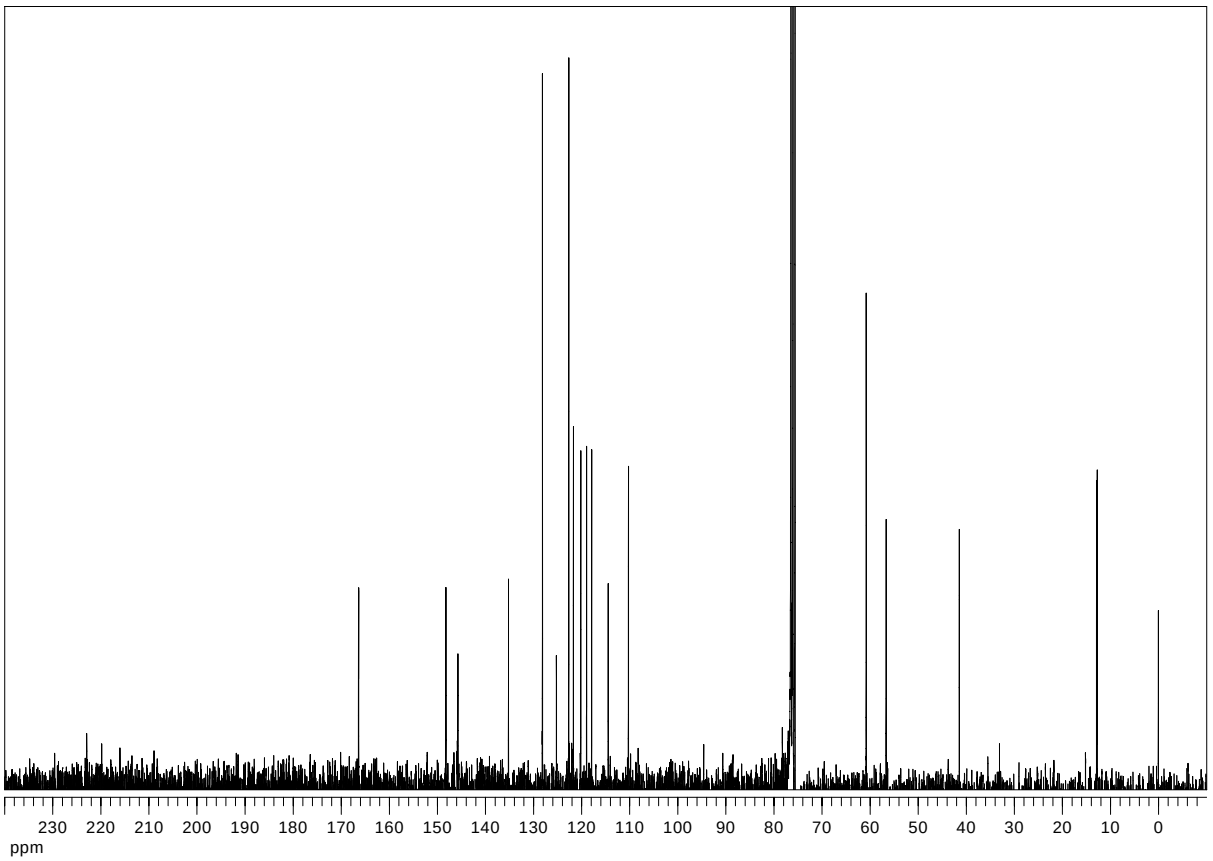

(*R*)-3-(2-nitro-1-phenylethyl)-1*H*-indole (186):

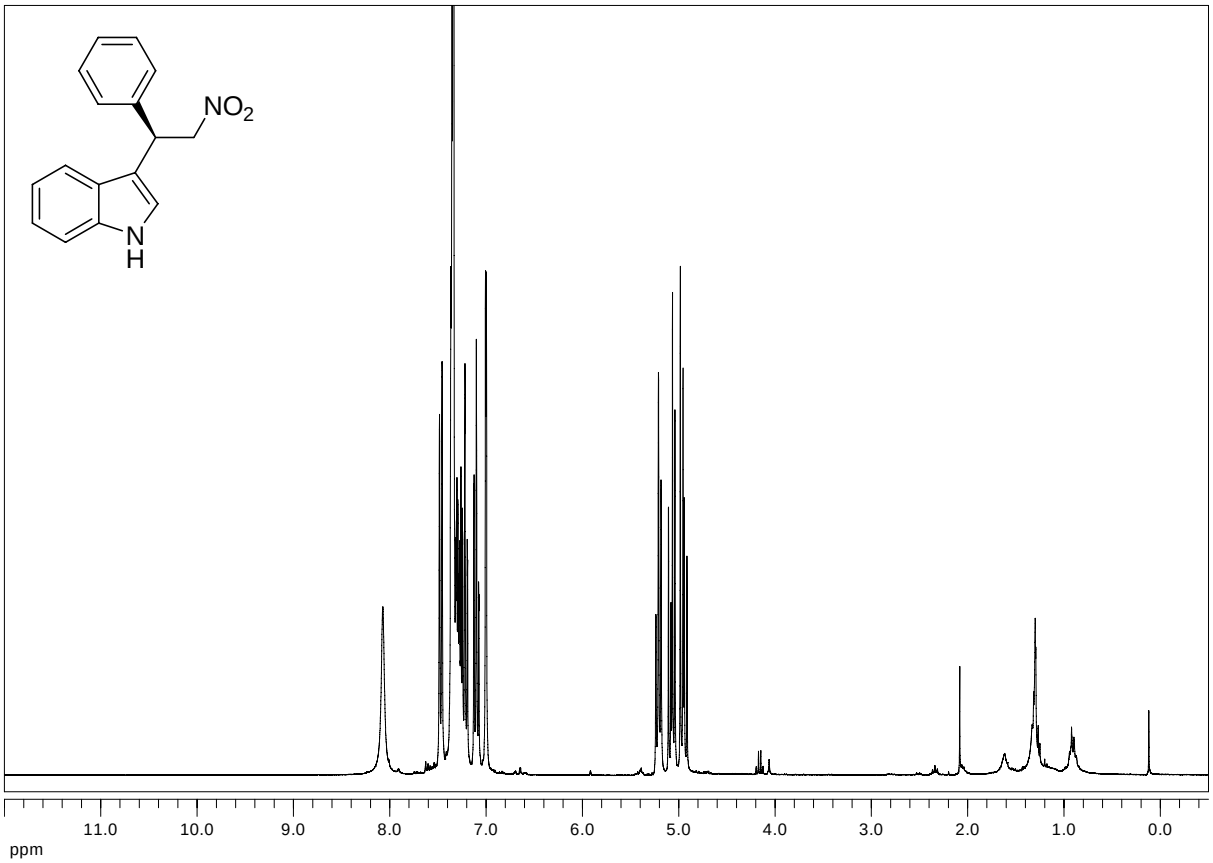

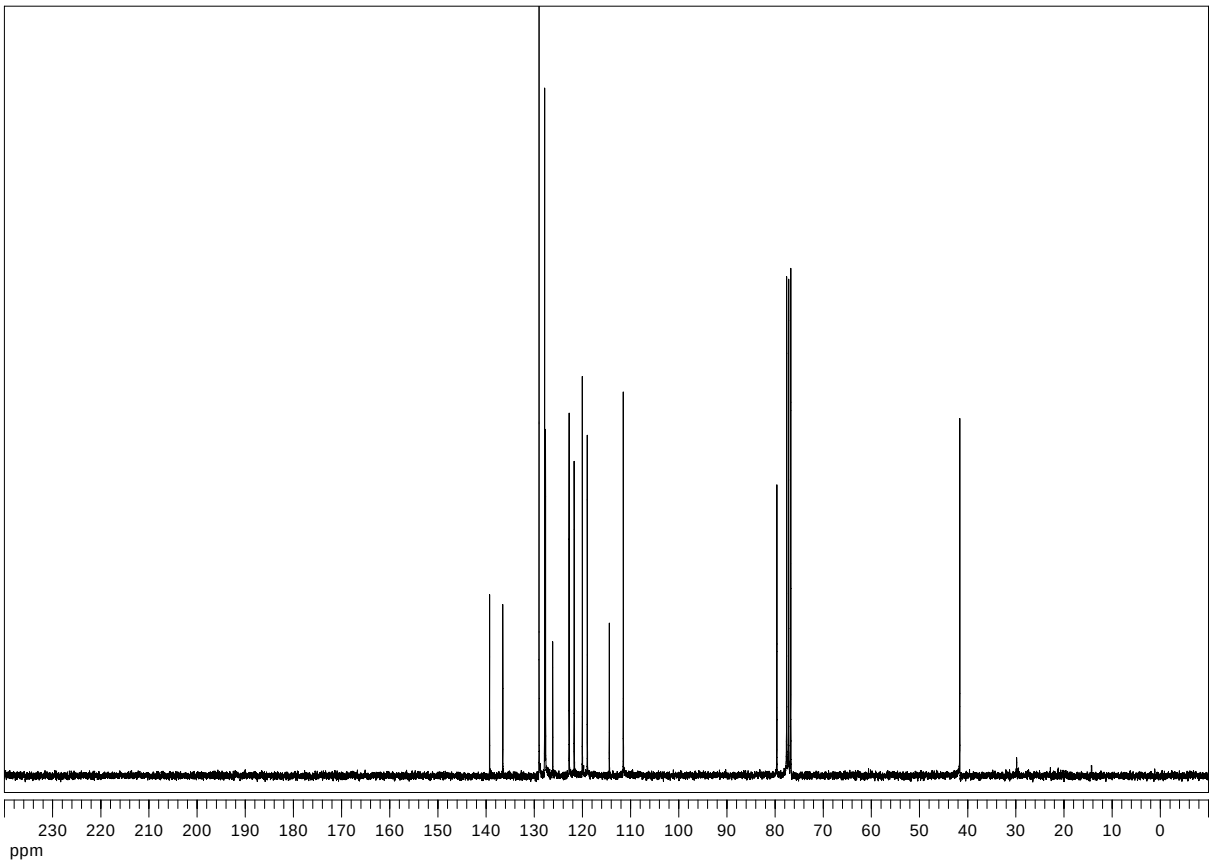

(*S*)-Isopropyl 2-hydroxy-2-phenylacetate (189):

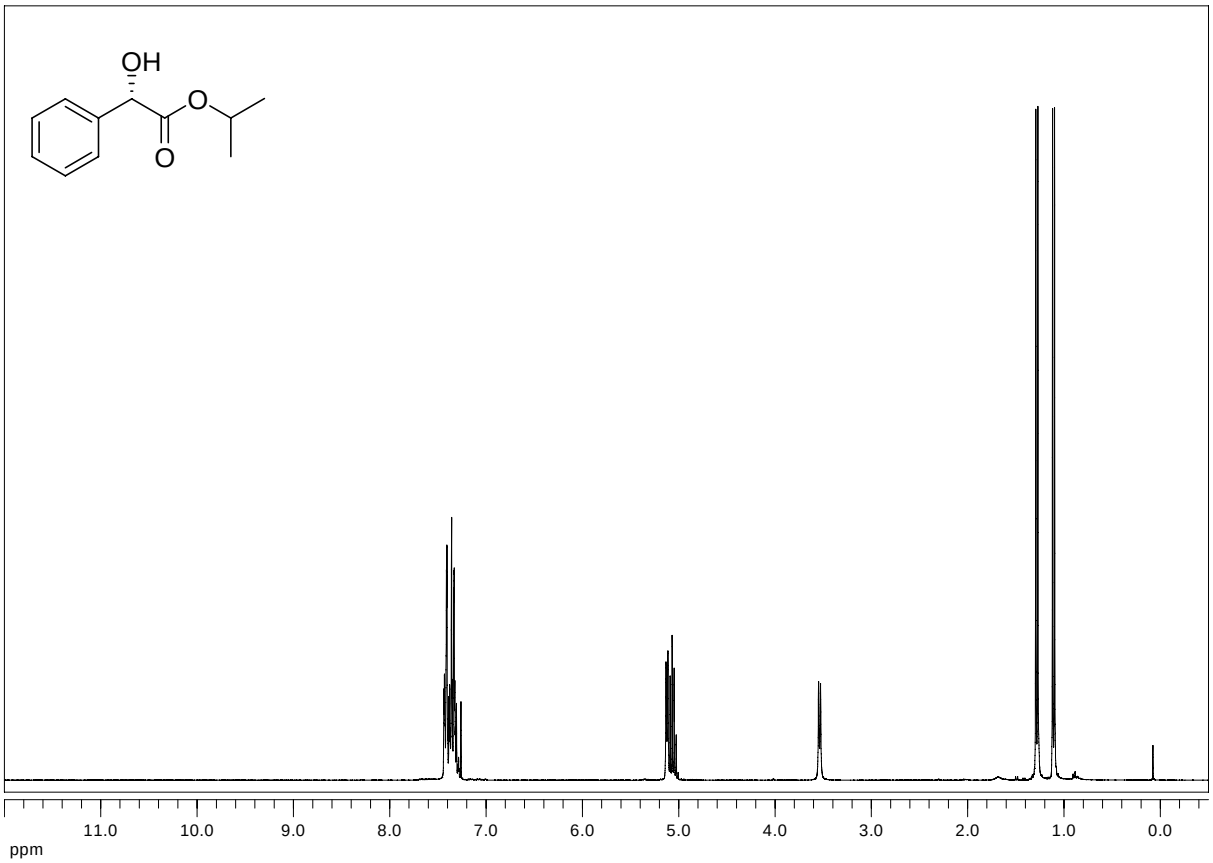

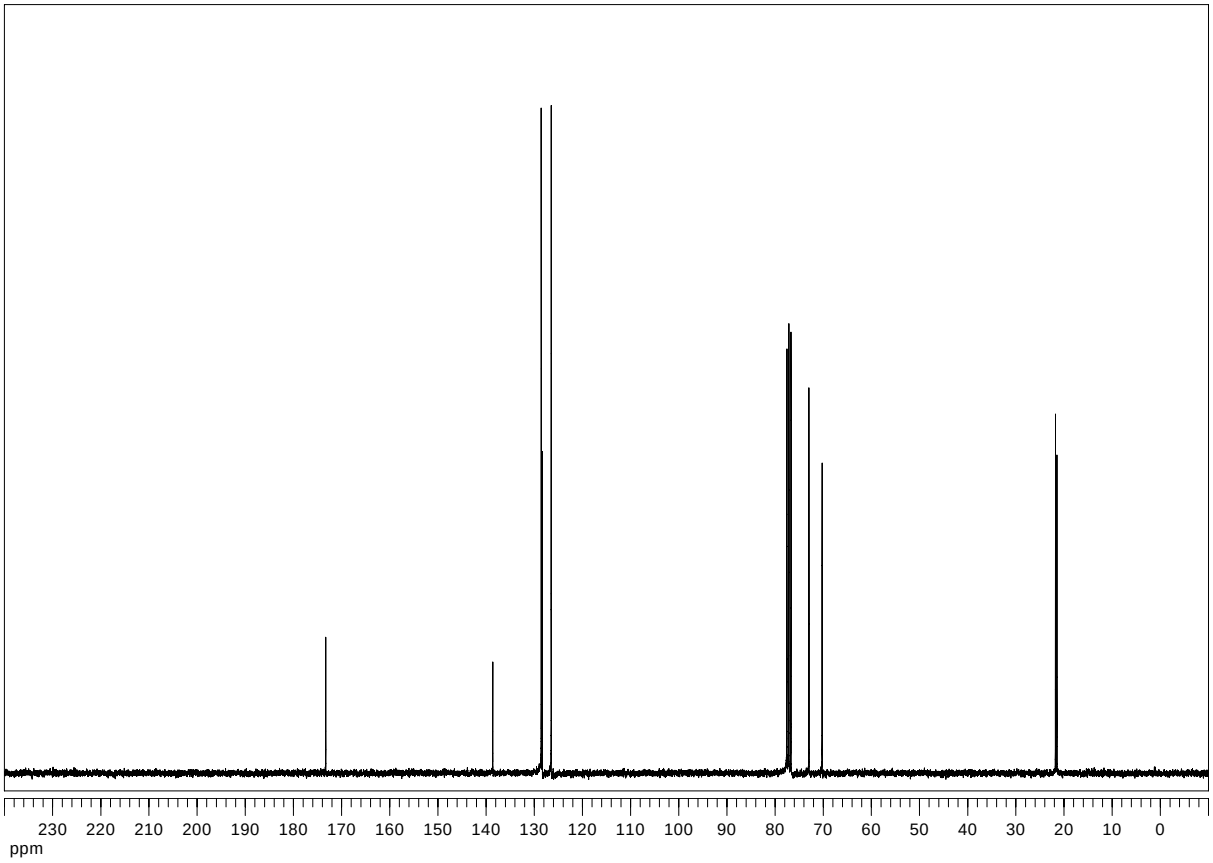

2. List of Publications

[1] Alexander Schätz, Alessandro Scarel, Ennio Zangrando, Luca Mosca, Carla Carfagna, Anja Gissibl, Barbara Milani, Oliver Reiser, *Organometallics* **2006**, *25*, 4065:
High Stereocontrol and Efficiency in CO/Styrene Polyketones Synthesis Promoted by Azabis(oxazoline)-Palladium Complexes

[2] Alexander Schätz, Ramesh Rasappan, Markus Hager, Anja Gissibl, Oliver Reiser, *Chemistry: A European Journal* **2008**, *14*, 7259:
Dependence of Enantioselectivity on Ligand/Metal-Ratio in the Asymmetric Michael Addition of Indole to Benzylidene Malonates: Electronic Influence of Substrate

[3] Alexander Schätz, Robert N. Grass, Oliver Reiser, Wendelin J. Stark, *Chemistry: A European Journal* **2008**, *14*, 8262:
TEMPO Supported on Magnetic C/Co-Nanoparticles: A Highly Active and Recyclable Organocatalyst

[4] Alexander Schätz, Markus Hager, Oliver Reiser, *Adv. Funct. Mater*. **2009**, Accepted:
Cu(II)-Azabis(oxazoline)-Complexes Immobilized on Superparamagnetic Magnetite@Silica-Nanoparticles: A Highly Selective and Recyclable Catalyst for the Kinetic Resolution of 1,2-Diols

3. Congresses and scientific meetings

International Symposium on Green Chemistry for Chemistry and Health, Helmholtz Center, Munich (Germany), October 13– 16 2008.
Poster presentation: **Recycling of Catalysts using Magnetic Nanoparticles**

Elite Network of Bavaria Evaluation Meeting, Tutzing (Germany), June 5 – 6 2008.
Oral contribution and poster presentation: **Magnetic TEMPO: A Highly Active and Recyclable Organocatalyst**

Frontiers in Organometallic Chemistry, Garching (Germany), April 17 – 18 2008.

DICHEM International Scientific Symposium, Burghausen (Germany), May 10 – 12 2007.

International Summer Course at BASF, Ludwigshafen (Germany), August 2006.
Poster presentation: **High Stereocontrol and Efficiency in CO/Styrene Polyketones Synthesis Promoted by Azabis(oxazoline)-Palladium Complexes**

European Network *PALLADIUM* Final Meeting, Grado-Trieste (Italy), June, 16 – 18 2006. Oral contribution: **Highly Efficient Stereocontrol in CO/Styrene Polyketones Synthesis Promoted by Azabis(oxazoline)-Palladium Complexes**

European Network *PALLADIUM* Meeting, Florence (Italy), October 21 – 23 2005.
Oral contribution: **Highly Efficient Stereocontrol in CO/Styrene Polyketones Synthesis Promoted by Azabis(oxazoline)-Palladium Complexes**

4. Curriculum Vitae

Personal Data

Name: Alexander Schätz

Date of Birth: 12/13/1979

Nationality: German

Email: alexander.schaetz@chemie.uni-regensburg.de

Education

01/2006 – Current	Ph.D. thesis within the Elite Network of Bavaria (ENB) under chairmanship of Prof. Dr. W. A. Herrmann, TU Muenchen and supervision of Prof. Dr. O. Reiser, University of Regensburg (Part of the international doctorate program NANOCAT - Nanodesign of High Performance Catalysts)
10/2005 – 12/2005	Research project in the group of Dr. B. Milani Università di Trieste, Italy: "*Synthesis of Isotactic Poly(styrene-alt-CO)*"
09/2005	Chemistry-Diploma with additional qualification in Medicinal Chemistry *Master of Science equivalent*
01/2005 – 09/2005	Diploma thesis in the research groups of Prof. Dr. O. Reiser and Dr. B. Milani (Università di Trieste, Italy): "*Asymmetric Copolymerization of Highly Isotactic Poly(1,4-ketones) using Pd(II)-Catalysts Based on Azabis(oxazolines)*"
10/2003 – 09/2005	Advanced studies in Medicinal Chemistry
10/2002	Intermediate exam (*Bachelor equivalent*)
10/2000 – 09/2005	Studies in Chemistry, University of Regensburg, Germany
09/1990 – 07/1999	Abitur (*A-levels*) Gymnasium (secondary school) Untergriesbach, Germany *High school Certificate equivalent*

Languages

German (native)

English (fluently)

Professional References:

Prof. Dr. Oliver Reiser
Institut für Organische Chemie
Universität Regensburg, Universitätsstr. 31
93053 Regensburg, Germany
Phone: +49 - 941 - 9434631
Email: oliver.reiser@chemie.uni-regensburg.de

Dr. Barbara Milani
Dipartimento di Scienze Chimiche
Università degli Studi di Trieste, Piazzale Europa 1
34127 Trieste, Italy
Phone: +39 - 040 - 5583955
Email: milani@dsch.univ.trieste.it

Prof. Dr. Wendelin J. Stark
Institut für Chemie- und Bioingenieurwissenschaften
Department Chemie und Angewandte Biowissenschaften
ETH Zürich, Wolfgang-Pauli-Strasse 10
8093 Zürich, Switzerland
Phone: +41 - 44 - 6320980
E-mail: wstark@ethz.ch

F. Acknowledgement

University of Regensburg

I would like to express my gratitude to ***Prof. Dr. Oliver Reiser*** for offering me the possibility to work on this highly interesting topic, the continuous support in publishing and for his guidance.

I am much obliged for the help provided by ***Dr. Peter Kreitmeier***, ***Dr. Kirsten Zeitler*** and ***Dr. Sabine Amslinger*** and for sharing their expertise. I am especially grateful for proof-reading by Kirsten and Sabine and thank Peter for his patience while realizing all kinds of setups.

Furthermore, I thank ***Georg Adolin***, ***Klaus Döring***, ***Andrea Roithmeier*** and ***Robert Tomahogh*** for doing all kinds of jobs that made everyday life much easier. The same is true for our secretaries ***Young Rotermund*** and ***Hedwig Ohli***.

I am grateful for the support of the central analytic department of the University of Regensburg.

For the productive and homelike environment in the institute I have to thank all current and former members of the Reiser group. My special thanks in this regard to ***Hans Zwicknagl***, ***Dr. Gudrun Geyer***, ***Markus Hager***, ***Dr. Eva Jezek***, ***Klaus Harrar***, ***Dr. Anja Gißibl***, ***Alexander Tereshchenko***, ***Dr. Yogesh Shinde, Florian Sahr***, ***Dr. Andreas Schall*** and ***Michael Kuhn*** for organizing and joining a multitude of trips, balcony barbecues and all the other occasions in order to socialize and have a beer occasionally. In addition, I thank ***Markus Hager*** and ***Sebastian Wittmann*** for proof-reading.

My labmates ***Tamilselvi Chinnusamy*** and ***Walter Olbrich*** deserve sincere thanks for the good atmosphere in the lab.

Thanks to my former interns ***Allan Wood***, ***Paul Baumeister***, ***Dennis Kühbeck*** and ***Quirin Kainz*** for carrying out a couple of reactions in place of me.

My fellows from outside the institute ***Dr. Matthias Stich***, ***Anna Hezinger***, ***Christian Schreiner***, ***Jens Bolle***, ***Fabian Glaab***, ***Dr. Markus Zistler*** and ***Dr. Philipp Wachter*** deserve my gratitude not only for their invaluable and immediate support in chemical matters but especially for their permanent friendship.

Last but not least, my friends during the years of study ***Renate Gleixner***, ***Anja Bernecker***, ***Tobias Pfaller***, ***Eva Schmitt***, ***Bernhard Sandig***, ***Regina Klein***, ***Christoph Beyer*** and ***Michael Egger*** have to be acknowledged.

TU München

I am grateful that ***Prof. Dr. W. A. Herrmann*** and ***Prof. Dr. F. E. Kühn*** enabled my employment at the *Lehrstuhl für Anorganische Chemie* within the international doctorate program NANOCAT.

I thank my co-supervisor ***Prof. Dr. T. Bach, Dr. Jörg Eppinger*** and especially ***Dr. Markus Drees*** for his efforts as network coordinator. The resources provided by NANOCAT were invaluable.

Finally, my special thanks to ***Daniel Stadler***, ***Dr. Philipp Rubenbauer*** and ***Sandra Zinner*** for making the NANOCAT meetings familiar and relaxing.

ETH Zürich

I have to acknowledge the outstanding work of ***Prof. Dr. W. J. Stark*** and ***Dr. Robert N. Grass*** as well as their hospitality. This work would have not been possible without their help, generous donations of cobalt nanoparticles and the fruitful cooperation with them.

Furthermore, I am very grateful for the support of the analytic department of the ETH Zürich.

Ganz besonderen und sicher den größten Dank schulde ich meinen Eltern und meiner Großmutter. Ohne Eure anhaltende Unterstützung wären weder mein Studium noch diese Arbeit möglich gewesen.